technische universität dortmund

MAX PLANCK INSTITUTE OF MOLECULAR PHYSIOLOGY

IDENTIFICATION AND CHARACTERIZATION OF INHIBITORS OF HEDGEHOG-INDUCED OSTEOBLAST DIFFERENTIATION

Dissertation

For the achievement of the academic degree of the

Doctor in Natural Sciences

(**Dr. rer. nat.**)

Submitted to

Faculty of Chemistry and Chemical Biology

TU Dortmund University

by

Jana Erika Flegel

born on 21.11.1992
in Ostercappeln, Niedersachsen

Dortmund 2022

Die vorliegende Arbeit wurde im Zeitraum von November 2017 bis Mai 2022 unter der Anleitung von Prof. Dr. Dr. h.c. Herbert Waldmann und Dr. Slava Ziegler an der Fakultät für Chemie und Chemische Biologie der Technischen Universität Dortmund und dem Max-Planck-Institut für molekulare Physiologie Dortmund angefertigt.

1. Gutachter: Prof. Dr. Dr. h.c. Herbert Waldmann

2. Gutachter: Prof. Dr. Daniel Rauh

ACKNOWLEDGEMENTS

A PhD is like a long journey: incredibly exciting, with ever new challenges and many ups and downs. For me, this time was extremely enriching, both personally and scientifically, and I would like to thank everyone who accompanied me on this journey.

First of all, I would like to thank Prof. Dr. Dr. h.c. Herbert Waldmann for the opportunity to join his research group for my doctorate and for entrusting me with highly exciting research projects. The access to high-end equipment, the excellent academic environment and the independent way of working have contributed significantly to my scientific maturation. I am very grateful for the encouraging project meetings and all the support I received during my PhD.

I would like to thank Prof. Dr. Rauh for taking over the second correction of this thesis.

I am very grateful to Dr. Slava Ziegler, my co-supervisor and group leader, who constantly guided, supported and encouraged me throughout my PhD. Her comments, ideas, and constructive suggestions were always very helpful in moving my scientific projects forward and getting the best out of them. Her open nature and appreciation for my work always motivated me to do my best. I would also like to thank her for proofreading my dissertation.

Particularly, I would like thank Dr. Saad Shaaban who worked with me on the Picoberin project. I really enjoyed our discussions on both, chemical and biological aspects of this project. As a chemist, he quickly accepted that biological experiments take a lot of time and he always patiently waited for news. I truly hope we will keep in tough in future.

Especially, I would like to thank Britta Schulte whom I supervised for her master thesis and who contributed to this thesis with her work on the Picoberin project. Her persistent, conscientious, and reliable attitude has led to several valuable results that have ultimately made this project a success. I would also like to thank Chantal Wientjens, who accompanied me during her bachelor thesis on the characterization of selected inhibitors of the Hh signaling pathway and who was always highly motivated to contribute to my projects with her scientific work and creative ideas. I would like to thank my two highly talented trainees, Michelle Saretzki and Julian Pretel for their assistance with diverse tasks in the lab. Moreover, I thank Neele Kleffner and Anke Flegel who both joined me for an internship and who very quickly became a great help to me in the lab thanks to their quick grasp of things. Likewise, my special thanks go to Alexandra Brause, who supported me in the lab, but also on a personal level throughout my PhD. Her always positive and cheerful attitude have contributed to this work, not only on a scientific level and I am sure our friendship will continue in future.

Furthermore, I would like to thank Dr. Zhijun Jia, Dr. Gang Shan, Dr. Houha Li, Dr. Stefan Zimmermann, Dr. Gregor Cremosnik for synthesis of compounds that I investigated throughout my research projects and for various fruitful scientific discussions. Furthermore, I thank Dr. Yilong Lian and Dr. Pedro Moura Alves from the Ludwig Cancer Research Institute Oxford for scientific discussions and collaboration on the Picoberin project.

I would like to particularly thank the mass spectrometry team of the MPI Dortmund, namely Dr. Petra Janning, Andreas Brockmeyer, Malte Metz, Dr. Elena Rudashevskaya and Jens Warmers for measuring my proteome profiling and TPP samples, for analyzing the mass spectrometry data and help me with the experimental design through constructive feedback and in general the introduction into the work with proteomics samples. Furthermore, I would like to thank the team of the COMAS, especially Dr. Sonja Sievers and Dr. Claude Ostermann for compound screening and Christiane Pfaff for culturing and providing the stem cells for my project. Additionally, I want to thank Dr. Sven A. H. Müller and Dr. Michael Schulz for their training and access to the confocal microscope and the flow cytometer. For help and support regarding all administrative issues, I want to express my gratitude to Brigitte Rose.

I really enjoyed being part of the International Chemical Biology Society (ICBS) Student Chapter Dortmund. Namely I would like to thank Dr. Elena Reckzeh, Dr. Annina Burhop, Aylin Binici, Jessica Nowacki, Pascal Hommen, Lara Dötsch and Kirujan Jeyakumar for their great work within this young research organization.

Moreover, I am highly thankful for the excellent working atmosphere, scientific discussions, summer BBQs and social events within this large international and highly collegial team of scientists. Without Aylin Binici, Dr. Nadine Kaiser, Dr. Lea Kremer, Dr. Fabian Weßeler, Dr. Michael Winzker, Sarah Zinken, Caitlin Davies, Dr. Georg Niggemeyer, Dr. Michael Gringalunas, Dr. Gregor Cremosnik, Dr. Soheila R. Adariani, Dr. Tim Förster, Dr. Alexandra Friese, Christine Nowack and Beate Schölermann this would not have been possible. Especially I would like to thank Dr. Annina Burhop, Dr. Tabea Schneidewind, Alexandra Brause and Lara Dötsch.

I am deeply grateful to Regine Siedentop and Anja Weitkamp for the very precious time-outs, which were so important to get my mind off work and to recharge my batteries.

My deepest and heartfelt appreciation goes to my partner Karsten Schrödter, my mother Babett Ahrens and my siblings Anke and Merlin Flegel for their constant personal support and encouragement. You have made me the person I am today and without you, none of this would have been possible.

TABLE OF CONTENTS

1 ABSTRACT

Hedgehog (Hh) signaling is one of the major pathways that is essentially required during embryonic development in vertebrates. Dysregulation during embryogenesis has been linked to severe developmental malformations including cyclopia and holoprosencephaly. Moreover, aberrant Hh signaling has been associated with several types of cancer, such as medulloblastoma and basal cell carcinoma. Over the past 40 years, studies have provided many insights into the current understanding of the Hh signaling pathway. Due promising potential for therapeutic modulation of this pathway, identification of small molecule modulators of Hh signaling is in high demand.

Throughout this thesis, six compounds were identified as potent inhibitors of Hh-dependent osteogenesis during a phenotypic screening. Five of these compounds inhibited GLI2/3-dependent reporter activity and expression of Hh target genes and were thus classified as novel Hh pathway inhibitors. While four compounds, a Furo[3,2-b]pyridine, quinoline, pyrroloquinoline and 20-membered macrocycle derivative bind to the key signaling molecule smoothened (SMO), one compound, a 4-arylisoquinolone does not bind to the heptahelical bundle of this protein.

An 8-oxotetrahydroprotoberberine derivate, termed Picoberin, inhibited Hh-dependent osteogenesis with a single-digit picomolar IC_{50} but did not modulate canonical Hh signaling. Despite its remarkable bioactivity, this small molecule was not cytotoxic at high concentrations in several cell lines. Global transcriptome and proteome profiling revealed that Picoberin activates Aryl hydrocarbon Receptor (AhR) signaling and led to the identification of AhR as the potential protein target. Subsequent functional evaluation of the influence of Picoberin on AhR signaling in several cell lines confirmed this target hypothesis. Moreover, chemical validations and genetic AhR depletion linked Picoberin mediated activation of AhR signaling to inhibition of Hh-dependent osteogenesis. Additionally, results obtained in this thesis provide evidence for crosstalk of AhR and Hh signaling and a functional role for AhR during osteoblast differentiation. AhR regulates xenobiotic metabolism as well as numerous physiological processes such as immune cell function, stem cell maintenance, and differentiation. Dysregulation of this ligand-activated transcription factor is observed in several diseases, including cancer. Historically, AhR is linked to mainly toxic effects. However, recent approval of the AhR agonist Tapinarof for treatment of plaque psoriasis and several studies exploring AhR in cancer provide evidence for potential therapeutic applications of AhR modulators. Picoberin could not only serve as a tool compound for AhR research but may potentially also provide a starting point for the development of further therapeutic AhR agonists.

ZUSAMMENFASSUNG

Der Hedgehog (Hh)-Signalweg ist einer der wichtigsten Signalwege während der embryonalen Entwicklung von Wirbeltieren, und seine Fehlregulation wurde mit schwerwiegenden Fehlbildungen wie Zyklopie oder Holoprosencephalie in Verbindung gebracht. Darüber hinaus führt eine übermäßige Aktivierung des Hh-Signalweges zu verschiedenen Krebsarten, z. B. Medulloblastomen und Basiliomen. In den letzten 40 Jahren wurden viele Erkenntnisse zum heutigen Verständnis des Hh-Signalweges gewinnen. Aufgrund des Potenzials einer therapeutischen Modulation ist die Identifizierung neuer Hh-Signalweg-Modulatoren von großem Interesse.

In einem phänotypischen Screening wurden sechs Verbindungen als potente Inhibitoren der Hh-abhängigen Osteogenese identifiziert. Fünf dieser Substanzen hemmen die GLI2/3 Aktivität und dadurch die Expression von Hh-Zielgenen. Sie wurden daher als Hh-Signalweg-Inhibitoren eingestuft. Während vier Verbindungen, ein Furo[3,2-b]pyridine, Chinolin, Pyrrolochinolin und eine 20-gliedrige makrozyklische Substanz an das Schlüsselprotein Smoothened binden, interagiert die fünfte Substanz, ein 4-Arylisochinolon, nicht mit dem heptahelikalen Bündel dieses Proteins.

Ein 8-Oxotetrahydroprotoberberin-Derivat, genannt Picoberin, hemmte die Hh-abhängige Osteogenese mit einem einstellig picomolaren IC_{50}-Wert, ohne den kanonische Hh-Signalweg zu beeinflussen. Trotz der bemerkenswerten Bioaktivität ist diese Substanz in mehreren Zelllinien auch bei hohen Konzentrationen nicht zytotoxisch. Globale Transkriptom- und Proteomanalysen zeigten, dass Picoberin den Aryl-Hydrocarbon-Rezeptor (AhR) aktiviert und führten zur Identifizierung des AhR als potenzielles Zielprotein. Anschließende funktionelle Untersuchungen des Einflusses von Picoberin auf den AhR in mehreren Zelllinien bestätigten diese Hypothese. Darüber hinaus verknüpften chemische Validierungen und genetische AhR-Depletion, die durch Picoberin vermittelte Aktivierung des AhR mit der Inhibition der Hh-abhängigen Osteogenese. Zusätzlich liefern die Ergebnisse dieser Arbeit Hinweise für ein Zusammenspiel von AhR- und Hh-Signalen und für eine funktionelle Rolle des AhR in der Osteogenese. Der AhR reguliert den Abbau von Xenobiotika und zahlreiche physiologische Prozesse, z.B. die Funktion von Immunzellen sowie die Erhaltung und Differenzierung von Stammzellen. In verschiedenen Krankheiten, einschließlich Krebs, werden Fehlregulationen des AhR Signalweges beobachtet. In der Vergangenheit wurde der AhR hauptsächlich mit toxischen Wirkungen in Verbindung gebracht. Die jüngste Zulassung des AhR-Agonisten Tapinarof zur Behandlung der Schuppenflechte und mehrere Studien zu AhR und Krebserkrankungen liefern jedoch Hinweise auf mögliche therapeutische Anwendungen von AhR-Modulatoren. Picoberin könnte somit nicht nur als Werkzeug für die AhR-Forschung dienen, sondern möglicherweise auch einen Ausgangspunkt für die Entwicklung weiterer therapeutischer AhR-Agonisten bilden.

2 INTRODUCTION

In recent years, significant progress has been made in the prevention and treatment of common diseases such as cancer, diabetes and heart diseases. However, there is still an urgent need for extensive research to gain more insights into diseases that affect millions of people worldwide on a molecular level. Detailed exploration of the underlying disease-related biological processes is an enormous challenge, requiring collaboration between different scientific disciplines, in order to include as many facets as possible, to interpret experimental results correctly and in context, and to draw the right conclusions. Chemical biology is a relatively new, highly interdisciplinary field of research that utilizes small molecules as tools to elucidate complex biological systems.[1] In the past, the functions of proteins and genes in cellular systems were mostly analyzed using genetic methods. In analogy to reverse and forward genetics, Chemical biology operates through reverse and forward 'chemical genetics'.[2] The discovery of novel bioactive small molecules, the identification of their molecular targets and the exploration of their mode of action in complex biological systems is at heart of Chemical Biology and medical research.[3]

2.1 Classical genetics vs. chemical genetics

Historically, conventional genetic approaches have been a powerful tool to gain insights into complex biological networks.[2, 4] Typically, the functions and relevance of proteins were studied by mutagenesis or genetic removal of proteins, followed by investigation of the phenotypic consequences for the model organism used, e.g. yeast, nematodes, zebrafish and mice.[5] In general, classical genetics can be divided into two opposing categories: a hypothesis-generating, forward directed approach and a hypothesis-based, reverse genetics approach (see Figure 1).[2, 4, 6] Classical reverse genetics operate through targeted mutagenesis or genetic deletion of a specific protein.[5, 6] In contrast, classical forward genetics aims to identify gene deletions and gene mutations that alter a phenotype of interest through phenotypic screening of randomly mutated model organisms.[5, 7] Classical genetic approaches have been able to shed light on the molecular basis of diverse biological processes, such as cell division in *Saccharomyces cerevisiae* and programmed cell-death in *Caenorhabditis elegans*.[5, 8] However, although genetic techniques are able to alter or delete virtually any protein, the study of complex biological systems through genetic manipulation has some drawbacks and limitations.[9] First, due to alternative splicing, RNA editing of the pre-messenger RNAs, and post-translational modifications, one single gene often codes for more than only one protein. Moreover, proteins usually have more than only one function. Thus, a gene knockout can have multiple unpredictable consequences. In addition, knockout of essential genes often results in increased or complete lethality, making genetics-based analysis of the function of these proteins impossible.

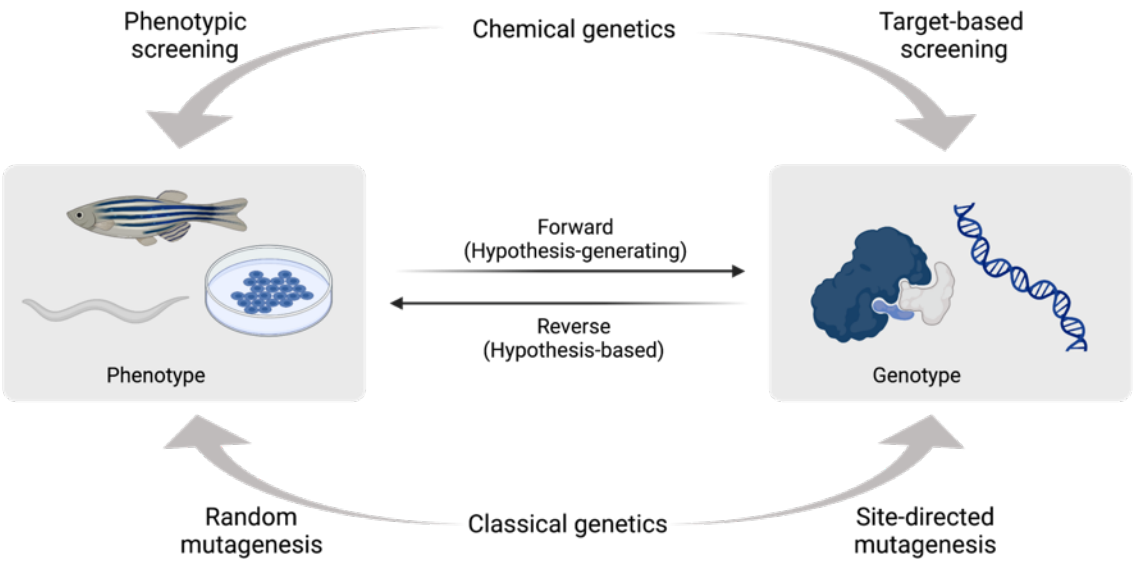

Figure 1: Classical genetics and chemical genetics approaches. Classical genetics uses random or site-directed mutagenesis to study the relationship between genes and phenotype. In contrast, chemical genetics uses small molecules for this purpose. A forward-looking study starts with the phenotype and by identifying the responsible genes or proteins, a hypothesis regarding the function of that gene is generated. Reverse approaches are based on a hypothesis. Proteins or genes are specifically manipulated and the effects on the phenotype are analyzed. Modified representation according to Kawasumi, 2007.[4]

Chemical genetics has evolved over the past 20 years as a complementary approach to classical genetics and in analogy, there is a forward and a reverse directed approach.[2, 4, 6] Instead of genetic interventions, chemical genetics uses small molecules to study complex biological systems.[2, 4, 9] These can be applied at any timepoint in the experiment, allowing temporal control, in contrast to genetic modifications. Small molecules usually act quickly, so that immediate or very early phenotypic effects can be monitored.[4, 9, 10] Most often, they act reversibly and can thus be washed out of the system again.[4, 10] Moreover, small molecules allow for quantitative control.[9, 10] Concentration gradients in many cases lead to the observation of graded phenotypic effects, providing greater confidence in the apparent biological effect of a small molecule.[9, 10] Perturbation of protein functions by small molecules does not mean that the entire protein is removed from the system.[11] Hence, only certain functions of the targeted proteins are altered, while the protein may still be able to accomplish other functions within the cell.[9-11] Chemical substances can be applied to all species and cell types at any developmental stage. Furthermore, they are not limited to only protein targets, but also have the potential to manipulate protein-protein interactions and other biomolecules, such as mRNA or DNA.[9, 10] However, the basic requirement for the study of biological processes using chemical genetics is the availability of selective biologically active chemical

substances.[4, 9] Consequently, the synthesis and identification of bioactive chemical entities that selectively and efficiently modulate a target in a cellular context is one of the biggest challenges in chemical biology.[9] In the last years, the availability of large compound collections has strongly increased via the accessibility of commercial libraries and public repositories.[4] In addition, concepts such as biology-oriented synthesis (BIOS) have led to the enrichment of compound libraries with substances that contain scaffolds that are biologically pre-validated by evolution.[12] In parallel, tremendous technical advances in high-throughput platforms, automated microscopy, and image analysis algorithms have fueled the development of forward chemical genetics.[8] Due to these developments, small molecule screening is no longer limited to industry.

2.1.1 Reverse chemical genetics

Reverse chemical genetics, like reverse genetics, is a hypothesis-based approach that begins with the targeted modulation of a protein of interest.[6, 9] To identify suitable chemical entities for the study of complex biological systems, reverse chemical genetics first requires biochemical or biophysical assays that detect either binding of a ligand to the protein of interest or a change in functionality of the target, and that are suitable for screening.[2] An important prerequisite for such an assay is the availability of the purified target, e.g. a protein of interest, in sufficient quantity and concentration. The hit compounds of such a screening are analyzed for their structure-activity relationship and subsequently optimized by rational design with respect to their selectivity and potency. The obtained optimized small molecules are then introduced into a cellular system to analyze the resulting phenotypic changes.[2, 6] For many diseases, therapeutic targets are already known. In these cases, the reverse chemical genetics approach has already been successfully used to study the functions of proteins in cells. However, simplified biochemical and biophysical assay setups never reflect the immense biological complexity of a cellular system or even whole organism. In a living system, even optimized small molecules may face membrane permeability issues or they may be metabolized and cleared quickly. Furthermore, within a cell, small molecules rarely bind selectively to only one single molecular target. Such polypharmacology can lead to undesired ‘off-target’ effects resulting in a poor translation in a more complex system like animals or humans. Since reverse chemical genetics is always based on a known molecular target, this approach cannot serve to efficiently identify new potential drug targets.

2.1.2 Forward chemical genetics

The hypothesis-generating forward chemical genetics approach starts at the phenotype of interest without any bias towards a specific molecular target.[9] Unlike target-base screenings,

this approach aims to identify and characterize bioactive small molecules that are able to induce a desired phenotype in a complex living system.[2] Detection of substances with the desired properties is achieved via phenotypic screenings, e.g. by measuring the activity of a reporter gene, a fluorescence or a luminescence signal, or detection of characteristic phenotypic changes using automated imaging techniques. Forward chemical genetics is used in academia to study rare diseases, characterize cellular signaling pathways, and provide chemical tools to modulate protein functions.[4] In contrast to reverse chemical genetics, forward chemical genetics offers the possibility of identifying new molecular targets related to the desired phenotype. Since the analysis of the substances is carried out within a complex biological system, critical factors such as off-target effects, toxicity or insufficient membrane permeability of small molecules can be identified at a very early stage. The term 'off-target effects' describes undesirable side effects triggered by the binding of a substance to cellular components. However, with regard to polypharmacology, so called 'off-targets' may even cause effects that could be beneficial in different contexts. In contrast to reverse chemical genetics, a phenotypic screen does not provide information about the molecular target of a bioactive small molecule. Since there is no generally applicable approach for target identification available, target identification and mode-of-action studies remain the main challenge of forward chemical genetics.

2.1.3 Target identification

Identification of the molecular target of bioactive small molecules is a crucial step in chemical genetics. Various methods are available for target identification, but not every technique is suitable for every compound and every molecular target. Therefore, the success of a target identification experiment strongly depends on the selection of the appropriate technology. This chapter is meant to give an overview about frequently used methodologies.

Affinity-based chemical proteomics (ABP) combines classical drug affinity chromatography with subsequent proteome profiling (see 2.2.3).[13] This method first requires the immobilization of the small molecule and an inactive analogue to a solid support, e.g., via a streptavidin-biotin interaction. Afterwards, lysates of cells or tissues are incubated with the immobilized compound, followed by extensive washing to remove unspecifically bound proteins. The remaining proteins bound to the probe are then eluted and analyzed via mass spectrometry. Proteins that are enriched with the active probe, but not with the inactive probe are considered as potential target proteins. The relationship of the identified target protein with the originally observed biological effect needs to be validated in further experiments.[10, 13] The major advantage of this approach is the absence of bias towards a specific protein target. However, this technology also has several limitations: First, ABP is dependent on the availability of a probe that can be immobilized on a solid support. This means that it is necessary to attach a

linker to the active small molecule, without influencing its biological activity.[13] Furthermore, this approach requires a negative probe for comparison of enriched proteins. These requirements assume a detailed understanding of the structure-activity relationship (SAR) of the compound class and especially the attachment of a linker may be highly complicated if not impossible for some compounds or target proteins.[10] Moreover, unspecifically bound proteins may also be identified in addition to the actual target proteins, which can lead to false-positive results.[10] Finally, ABP may not allow for identification of proteins that are insoluble in the buffer used during cell lysis and target enrichment.[13]

Another frequently used approach is the so-called activity-based proteome profiling (ABPP).[13, 14] This technology requires an activity-based probe that covalently labels the active site of enzymes and that is equipped with an affinity tag.[14] The probes are incubated with living cells, lysates, or tissue homogenates to allow binding of their target proteins. Afterwards, probe-labelled enzymes are captured using the affinity tag, e.g. via biotin - streptavidin interaction, and identified by means of mass spectrometry.[13, 14] One major advantage of ABPP is the ability to detect the availability of the active site of enzymes directly rather than being limited to protein or mRNA abundance.[14] However, similar to affinity chromatography-based approaches, also ABPP requires the availability of a probe and thus attachment of a linker to the active molecule.

To circumvent the drawbacks of attachment of a linker to a bioactive small molecule, label-free target identification approaches can be applied. One example for such an approach is thermal proteome profiling (TPP), which couples a cellular thermal shift assay (CETSA) to proteome profiling by mass spectrometry.[15, 16] CETSA is based on the concept, that binding of a small-molecule causes a change of the thermal stability of the target protein.[15] A shift in a protein's melting temperature upon treatment of cell lysates, or living cells with a compound of interest can therefore be considered as a proof of binding and thus, this method is frequently used for target engagement. However, TPP monitors changes of thermal stability of proteins upon compound treatment across the whole proteome and is, thus, an approach for target identification that in unbiased with respect to a specific target protein.[16]

2.1.4 Target validation

Validation of a putative molecular target of a small molecule is required to verify that modulation of this target mediates the effect of the compound observed during the phenotypic screening.[17] Diverse approaches for target validation are available, but the choice of appropriate methods for target validation highly depends on the chemistry, the putative molecular target and the cellular phenotype associated with the small molecule. Target validation includes confirmation of the direct binding of the small molecule to the putative molecular target. However, only validation of binding of a small molecule to a particular protein

does not guarantee that this protein is also the physiologically relevant target that is responsible for the observed phenotype.[17] Thus, diverse aspects must be explored, including binding studies, chemical, functional and genetic validations (Figure 2).

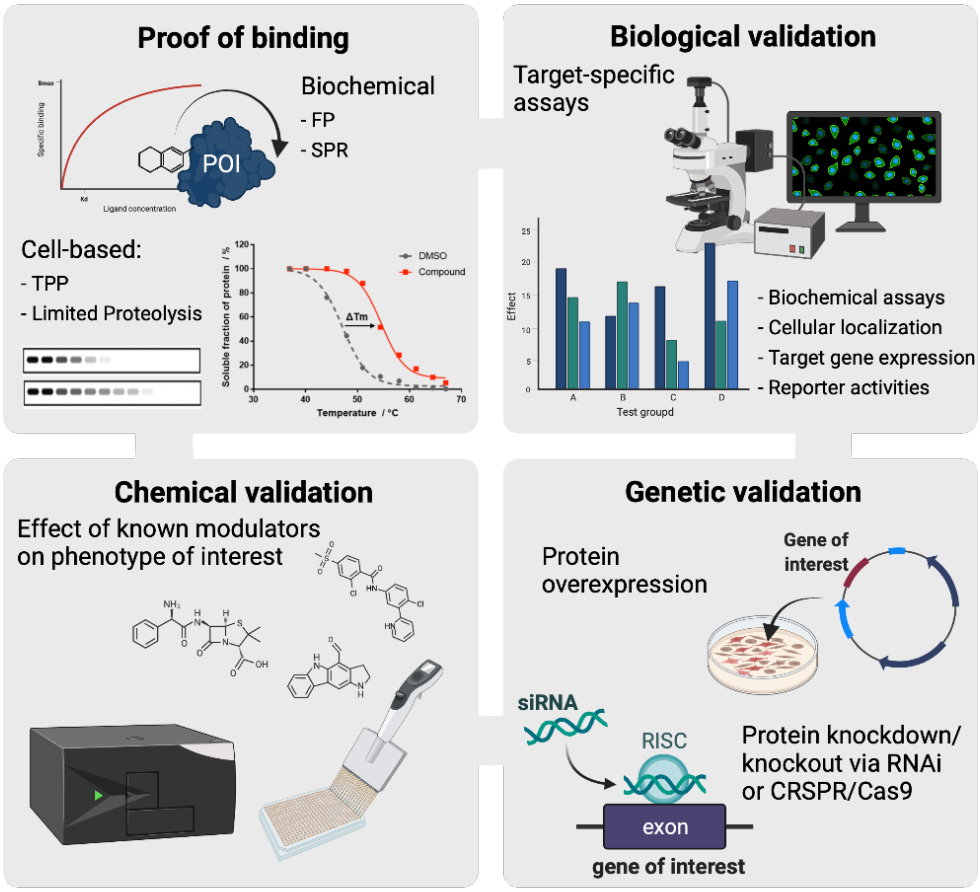

Figure 2: Schematic overview about common validation strategies for target validation. Validation of a hypothetical (protein) target include chemical, functional and genetic validations and proof of binding of the small molecule to the target. Suitability of specific approaches highly depends on the specific compound and target. FP: Fluorescence polarization. SPR: Surface plasmon resonance. TPP: Thermal proteome profiling.

One very important aspect of target validation is the confirmation of a direct physical interaction of the small molecule with the putative target. As already mentioned in chapter 2.1.3, CETSA allows detection of changes in the thermal stability of proteins (in lysate or in cells) in presence of a small molecule and can thus proof binding.[15] However, not every interaction leads to changes of the melting behavior of a protein. For this reason, biophysical methods, such as fluorescence polarization (FP), Surface plasmon resonance (SPR) or isothermal titration calorimetry (ITC) are commonly used to explore binding events.[18, 19] These methods however require sufficient amount of purified protein. Furthermore, FP and SPR require chemical modifications of the small molecule.[18] Biological validations comprise diverse types of biochemical and cellular experiments, that fully depend on the particular protein of interest (POI) and the phenotype that is explored. These experiments aim for validation of the influence of a small molecule on the functions of the POI. Experiments may include immunofluorescence

microscopy e.g. to monitor co-localization of the compound and the putative target protein, or changes in the cellular localization of the POI upon compound treatment. Furthermore, gene expression analysis may be used to explore differential gene expression or alterations in protein levels in presence of the small molecule. Moreover, target protein-specific reporter gene assays, assays that monitor enzymatic activities (biochemical and cell-based) or downstream signaling allow exploring effects of a small molecule and its analogues. If a congruent SAR could be observed in the phenotypic assay, correlation of the SAR in a target specific assay clearly strengthens a target hypothesis.[17] Furthermore, bioluminescence resonance energy transfer (BRET) or application of proteolysis targeting chimera (PROTAC) can be used to show target engagement.[20, 21] The next step in target validation is to verify the physiological relevance of the target to the phenotype of interest. This can be done via chemical and genetic validations.[17, 22] Chemical validation is highly useful to explore, if known small molecule modulators of a putative molecular target induce the same phenotype observed for the research compound in the phenotypic assay.[22] In case of putative inhibitory functions of the research compound, known activators of the POI may potentially rescue this effect and vice versa. However, chemical validations depend on the availability of well characterized and specific small molecule modulators of the POI, which is not given for every protein.[22] Even if specific modulators are available, these could still modulate the protein differently than the research compound, e.g. because of a different binding site or modulation of only one specific function or the localization of the protein. Consequently, chemical validations have the potential to support a target hypothesis. Genetic validation is highly important to explore the effect of target depletion or plasmid-mediated upregulation of the POI on the phenotype of interest. Furthermore, the influence of decreased or increased levels of the POI on the bioactivity of the small molecule may provide strong evidence for a causal link between the putative target and the biological activity of the small molecule.[17, 22] While siRNA-mediated knockdown of the putative target may only show slight and in best case graded effects on the bioactivity of the small molecule, a compound should be completely inactive in cells with a CRISPR-Cas9-mediated knockout of the target protein.[17]

Since no generic roadmap is available, target identification and validation represent the most challenging part of a forward chemical genetics project. However, the diverse assays that can be applied may already give hints towards a mode of action of the compound.

2.2 *'Omics'* approaches for bioactivity profiling

Since the beginning of the human genome project, tremendous advances in time and cost-effective high-throughput screening technologies have enabled scientists to run a vast number of parallel molecular measurements in cells or tissues.[23, 24] In contrast to phenotypic screenings, which are unbiased with regard to a specific molecular target, but still focused on

a single bioactivity of interest, *'omics'* approaches allow for global profiling of DNA (genomics), RNA (transcriptomics), proteins (proteomics) or metabolites (metabolomics) etc.[25] The access to such large profiling data sets has revolutionized biological and pharmaceutical research.[24] They have been able to significantly improve the understanding of complex biological processes and disease-related phenotypes and provide important information that enables personalized medicine, e.g. for the treatment of cancer.[24, 26] Moreover, profiling approaches have strongly advanced drug discovery research.[26]

The central dogma of molecular biology outlines the information flow from genes, which are transcribed into mRNA and subsequently translated into proteins (see Figure 3).[27]

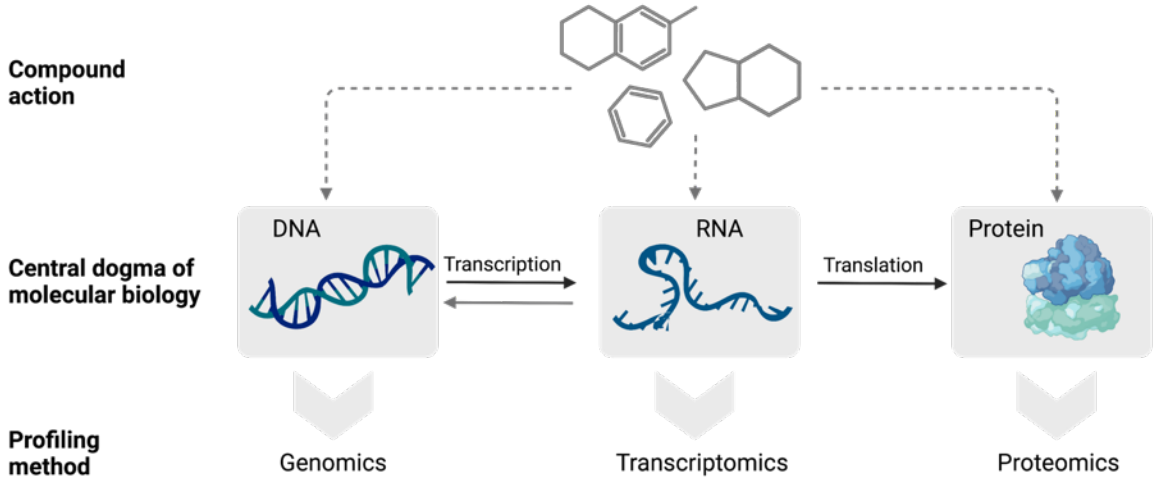

Figure 3: Schematic overview on gene expression profiling approaches along the central dogma of molecular biology for investigation of compound actions in a biological system. The central dogma of molecular biology describes the information flow during gene expression. DNA is transcribed into mRNA, followed by translation to proteins. Each of these steps can be analyzed using genomics, transcriptomics, and proteomics approaches, respectively. The action of small molecules can affect gene expression at any level and can thus be explored by means of 'omics' approaches.

The exposition of a cell or an organism to an external stimulus, such as a small molecule, can influence gene expression at any level.[27] Conclusively, profiling approaches can be utilized to identify their molecular targets, to investigate their mode of action (MoA) and, also potential side effects.[26] However, although these profiling approaches open exciting opportunities for detailed exploration and understanding of biological processes on a molecular level, the sheer amount of data is a major challenge for biologists, computational biologists and bioinformaticians.[24, 25] Recently, major efforts have been made to collect and curate data from various *'omics'* experiments and to make them available in public repositories, such as Gene Expression Omnibus (GEO), The Cancer Genome Atlas (TCGA) or the Omics Discovery Index (OmicsDI).[28-31] Data sharing prevents unnecessary repetitions of investigations that were already carried out by others and, more importantly, allows integration of multiple omics data sets.

2.2.1 Genome profiling

The term ‘genome’ describes the totality of all DNA in a cell, tissue or organism, that can be found in the cell nucleus or in mitochondria.[23, 32] The central requirement for genome profiling is the availability of DNA sequencing technologies, which have undergone tremendous development over the past 50 years. First-generation sequencing technologies include the chain termination method using labelled di-deoxynucleotide triphosphates (ddNTPs) developed by Frederick Sanger and co-workers (1975) or the chemical chain degradation method invented by Maxam and Gilbert during 1976 and 1977.[32-34] Until the end of the 20th century, the Sanger method has clearly dominated the field of DNA sequencing. However, this technology is restricted to mostly relatively small genomes.[32, 34] With the beginning of the 21st century, new massively parallel DNA microarray and next-generation sequencing (NGS) platforms were developed that enabled accurate sequencing of whole genomes and transcriptomes within a very short time.[32, 33] These technologies enabled high-throughput analysis of genotype-to-phenotype relationships and strongly advanced genetically informed drug discovery.[26] However, these second-generation sequencing methods are currently already being augmented by third-generation real-time sequencing (TGS) methods of single molecules.[32]

2.2.2 Transcriptome profiling

The ‘transcriptome’ is defined as the complete set of RNA in a cell or a tissue at a specific developmental stage and physiological condition.[23, 35] This includes messenger RNA (mRNA), ribosomal RNA (rRNA), transfer RNA (tRNA), micro RNA (miRNA), and other non-coding RNA (ncRNA).[23, 36] Each of these RNA molecules plays a central role in the regulation of biological processes and thus in the physiological response of cells to external stimuli, such as small molecules. Thus, investigation of how these biomolecules are regulated is of great importance for a better understanding of small-molecule mode of actions and the entire functional genome.[36]

One method for transcriptome profiling is the application of gene expression microarrays, also referred to as GeneChip or DNA/RNA chip, which were invented in the 1990s.[35] This technique requires the assembly of a large number of known nucleic acid sequences on a solid support. Isolated RNA from a biological sample or complementary DNA (cDNA) is fluorescently labelled and added to the immobilized nucleic acid sequences, followed by extensive washing to remove any RNA or cDNA that did not hybridize with sequences on the solid support. Scanning of the microarray using a laser allows the detection of fluorescent signals of hybridized nucleic acid sequences and, thus, identification of the respective sequences.[35, 37] The microarray technology enables collection of large data set with high accuracy within a short time and allows analysis of different types of RNA, including mRNA and lncRNA.[35]

However, microarray-based technologies are dependent on the availability of already known reference sequences.[35]

Another key method for transcriptome profiling that has developed rapidly over the past decade is the use of NGS-based RNA sequencing (RNA-Seq).[34, 38] In contrast to microarrays, RNA-Seq of cells, tissue or an organism can complement and expand the known set of genes of the respective species and discover new functional genes.[34, 35] Furthermore, RNA-Seq allows quantification of RNA over a broader dynamic range as compared to microarrays and even detection of alternative spicing events is possible.[27, 34, 38] Investigation of the transcriptome using RNA-Seq requires first isolation and purification of RNA, followed by library preparation, clonal amplification and sequencing, e.g. sequencing by synthesis.[24, 39] Afterwards, extensive data processing is required, including data cleaning, filtering, and assembly, followed by a sequence alignment of the obtained gene reads to a reference genome or transcriptome and gene or transcript annotation.[24] If no reference genome is available, *de novo* genome assembly is possible and required.[24, 34] Afterwards, detection of differentially expressed genes, e.g. in disease-state samples compared to control samples or small molecule treated samples compared to vehicle treated samples, allows functional analysis of the dataset obtained.[24] Over the last decade, RNA-Seq has emerged to the most popular transcriptome profiling approach used in research. However, also this approach suffers from several inherent limitations. For example, it fails to identify multiple full-length transcripts reconstructed from the short reads.[34]

In contrast to the above-described approaches, single-molecule long-read sequencing-based transcriptome profiling techniques (third generation sequencing) have the inherent advantage of rendering a full-length transcript sequence without depending on the error-prone, computational step of transcriptome assembly.[34] However, only a small percentage of the genome is represented in the transcriptome as protein-encoding genes. Furthermore, the sum of all mRNA transcripts does not represent the number of proteins present in a cell or an organism, since post-translational modifications also contribute to the phenotype. Moreover, the amount of mRNA present in a cell does not automatically correlate with the amount of the corresponding protein in the cell, as translational control mechanism, such as RNA interference (RNAi) may come into play.[40] Consequently, additional analysis of the proteome will allow a more holistic understanding of biological effects or physiological conditions of interest.

2.2.3 Proteome profiling

The ‘proteome’ is defined as the totality of proteins present in a cell or tissue. The analysis of the global proteome (also called proteome profiling) is very complex because proteins can undergo post-translational changes such as acetylation, phosphorylation and glycosylation. In

addition, proteins have specific configurations and intracellular localizations. Moreover, they may be part of a multi-protein complex or associate with other biomolecules, such as DNA, RNA or lipids.[23] Proteins can be detected by means of mass spectrometry (MS) analysis of cell lysates and recent advances in this technology have strongly improved the detection sensitivity of this method. Preparation of samples for proteome profiling include collection of samples using an appropriate lysis condition and method to extract the proteins from the cells. Afterwards, the proteins are enzymatically digested, followed by fractionation using liquid chromatography (LC) and subsequent MS and identification and quantification of the detected peptides.[24] Proteome profiling can on the one hand be used to identify differentially expressed proteins in a sample of interest compared to a control. This approach allows taking snap shots of a cellular state under a specific condition and at a specific timepoint, which can serve to identify the MoA of a small molecule. On the other hand, so called chemical proteomics approaches, which couple classical drug affinity chromatography to subsequent high-resolution MS, can be used to deconvolute the target proteins of bioactive compounds. In general, chemical proteomics approaches can be divided into two main categories: activity-based protein profiling (ABPP) and compound-centric chemical proteomics.[13] Furthermore, thermal proteome profiling can be used for target identification and MoA analysis of small molecules (see chapter 2.1.3).[16]

2.3 Hedgehog signaling

The Hedgehog (Hh) morphogen was discovered in 1980 by the Nobel laureates Christiane Nusslein-Volhard and Eric F. Weischaus during a genetic screening of the fruit fly *Drosophila melanogaster*.[41, 42] Embryos lacking the Hh alleles developed a lawn of disordered, hair-like bristles, that resembled the spines of a hedgehog, which is why this morphogen earned its name.[42] Hedgehog signaling plays a crucial role in the regulation of organogenesis, during embryonic development, as well as stem cell regeneration and tissue homeostasis.[42, 43] In particular, Hh signaling plays an important role in osteoblast differentiation and post-natal bone-homeostasis, which will be described in more detail in chapter 2.4.1.[44] Unlike *Drosophila*, mammalian cells possess three homologous Hh proteins with different spatial and temporal occurrence: Sonic Hh (SHH), Indian Hh (IHH), and Desert Hh (DHH).[42, 43] A schematic overview of mammalian canonical Hh signaling is shown in Figure 4.

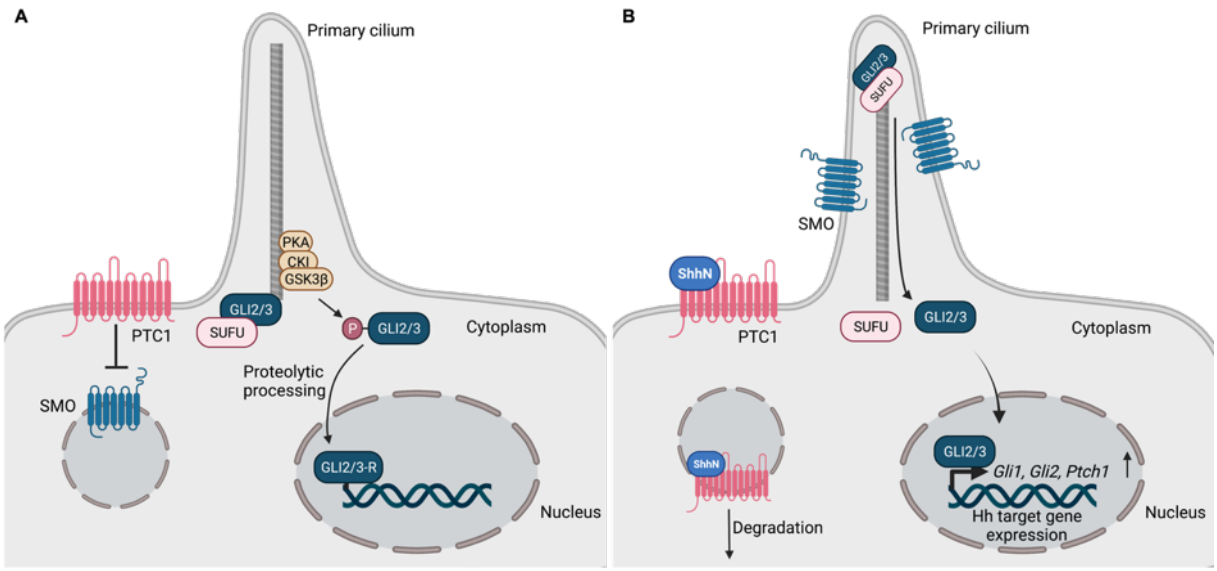

Figure 4: Hedgehog signaling in vertebrates. A: In the inactive state, the transmembrane receptor Patched 1 (PTC1) is localized in the plasma membrane in and around the primary cilium. PTC1 inhibits the transmembrane protein Smoothened (SMO) and prevents its migration into the primary cilium. The transcription factors glioma associated oncogene 2 and 3 (GLI2/3) are phosphorylated by protein kinase A (PKA), casein kinase 1 (CK1) and glycogen synthase kinase 3β (GSK3β) and C-terminally proteolytic cleaved to their transcriptional repressor form (GLI2/3R). **B:** Upon binding of a Sonic Hedgehog (SHH) ligand to PTC1, PTC1 is internalized and undergoes proteasomal degradation. SMO is not inhibited and can migrate to the cilium, thereby causing the dissociation of the Suppressor of Fused (SUFU) and GLI2/3 complex. In addition, phosphorylation of the transcription factors and, thus, their proteolytic cleavage is prevented. Full-length GLI2/3 enter the nucleus and induce expression of Hh target genes. Modified representation according to J. Briscoe, 2013.[42]

In vertebrates, Hh signaling takes place in the primary cilium, a highly specialized, microtubule-based organelle of the cell.[42, 45] In the absence of a Hh ligand, the 12-pass transmembrane receptor Patched1 (PTC1) is located in the plasma membrane and represses the 7-pass transmembrane protein Smoothened (SMO) and, thus, prevents its accumulation in the plasma membrane. In this inactive state, the glioma associated oncogenes 2 and 3 (GLI2/3) are bound by the negative regulator Suppressor of Fused (SUFU), which prevents their translocation to the nucleus and thereby pathway activation. The mechanistic details regarding GLI inhibition by SUFU are only partially understood so far.[43] However, full-length GLI proteins are phosphorylated by protein kinase A (PKA), casein kinase 1 (CK1) and glycogen synthase kinase 3β (GSK3β), followed by a C-terminal proteolytic cleavage resulting in the repressor form GLI2/3-R. The truncated GLI2/3-R moves into the nucleus and represses the transcription of Hh target genes. Binding of a Hh ligand, e.g. SHH, to PTC1 leads to its proteasomal degradation and, thus, to disruption of PTC1-mediated repression of SMO. This causes translocation of SMO into the plasma membrane of the primary cilium and accumulation and subsequent dissociation of the SUFU-GLI2/3 complex at the tip of the primary cilium. Full length GLI2/3 is released and can move into the nucleus, where it induces transcription of Hh

target genes, including *Ptch1* and *Gli1*, resulting in a negative and positive feedback loop, respectively.[42, 43, 45]

2.3.1 Hh signaling in carcinogenesis and cancer progression

While controlled Hh signaling is required for several biological processes throughout embryonic development, tissue homeostasis and regeneration, aberrant Hh signaling is involved in numerous types of cancer, including basal cell carcinoma (the most common kind of skin cancer in western world), medulloblastoma (the most common type of brain tumor in children) and rhabdomyosarcoma (the most frequent soft tissue cancer in children).[44, 46] Additionally, inadequate Hh signaling is involved in cancers of the lung, colon, stomach, pancreas, ovarie and breast, as well as in malignant hematological cancers. Moreover, accumulating evidence suggests a function of Hh signaling in cancer stem cells (CSC) in various tumors.[47]

In principle, dysregulation of any component within the Hh pathway may be involved in tumorigenesis and cancer progression.[44, 48] However, three main mechanisms of aberrant Hh pathway activation in cancer are described in the literature. The first type of Hh-dependent tumors includes basal cell carcinoma and medulloblastoma and is characterized by a ligand-independent activation of Hh signaling. In these cancers, aberrant Hh signaling is caused by activating mutations of SMO or inactivating mutations of PTC1 or SUFU. In these cases, a Hh ligand is no longer required for activation of Hh signaling.[44, 49] The second type of tumors caused by Hh signaling are characterized by overexpression of Hh ligands which either act on the ligand-secreting tumor cell it-self (autocrine) or on a neighboring tumor cell (juxtracrine).[49] This ligand-dependent mechanism is found in several types of cancer, including prostate, digestive tract, ovarian, colorectal, liver, breast, and brain cancer as well as in melanoma.[44, 49] The third type is ligand-dependent paracrine activation of Hh signaling. In these types of cancer, tumor cells secrete Hh ligands, which activate Hh signaling in stromal cells. As a response, these stromal cells start to express and secrete several growth factors and morphogens, which act on the ligand-secreting tumor cells and thereby induce tumor cell growth and proliferation.[44, 49]

Due to the high relevance of Hh signaling in carcinogenesis and cancer progression, therapeutic inhibition of Hh signaling is of high interest for medical research and indeed several Hh pathway inhibitors have shown promising results in clinical trials.[44]

2.3.2 Small-molecule modulators of Hh signaling

Application of small molecule inhibitors of Hh signaling is a therapeutic strategy for treatment of Hh dependent types of cancer, such as locally advanced basal cell carcinoma and acute

myeloid leukemia. However, still only a few Hh pathway inhibitors have been approved for clinical applications and most of them target SMO. Clinical application of SMO inhibitors is limited by mutations in SMO that confer drug resistance in residual cancer cells. These mutations include the SMO-D4738H mutation, which was found in 42.5 % of basal cell carcinoma patients with acquired drug resistance and which blocked binding of SMO antagonists to SMO.[44] Furthermore, mutations of Hh components downstream of SMO (e.g. in PTCH1 or SUFU) mediate SMO-independent activation of Hh signaling and, thus, resistance to SMO antagonists.[50] Consequently, identification of novel types of Hh inhibitors that overcome these resistances is of high interest for medical research. The next chapters provide an overview about some of the most relevant small molecule modulators of Hh signaling.

2.3.2.1 SMO antagonists

Cyclopamine (Figure 5A) was the first Hh pathway antagonist that was identified in corn lily plants (*Veratrum californicum*). Consumption of this plant by sheep led to severe craniofacial defects in lamb embryos.[51, 52] Subsequent studies showed that Cyclopamine inhibits Hh signaling through binding and inhibition of SMO and it inhibited tumor growth and invasion in mouse xenografts. However, it also had severe side effects, including death and, thus, it was never approved for clinical applications.[50, 51]

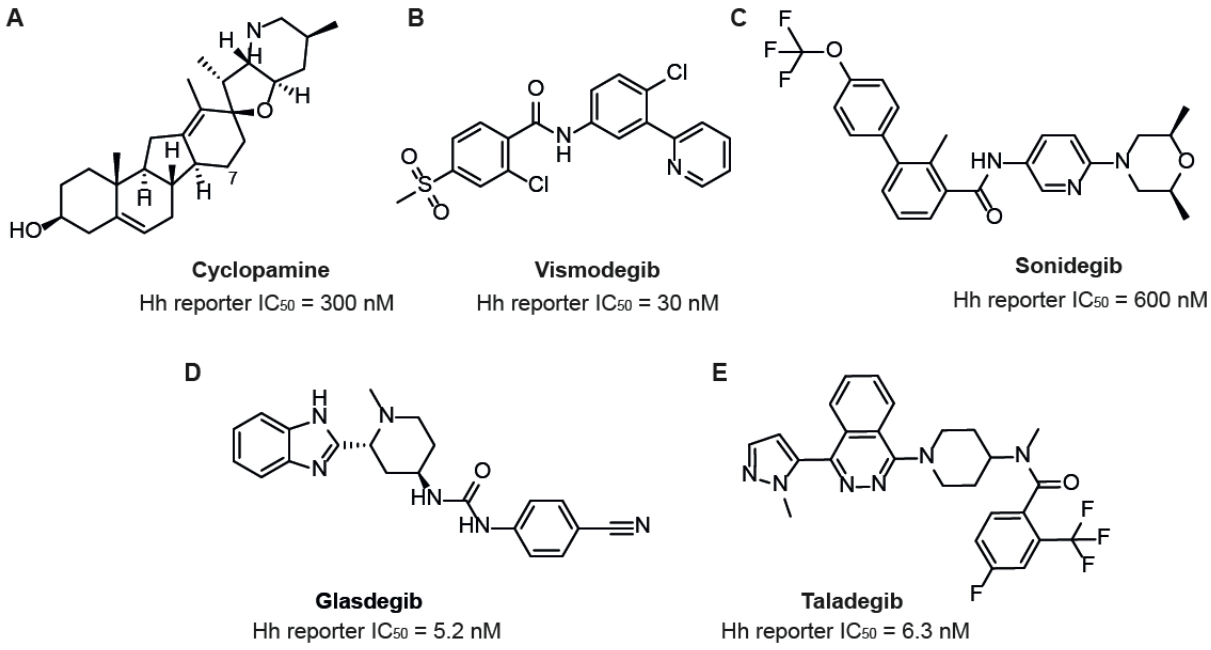

Figure 5: Selected SMO antagonists. A: Cyclopamine (Hh reporter IC_{50} obtained from Chen et al.).[52] **B:** Vismodegib (GDC-0449, Erivedge, Hh reporter IC_{50} was taken from Wu et al.).[53] **C:** Sonigedib (LDE225, Erismodegib or ODOMZO, Hh reporter IC_{50} was taken from Pan et al.).[54] **D:** Glasdegib (PF-04449913 or DAURISMO, Hh reporter IC_{50} was obtained from Norsworthy et al.).[55] **E:** Taladegib (LY2940680, Hh reporter IC_{50} was taken from Ghirga et al.).[56]

The SMO antagonist Vismodegib, also known as GDC-0449 or Erivedge (Figure 5B) was the first Hh inhibitor that was approved in 2012 by the Food and Drug Administration (FDA) for treatment of symptomatic metastatic and locally advanced basal cell carcinoma.[50, 56, 57] Sonidegib, also known as LDE225, Erismodegib or ODOMZO (Figure 5C) is another SMO antagonist that is approved for clinical application by FDA and European Medicines Agency (EMA).[56, 58] It is indicated for treatment of adult patients with locally advanced basal cell carcinoma, who are not candidates for curative surgery or radiation therapy.[50, 58] Glasdegib also referred to as PF-04449913 or DAURISMO (Figure 5D) the first FDA-approved SMO antagonist for treatment of acute myeloid leukemia.[50] Taladegib, also known as LY2940680 (Figure 5E) is currently tested in clinical trials for treatment of chronic myelogenous leukemia and a range of solid tumors.[50, 51] In contrast to other SMO antagonists, this small molecule was reported to inhibit the D473H mutant of Smoothened, which confers clinical resistance to Vismodegib treatment of patients.[50, 56, 59]

2.3.2.2 SMO independent Hh pathway inhibitors

Besides SMO-binding Hh pathway inhibitors, only few Hh inhibitors have been identified that do not target SMO. A selection of SMO independent Hh inhibitors is depicted in Figure 6.

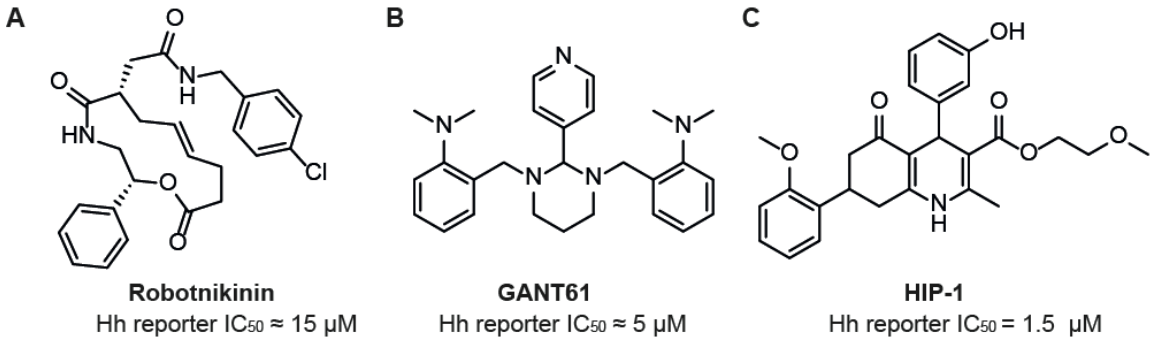

Figure 6: Selected non-SMO binding Hh pathway inhibitors. A: Robotnikinin (Hh reporter IC_{50} was taken from Stanton et al.)[60]. **B:** GANT61 (Hh reporter IC_{50} was taken from Lauth et al.)[61] **C:** HIP-1 (Hh reporter IC_{50} was taken from Hyman et al.).[62]

The macrocyclic small molecule Robotnikinin (Figure 6A) binds to extracellular Sonic Hedgehog protein and thereby prevents binding of SHH to PTC1 and, thus, Hh-ligand induced activation of Hh signaling.[60] In contrast, Gli-ANTagonist 61 (GANT61, Figure 6B) acts downstream of SMO. It causes accumulation of GLI1 in the nucleus, but at the same time it inhibits GLI1 transcriptional activity, most likely by preventing proper binding of GLI1 to DNA, or destabilization of GLI1-DNA complexes.[61] HIP-1 (Figure 6C) does not bind to SMO and it does also not influence ciliogenesis or SMO localization in cilia. Hyman *et al*. state that it acts downstream of SUFU as it inhibits Hh signaling induced by loss off SUFU and GLI overexpression.[62]

2.3.2.3 SMO agonists

Besides the identification of novel Hh pathway inhibitors, also the characterization of selective small-molecule activators of Hh signaling is highly important. Identification of Hh pathway inhibitors requires at first activation of Hh signaling. Thus, Hh activating compounds are needed as tool compounds and facilitate cell-based screening for and characterization of Hh pathway inhibitors and exploration of Hh signaling in general.

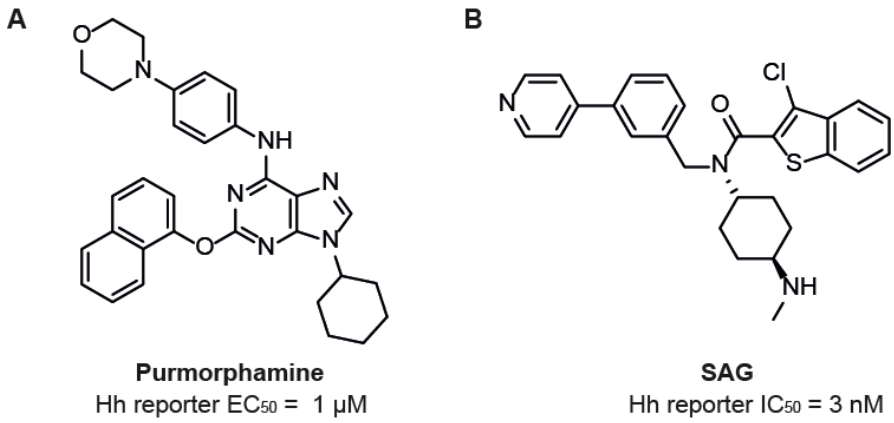

Figure 7: Selected SMO agonists. A: purmorphamine (Hh reporter EC_{50} was taken from Sinha et al.).[63] **B:** SMO agonist (SAG, Hh reporter EC_{50} was taken from Chen et al.)[64].

Purmorphamine (Figure 7A) is a SMO agonist that binds to the heptahelical bundle of SMO to activate Hh signaling and thereby induce osteoblast differentiation of murine mesenchymal stem cells.[63, 65] In this thesis, purmorphamine was mostly used to activate Hh signaling and to induce osteoblast differentiation of C3H10T1/2 cells. SMO AGonist (SAG, Figure 7B) is another Hh pathway activator that binds to the same SMO binding pocket as purmorphamine.[64]

2.4 Osteoblast differentiation

Bone is formed through two different processes: Endochondral ossification, in which at first cartilage is formed that is later replaced by bone cells, and intermembranous ossification, in which mesenchymal stem cells (MSCs) directly differentiate into bone cells, without intermediate cartilage state.[66] Osteoblasts are the key bone-building cells that derive from mesenchymal stem cells.[67-69] Differentiation of MSCs into osteoblasts is a tightly regulated and highly complex process that is only partially understood.[68, 70] This is at least in part due to the lack of reliable model systems and the use of diverse cell lines with different characteristics and differentiation status, which makes it hard to draw a clear roadmap of osteoblast differentiation.[68] The basic steps of osteoblast differentiation according to the current knowledge are depicted in Figure 8.

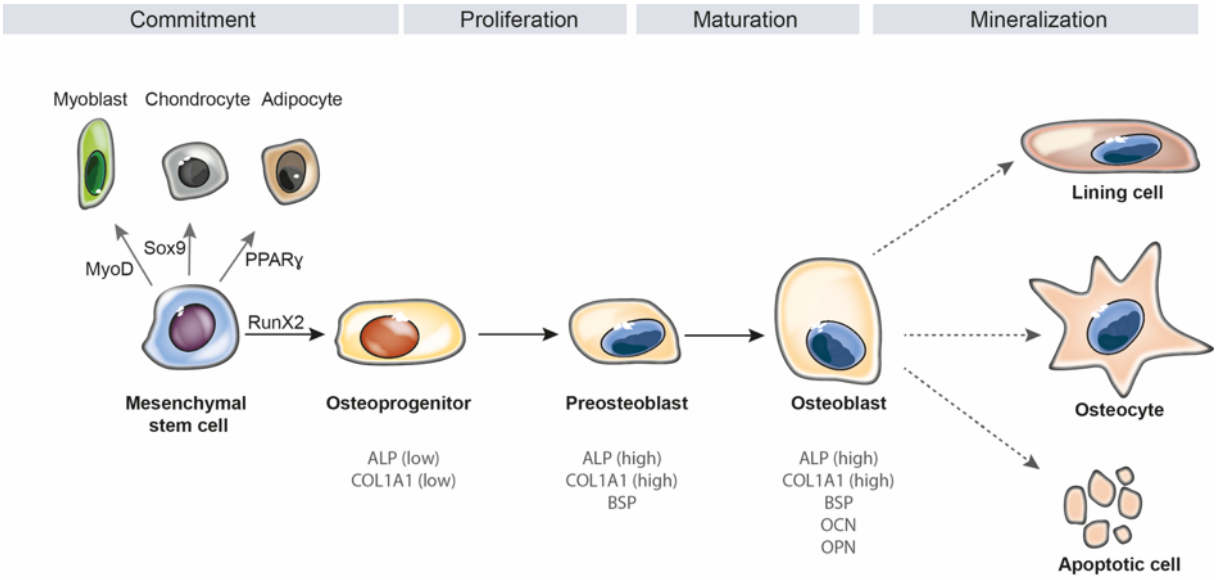

Figure 8: Osteoblast differentiation. Multipotent mesenchymal stem cells (MSCs) differentiate into different cell types, depending on the master regulator that is expressed and activated. Myogenic differentiation protein 1 (MyoD) is the master regulator of myogenic differentiation, sex determining region Y-box 9 (SOX-9) is the key regulator of chondroblast differentiation, peroxisome proliferator-activated receptor gamma (PPARγ) regulates adipogenesis and Runt-related transcription factor 2 (RUNX2) is the master regulator of osteoblast differentiation. Upon lineage commitment, osteoprogenitors undergo three differentiation stages: cell proliferation, extracellular matrix maturation and matrix mineralization. At each state, cells express specific marker genes, such as Alkaline Phosphatase (ALP), Collagen type 1 (COL1A1), Bone Sialoprotein (BSP), Osteocalcin (OCN) and Osteopontin (OPN). Osteoblasts finally mineralize into osteocytes, bone lining cells, or they undergo apoptosis. Modified figure, adopted from L. Arboleya and S. Castañeda et. al.[69, 71]

MSCs are multipotent and able to differentiate into myoblasts, adipocytes, chondroblasts or osteoblasts, depending on specific molecular factors, so-called ‘master regulators’ that are present and activated in their micro-environment.[67, 69, 71] Differentiation of MSCs into osteoblasts is initiated by the master regulator runt-related transcription factor 2 (RUNX2) and, later on, the transcriptional regulator osterix (OSX) is essential for regulation of osteogenic gene expression.[71, 72] Upon commitment of mesenchymal stem cells to the osteoblastic lineage, osteoprogenitor cells undergo three developmental stages: cell proliferation, extracellular matrix maturation and matrix mineralization.[69, 72] In the stage of cell proliferation, osteoprogenitors undergo active proliferation and alkaline phosphatase (ALP) and collagen type 1 alpha 1 chain (COL1A1) expression levels start to be up-regulated. During matrix maturation, cell proliferation is downregulated, high levels of ALP are expressed and COL1A1, the major constituent of the extracellular matrix, is secreted. In the third stage, matrix mineralization proceeds through expression of bone sialoprotein (BSP), osteocalcin (OCN), osteopontin (OPN) and continued expression of high levels of ALP and COL1A1.[69] Finally, mature osteoblasts are progressively incorporated into the bone matrix as terminally differentiated osteocytes, transform into bone-lining cells or undergo apoptosis.[69, 71] Osteoblast differentiation is regulated by multiple signaling pathways, including Wnt signaling,

BMP signaling, TGFβ signaling and Hh signaling.[72] Since this thesis focusses on Hh signaling-induced osteogenesis, the next chapter will provide an overview of the role of this pathway in osteogenesis.

2.4.1 Hedgehog signaling in osteoblast differentiation

Besides other pathways, Hh signaling is critical for bone development and repair, and mis-regulation of Hh signaling is observed in several bone-related diseases, including osteoarthritis, osteoporosis and bone fracture.[45, 73] Of the three Hh ligands, IHH and SHH are involved in osteoblast development.[72] However, the ability of mesenchymal cells to undergo osteogenesis upon activation of Hh signaling seems to be dependent on the differentiation status of the cells. While the multipotent mesenchymal stem cell line C3H10T1/2 responds to SHH and also purmorphamine mediated activation of Hh signaling, the more committed osteoprogenitor cell line MC3T3-E1 does not.[65, 72] Furthermore, SHH upregulates the osteogenic markers ALP, RUNX2 and OCN and at the same time downregulates the adipogenesis marker Peroxisome proliferator-activated receptor γ (PPARγ). Therefore, it is assumed that SHH is especially important for early stages of differentiation, e.g., the commitment of pluripotent mesenchymal stem cells into the osteoblast lineage on the expenses of adipocyte differentiation.[72] Furthermore, there is evidence for crosstalk between Hh and Wnt signaling during osteoblast differentiation, however this crosstalk is highly complex. Several studies have shown that inhibition of Wnt signaling reduces Hh-induced ALP expression in C3H10T1/2 cells.[74, 75] Conversely, inhibition of Hh signaling does not lead to a reduction in Wnt-induced ALP expression. Consequently, Hh signaling acts upstream of Wnt signaling during osteoblast differentiation.[74] In conjunction with bone morphogenic protein 2 (BMP-2), Hh signaling synergistically induces expression of ALP, especially in murine mesenchymal stem cells.[72]

2.4.2 Other pathways involved in osteoblast differentiation

In this thesis, Hh signaling is used to induce osteoblast differentiation. However, besides Hh signaling, various other signaling pathways are involved in this highly complex process. In recent years it became clear, that there is extensive crosstalk between different signaling pathways and during osteogenesis and tight temporal regulation and sequential activation of different pathways is essential.[70, 76] This chapter provides a brief overview of the major signaling pathways involved in this differentiation process (Figure 9).[76]

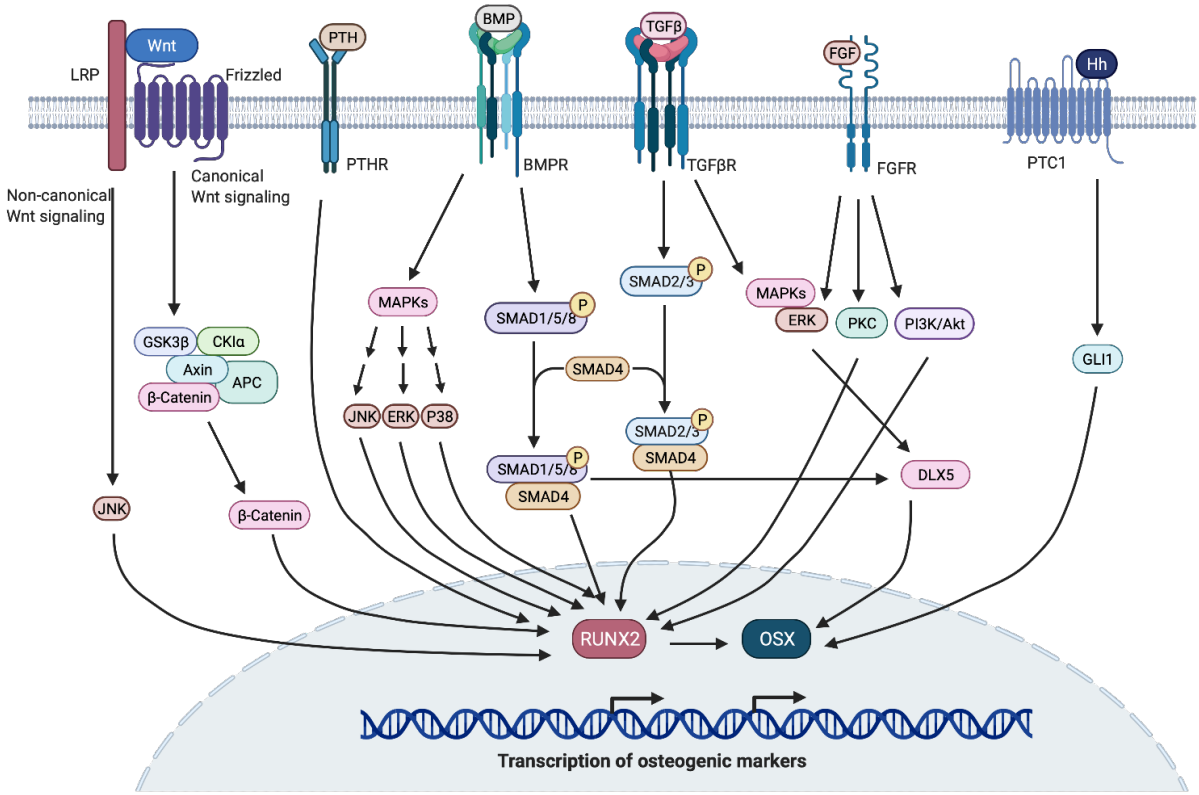

Figure 9: Key signaling pathways involved in osteoblast differentiation. Figure was adopted and modified from D. S. Amarasekara *et al.*[76] LRP: Low-Density Lipoprotein Receptor-Related Protein. PTH: Parathyroid hormone. PTHR: PTH receptor. TGFβ: Transforming growth factor β. TGFβR: TGFβ receptor. FGF: fibroblast growth factor. FGFR: FGF receptor. Hh, Hedgehog. PTC1: Patched 1. RUNX2: Runt-related transcription factor 2. OSX: Osterix. JNK: c-jun N-terminal kinase. PKC: Protein kinase C. APC: Adenomatosis polyposis coli. CK1α: casein kinase 1α. GSK3β: glycogen synthase kinase 3β. PKA: protein kinase A. DLX5: distal-less homeobox 5. MAPK: mitogen-activated protein kinase. ERK: extracellular receptor kinase. PLC: phospholipase. AKT: protein kinase B. GLI1: glioma-associated oncogene 1.

As already mentioned in chapter 2.4.1, Wnt signaling plays a critical role during osteoblast differentiation. The first evidence for this role became apparent from human studies that revealed a causal link between mutations in the Wnt co-receptor Low-Density Lipoprotein Receptor-Related Protein 5 (LRP5) and alterations in human bone mass.[70, 77] In agreement with this, activation of canonical Wnt signaling and upregulation of β-catenin induce expression of early osteogenesis markers, such as *Alpl* and *Runx2*, *in vitro*. On the other hand, the non-canonical Wnt-ligand Wnt5a interferes with BMP-2 signaling and suppresses the expression of osteogenic markers, e.g. ALP, BSP and Osterix.[77, 78] Consequently, during research of signaling in bone biology it is highly important to consider, that both, canonical and non-canonical Wnt signaling may be regulated differently and independently of each other at different stages of differentiation.[77]

Several members of the transforming growth factor β (TGFβ) superfamily, such as bone morphogenic proteins (BMPs) have potent regulatory functions for both, chondroblast and osteoblast differentiation.[70, 76] BMPs are highly conserved signaling molecules that were

initially identified due to their ability to induce endochondral ossification. Several BMPs are expressed in skeletal tissue (e.g. BMP-1 and BMP-7) and in osteoblast cell cultures (including BMP-2, -4, and -6). However, while some BMPs, such as BMP-2, BMP-6, BMP-7 and BMP-9, promote osteoblast differentiation, BMP-3 suppresses bone formation.[70] Upon receptor activation, BMPs act through Mothers against decapentaplegic (Smad)-dependent and Smad-independent signaling.[76] Smads are major signaling molecules of serine/threonine kinase receptors that can be activated by TGFβ and/or BMPs and they can have both, positive and negative regulatory functions on target genes controlling the osteogenic program.[70] Inhibition of BMP signaling impairs RUNX2 expression and function via a Smad-dependent mechanism, including transcriptional regulation of homeobox gene Dlx5, an upstream target of BMP-2.[76] However, BMP-2 induces expression of the osteogenic marker and transcriptional regulator Osterix (OSX) in murine osteoprogenitor cells, via a mechanism independent of RUNX2.[79] Smad-independent regulation of BMPs include activation of extracellular receptor kinase (ERK), c-jun N-terminal kinase (JNK) and P38 in osteoblastic cells and there is evidence, that these MAP kinases have distinct functions in the regulation of alkaline phosphatase and osteocalcin expression.[76]

Other pathways involved in osteoblast differentiation include Notch signaling, Ephrin signaling, parathyroid hormone receptor (PTHR) signaling, fibroblast growth factor (FGF) signaling and diverse other factors and proteins including G-protein coupled receptors (GPCRs) and nuclear receptors (NRs).[70, 72, 80, 81]

3 AIM OF THIS THESIS

Hh signaling is essential during embryogenesis and has complex regulatory functions in bone formation. Furthermore, it is involved in tumorigenesis and progression of different types of cancer, including basal cell carcinoma and medulloblastoma.[42] In the last decade, Hh antagonists targeting the key signaling protein SMO have been successfully applied for treatment of Hh-dependent types of cancer.[56, 58] However, low target diversity, the emergence of acquired drug resistance upon drug treatment and identification of cancers with SMO-independent dysregulation of Hh signaling have led to a large scientific interest in the discovery of novel Hh pathway inhibitors. Especially identification of small molecules that could overcome resistance mutations by targeting other proteins involved in Hh signaling is in high demand. Besides offering potentially new approaches for therapeutic treatment of Hh dependent cancers, such small molecules could be used as tool compounds and might confer new insights into so far unknown aspects of Hh signaling.

The aim of this thesis was the identification and characterization of small molecule modulators of Hh-induced osteoblast differentiation and thereby potentially identification of novel chemotypes that are able to inhibit Hh signaling. A phenotypic Hh-dependent osteoblast differentiation assay monitoring the expression of the early osteogenesis marker alkaline phosphatase upon activation of Hh signaling and thereby induction of osteogenesis was used to identify potential “hit” candidates. Potent hit compounds should be characterized with regard to their ability to inhibit the Hh pathway using orthogonal assays, followed by exploration of their ability to target the key protein SMO. For interesting compound classes, the underlying structure activity relationship (SAR) should be explored in detail, to identify suitable sites for chemical modifications. Afterwards the molecular targets should be identified, and mode of action studies should be carried out to gain new insights into both, the Hh signaling network and Hh-induced osteoblast differentiation.

4 MATERIAL AND METHODS

4.1 Material

4.1.1 Chemicals and reagents

Compounds, that are mentioned in this thesis, but not in this chapter were synthesized by the chemists Dr. Saad Shaaban, Dr. Zhijun Jia or Dr. Gang Shan, Dr. Georg Niggemeyer and Dr. Jie Liu at the Max Planck Institute of Molecular Physiology in Dortmund, in the department of Chemical Biology. The Furo[2,3]pyridines were kindly provided by the group of Dr. Kamil Paruch at Masaryk University in Czech Republic. Quinoline compounds were provided by the group of Dr. Marta Gutiérrez Rodríguez from the Institute of Medical Chemistry at CSIC in Madrid.

Chemical / Reagent	Catlog No.	Supplier
2-(4-(2- hydroxyethyl)-1-piperazine ethane sulfonic acid (HEPES)	#1009.0250	GERBU Biotechnik
4',6-Diamidino-2-phenylindol (DAPI)	#D9542	Sigma-Aldrich
6-Formylindolo[3,2-*b*]carbazole (FICZ)	#SML1489-1MG	Sigma-Aldrich
Acetonitrile, HPLC grade	#A/0400PB15	Fisher Chemical
Acrylamide (30 %)	#A1672	AppliChem
Alizarin Red S	#sc-205998A	ChemCruz
Ammonium persulfate (APS)	#13375	Serva
Ampicillin	#10416.0050	GERBU Biotechnik
Aqua-Poly/Mount	#18606-20	Polysciences
Blasticidin	# SBR00022	Sigma-Aldrich
BMP-4	#314-BP-010	R&D Systems
Bodipy-Cyclopamine	#FBI18988	Carbosynth Limited
Bovine serum albumin (BSA)	#11945.03	Serva
Bromphenol blue	#A512.1	Carl Roth
CDP-Star	#11685637001	Roche Diagnostics
Cell dissociation buffer enzyme-free, PBS based	#13151-014	Gibco
cOmplete™, EDTA-free protease inhibitor cocktail	#11873580001	Sigma-Aldrich
Cosmic calf serum (Hyclone™)	#SH30087	GE Healthcare
DharmaFECT 1	#T-2001-02	Dharmacon™
Dimethyl sulfoxide (DMSO)	#41639	Sigma-Aldrich
Dithioerythritol (DTE)	#1007.0025	GERBU Biotechnik
Dithiothreitol (DTT)	#1008.0005	GERBU Biotechnik
DNA loading dye (6x)	#R0611	Thermo Fisher
Dulbecco's modified eagle medium (DMEM)	#P04-03550	PAN™-Biotech
Ethanol (EtOH), absolute	#UN1170	Fisher Chemical
Ethylene diamine tetra acetic acid (EDTA)	#1034	GERBU Biotechnik
Fetal bovine serum (FBS)	#10270-106	Gibco
Formaldehyde (37 %)	#A3592	AppliChem

Chemical / Reagent	Catlog No.	Supplier
FuGENE® HD	#E2311	Promega
GeneRuler 1kb, DNA Ladder	#SM0313	Thermo Fisher
GeneRuler Ultra Low Range DNA Ladder	#SM1213	Thermo Fisher
Geneticin (G418) disulfate salt solution	#G8168	Sigma-Aldrich
Glycerol	#783.1	Carl Roth
Glycin	#3790.2	Roth
Hydrochloric acid (HCl)	#A0658	AppliChem
Iodacetamide	#A1666.0025	AppliChem
2-propanol	#6067	J.T. Baker
Kanamycin	#1091	GERBU Biotechnik
L-ascrobic acid, cell culture grade	#8960-5G	Sigma-Aldrich
Levamisole hydrochloride	#ab141217	Abcam
Lipofectamine® 2000	#11668019	Thermo Fisher
Lipofectamine® LTX	#15338100	Thermo Fisher
Magnesium chloride hexahydrate	#A3618	AppliChem
MEM non-essential amino acids (NEAA) (100x)	#P08-32100	PAN™-Biotech
Methanol	#32213-2.5L	Honeywell
NP-40 Alternative	#492016	Merck
Odyssey blocking buffer (PBS)	#927-40000	Li-COR Biosciences
PBS tablets	#AK-102P-L	Jena Bioscience
PhosSTOP phosphatase inhibitors	#04906837001	Sigma-Aldrich
Phusion flash high-fidelity PCR master mix	#F-548	Thermo Fisher
Ponceau S solution (0.2 %)	#3342.7	Serva
Potassium chloride (KCl)	#0509	J.T. Baker
purmorphamine	#10009634	Cayman Chemical
Puromycin	#15490717	Thermo Fisher
Red Safe™ DNA stain	#21141	iNtRON
RNaseZAP™	#R2020	Sigma-Aldrich
RT-PCR grade water	#AM9935	Invitrogen™
Smoothened agonist (SAG1.3)	#566660	Calbiochem
Sodium azide	#11476272	MP Biomedicals
Sodium chloride	#27810.295	VWR
Sodium dodecyl sulfate (SDS) pellets	#CN30.2	Carl Roth
Sodium hydroxide (NaOH)	#7036	J.T. Baker
Sodium pyruvate	#P04-43100	PAN™-Biotech
SsoAdvancedTMUniversal SYBR® Green Supermix	#1725274	Bio-Rad
Tapinarof	#S9700	Selleckchem
TCDD	#ED-5607	Camebridge Isotope Laboratories, Inc.
TCEP HCl	#20491	Thermo Fisher
Tetramethylethylenediamine (TEMED)	#2367.3	Carl Roth
TGFβ-I	#78067	STEMCELL Technologies
TMT10PLEX labelling reagent	#15285743	Thermo Fisher

Chemical / Reagent	Catlog No.	Supplier
Triethylammonium bicarbonate (TEAB)	#T7408	Sigma-Aldrich
Trifluoroacetic acid (TFA)	#106232	Sigma-Aldrich
TRIS	#4855.2	Roth
Triton® X-100	#39795.02	SERVA
Trypan Blue	#T10282	Invitrogen™
Trypsin rec., proteomics-grade	#03708969001	Roche Diagnostics
Trypsin/EDTA solution	#P10-023100	PAN™-Biotech
Tween 20	#BB337-100	Fisher Bioreagents
UltraPure™ Agarose	#16500	Thermo Fisher
Vismodegib	#S1082	Selleckchem
YH439	#HY-100242	MedChemExpress
Zeocin	#ant-zn-1	Invivogen
β-glycerophosphate (BGP) disodium salt	#G9422	Sigma-Aldrich
2-mercaptoethanol	# 28625.01	Serva

4.1.2 Buffers and solutions

Buffer / Solution	Components	Method
50x TAE buffer	242 g/l TRIS (pH 8.0), 10 % 0.5 M Na_2EDTA, 57.1 mL/L acetic acid	Agarose gel electrophoresis
Alizarin Red staining solution	2 % Alizarin Red S in mH2O, pH 4.1 adjusted with NH_4OH (10 %)	Mineralization assay
Alkylation solution	375 mM iodoacetamide, 200 mM TEAB, in mH_2O	Proteome profiling
Blocking buffer A	0.3 % BSA in PBS	Immunofluorescence
Blocking buffer B	1 % FBS in PBS	Immunofluorescence
Blotting buffer (1X)	25 mM TRIS, 190 mM glycine, 5 % methanol in mH_2O	Wet blotting
CETSA lysis buffer 1	50 mM TRIS (pH 8.0), 150 mM NaCl, 1 % NP-40 in mH_2O	CETSA
CETSA lysis buffer 2	0.4 % NP-40 in PBS, protease and phosphatase inhibitor cocktail	TPP
Fixation buffer	3.7 % formaldehyde in PBS	Fixation of cells
Osteogenesis Lysis buffer	12.1 g/L TRIS (pH 9.5), 14.6 g/L NaCl, 5,325 g/L $MgCl_2$, 1 % Triton X-100, sterile filtered, 1 % CDP-Star	osteoblast differentiation assays
PBS-T	PBS supplemented with 0.1 % Tween20	General washing buffer
PBS-Tx	PBS supplemented with 0.1 % Triton X-100	General washing buffer
Permeabilization buffer	0.3 % Triton X-100 in PBS	Immunofluorescence

Buffer / Solution	Components	Method
Phosphate buffered saline (PBS)	1 PBS tablet dissolved in 500 mL mH_2O	General washing buffer
Reduction solution	200 mM TCEP, 200 mM TEAB in mH_2O	Proteome profiling
SDS running buffer	250 mM TRIS, 2M glycine and 5 % MeOH in mH2O	SDS-PAGE
SDS sample buffer (5X)	0.5 M TRIS, 8 % SDS, 40 % glycerol, 0.4 M DTE, 0.02 % bromophenol blue in mH2O	SDS-PAGE
SDS separation gel	8-10 % acrylamide, 0.1 % SDS, 1.5 M TRIS-HCl (pH 8.8), 0.1 % APS, 0.004% TEMED in mH2O	SDS-PAGE
SDS stacking gel	5 % acrylamide, 1 M TRIS-HCl, pH 6.8, 0.1 % SDS, 0.1 % APS, 0.01% TEMED in mH2O	SDS-PAGE
Stabilization buffer	10 mM glycin, 0.2 % sodium azide in PBS	SMO binding assays
TEAB buffer	100 mM TEAB in mH2O	Proteome profiling
TRIS-HCl buffer	50 – 1000 mM TRIS-HCl (pH 6.8 – 8.1) in mH2O	General buffer, several applications
Trypsin solution	2.2 mL 100 mM TEAB, 165 µl 0.4 µg/µL Trypsin rec., proteomics-grade in 100 mM HCl	Proteome Profiling
Whole cell lysis buffer	50 mM TRIS (pH 8.0), 150 mM NaCl, 0.5 % sodium deoxycholate, 1 % NP-40 in mH_2O	Western blot

4.1.3 Cell lines

All cell lines were cultivated in an MCO-230AICUV-PE incubator, in a humidified atmosphere and at 37°C and 5 % CO2.

Cell line	Description	Culture conditions	Source
C2C12	Mouse myoblast cells	C2C12 growth medium	ATCC®CCL-1772
C3H10T1/2	Mouse embryonic stem cells	C3H10T1/2 growth medium	ATCC®CCL-226™
HaCaT XRE:fluc_ PGK:rluc	Human keratinocytes virally infected with a construct for XRE-dependent firefly luciferase and a construct for constitutively expressed *Renilla* luciferase	HEK293T growth medium	Alves group (Oxford)

Cell line	Description	Culture conditions	Source
C2C12	Mouse myoblast cells	C2C12 growth medium	ATCC®CCL-1772
HEK293T	Human embryonic kidney cells	HEK293T growth medium	ATCC, CRL1268
HepG2	Human hepatoblastoma cells	HepG2 growth medium	DZMS, ACC-180
L	Murine fibroblast cells	L-cell growth medium	ATCC, CRL-2648
L-Wnt-3A	Murine fibroblast cells stably transfected with Wnt-3A	L-cell growth medium	ATCC, CRL-2647
NIH-3T3	Murine embryonic fibroblasts	NIH-3T3 growth medium	DZMS, ACC-59
NIH-3T3-XRE:fluc_pbas:rluc	Murine embryonic fibroblasts virally transfected with XRE dependent firefly luciferase and constitutively expressed *Renilla* luciferase	NIH-3T3 growth medium	
Shh-LIGHT2	Murine embryonic fibroblasts, stabile infected with a plasmid encoding for GLI-dependent firefly luciferase and pSVNeo (G418 resistance), and a plasmid enconding for pRLTK (constitutive *Renilla* luciferase expression vector) and pVgRXR (Zeocin resistance)	Shh-LIGHT2 growth medium	Taipale *et al.* [64]

4.1.4 Bacterial strains

Bacterial Strain	Description	Catalog No.	Supplier
OmniMAX™ 2 T1R	Chemically competent *Escherichia Coli*	#C854003	Thermo Fisher

4.1.5 Media and supplements

Media / Supplement	Components	Supplier
C2C12 growth medium	DMEM (#P04-03550) supplemented with 6% heat-inactivated FBS, GlutaMAX, and penicillin−streptomycin	PAN™-Biotech
C3H10T1/2 growth medium	DMEM (#P04-03550) supplemented with 10 % FCS and 1 mM sodium pyruvate	PAN™-Biotech
HEK293T assay medium	DMEM (#P04-03550) supplemented with 0.5 % FBS	PAN™-Biotech

Media / Supplement	Components	Supplier
HEK293T growth medium	DMEM (#P04-03550) supplemented with 10 % FBS, 1 mM sodium pyruvate and 1 mM MEM NEAA	PAN^{TM}-Biotech
HepG2 growth medium	DMEM (#P04-03550) supplemented with 10 % FBS, 1 mM sodium pyruvate and 1 mM MEM NEAA	PAN^{TM}-Biotech
L-cell growth medium	DMEM (#P04-03550) supplemented with 10 % FBS, 1 mM sodium pyruvate and 1 mM MEM NEAA	PAN^{TM}-Biotech
Lysogeny broth (LB) medium	10 g/L bacterial tryptone, 5 g/L yeast extract, 10 g/L NaCl in mH_2O	Central Biotechnology Facility, Dortmund
NIH-3T3 assay medium	DMEM (#P04-03550) supplemented with 0.5 % FCS and 1 mM sodium pyruvate	PAN^{TM}-Biotech
NIH-3T3 growth medium	DMEM (#P04-03550) supplemented with 10 % FCS and 1 mM sodium pyruvate	PAN^{TM}-Biotech
Serum free medium	Opti-MEM (#31985-062)	Gibco
Shh-LIGHT II assay medium	DMEM (#P04-03550) supplemented with 0.5 % FCS, 1 mM sodium pyruvate and 5 mM HEPES	PAN^{TM}-Biotech
Shh-LIGHT II growth medium	DMEM (#P04-03550) supplemented with 10 % FCS and 1 mM sodium pyruvate	PAN^{TM}-Biotech

4.1.6 Primary antibodies

Antigen	Host, Clonality	Condition	Catalog No.	Supplier
Acetylated Tubulin (ac-Tubulin)	Mouse, monoclonal	1:1000 in cilia blocking and permeabilization buffer	T6793	Sigma-Aldrich
AhR	Mouse, monoclonal	1:500 in Li-COR blocking buffer	sc-133088	Santa Cruz
FLAG	Mouse, monoclonal	1:1000 in Li-COR blocking buffer	F3165	Sigma-Aldrich
Lamin A	Mouse, monoclonal	1:1000 in Li-COR blocking buffer,	sc-71481	Santa Cruz
SMO	Mouse, monoclonal	1:200 in cilia blocking and permeabilization buffer	Sc-166685	Santa Cruz
β-Actin	Rabbit, polyclonal	1:5000 in Li-COR blocking buffer	ab8227	Abcam
β-Tubulin	Mouse, monoclonal	1:5000 in Li-COR blocking buffer	T5076	Sigma-Aldrich

4.1.7 Secondary antibodies

Antigen	Conjugate	Host, Clonality	Condition	Catalog No.	Supplier
mouse	800CW dye	donkey	1:5000 in Li-COR blocking buffer (PBS)	926-32210	Li-COR Biosciences
mouse	Alexa488	donkey	1:5000 in the same buffer as for the used primary antibody,	A-21202	Thermo Fisher
rabbit	800CW dye	donkey	1:5000 in Li-COR blocking buffer (PBS)	926-32213	Li-COR Biosciences
rabbit	Alexa549	goat	1:500 in the same buffer as for the used primary antibody	A11012	Thermo Fisher

4.1.8 Plasmids

Plasmid	Description	Catalog No.	Supplier
pcDNA3.1	Empty vector, Ampcillin (Amp) resistance	#V79020	Thermo Fisher
M50 Super 8x TOPFlash	TCF/LEF binding sites upstream of a luciferase reporter, Amp resistance	#12456	Addgene
pcDNA3.1-mAhR-FLAG	Murine AhR, MYC-DDK tagged ORF Clone, NM_013464, Kanamycin resistance	#OMu19221	GeneScript
pcDNA3.1 ShhN	Murine SHH, Amp resistance	#37680	Addgene
pGen-mSMO	Murine SMO cDNA, Kanamycin resistance	#37673	Addgene
pGL4.54[luc2/TK]	XRE-dependent firefly luciferase, Amp resistance	#9PIE412	Promega
pRL-TK-Rluc	Rluc control vector, Amp resistance	#E2241	Promega
pBV-SBE4-Luc	TGF-β dependent firefly luciferase	#16495	Addgene
SMO-BFP	Ntag-BFP, Kanamycin resistance	Generated by Lea Kremer at MPI Dortmund	Kremer *et al.*[82]
pcDNA3.1-Wnt-3A	pcDNA-Wnt-3A, Amp resistance	#35908	Addgene

4.1.9 Primers

Primer	Forward (fw) Sequence Reverse (rv) Sequence	RefSeq
mouse *AhR*	fw: 5‘-CTGGTTGTCACAGCAGATGCCT-3‘	NM_013464
	rv: 5‘-CGGTCTTCTGTATGGATGAGCTC-3‘	
mouse *Alpl*	fw: 5‘-ATCTTTGGTCTGGCTCCCATG-3‘	NM_007431.3
	rv: 5‘-TTTCCCGTTCACCGTCCAC-3‘	
mouse *Ap3d1*	fw: 5‘-CAGAGGGCTCATCGGTACAC-3‘	NM_007460
	rv: 5‘-GCCGGAAGTCCAACTTCTCA-3‘	
mouse *Cyp1b1*	fw: 5´-GGATGTGCCTGCCACTATTA -3´	NM_009994.2
	rv: 5´- TGAACATCCGGGTATCTGGT -3´	
mouse *Gapdh*	fw: 5‘-CAGTGCCAGCCTCGTC-3‘	NM_008084.3
	rv: 5‘-CAATCTCCACTTTGCCACTG-3‘	
mouse *Gli-1*	fw: 5’-CACCGTGGGAGTAAACAGGCCTTCC-3‘	NM_010296.2
	rv: 5‘-CCAGAGCGTTACACACCTGCCCTTC-3‘	
mouse *Ptch1*	fw: 5’-CTCTGGAGCAGATTTCCAAGG-3‘	NM_008957.3
	rv: 5‘-TGCCGCAGTTCTTTTGAATG-3‘	
mouse *Ptch2*	fw: 5‘-GGCACTCACATCCGTCAACAAC-3‘	NM_008958.3
	rv: 5‘-GAAGACGAGCATTACCGCTGCA-3‘	
mouse *Smo*	fw: 5’-GAGGCTACTTCCTCATCAGAGG-3’	NM_176996.4
	rv: 5’-GCTGAAGGTGATGAGCACAAAGC-3’	

4.1.10 siRNAs

All siRNAs were purchased from Horizon Discovery Biosciences Limited.

Name	Sequence	Catalog No.
Control siRNA	UGGUUUACAUGUCGACUAA	D-001810-01-05
murine AhR – 1	GUGCAGAGUUGAGGUGUUU	J-044066-06-0005
murine AhR – 2	UCAGAGCUCUUUCCGGAUA	J-044066-07-0005
murine AhR – 3	CAAGGGAGGUUAAAGUAUC	J-044066-08-0005
murine AhR – 4	CGACAUAACGGACGAAAUC	J-044066-05-0005

4.1.11 Commerical kits

Kit	Catalog No.	Supplier
DC™ Protein Assay Kit II	#000112	BioRad
Dual-Luciferase® Reporter Assay System	#E1960	Promega
EndoFree Plasmid Maxi Kit	#12163	Qiagen
MycoAlertTM Mycoplasma Detection Kit	#LT07-318	Lonza
P450-Glo™ CYP1A1 Assay System	#V8751	Promega
QuantiFast SYBRgreen Kit	#204054	Qiagen
QuantiTect® Reverse Transcription Kit	#205313	Qiagen
Qubit™ RNA BR Assay Kit	#Q10210	Thermo Fisher
Qubit™ RNA HS Assay Kit	#Q32852	Thermo Fisher
Qubit™ RNA IQ Assay Kit	#Q33221	Thermo Fisher
Rnase-Free Dnase Set	#79256	Qiagen
Rneasy Mini Kit®	#74106	Qiagen
Ultra™ II Directional RNA Library Prep Kit	#E7760	New England Biolabs

4.1.12 Laboratory devices

Device	Name	Supplier
Agarose gel chamber	SUB-CELL® GT	BioRad
Automated cell counter	Countless™ II	Thermo Fisher
Centrifuges	5415 R	Eppendorf AG
	5424 R	Eppendorf AG
	5702	Eppendorf AG
	5810 R	Eppendorf AG
	Concentrator plus	Eppendorf AG
	MiniSpin	Eppendorf AG
	Optima™ MAX-XP Ultracentrifuge	Beckman Coulter
Clean benches	DNA/RNA UV-Cleaner Box	LTF Labortechnik
	MSC Adventage 1.2	Thermo Fisher
	NU437-600E	NuAire
Flow Cytometer	FACS LSRII Flow Cytometry System	Becton Dickinson
Fluorometer	Qubit 4.0	Thermo Fisher
Holder for SDS gels	Mini-PROTEAN® Tetra Electrode Assembly	Bio-Rad
Holder for wet protein transfer	2-Gel Tetra and Blotting Module	Bio-Rad

Device	Name	Supplier
Imaging systems	ChemiDoc™ MP Imaging System	BioRad
Incubator	INE400	Memmert
	MCO-230AICUV-PE, CO_2 Incubator	phcbi
Life cell microscope	IncuCyte ZOOM	Sartorius AG
Light microscope	Primo Vert	Zeiss
Liquid handling station	Biomek i7	Beckman Coulter
Mass spectrometer	Q Exactive! HF Plus Hybrid Quadropole-Orbitrap	Thermo Fisher
Multi-channel pipettes (10 µL and 300 µL)	Research® Plus	Eppendorf AG
Oil objective (63x)	Plan-Apochromat 63x/1.40 Oil DIC M27 objective	Zeiss
PCR cycler	Mastercycler epgradientS	Eppendorf AG
	C1000 Touch™ Thermal Cycler, CFX96™ Real-Time System	Bio-Rad
pH meter	Bench top pH meter FiveEasy Plus™ (FEP20)	Mettler Toledo
Pipette controllers	Accu-Jet® Pro	BRAND
Plate reader	TecanSpark®	Tecan trading AG
	Paradigm Reader	Molecular Devices
Pipetting robot	Echo Liquid Handler	Labcyte
Power supply	PowerPac™ Basic Power Supply	Bio-Rad
Scale	Analytical Plus	Ohaus
Sequencer	Illumina HiSeq 3000	Illumina
Shaker	KS 130 basic	IKA®
	Rotator SB3	Stuart®
Single-channel pipettes (10, 20, 100, 200 and 1000 µL)	Research® Plus	Eppendorf AG
SpeedVac	Concentrator 5301	Eppendorf AG
Spectrophotometer	NanoDrop™2000c	Thermo Fisher
Thermomixer	Thermomixer comfort	Eppendorf AG
Ultrasound bath	Sonorex Super	Bandelin
Vacuum pump	Integra Vacusip (#159010)	Integra Biosciences
Vortexer	Vortex Genie 1	Scientific Industries
Water bath	Typ 1004	GFL GmbH
Widefield fluorescence microscope	Observer Z1 (AxioCam HRc, AxioCam MRm)	Zeiss

4.1.13 Consumables

Consumable	Catalog No.	Supplier
12-well plate, standard F	#83.3921	Sarstedt
24-well plate, standard F	#83.3922	Sarstedt
50 ml SuperClear® Centrifuge Tubes with Plug Style Caps	#525-0304	VWR
6-well plate, standard F	#83.3920	Sarstedt
96-well hard-Shell® PCR plates, low profile, thin wall, skirted, white/clear	#HSP9601	BioRad
96-well plate, clear wall, clear and flat bottom	#353075	Corning
96-well plate, conical wells, C	#82.1583001	Sarstedt
96-well plate, standard F	#83.3924	Sarstedt
96-well plate, white wall, clear and flat bottom	#655098	Greiner Bio-one
Breathe-Easy foil	#BEM-1	Diversified Biotech
Countless™ cell counting chamber slides	#C10283	Thermo Fisher
Cryo vials	#72.379.992	Sarstedt
Falcon tube, 15 mL	#62.554.502	Sarstedt
Falcon tube, 50 mL	#62.547.254	Sarstedt
Falcon 5mL round bottom polystyrene test tube, with cell strainer snap cap for flow cytometry	#352235	Corning
Filtropur S 0.2 µm	#83.1826.001	Sarstedt
Glass coverslips (Ø 12 mm)	#12-545-80	Thermo Fisher
Immobilon-FL PVDF membrane	#IPFL00010	Merc
KIMTECH® Science precision tissues	#AA63.2	Carl Roth
Microscope slides	#02 1102	Diagonal
Microseal® 'B' PCR plate sealing film, adhesive	#MSB1001	BioRad
Omnifix® Luer Lock Solo	#4617509F	Braun
PARAFILM® M	#PM-996	Parafilm
Pipette tip stacks 10 µL		Sarstedt
Pipette tip stacks 200 µL	#70.3030.100	Sarstedt
Poly-D-Lysine coated coverslips	#GG-12-1.5-PDL	Neuvitro Corporation
PCR tubes	#16960	Sorenson
Protein LoBind Tube, 0.5 mL	#0030108094	Eppendorf AG
Protein LoBind Tube, 1.5 mL	#0030108116	Eppendorf AG
Protein LoBind Tube, 2.0 mL	#0030108132	Eppendorf AG
QIAshredder	#79656	Qiagen
Qubit™ assay tubes	#Q32856	Thermo Fisher
SafeSeal tubes, 0.5 mL	#72.704	Sarstedt
SafeSeal tubes, 1.5 mL	#72.706	Sarstedt
SafeSeal tubes, 2.0 mL	#72.695.500	Sarstedt
SafeSeal-Tips® premium, 10 µL	#693010X	Biozym
SafeSeal-Tips® premium, 100 µL	#692066X	Biozym
SafeSeal-Tips® premium, 1000 µL	#692078X	Biozym
SafeSeal-Tips® premium, 200 µL	#692069X	Biozym

Consumable	Catalog No.	Supplier
Serological pipette, 1 mL	#86.1251.001	Sarstedt
Serological pipette, 10 mL	#86.1254.001	Sarstedt
Serological pipette, 25 mL	#86.1685.001	Sarstedt
Serological pipette, 5 mL	#86.1253.001	Sarstedt
Serological pipette, 50 mL	#86.1256.001	Sarstedt
TC Flask T25 Stand.,Vent. Cap	#83.3910.002	Sarstedt
TC Flask T715 Stand.,Vent. Cap	#83.3912.002	Sarstedt
TC Flask T75 Stand.,Vent. Cap	#83.3911.002	Sarstedt
Ultracentrifuge tubes (thick wall, polycarbonate, 8 x 34 mm vials)	#343776	Beckman Coulter
Whatman® gel blotting paper, Grade GB005	#WHA10426994	Sigma-Aldrich
µltraAmp PCR tubes, 0.2 mL	#16950	Sorenson™

4.1.14 Software

Description	Name	Supplier
Chemical analysis software	ChemDraw	PerkinElmer, Inc., USA
Data analysis software	Excel	Microsoft, USA
Data analysis software	Prism 7.0	GraphPad software, USA
Description	Name	Supplier
FACS analysis software	FlowJo	TreeStar Inc.
Gel/Blot analysis software	ImageLab	Bio-Rad Laboratories, Inc., USA
Image analysis software	Fiji	Open source
Image analysis software	ZEN	Carl Zeiss AG, Germany
Live-cell imaging software	IncuCyte ZOOM	Sartorius AG, Germany
Live-cell imaging software	IncuCyte S3	Sartorius AG, Germany
NGS data analysis	CLC Workbench 12	Qiagen
Pathway analysis	IPA	Qiagen
Proteome profiling data analysis	MaxQuant[83]	Free download
Proteome profiling data analysis	Perseus[84]	Free download
qPCR analysis	CFX Maestro	BioRad
Tool for Figures	Illustrator	Adobe
Tool for scientific images	BioRender	Bio RENDER
Tool for volcano plots	VolcaNose R[85]	Free download

4.2 Methods

4.2.1 Cell culture methods

All work with living cells was performed under sterile conditions, using appropriate sterile equipment and a clean bench. Unless stated differently, standard disposable cell culture materials were used.

4.2.1.1 Cultivation of cells

I Thawing of cryopreserved cells

To thaw cryopreserved cells, frozen cells were removed from the liquid nitrogen tank and thawed in a water bath at 37°C. The cell suspension was transferred into a 50 mL falcon tube containing 5 mL of the cell type specific growth medium and was centrifuged for 5 min and 300 rpm, to pellet the cells. Afterwards the supernatant was removed, and the cell pellet was suspended in fresh growth medium. In case of NIH-3T3 or Shh-LIGHT2 cells, the pellet was suspended in 6 mL growth medium and filled in a T25 cell culture flask. HEK293-T cells, HepG2 cells, Wnt-3A cells and L-cells were suspended in 13 mL growth medium and filled into a T75 cell culture flask. Cells were cultured at 37°C and 5 % CO_2 until they reached a confluence of 80 % and were only used after one more passage. C3H10T1/2 cells were suspended in a volume of 4 mL growth medium after centrifugation. These cells were directly counted (see 4.2.1.1-II) and seeded as required for the respective experiment.

II Cell passaging and seeding

All cell lines were cultured in a humidified atmosphere at 37°C and 5 % CO_2. Cells were sub-cultured at 80 % confluence. For this, the culture medium was removed and the cell monolayer was washed with PBS. Afterwards, cells were treated with a minimal volume of Trypsin/EDTA (e.g. 2 mL for a T75-flask) for 2 – 5 min and at 37°C. Detached cells were suspended in 5-9 mL of the appropriate growth medium. For sub-cultivation, an appropriate volume of the cell suspension was added to a new flask, in a total volume of 6 mL (T25), 13 mL (T75) or 26 ml (T175). For seeding of cells for an experiment, the cell suspension was collected in a 50 mL falcon tube. Cells were counted with the automated cell counter Countness II, using trypan blue staining for identification of dead cells. The desired number of cells was diluted in the required volume of the appropriate growth medium and the cell suspension was filled into cell culture dishes.

III Cryopreservation of mammalian cells

For long-term storage, cells were cryo-conserved and kept in the gas phase of a liquid nitrogen tank. For cryopreservation cells were harvested as described in 4.2.1.1-II. The cell suspension

was supplemented with 10 % DMSO (Shh-LIGHT2, NIH-3T3, Wnt-3A, L- and HepG2 cells) or 5 % DMSO (HEK293-T cells), aliquoted into cryo vials and transferred to a CoolCell® Freezing container. Afterwards the cells were kept at -80°C for 24 h, to slowly cool them down (1°C/min) and were then transferred to the liquid nitrogen tank.

IV Tests for mycoplasma contaminations

Cells were analysed for mycoplasma contaminations before cryo-conservation and regularly during culturing. For this, the commercially available MycoAlert™ Mycoplasma detection kit was applied, according to the manufacturer's instructions.

4.2.1.2 Analysis of cell growth and viability

To explore the influence of small molecules on C3H10T1/2 cell growth and viability, cell confluence was monitored over time using the live-cell imaging system IncuCyte® ZOOM (Sartorius). Briefly, 2000 C3H10T1/2 cells were seeded per well in 96-well plates (Corning) and incubated at 37°C and 5 % CO_2 overnight. For compound treatments, 4 mM, 2 mM and 1 mM pre-dilutions of the compounds in DMSO were prepared. These pre-dilutions were then 40-fold diluted in growth medium. For this purpose, 39 µL growth medium were mixed with 1 µL of the compounds. Next, the medium was removed from the cells and was replaced by 90 µl fresh growth medium. Subsequently, 10 µl of the compound dilutions in medium were added to the respective wells, to final concentrations of 10 µM, 5 µM or 2.5 µM. Control samples were only treated with DMSO following the same dilution steps described above. The final DMSO concentration was 0.25 % in all wells. Cells were placed into the live cell imaging system IncuCyte® ZOOM and brightfield microscopy images were taken every two hours for in total 72 h. To determine the cell confluence, the area covered with cells was quantified using the live-cell imaging software IncuCyte® ZOOM. For each condition three technical and three biological replicates were analyzed.

4.2.1.3 Transfection of cells

I Transfection of plasmid DNA

All transfections were performed using the lipid-based transfection technology according to the manufacturer's instructions of the respective transfection reagent. First, plasmid DNA was diluted in Opti-MEM. Depending on the manufacturer's instructions, the transfection reagent was either added directly to the same tube or was pre-diluted in Opti-MEM, in a separate tube and the DNA solution was transferred to the liposomes after 5 min of incubation. Afterwards, transfection mixtures were incubated for 15-30 min at room temperature, prior to dropwise addition to the cells. The transfection conditions used for the experiments are summarized in Table 1.

Table 1: Conditions used for plasmid transfections.

Cells	Plasmid	Nucleic acid concentration	Transfection reagent	Ration DNA (µg): reagent (µL)	Incubation time (h)
C3H10T1/2	pcDNA3.1-mAhR-FLAG	0.5 µg/mL	Lipofectamine LTX & Plus	1:6:1	24-72
HEK293T	pGen-mSMO	1 µg/mL	Fugene HD	1:3	48
HEK293T	mSMO-BFP	1 µg/mL	Fugene HD	1:3	48
HEK293T	pcDNA3.1-Shh-N	1 µg/mL	Fugene HD	1:1.5	120
HEK293T	pcDNA3.1	1 µg/mL	Fugene HD	1:1.5	120
HEK293T	pRL-TK-Rluc	0.06 µg/mL	Lipofectamine 2000	1:3	24
HEK293T	pcDNA3.1-Wnt-3A	0.6 µg/mL	Lipofectamine 2000	1:3	24
HEK293T	M50 Super 8x TOPFlash	0.6 µg/mL	Lipofectamine 2000	1:3	24
HEK293T	pGL4.54[luc2/TK]	1.1 µg/mL	Fugene HD	1:5	24
HEK293T	SBE4-Luciferase	0.8 µg/mL	Lipofectamine 2000	1:3	24
HEK293T	pcDNA3.1-mAhR-FLAG	1 µg/mL	Fugene HD	1:3	48

II Transfection of siRNA

For genetic knockdown experiments, C3H10T1/2 cells were reversely transfected with siRNA targeting the gene of interest. Briefly, siRNAs (see 4.1.10) were diluted in a ratio of 1:20 in Opti-MEM. The transfection reagent DharmaFECT1 was diluted 1:50 in a separate low-binding tube. After 5 min of incubation at room temperature, the siRNA solution was added to the lipid solution in a ratio of 1:1 and incubated for 20 min at room temperature, to allow complex formation. Meanwhile, $6x10^5$ C3H10T1/2 cells were diluted in 4 mL of the corresponding growth medium. After completion of the complex formation, the lipid:siRNA solution was dropwise added in a ratio of 1:5 to the diluted C3H10T1/2 cells, which were then transferred to a T25 cell culture flask. Cells were incubated for 24 h at 37°C and 5 % CO_2 prior to re-seeding for subsequent osteoblast differentiation assays (see 4.2.1.5) or gene expression analysis (see 4.2.1.13).

4.2.1.4 Production of conditioned media

SHH-N- and Wnt-3A-conditioned media were used to activated Hh signaling and Wnt signaling, respectively, without application of any compound.

I SHH-conditioned medium

To obtain SHH-N-conditioned medium, 2×10^6 HEK293-T cells were seeded into T75 cell culture flasks and incubated overnight at 37°C and 5 % CO_2. Cells were transfected with a pcDNA3.1-Shh-N plasmid for SHH expression or a pcDNA3.1 plasmid, as a control, as described in 4.2.1.3. After 24 h, transfection medium was replaced by 13 mL fresh HEK293-T assay medium. After another 24 h of incubation, the conditioned medium was collected in a 50 mL falcon tube and cells were supplemented again with 13 mL fresh HEK293-T assay medium and incubated for another 24 h at 37°C and 5 % CO_2. Afterwards, the second part of conditioned medium was harvested and combined with the medium from the previous day. To remove any cells and debris, the conditioned medium was centrifuged at 1000 x g for 15 min and passed through a 0.2 µm syringe filter. Afterwards, the conditioned medium was diluted 1:3 with fresh assay medium and stored at 4°C until further usage. If the medium was used for induction of C3H10T1/2 cells, it was supplemented with 10 % FCS.

II Wnt-3A-conditioned medium

To obtain Wnt-3A-conditioned medium, 2.5×10^5 L-cells stably transfected with a Wnt-3A plasmid or untransfected L-cells, as a control, were seeded in 25 mL growth medium into a T175 cell culture flask. After incubation for four days, the medium was collected in a 50 mL falcon tube and cells were supplemented with 25 mL fresh growth medium. The harvested medium was centrifuged for 15 min at 1000 x g and passed through a 0.2 µm syringe filter to remove any residual cells and debris. After another three days of incubation at 37°C and 5 % CO_2, conditioned medium was harvested for a second time as described above. Both parts of the conditioned medium were combined and stored at 4°C until further usage.[86]

4.2.1.5 Osteoblast differentiation assay

The Hh-dependent osteoblast differentiation assay was used to evaluate the effect of small molecules on Hh-induced osteoblast differentiation of murine mesenchymal stem cells.[65, 87] For this purpose, 6000 C3H10T1/2 cells were seeded in a volume of 80 µL per well into a white 96-well cell culture plate with clear bottom and incubated for 6 h at 37°C and 5 % CO_2 to allow cell attachment. Afterwards, the small molecules were added to the cells. For this purpose, a dilution series of the compounds in DMSO was prepared. The DMSO-dilutions of the compounds were diluted in medium (dilution factor: 33.33) and mixed by pipetting several times up and down. Subsequently, 10 µL of the compound dilutions were transferred to each well of the cell plate. After 10 min of pre-incubation with the small molecules, 1.5 µM purmorphamine was added to the cells. Therefore, 1 mM purmorphamine was diluted to a concentration of 15 µM in medium. Finally, 10 µL of the pre-diluted purmorphamine was added to each well of the cell culture plate. The final volume on the cell culture plate was 100 µL per

well and the final DMSO concentration was 0.45 %. After 96 h of incubation at 37°C and 5 % CO_2, cells were lysed using the osteoblast differentiation lysis buffer and the ALP protein level was accessed using the chemiluminescent ALP substrate CDP-Star. The luminescence signals were read using the Tecan Sparks plate reader. The signal of cells treated with purmorphamine-DMSO was set to 100 % and all other values were related to this value. To determine IC_{50} values, non-linear regression was performed using a four-parameter fit (GraphPad Prism 7, GraphPad software, USA). For each condition, three technical and three biological replicates were analyzed.

For BMP-4-dependent osteoblast differentiation assays were $2x10^3$ C2C12 cells per well were seeded in 384-well plates and incubated for 16 h at 37°C and 5 % CO_2. Compounds or DMSO were added in triplicates with the Echo Liquid Handler (Labcyte). Afterwards, 7.5 ng/µL BMP-4 and/or 1 µM purmorphamine were added to the wells to a final volume of 50 µL/well. After 72 h, cells were treated with CDP-Star and ALP activities were detected using the Paradigm Reader. For analysis, ALP-activity of cells treated with BMP-4 or BMP-4 and purmorphamine was set to 100 % and all other values were related to this. For each condition, three technical and three biological replicates were analyzed.

4.2.1.6 ALP activity assay

As a counter assay of the Hh-dependent osteoblast differentiation assay, an alkaline phosphatase activity assay was employed to exclude potential effects of hit compounds on the ALP enzymatic activity. For this purpose, 6000 C3H10T1/2 cells were seeded in a volume of 90 µL per well into a white 96-well cell culture plate with clear bottom and incubated for 6 h at 37°C and 5 % CO_2 to allow cell attachment. Afterwards, cells were treated with 1.5 µM purmorphamine to induce ALP expression, as described in 4.2.1.5. After 96 h of incubation at 37°C and 5 % CO_2, cells were lysed using the osteoblast differentiation lysis buffer containing the ALP substrate CDP-Star and different concentrations of the small molecules for 1 h at room temperature. The commercially available ALP inhibitor Levamisole was used as a control for inhibition of the ALP enzymatic activity. The luminescence signals were detected and analysed as described in 4.2.1.5 . For each condition three technical and three biological replicates were analyzed.

4.2.1.7 GLI2/3-dependent reporter gene assay

The GLI2/3-dependent reporter gene assay was used as an orthogonal approach to the Hh-dependent osteoblast differentiation assay to characterize hit compounds regarding their direct effect on canonical Hh signalling. For this purpose, NIH-3T3 cells stably transfected with a GLI2/3-responsive firefly luciferase reporter and a constitutively expressed *Renilla* luciferase

reporter (Shh-LIGHT2 cells)[64] were used. For this experiment, 2.5×10^4 cells per well were seeded into a 96-well cell culture plate and grown at 37°C and 5 % CO_2. After overnight incubation the growth medium was replaced by 80 µL of fresh NIH-3T3 assay medium and the compounds were added as described in 4.2.1.5. A final purmorphamine concentration of 2 µM was used in this assay. After 48 h incubation at 37°C and 5 % CO_2, cells were lysed using 50 µL of a passive lysis buffer per well and incubated while shaking at 650 rpm and room temperature. After 20 min, the luciferase activities were detected using the Dual-Glo® Luciferase Assay Kit and the Tecan Sparks plate reader, according to the manufacturer's instructions. The firefly luciferase signals were normalized to the corresponding *Renilla* luciferase signals. Values for cell that were treated with DMSO-purmorphamine were set to 100 %. To obtain IC_{50} values, non-linear regression was performed using a four-parameter fit (GraphPad Prism 7, GraphPad software, USA). For each condition three technical and three biological replicates were analyzed.

4.2.1.8 TCF/LEF-dependent reporter gene assay

The TCF/LEF-dependent reporter gene assay was used to characterize small molecules regarding their effect on canonical Wnt signalling. For this purpose, HEK293-T cells were transfected with plasmids encoding for Wnt-3A, a TCF/LEF-dependent SuperTop-Flash luciferase (pSTF) and a constitutively expressed *Renilla* luciferase as described in 4.2.1.3 and incubated for 6 h at 37°C and 5 % CO_2. Afterwards, transfected cells were collected in a 50 mL falcon tube and counted as described in 4.2.1.1. Next, 2.5×10^4 cells per well were seeded into a transparent 96-well cell culture plate in a volume of 90 µL. After 1 h of incubation at 37°C and 5 % CO_2, cells were treated with the compounds. For this purpose, a dilution series of the compounds in DMSO was prepared. Afterwards the DMSO-dilutions of the compounds were diluted in HEK293-T growth medium (dilution factor: 33.33) and mixed by pipetting several times up and down. Subsequently, 10 µL of the compound dilutions were added to each well of the cell plate. The final DMSO concentration in all wells was 0.3 %. After 24 h of incubation at 37°C and 5 % CO_2, cells were lysed, and the luciferase signals were detected and analysed as described in 4.2.1.7. For each condition three technical and three biological replicates were analyzed.

4.2.1.9 SMAD-4 binding element (SBE-4) -dependent reporter gene assay

The SBE-4-dependent reporter gene assay was employed to investigate the effect of small molecules on TGFβ signaling. For this purpose, 3×10^6 HEK293-T cells were seeded into a T25 cell culture flask and were bulk transfected with plasmids encoding for a SBE-4-dependent firefly luciferase and a constitutively expressed *Renilla* luciferase, as described in 4.2.1.3. After

incubation for 12 h at 37°C and 5 % CO_2, cells were collected in a 50 mL falcon tube and 2×10^4 cells per well were seeded into a transparent 96-well cell culture plate. The cells were allowed to attach for 1 h and were then treated with the compounds or DMSO as solvent control. For this purpose, DMSO-dilution series of the compounds were prepared. These were subsequently diluted in culture medium (dilution factor: 33.33). Afterwards, 10 µL of the compound dilutions were transferred to each well of the cell plate, in triplicate. To induce TGFβ signalling, the cells were additionally treated with 20 ng/mL TGFβ-I, or DMSO as a control. The final DMSO concentration was 0.3 % in all wells. After 24 h of incubation at 37°C and 5 % CO_2, cells were lysed, and the luciferase signals were detected as described in 4.2.1.7. For each condition three technical and three biological replicates were analyzed.

4.2.1.10 XRE-dependent reporter gene assay

The XRE-dependent reporter gene assay was performed to evaluate the effect of small molecules on the activity of the aryl hydrocarbon receptor. In case of HepG2 cells, 3×10^6 cells were reversely transfected with plasmids encoding for an XRE-dependent firefly luciferase and a constitutively expressed *Renilla* luciferase (see 4.2.1.3) and seeded into a T25 cell culture flask. After incubation for 24 h at 37°C and 5% CO_2 the cells were collected in a 50 mL falcon tube and subsequently, $2.5\text{x}10^4$ cells were seeded in a volume of 90 µL per well into a 96 well cell culture plate. After 1 h, cells were treated with several concentrations of the test compounds as described in chapter 4.2.1.8 and were incubated at 37°C and 5% CO_2 for 4 h or 24 h prior to assay readout (see 4.2.1.7). The firefly luciferase signals were normalized to the respective *Renilla* luciferase signals. To obtain fold changes all normalized signals were divided by values obtained from wells which were only treated with DMSO. As a control for XRE induction, the known aryl hydrocarbon receptor agonist FICZ was used as a reference.
In case of stably transfected NIH-3T3 cells (NIH-3T3-XRE:fluc_pbas:rluc), $1\text{x}10^4$ cells were seeded into each well of a 96-well cell culture plate. In case of stably transfected HaCaT cells (HaCaT-XRE:fluc_PGK:rluc), $2\text{x}10^4$ cells per well were seeded into 96-well plates. In both cases, cells were incubated at 37°C and 5 % CO_2 for 24 h, prior to compound treatment and assay readout, following the same procedure, as described above. For each condition three technical and three biological replicates were analyzed.

4.2.1.11 Luciferase activity assay

The luciferase activity assay was used as a counter assay for luciferase-based reporter gene assays, to avoid false-positive results, i.e. to identify compounds that directly impair the enzymatic activity of Fluc or Rluc. For this purpose, HEK293-T cells were transfected with pRL-TK-Rluc, pcDNA-Wnt-3A and M50 Super 8x TOPFlash plasmids as described in 4.2.1.3 and

were seeded into T25 cell culture flasks. After 24 h, cells were lysed in 1 mL passive lysis buffer for 20 min at 650 rpm. Afterwards, lysates were snap frozen and stored at -80°C until further usage or were directly used for luciferase activity assays. Briefly, 9 µL of the lysates were transferred to each well of a white 96-half-well plate. For treatment of the cell lysates with small molecules, serial dilutions of the compounds in DMSO were prepared and these were diluted in a ratio of 1:10 in passive lysis buffer. Afterwards, 1 µL of these dilutions were added to the 9 µL of the cell lysates and samples were incubated for 1 h at room temperature. Afterwards, the luciferase signals were detected using the Dual-Glo® Luciferase Assay Kit and the Tecan Sparks plate reader according to the manufacturer's instructions. The luminescence signals of firefly and *Renilla* luciferases in lysates of cells that were treated with DMSO were set to 100 %. To obtain IC_{50} values, non-linear regression was performed using a four-parameter fit (GraphPad Prism 7, GraphPad software, USA). For each condition three technical and three biological replicates were analyzed.

4.2.1.12 BODIPY-cyclopamine displacement assay

The BODIPY-cyclopamine displacement assay was adopted from Chen *et al.*[52] and was used to evaluate whether a compound binds to the heptahelical bundle of the SMO protein. For this purpose, HEK293-T cells were seeded at a concentration of 5×10^4 cells per well into 24-well plates equipped with poly-D-lysine coated coverslips, or at a concentration of 6×10^5 cells per well into 6-well plates. After 24 h of incubation at 37°C and 5 % CO_2, cells were transfected with pGen_mSMO plasmid (24-well plate) or SMO-BFP plasmid (6-well plate) as described in 4.2.1.3, for 48 h at 37°C and 5 % CO_2.

I Immunocytochemistry

After two days, the pGen_mSMO-transfected cells (24-well plate) were fixed for 10 min. Fixed cells were washed twice with PBS for 5 min and were then stabilized with PBS containing 10 mM glycine and 0.2 % sodium azide for 5 min. Afterwards, cells were washed three times with PBS and were subsequently treated with the compounds or DMSO in HEK293-T assay medium, containing 5 nM BODIPY-cyclopamine, for 4 h at room temperature and in the dark. Next, cells were washed with PBS and incubated with 1 µg/mL DAPI in PBS for 10 min to stain the nuclei. The coverslips were washed again with PBS and were mounted onto glass slides. For analysis, the samples were analysed by means of fluorescence microscopy using the Zeiss Observer Z1 (Carl Zeiss, Germany) and a Plan-Apochromatic 63x/1.40 Oil DIC M27 objective.

II Fluorescence assisted cell sorting (FACS)

The SMO-BFP-transfected cells (6-well plate) were treated with compounds or DMSO as a control. For this purpose, the compounds were pre-diluted in DMSO. Afterwards, 16 µL of the

pre-diluted compounds or DMSO were pipetted into 3.2 mL HEK293-T assay medium, containing 5 nM BODIPY-Cyclopamine. Next, 3 mL of the compound dilutions or DMSO were added to the cells. After 4 h of incubation at 37°C and 5 % CO_2, cells were detached using PBS and collected in 15 mL falcon tubes. After centrifugation for 5 min at 300 x g, the cells were suspended and washed twice with 0.5 mL PBS. Afterwards, cells were filtered through the grid of a FACS tube lid. Finally, cells were subjected to flow cytometry employing the BD LSR II Flow Cytometer (BD Biosciences, USA) (laser line: 488 nm, emission filter: 530/30 for BODIPY and laser line: 405 nm, emission filter: 450/50 for BFP).

4.2.1.13 Gene expression analysis

For gene expression analysis via RT-qPCR or next generation sequencing analysis (NGS) $1x10^5$ C3H10T1/2 cells were seeded per well into 6-well plates and cultured for 48 h at 37°C and 5 % CO_2 to a confluence of 80 %. For compound treatment, 1 mM purmorphamine was diluted in C3H10T1/2 growth medium to a concentration of 1.5 µM (0.15 % DMSO, purmorphamine medium). For negative controls 0.15 % DMSO medium was prepared accordingly. Afterwards, compounds or DMSO as a control were diluted in a ratio of 1:1000 in 3.2 mL purmorphamine medium, or DMSO medium in case of the negative control, resulting in a final DMSO concentration of 0.25 %. Samples were mixed well by vortexing. Afterwards, the medium was removed from the cells and 3 mL of the compound medium was added to each well. Finally, cells were incubated for 24 h, 48 h, 96 h or 7 days at 37°C and 5 % CO_2 prior to RNA isolation (see 4.2.2.6), reverse transcription (see 4.2.2.7) and qPCR analysis (see 4.2.2.8) or submission for NGS (see 4.2.2.10).
For gene expression analysis in NIH-3T3 cells, $2x10^4$ cells were seeded into each well of a 24-well plate and incubated for 24 h at 37°C and 5 % CO_2. For compound treatment 1 mM purmorphamine was diluted in NIH-3T3 assay medium to a concentration of 2 µM (purmorphamine medium). Afterwards, compounds or DMSO as a control were diluted in purmorphamine medium in a ratio of 1:400 and a volume of 550 µL per sample. The compound dilutions were mixed by vortexing. Afterwards, the medium was removed from the cells and replaced by 500 µL of the corresponding compound dilution. Cells were incubated for 48 h at 37°C and 5 % CO_2 prior to RNA isolation (see 4.2.2.6), reverse transcription (see 4.2.2.7) and qPCR analysis (see 4.2.2.8).

4.2.1.14 Matrix mineralization assay

To evaluate the effect of small molecules on late-stage osteoblast differentiation a matrix mineralization assay using Alizarin Red S for staining of hydroxyapatite (molecular formula: $Ca_3(PO_4)_2$) was used. For this purpose, $6×10^4$ C3H10T1/2 cells per well were seeded into 12-

well plates and grown at 37°C and 5 % CO_2 for 48 h, to a confluence of 80 %. Afterwards, the cells were treated with mineralization medium (SHH-N-conditioned medium containing 50 µg/mL L-ascorbic-3-phosphate, 10 mM β-glycerophosphate and 10 % heat-inactivated FCS) or control medium (empty vector-conditioned medium containing 50 µg/mL L-ascorbic-3-phosphate, 10 mM β-glycerophosphate and 10 % heat-inactivated FCS) and compounds or DMSO as a solvent control. For this purpose, compounds were pre-diluted in DMSO first and added in a ratio of 1:1000 to 1.2 mL of mineralization medium, so that the final DMSO concentration in all wells was 0.1 %. The growth medium on the cells was aspirated and replaced by 1 mL of the desired mineralization/control medium. Cells were cultured at 37°C and 5 % CO_2 for 21 days and the medium was exchanged every 3 to 4 days. Afterwards cells were fixed in 3.7 % formaldehyde, washed twice with ddH_2O and stained with 40 mM Alizarin Red S solution (pH = 4.1, adjusted using 10 % ammonium hydroxide) for 40 min. To remove unspecific staining, cells were washed 5 times with ddH_2O and were finally supplied with PBS. To evaluate the matrix mineralization, stained cells were observed and imaged using a Zeiss Observer Z1 (Carl Zeiss, Germany).

4.2.1.15 CYP450 Glo assay

CYP1A1 activity was assessed using the P450-Glo™ CYP1A1 Assay system (Promega), according to the instructions of the manufacturer. Briefly, $4x10^4$ HepG2 cells per well were seeded into 96-well plates and incubated for 24 h at 37°C and 5 % CO_2. The next day, the HepG2 growth medium was discarded and replaced by 80 µL of HepG2 assay medium. Cells were then treated with different concentrations of the compounds or DMSO as a control, as described in 4.2.1.8. After 24 h the 50 AM CEE substrate was added to the cells for 3 h at 37°C and 5 % CO_2. The luminescence signals were measured using the Tecan Sparks plate reader, 24 h after addition of the compounds. To obtain fold changes all values obtained for samples that were treated with compounds were divided by the mean value obtained for cells that were treated with DMSO. To obtain EC_{50} values, non-linear regression analysis was performed using a four-parameter fit (GraphPad Prism 7, GraphPad software, USA). For each condition three technical and three biological replicates were analyzed.

4.2.1.16 GPCR Panel

The gpcrMAX panel contained 168 GPCRs and was performed by the LeadHunter service at Eurofins DiscoverX. Picoberin was tested at a single concentration of 500 nM using the PathHunter β-Arrestin assay in agonist and antagonist mode. The dose dependent CXCR4 calcium flux assay was performed Eurofins Discovery in agonist and antagonist mode.

4.2.1.17 Nuclear receptor panel

The nhrMAX Biosensor panel included in total 19 nuclear receptors and was performed by the LeadHunter service at Eurofins DiscoverX. Compounds were tested at a single concentration of 500 nM using the PathHunter Nuclear hormone receptor assay in agonist and antagonist mode.

4.2.1.18 Immunocytochemistry

For evaluation of the cellular localization of the AhR in C3H10T1/2 cells, 24-well plates were supplemented with 12 mm glass coverslips. Afterwards, $2x10^4$ C3H10T1/2 cells, which were reversely transfected with mAhR-FLAG plasmid (see 4.2.1.3) were seeded into each well in a volume of 500 µL C3H10T1/2 growth medium. Cells were incubated for 24 h at 37°C and 5 % CO_2 and were then treated with different concentrations of the test compounds or DMSO as a control. The final DMSO concentration was 0.1 % in all samples. After 24 h, the medium was aspirated and 500 µL fixation buffer was added to each well for 5 min. Afterwards, the fixation buffer was aspirated and cells were washed once with PBS, followed by incubation with 500 µL permeabilization buffer per well. Cells were then washed three times for 5 min with PBS. After blocking with 3 % BSA in PBS for 40 min, a primary antibody against the FLAG-tag was added to the samples (see 4.1.6 for description and dilution details). After overnight incubation at 4°C, the primary antibody solution was removed and samples were washed three times for 5 min with PBS, prior to addition of the secondary antibodies (anti-mouse-Alexa488, see 4.1.6) and 1 µg/mL DAPI. After incubation for 1 h at room temperature and in the dark, the antibody-DAPI solution was removed, and cells were again washed three times for 5 min with PBS. Finally, the coverslips were mounted on glass slides and dried for at least 24 h. Fluorescence staining was examined by means of fluorescence microscopy using the Zeiss Observer Z1 and a Plan-Apochromat 53x/1.40 Oil DIC M27 objective.

To explore the cellular AhR localization in HepG2 cells, 24-well plates were equipped with poly-D-lysine coated coverslips and $5x10^4$ cells were seeded in a volume of 500 µL HepG2 growth medium per well. Cells were incubated for 6 h at 37°C and 5 % CO_2 until they were attached to the coverslips, prior to treatment with different concentrations of the test compounds or DMSO, as described above, for 15 min. Cells were then fixed, washed and blocked as described above. Afterwards, cells were incubated with a primary antibody against AhR (see 4.1.6 for antibody description and dilution details) at 4°C and overnight. Afterwards, samples were further processed, as described above.

4.2.1.19 Generation of cell lysates

For the detection and quantification of cellular proteins, the cells needed to be lysed. Depending on the follow up experimental procedure, different lysis protocols were applied.

I Direct lysis of cells using SDS lysis buffer

For the direct lysis of cells using SDS lyses buffer, first the medium was aspirated from all wells and cells were washed once with PBS. Depending on the size of the multi-well plates and cell density, 20 – 60 µL SDS lysis buffer without bromphenol blue and DTE were added to the cells. To collect all cells, cells were scrapped with a cell scrapper and the lysates were collected in 1.5 mL tubes. Lysates were sonicated (10 %, 7 cycles) and the protein concentrations were determined using the DC protein assay (see 4.2.3.1). Afterwards 0.2 % bromphenol blue and 0.08 M DTE were added, and samples were heated to 95 °C for 10 min to denature the proteins. Finally, samples were stored at -20 °C until further usage.

II Generation of whole cell lysates for proteomics

For subsequent proteome profiling of C3H10T1/2 cells (see chapter 4.2.1.19), cell culture medium was removed from each T75 flask and cells were washed with 10 mL PBS per flask. Afterwards, 2 mL Trypsin/EDTA solution were added to the flasks and cells were incubated at 37°C. When the cells were detached, 8 mL growth medium was added to each flask and the cells were collected in 50 mL falcon tubes and centrifuged at 340 x g and 4°C for 5 min. After aspiration of the supernatant, cells were washed with 10 mL cold PBS per sample and were again centrifuged at 340 x g and 4°C for 5 min. The PBS was discarded, and cells were suspended in 5 mL ice-cold PBS and centrifuged again as described above. The supernatant was discarded, and cells were suspended in 1 mL cold PBS, transferred to 1.5 mL low binding tubes and centrifuged again. Afterwards, cells from each flask were resuspended in 100 µL cold PBS containing 0.4 % NP-40 and protease and phosphatase inhibitors, followed by four freeze-thaw cycles in liquid nitrogen. Finally, the samples were centrifuged for 15 min at 16000 x g and supernatants were transferred to fresh low binding tubes. Protein concentrations were determined using the DC protein assay (see 4.2.3.1) and samples were snap frozen and stored at -80°C until further usage.

III Generation of whole cell lysates for CETSA and TPP

For generation of cell lysates for CETSA or TPP (see 4.2.1.18), $4x10^6$ HepG2 cells or $2x10^6$ C3H10T1/2 cells were seeded in a volume of 26 mL into T175 cell culture flasks. In both cases, cells were confluent after 72 h of incubation at 37°C and 5 % CO_2. The culture medium was removed from the cell culture flasks and cells were washed with 10 mL PBS per flask. Afterwards, 3 mL of a cell dissociation solution was added to each flask and cells were

incubated at 37°C until they detached. Cells were re-suspended in a volume of 7 mL growth medium, collected in a 50 mL falcon tube, and centrifuged at 340 x g and 4°C for 5 min. The supernatant was discarded, cells were washed three times in 10 mL, 5 mL and 1 mL ice-cold PBS and centrifuged again at 340 x g and 4°C for 5 min. The supernatant was discarded, and the cell pellet was suspended in 1.2 mL CETSA lysis buffer 1 (for HepG2 cells, see 4.1.2) or 1.2 mL CETSA lysis buffer 2 (C3H10T1/2 cells, see 4.1.2) followed by four freeze-thaw cycles in liquid nitrogen. To remove all cell debris, lysates were ultra-centrifuged for 20 min at 100 000 x g and 4°C. The supernatants containing the soluble proteins were transferred into fresh low-binding tubes and samples were snap frozen and stored at -80°C until further usage.

4.2.1.20 Cellular thermal shift assay and thermal proteome profiling

I CETSA or TPP with cell lysates

For in-lysate CETSA or TPP, cell lysates were generated as described in 4.2.1.17-II. After determination of the lysate concentration (see 4.2.3.1), the lysate was diluted to a concentration of 5 mg/mL (HepG2 cells) or 4 mg/mL (C3H10T1/2 cells) and split into two vials, with 600 µL (WB based CETSA) or 1.4 mL (TPP) per vial. Afterwards, one aliquot was incubated with Picoberin (20 µM for HepG2 cells, 100 nM in case of C3H10T1/2 cells), the other aliquot was incubated with DMSO (HepG2: 0.5 %, C3H10T1/2: 0.1 %) for 10 min at room temperature. Lysates were then split into nine aliquots and incubated at different temperatures ranging from 35.9°C to 67.0°C for 3 min. After the heat treatment, the samples were stored on ice and transferred to polycarbonate vials for ultracentrifugation. After ultracentrifugation at 100 000 x g at 4°C for 20 min, supernatants were carefully transferred into fresh 1.5 mL tubes, without disturbing the pellets. Samples were then snap frozen in liquid nitrogen until further usage. For protein separation via SDS-PAGE, followed by immunoblotting, samples were treated as described in 4.2.3.2. For TPP, 75 µL of the samples were prepared for MS/MS analysis as described in chapter 4.2.1.19-I.

II In-cell CETSA

For in-cell CETSA, $2x10^6$ HepG2 cells were seeded into two T75 cell culture flasks and cultured at 37°C and 5 % CO_2 for 72 h. For compound treatments, two 50 mL falcon tubes were filled with 3 mL HepG2-growth medium and 15 µL of 4 mM of the compound or DMSO as a control was added to the respective tube. The final compound concentration was 20 µM and the final DMSO concentration was 0.5 %. The medium was removed from the cells and was replaced by 3 mL of the respective compound or DMSO-containing medium. Cells were then incubated for 15 min at 37°C and 5 % CO_2 to allow the compound to bind to its molecular target. Afterwards, the medium was removed from the cell culture flasks, cells were washed once with 6 mL PBS and 2 mL of a cell dissociation solution was added to each flask. Cells were

incubated at 37°C until they were detached, 5 mL growth medium was added to each flask and cells were suspended and collected in two 15 mL falcon tubes. After centrifugation at 340 x g and 4°C for 5 min, the supernatant was aspirated, and cells were washed with 1 mL PBS and centrifuged again as described above. The supernatant was again discarded, and cells were suspended in 0.6 mL TRIS-NaCl buffer. Cell suspensions were then split into nine aliquots of 50 µL and incubated at different temperatures for 3 min. Subsequently, 5 µL of lysis buffer containing 11 % NP-40 and 5.5 % sodium deoxycholate in TRIS-NaCl buffer was added to each tube and cells were lysed by three freeze-thaw cycles. Samples were transferred to polycarbonate vials for ultracentrifugation at 100 000 x g at 4°C for 20 min. Afterwards, supernatants were carefully transferred into fresh 1.5 mL low-binding tubes, without disturbing the pellets. Samples were then prepared for protein separation via SDS-PAGE, followed by immunoblotting, as described in 4.2.3.2.

4.2.1.21 Global proteome profiling

For proteome profiling, C3H10T1/2 cells were thawed as described in 4.2.1 and 8.5×10^5 cells were seeded into seventeen T75 cell culture flasks, in a volume of 10 mL growth medium. The cells were incubated at 37°C and 5 % CO_2 for 48 h until 80 % confluence. For compound treatment 14 mL of 15 µM purmorphamine medium was prepared. For this purpose, 210 µL of 1 mM purmorphamine was added to 13.79 mL of growth medium (1.5 % DMSO) and mixed well. For negative controls, 7 mL of DMSO-containing medium A was prepared (105 µL DMSO + 6.895 mL growth medium, 1.5 % DMSO). Furthermore, a predilution of 10 nM compound was prepared by addition of 70 µL of 1 mM compound to 6.930 mL growth medium (1 % DMSO). For non-compound treated samples, 12 mL of DMSO medium B (120 µL DMSO + 11.89 mL growth medium, 1 % DMSO) was prepared. Afterwards, medium was removed from the cells and 8 mL fresh growth medium were added to each flask. To five flasks, 1 mL of purmorphamine medium and 1 mL of 10 nM compound medium were added, resulting in a final purmorphamine concentration of 1.5 µM, a final concentration of 1 nM compound and in total 0.25 % DMSO. For positive controls, five flasks were supplemented with 1 mL purmorphamine medium and 1 mL DMSO medium B, resulting in a final purmorphamine concentration of 1.5 µM purmorphamine and 0.25 % DMSO, respectively. For negative controls, five flasks were supplemented with 1 mL of DMSO medium A and 1 mL of DMSO medium B, to reach a final DMSO concentration of 0.25 %. Cells in the residual two flasks were not treated with any compound and served as control for untreated cells. Cells were incubated at 37°C and 5 % CO_2 for 0 h, 24 h, 48 h, 96 h or 7 days.

At each timepoint, one flask of cells that were treated with compound and purmorphamine, one flask of cells that were treated with purmorphamine and DMSO and one flask of cells that were only treated with DMSO were lysed as described in 4.2.1.17. Untreated cells were lysed

and pooled at time point 0 h. After determination of the protein concentrations (see 4.2.3.1), samples were snap frozen and stored at -80°C until further usage.

I Reduction, alkylation and digestion

To prepare the samples for MS analysis, dilutions of a total amount of 200 µg protein in a volume of 75 µL lysis buffer were prepared in fresh low-binding tubes and 75 µL of a 100 mM triethylammonium bicarbonate (TEAB) solution was added to each sample. Afterwards, 7.5 µL of a 200 mM TRIS(2-carboxyethyl)phosphine hydrochloride (TCEP) solution in 200 mM TEAB was added to each sample, and samples were directly inverted several times and vortexed for proper mixing. After a short centrifugation to collect the liquid in the bottom of the tubes, samples were incubated for 1 h at 55°C and protected from light. Immediately before use, a 375 mM solution of iodoacetamide in 200 mM TEAB buffer was prepared and 7.5 µL of this solution was added to each sample. After an incubation for 30 min at room temperature and in absence of light, 900 µL of ice-cold acetone (proteomics grade) was added to the samples for protein precipitation. For complete precipitation, samples were stored at -20°C overnight. The next day, samples were centrifuged at 8000 x g for 10 min, supernatants were removed, and pellets were dried for 30-45 min. In the meantime, a solution 0.4 µg/mL Trypsin (HPLC grade) in 10 mM HCl and a fresh 200 mM TEAB solution were prepared. Afterwards, 220 µL of the trypsin solution were dissolved in 2200 µL of the 200 mM TEAB buffer and 107.5 µL of this solution were added to each pellet. Samples were vortexed vigorously to dissolve the pellets completely. After a short centrifugation to collect the liquids, samples were incubated at 37°C and 300 rpm for 2 h. Samples were then vortexed again, prior to incubation overnight at 37°C, 300 rpm and in the absence of light.

II TMT labelling of the samples

Subsequent sample preparation was conducted by the mass spectrometry team of the MPI Dortmund. Briefly, each sample was labelled with 41 µL labelling solution of one TMT11plex™ label and incubated at room temperature. After 2 h, reactions were quenched by the addition of 8 µL of a quenching solution and incubation at 15 min at room temperature. Afterwards, all samples of a timepoint (including all three biological replicates) were combined and dried in vacuum. Next, the samples were dissolved in 120 µL of a 20 mM NH_4COO solution (pH = 11), ultra-sonicated for 2 min, vortexed for 1 min and finally centrifuged for 3 min at 13,000 rpm. After prefractionation, samples were dried completely in vacuum.

III Fractionation of the samples

For reduction of sample complexity and to thereby increase the number of quantified proteins, the samples were fractionated into ten fractions using a C18 column and high pH conditions,

prior to nanoHPLC-MS/MS analysis. For this purpose, samples were dissolved in 120 µL of a 20 mM ammonium formate (HCOONH4) solution (pH 11.0), followed by ultra-sonication (15 min), incubation while rotating (15 min) and centrifugation at 8000 x g for 3 min at room temperature. For separations of the samples, 50 µL of the supernatants were injected onto a Xbridge C18 column (130 A°, 3.5 mm, 1 mm x 150 mm) using a U3000 capHPLC system (ThermoFisher Scientific) and a flow rate of 50 µL/min. Table 2 and Table 3 show the solvents and steps used for sample separation.

Table 2: Solvent composition.

Solvent	Composition
A	20 mM $HCOONH_4$ pH 11 in H2O
B	40 % 20 mM $HCOONH_4$ pH 11 in H2O premixed with 60 % acetonitrile

Table 3: Separation conditions.

Step	t/ min	Separation condition
1	10	95 % solvent A, 5 % solvent B, isocratic
2	5	Linear gradient up to 25 % solvent B
3	60	Linear gradient up to 65 % solvent B
4	10	Linear gradient up to 100 % solvent B
5	14	100 % solvent B

Proteins were detected at a wavelength of 214 nm and the eluate between 15 and 100 min was collected in 10 fractions, with 30 s per fraction using circular fractionation. Fractions were dried in a SpeedVac at 30°C and subjected to nanoHPLC-MS/MS analysis.

IV Mass spectrometry

For MS/MS analysis, all samples were dissolved in 20 µL 0.1 % TFA in water (HPLC grade) and 3 µL of these solutions were injected onto the UltiMateTM 3000 RSL Cnano system (ThermoFisher Scientific), online coupled to a Q Exactive! HF Plus Hybrid Quadrupole-Orbitrap Mass Spectrometer equipped with a nanospray source (Nanospray Flex Ion Source, Thermo Scientific). For desalting, samples were injected onto a pre-column cartridge (5 µm, 100 A°, 300 mm ID * 5 mm, Dionex, Germany) using 0.1 % TFA in water as eluent with a flow rate of 30 mL/min. Afterwards, desalting was performed with eluent flow to waste followed by back-flushing of the sample during the whole analysis from the pre-column to the PepMap100 RSLC C18 nano-HPLC column (2 µm, 100 A˚, 75 mm ID 3 50 cm, nanoViper, Dionex, Germany) using the steps indicated in Table 4 and Table 5 and a flow rate of 300 nL/min. The nanoHPLC was online coupled to a Quadrupole-Orbitrap Mass Spectrometer using a standard coated SilicaTip (ID 20 mm, Tip-ID 10 mM, New Objective, Woburn, MA, USA). The mass range of m/z 300 to 1650 was acquired with a resolution of 70000 for full scan, followed by up to 10 high energy collision dissociation (HCD) MS/MS scans of the most intense at least doubly

charged ions using a NCE energy of 35 % and a resolution of 35000. Data analysis is described in 4.2.4.3.

Table 4: Solvent composition II.

Solvent	Composition
A	0.1 % formic acid in H_2O (HPLC-grade)
B	Acetonitrile containing 0.1 % formic acid (HPLC-grade)

Table 5: Separation conditions II.

Step	t/ min	Separation condition
1	0	95 % solvent A, 5 % solvent B
2	120	Linear gradient up to 40 % solvent B
3	5	Linear gradient up to 60 % solvent B
4	5	Linear gradient up to 95 % solvent B
5	5	95 % solvent B
6	1	Linear gradient back to starting conditions
7	14	Re-equilibration to starting conditions

4.2.2 Molecular biology methods

4.2.2.1 Transformation of competent cells

Heat shock transformation of chemically competent *E. coli* (One Shot® OmniMAX) was performed to insert plasmid DNA into a bacterial strain. For this purpose, 100 µL of competent *E. coli* cells were mixed with 50 – 100 ng of the plasmid DNA. The mix was incubated on ice for 30 min. Subsequently, cells were exposed to 42°C for 2 min (heat shock) and were then transferred to ice for 1 minute. After addition of 900 µL fresh LB medium, cells were incubated at 37°C and 350 rpm. After 1 h, cells were centrifuged at 8000 x g for 5 min, the supernatant was aspirated, and the pellet was suspended in 100 µL fresh LB medium. The resulting cell suspension was distributed on three agar plates (volumes of 10 µL, 30 µL and 60 µL) containing the respective selection antibiotics (100 ng/mL ampicillin or 50 ng/mL kanamycin). After overnight incubation at 37°C, plates were inspected for clones and isolated clones were expanded as described in 4.2.2.2 for generation of a glycerol stock.

4.2.2.2 Preparation of glycerol stocks

For the preparation of glycerol stocks, a positive clone was picked from an agar plate and transferred to 4 mL LB-medium containing the respective selection antibiotic (100 ng/mL ampicillin or 50 ng/mL kanamycin). The suspension was incubated for 5 h for bacterial amplification. Afterwards, 500 µL of the cell suspension was mixed with 500 µL sterile glycerol. The mixture was snap frozen in liquid nitrogen and stored at -80°C.

4.2.2.3 Plasmid amplification

To amplify a plasmid of interest, 300 mL LB medium containing the required selection antibiotic (100 ng/mL ampicillin or 50 ng/mL kanamycin) were inoculated with positive clones from a glycerol stock. The bacterial cultures were incubated at 37°C and 180 rpm overnight.

4.2.2.4 Plasmid isolation

To harvest the cells after plasmid amplification, bacterial cultures were centrifuged at 6000 x g and 4°C for 15 min. Afterwards, plasmids were isolated using the EndoFree Plasmid Maxi Kit according to the instructions of the manufacturer. Isolated plasmids were suspended in sterile water and DNA concentration was determined spectrophotometrically, using the NanoDrop2000.

4.2.2.5 DNA sequencing

Sequencing of plasmid DNA was performed using the Sanger sequencing technique at Microsynth Seqlab GmbH.

4.2.2.6 RNA isolation

To obtain total RNA from mammalian cells, the culture medium was aspirated, and the cells were washed with PBS once. Afterwards, RNA was isolated using the Rneasy Mini Plus kit according to the instructions of the manufacturer. Depending on the size of the cell culture dish, different volumes of the RLT lysis buffer provided in the kit were used: 350 µL (24-well plate), 450 µL (12-well plate) or 600 µL (6-well plate). In case of NIH-3T3 cells, the resulting cell lysates were applied to QIAshredder columns and centrifuged for 1 min at 16000 x g for homogenization. C3H10T1/2 cell lysates were snap frozen once in liquid nitrogen and vortexed several times for homogenization. RNA concentrations were determined using the NanoDrop 2000 spectrophotometer. Additionally, RNA concentrations and qualities were assessed with the Qubit 4.0 fluorometer, using the Qubit™ RNA BR assay kit and the Qubit™ RNA IQ assay kit according to the instructions of the manufacturer. Until further use, isolated RNA was snap frozen and stored at -80°C.

4.2.2.7 Reverse transcription

Complementary DNA (cDNA) was obtained via reverse transcription of total RNA using the QuantiTect reverse transcription kit according to the instructions of the manufacturer. Briefly, 500 ng RNA were diluted in PCR-grade water to a final volume of 12 µL, supplemented with 2 µL gDNA Wipeout buffer and samples were incubated at 42°C for 2 min to eliminate genomic

DNA (gDNA). Afterwards, 6 µL of a master mix containing the reverse transcriptase, random primers and buffer was added. Samples were incubated for 15 min at 42°C for reverse transcription. After inactivation of the reverse transcriptase at 95°C for 2 min, samples were stored until further use at -20°C.

4.2.2.8 Quantitative PCR (qPCR)

The quantitative PCR (qPCR) was performed using the SsoAdvanced™ Universal SYBR® Green Supermix according to the instructions of the manufacturer. Briefly, cDNA obtained as described in 4.2.2.7 was diluted in PCR-grade H_2O and 3 µL of the cDNA solution was mixed with 7 µL of SYBR® Green master mix containing the respective primers. All primers used are listed in 4.1.9. All qPCR reactions were performed using the CFX96 Tough Bio-Rad PCR cycler. To obtain relative gene expression levels, the $2^{-\Delta\Delta Ct}$ method was employed.[88]

4.2.2.9 Agarose gel electrophoresis

For the analysis of PCR products, agarose gel electrophoresis was carried out. For this purpose, 1.8 % agarose gels were prepared by dissolving 3.6 g agarose in 200 mL TEA buffer using a microwave. After the solution cooled to about 60°C, 10 µL RedSafe™ were added, which is a dye that intercalates into DNA and allows for DNA detection using UV light. The agarose solution was transferred to a gel chamber and allowed to solidify for 30 min. Samples were mixed with DNA loading buffer and then 10 µL of the sample were loaded into the gel pockets. To determine the fragment sizes, the DNA markers GeneRuler 1 kb DNA Marker and GeneRuler Ultra Low Range DNA marker were loaded onto the gel. For separation of DNA fragments, a voltage of 5 V per cm was applied. The detection of DNA bands was carried out with Documentation system Logic 200 Imaging System by irradiation with UV light.

4.2.2.10 Next generation sequencing (NGS)

Next generation sequencing was performed at the Max Planck Genome Centre (MP-GC) in Cologne (Germany) under the responsibility of Dr. Bruno Hüttel.

Briefly, RNA quality and quantity was assessed by Agilent Bioanalyzer Nanochip. Poly-A RNA was then enriched from 500 ng total RNA using the ®Poly(A) mRNA Magnetic Isolation Module (New England Biolabs) and directional RNA-seq libraries were prepared as described in Ultra™ II Directional RNA Library Prep Kit for Illumina (New England Biolabs). Library concentration was enriched by PCR with dual barcoded primers. Concentration of the libraries were determined by Qubit HS kit (Thermo) and the fragment size and quality of libraries screened by Agilent TapeStation. The libraries were then diluted and pooled on a liquid handling station (Biomek i7, Beckman Coulter). Afterwards, sequencing-by-synthesis was

done on an Illumina HiSeq 3000 device in paired-end read mode 2 x 150 bp with a HiSeq 3000 PE Cluster Kit and a HiSeq 3000 SBS Kit (300 cycle). The obtained data was finally trimmed to 1 x 150 bp.

4.2.3 Biochemical methods

4.2.3.1 Determination of protein concentration (DC protein assay)

The DC protein assay is a colorimetric assay that allows the determination of protein concentrations after prior detergent-based cell lysis. This method is based on a reaction of proteins with copper ions and the oxidation of basic amino acids. For quantification of the protein content of a sample, a BSA standard dilution series was measured in parallel for each assay. Each sample was measured in duplicate following the manufacturer's instructions. Briefly, 5 µL of the samples or standards were mixed with 25 µL of the copper tartrate-containing solution in a transparent 96-well plate and subsequently 200 µL of the Folin reagent was added to each well. After 15 min of incubation in the absence of light, the absorbance at 750 nm was measured. Based on the measured absorptions of the standards, a calibration line was obtained, and the protein concentrations of the samples were determined.

4.2.3.2 SDS polyacrylamide gel electrophoresis (SDS-PAGE)

Separation of proteins contained in lysates was achieved using discontinuous SDS-polyacrylamide gel electrophoresis (SDS-PAGE) according to Laemmli.[89] For this purpose, 0.2 % bromphenol blue and 0.08 M dithioerythritol were added to the lysates after concentration determination. Samples were heated to 95°C for 10 min to disrupt the secondary and tertiary structures of proteins. Afterwards, samples were loaded onto SDS polyacrylamide gels, which were prepared using the recipe described in 4.1.2, with different acrylamide concentrations, depending on the size of the protein of interest. The gels were placed into a Mini-PROTEAN® Tetra Cell gel chamber and 1x SDS-running buffer was filled into the tank. The samples and 8 µL of the PageRuler™ Plus prestained protein ladder were loaded into the pockets of the gel. Afterwards, the proteins were stacked into the stacking gel by applying a voltage of 80 V. After 15 min, the voltage was increased to 120 V. This voltage was kept constant until the running front reached the end of the gel. Finally, gels were transferred to a lab dish containing mH_2O or transfer/wet blotting buffer. Proteins of interest were detected either via Coomassie staining or via immunoblotting.

4.2.3.3 Immunoblotting

Immunoblotting is a technique that combines the resolution of proteins that is achieved by SDS-PAGE with specific protein detection using primary and secondary antibodies. For this purpose, the proteins need to be transferred to a suitable membrane, which allows for specific anti body binding and detection.

I Wet blotting

After protein separation via SDS-PAGE, the gel was transferred to a lab dish containing 1x wet blotting buffer for approx. 10 min. The polyvinylidene fluoride (PVDF) membrane was activated using 100 % methanol for approx. 30 s and was subsequently transferred into wet blotting buffer for equilibration. The stacking gel was removed, and the separation gel was transferred to a wet blotting chamber, together with the Whatman filter papers and the PVDF membrane in a staggered manner. For this, the transfer cassette was placed into a tank filled with 1x blotting buffer. The fibre pad was placed in the cassette first, followed by a Whatman blotting paper, the activated PVDF membrane and the equilibrated protein gel. Afterwards, another Whatman filter paper and a second fibre pad were added. All air bubbles were removed using a plastic roller and the cassette was closed and placed into the wet blotting chamber. The chamber was filled with 1x wet blotting buffer, and an ice pack and a magnetic stirrer were added. For the transfer of the proteins to the PVDF membrane, a voltage of 100 V was applied for 60 min. Prior to immunostaining, the membrane was washed in mH_2O thrice for 5 min.

II Fast blotting

After protein separation, the SDS-gel was washed three times in mH_2O and equilibrated in Pierce™ 1-Step transfer buffer for 5 min. The PVDF membrane was activated in 100 % methanol for approx. 30 s and equilibrated in Pierce™ 1-Step transfer buffer. Afterwards, the membrane was placed into the Pierce™ Fast Blotter, onto a pre wetted Whatman paper. The SDS- gel was placed onto the membrane, followed by another pre-wetted Whatman paper. All air bubbles were removed using a plastic roller. The protein transfer was carried out at a constant voltage of 25 V for 5 – 10 min, depending on the size of the protein of interest. Afterwards, the membrane was washed three times in mH_2O prior to immunostaining.

III Immunodetection of proteins

Depending on the protein of interest and the optimal conditions for the corresponding primary antibodies the PVDF membrane was blocked for 40 min either in LI-COR blocking buffer or in 5 % milk to saturate any unspecific binding sites. Afterwards, the primary antibodies were diluted in the same blocking solution as described in 4.1.6 and the membrane was incubated with the primary antibody solution overnight at 4°C. On the next day, the PVDF membrane was

washed once with PBS-T for 5 min followed by another two 5 min washing steps in PBS. Afterwards, the secondary antibodies were diluted in the respective blocking solution as described in 4.1.7 and the membrane was incubated with these antibody dilutions for 1 h at room temperature. After another 3 x 5 min washing step in PBS, proteins bands were detected using the ChemiDoc imaging system (Bio-Rad). Band intensities were quantified using the software Image Lab (Bio-Rad).

4.2.4 Data analysis

4.2.4.1 FACS analysis

FACS-based SMO-binding data were analysed using the software FlowJo (TreeStar Inc., USA). At first, all detected events were visualized in a forward scatter height (FCS-H) vs. forward scatter area (FSC-A) density plot, which was used to identify and exclude doublets from the analysis. To select only the living cells, all singlets were visualized in an SSC-A vs. FSC-A plot and debris with very low size and granularity, which were located in the bottom left corner of the density plot, were excluded from further analysis steps. Afterwards, fluorescence intensities of the BFP channel (emission filter: 450/50) were depicted as a histogram and a gate for the population with high BFP fluorescence intensities was set to select only successfully transfected, BFP-positive cells. Finally, median BODIPY fluorescence intensities (emission filter: 530/30) were determined only for these cells. Median fluorescence values obtained for samples, which were treated with DMSO were set to 100 % and the BODIPY fluorescence intensities of all other samples were related to this sample.

4.2.4.2 NGS analysis

Processing of NGS raw data was performed at the Max Planck Genome Centre in Cologne (Germany) by Dr. Christian Woehler, functional analysis and interpretations were performed at MPI Dortmund as part of this thesis.

Briefly, for NGS data analyses the CLC Workbench (version 12.0 & CLC Genomics Server version 11.0) was used. For this purpose, the operations ‘Trim Reads’, ‘RNA-Seq Analysis’ (‘Strand specific = Reverse’) and ‘Differential Expression for RNA-Seq’ functions were applied to the data in that order. Mouse genome version GRCm38 was used as reference.

For pathway-overrepresentation analysis, log2(Fold change) data were uploaded to the Ingenuity Pathway Analysis software (IPA, Qiagen). To identify significantly regulated pathways, the significance threshold was set to $p < 0.05$ and only genes with a $\log_2$(Fold change) of ± 0.2 were considered during this analysis. Volcano plots were generated using the web-based tool VolcaNoseR.[85] Heat maps were generated using the software GraphPad Prism 7.0 (GraphPad software, USA).

4.2.4.3 Proteomics analysis

Data analysis was performed using the software MaxQuant including the Andromeda search algorithm was used.[90] Proteins were assignment based on the murine reference proteome (Uniprot database, UP000000589) and the search was performed for full enzymatic trypsin cleavages allowing two miss-cleavages. Oxidation of methionine and acetylation of the N-terminus were considered as variable protein modifications and carbamidomethylation was selected as fixed. The type ‘‘reporter ion MS2’’ was chosen for relative quantification and TMT labels were defined for all lysines and peptide N-termini. The mass accuracy for full mass spectra was set to 20 ppm (first search), to 4.5 ppm (second search) and to 20 ppm for MS/MS spectra. The false discovery rates for peptide and protein identification were set to 1 % and only proteins with at least two quantified peptides were selected. Relative quantification of proteins was performed using the reporter ion MS2 algorithm that is implemented in MaxQuant and saved as a proteinGroups.txt file, which was used for further analysis. Afterwards, proteins that were not identified with at least two razor and unique peptides in at least one biological replicate were excluded. Further data analysis was carried out using the software Perseus, version 1.6.2.3.[91] The “Reporter intensities corrected” from the proteinGroups.txt table were set as main columns. Proteins resulting from the reverse database search, just identified by site, and typical contaminants were filtered out. The ‘‘Reporter intensities corrected’’ were then logarithmized (log_2) and normalized to the median. Differentially regulated proteins were identified using a paired two-sided t-tests that was performed for each time point, separately. Only proteins with a p-value < 0.05 were considered as statistically significantly up- or down-regulated, depending on the direction of change. For pathway-overrepresentation analysis the Ingenuity Pathway Analysis tool (IPA, Qiagen) was employed. To identify significantly regulated pathways, the significance threshold was set to $p < 0.05$ and only genes with a log_2(Fold change) of ± 0.2 were analysed. For generation of volcano plots the web-based tool VolcaNoseR was used.[85]

4.2.4.4 Statistical analysis

For all experiments, at least three biological replicates ($n \geq 3$) were performed, with three technical replicates ($N = 3$) per biological replicate. Statistical analysis was performed for at least three biological replicates via an unpaired t-test using the software GraphPad Prism 7. Only data with p-values < 0.05 were considered as significant.

5 Results

5.1 Furo[3,2-b]pyridine, quinoline, pyrroloquinoline and a 20-membered macrocycle derivatives as Hh pathway inhibitors

Phenotypic screening of the in-house library of the department for Chemical Biology (MPI Dortmund) at the Compound Management and Screening Center (COMAS) led to the identification of several Furo[3,2-b]pyridine, quinoline, pyrroloquinoline and 20-membered macrocycle derivatives as potent inhibitors of Hh-dependent osteoblast differentiation of C3H10T1/2 cells. The chemical structures of the most potent derivatives are depicted in Figure 10A. The Furo[3,2-b]pyridine **1** was synthesized in the group of Dr. Kamil Paruch, the quinoline derivative **2** was provided by the group of Dr. Marta Gutiérrez Rodríguez, the pyrroloquinoline **3** and the macrocycle **4** were synthesized at the Max Planck Institute of Molecular Physiology by Dr. Jie Liu and Dr. Georg Niggemeyer[92], respectively. Figure 10B shows the dose-response curves of these compounds in the Hh-dependent osteoblast differentiation assay.

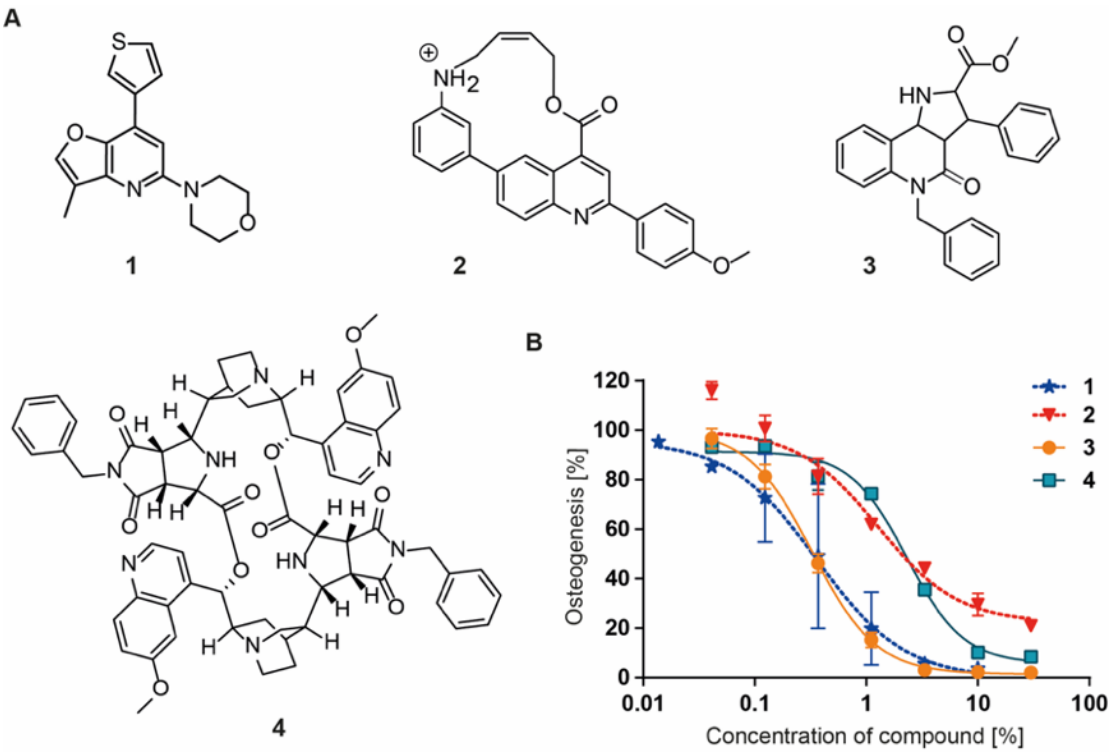

Figure 10: Identification of diverse small-molecule scaffolds as inhibitors of Hh-dependent osteoblast differentiation. A: Chemical structures of the most potent Furo[3,2-b]pyridine derivative (compound **1**), quinoline (compound **2**), pyrroloquinoline (compound **3**) and 20-membered macrocycle derivative (compound **4**). **B:** Osteoblast differentiation assay. C3H10T1/2 cells were treated with 1.5 µM purmorphamine and different concentrations of the compounds or DMSO as a control. Activity of the osteogenesis marker Alkaline phosphatase was measured after 96 h using a chemiluminescent readout. Data were normalized to values of samples that were treated with 1.5 µM purmorphamine and DMSO, which was set to 100 %. All data are mean values of three biological replicates (N = 3, n = 3) ± SD.

The compounds inhibited Hh-dependent osteoblast differentiation with IC_{50} values of 300 ± 100 nM (compound **1**), 1.3 ± 0.2 µM (compound **2**), 300 ± 150 nM (compound **3**) and 1.2 ± 0.1 µM (compound **4**).

5.1.1 Confirmation of Hh pathway inhibition

As described in chapter 2.4.1 and 2.4.2, besides Hh signaling several other pathways are involved in osteoblast differentiation. For this reason, compounds **1** – **4** were tested in an orthogonal GLI2/3-dependent reporter gene assay (Figure 11A) to confirm inhibition of Hh signaling.

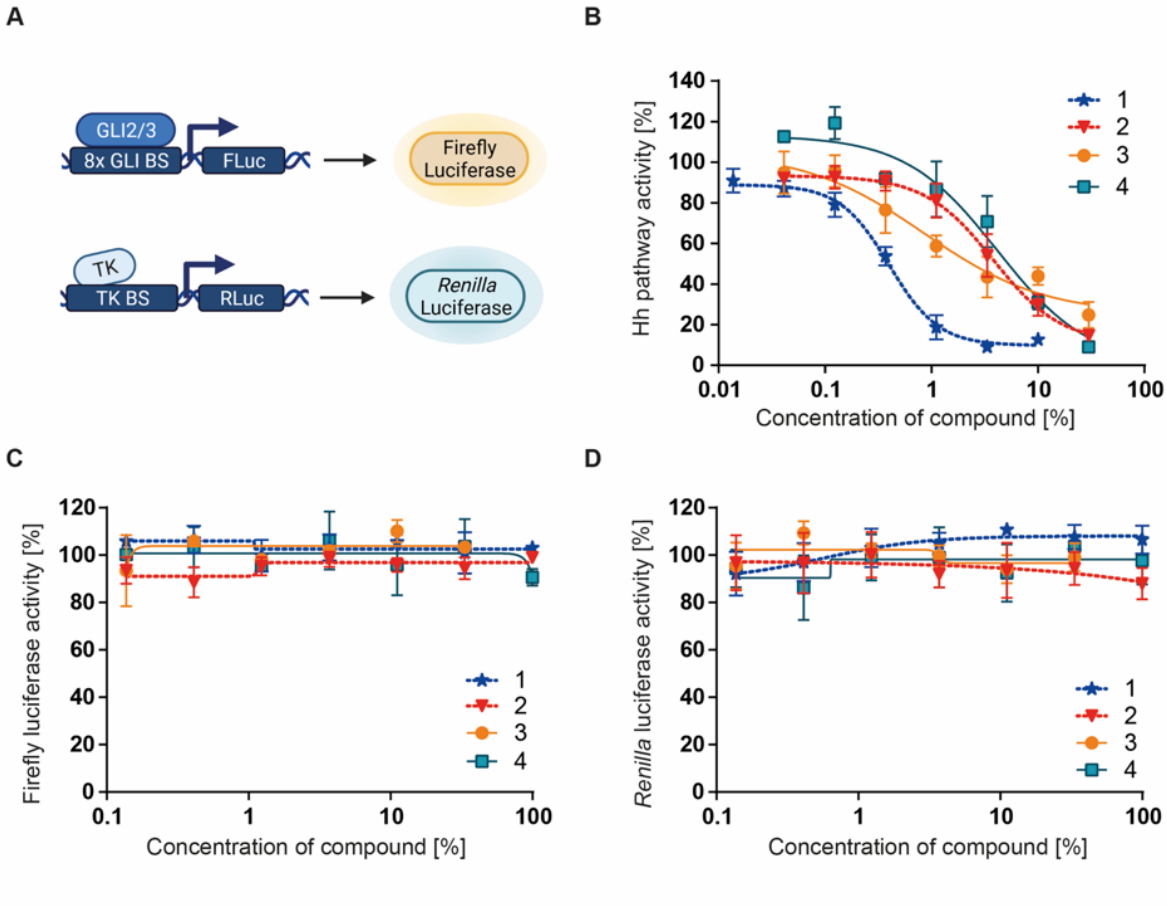

Figure 11: Confirmation of Hh pathway inhibition using a GLI2/3-dependent reporter gene assay. A: Schematic representation of the assay principle. **B:** Dose-response curves of compound **1**, **2**, **3** and **4** obtained with the GLI2/3-dependent reporter gene assay. Shh-LIGHT2 cells were treated with 2µM purmorphamine and different concentrations the compounds or DMSO as a control for 48 h. Values obtained for the Hh-responsive firefly luciferase were divided by the respective *Renilla* luciferase values and normalized to values of purmorphamine and DMSO treated cells. Data are mean values of three biological replicates (N = 3, n = 3) ± SD. **C** and **D:** Direct influence of compounds **1** – **4** on firefly l and *Renilla* (**D**) luciferase activities. Lysates of firefly and *Renilla* luciferase expressing cells were treated with different concentrations the compounds or DMSO as a control for 1 h. Data were normalized to values of samples that were treated with DMSO, which was set to 100 % and are mean values of three biological replicates (N = 3, n = 3) ± SD.

Reporter gene assays allow exploration of gene expression via measurement of the activity of a reporter protein. In this case, a GLI2/3-dependent reporter gene assay was performed, using the cell line Shh-LIGHT2[62] (see 4.1.3). Upon stimulation of Hh signaling, these cells express firefly luciferase (Fluc), which is under the control of an 8x GLI binding side (8x GLI BS). In addition, the cells constitutively express *Renilla* luciferase (Rluc), which is under the control of a thymidine kinase (TK) promoter, as a growth control. The GLI2/3-dependent reporter gene assay results obtained for compound **1** – **4** are shown in Figure 11B. All four compounds dose-dependently inhibited the Hh pathway activity with IC_{50} values of 400 ± 100 nM (compound **1**), 1.1 ± 0.3 µM (compound **2**), 2.5 ± 1.1 µM (compound **3**) and 4.1 ± 0.4 µM (compound **4**). The IC_{50} values obtained for compounds **1** and **2** fit well to the results obtained via the osteoblast differentiation assay. However, compounds **3** and **4** show a reduced potency in the GLI2/3-dependent reporter gene assay. To exclude potential effects of the compounds on the reporter gene assay readout, the direct influence of the compounds on firefly and *Renilla* luciferase activities were evaluated (Figure 11C and D, respectively). The compounds did not influence the luciferases' enzymatic activities. The effects observed in the GLI2/3-dependent reporter gene assay were thus caused by compound-mediated inhibition of Hh signaling. Analysis of the expression of Hh target genes (e.g. *Gli1* and *Ptch1*) by means of RT-qPCR allows to directly investigate the state of Hh pathway activity in cells, without an intervening reporter. The influence on Hh target gene expression was evaluated for the most potent derivatives **1**, **2**, and **3**. The corresponding results are shown in Figure 12.

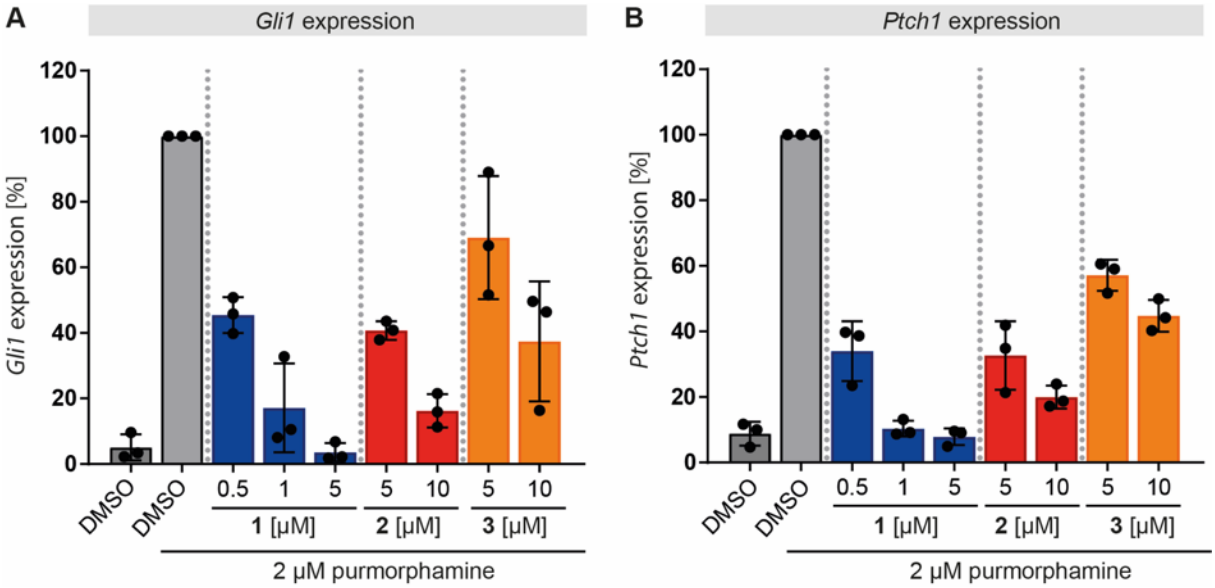

Figure 12: Evaluation of Hh target gene expression. NIH-3T3 cells were treated with 2 µM purmorphamine and different concentrations of the compounds or DMSO as a control for 48 h. For quantification of *Gli1* (**A**) and *Ptch1* (**B**) gene expression, RT-qPCR was performed with primers specific for *Gli1* and *Ptch1* as Hh target genes and *Gapdh* as housekeeping gene. Data were normalized to values of samples that were treated with purmorphamine and DMSO (100 %) and are mean values of three biological replicates (N = 3, n = 3) ± SD.

All three compounds dose-dependently inhibited the expression of the Hh target genes *Gli1* (Figure 12A) and *Ptch1* (Figure 12B). At a concentration of 5 µM, compound **1** reduced the expression of both target genes down to the level of samples that were treated with DMSO. At a concentration of 0.5 µM, the expression of *Gli1* was decreased to 45 % and *Ptch1* was reduced to 40 %. Compound **2** reduced *Gli1* and *Ptch1* expression levels to 15 % and 20 %, respectively, at a concentration of 10 µM. After treatment of cells with 10 µM of compound **3**, *Gli1* and *Ptch1* expression levels were reduced to 35 % and 40 %, respectively.

In summary, the results presented in this chapter could clearly confirm compounds **1** – **4** as Hh pathway inhibitors.

5.1.2 Characterization of SMO as the potential molecular target

Most of the already known Hh pathway inhibitors target the transmembrane protein SMO (see 2.3). For this reason, a BODIPY-cyclopamine displacement assay was employed to evaluate the ability of compounds **1**, **2**, **3** and **4** to bind to the heptahelical bundle of SMO. Cyclopamine is a known Hh pathway inhibitor that directly binds to the heptahelical bundle of SMO (see 2.3.2.1). For displacement assays, BODIPY-labelled cyclopamine was added to SMO-expressing HEK293-T cells. In the absence of a SMO antagonist, BODIPY-cyclopamine binds to SMO and the resulting green fluorescence can be detected via fluorescence microscopy or fluorescence-assisted cell sorting (FACS). In the presence of a SMO antagonist, such as Vismodegib that targets the same binding site, BODIPY-cyclopamine is competed out of the heptahelical bundle, resulting in reduction or complete loss of the fluorescence signal. The results obtained for compounds **1**, **2**, **3** and **4** are shown in Figure 13.

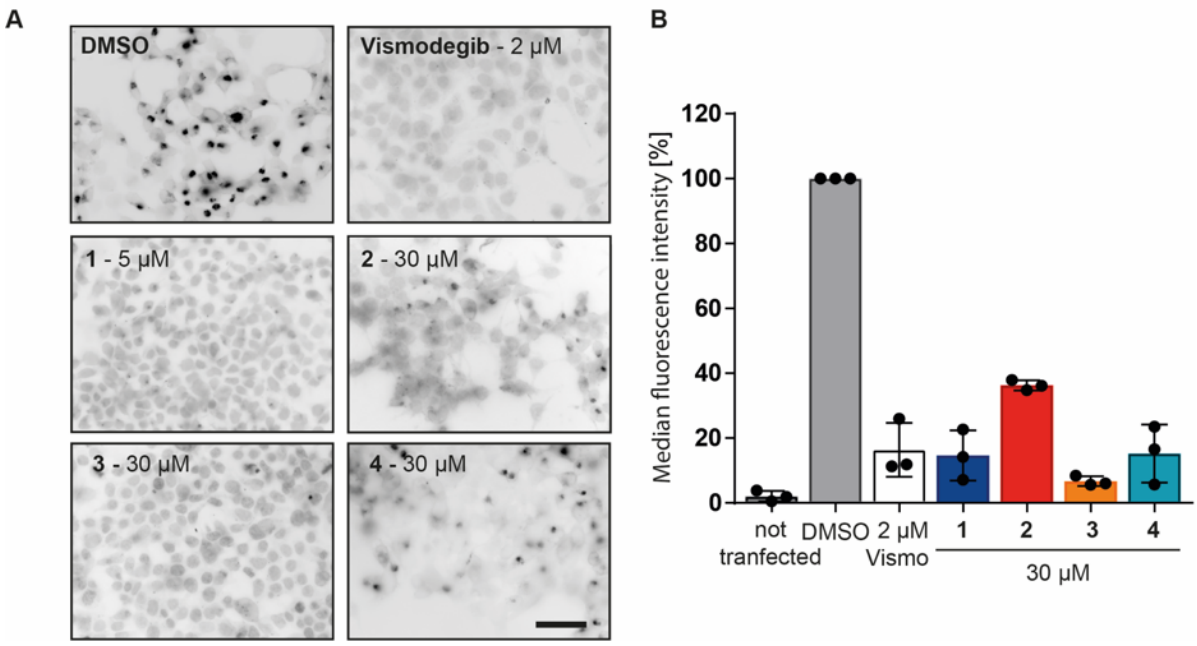

Figure 13: Compounds 1, 2, 3 and 4 bind to the heptahelical bundle of SMO. **A:** HEK293-T cells transiently transfected with a plasmid encoding for SMO were fixed and treated with 5 nM BODIPY-cyclopamine and different concentrations of the compounds or DMSO as a control for 4 h. BODIPY fluorescence was assessed by means of fluorescence microscopy. Images are representative for three biological replicates (n = 3). **B:** HEK293-T cells transiently transfected with a plasmid encoding for BFP-SMO were treated with 5 nM BODIPY-cyclopamine and different concentrations of the compounds or DMSO as a control for 4 h. Fluorescence signals were detected by means of flow cytometry. Data were normalized to values of DMSO-treated samples (100 %) and are mean values of three biological replicates (n = 3).

The microscopy images in Figure 13A clearly show that compound **1** at a concentration of 5 µM and compound **3** at a concentration of 30 µM were able to completely abolish the BODIPY fluorescence. Compound **4** at a concentration of 30 µM almost completely abolished the fluorescence signal, however, some few, weekly fluorescent dots were detected. These observations are in line with the results obtained using flow cytometry (Figure 13B). Compound **1**, **3** and **4** clearly reduced the median BODIPY-fluorescence intensity down to a level of 10 % to 20 % compared to DMSO, which is comparable to the effect of the known SMO binder Vismodegib at a concentration of 2 µM. In the microscopy experiment, compound **2** showed reduced fluorescence intensities at a concentration of 30 µM but was not able to completely displace BODIPY-cyclopamine from the heptahelical bundle of SMO (Figure 13A). In line with this observation, quantification of the BODIPY-fluorescence intensity by means of flow cytometry confirmed a reduction of the median BODIPY-fluorescence intensity to a level of 40 % compared to DMSO (Figure 13B). Since this compound is less potent than the other compounds tested in this experimental setup, higher concentrations of **4** may be required for complete displacement of BODIPY-cyclopamine. However, based on these data, all four compounds were classified as SMO binders.

The most potent compound (**1**) was furthermore tested in a GLI2/3-dependent reporter gene assay in which SHH was used to activate Hh signaling. While purmorphamine activates Hh signaling via direct binding to and activation of SMO, SHH activates Hh signaling upstream of SMO via disruption of PTC1-mediated inhibition of SMO. Consequently, compounds that act via binding to SMO should be able to inhibit SHH-induced Hh signaling more potently compared to purmorphamine induced Hh-signaling. The results obtained are presented in Figure 14.

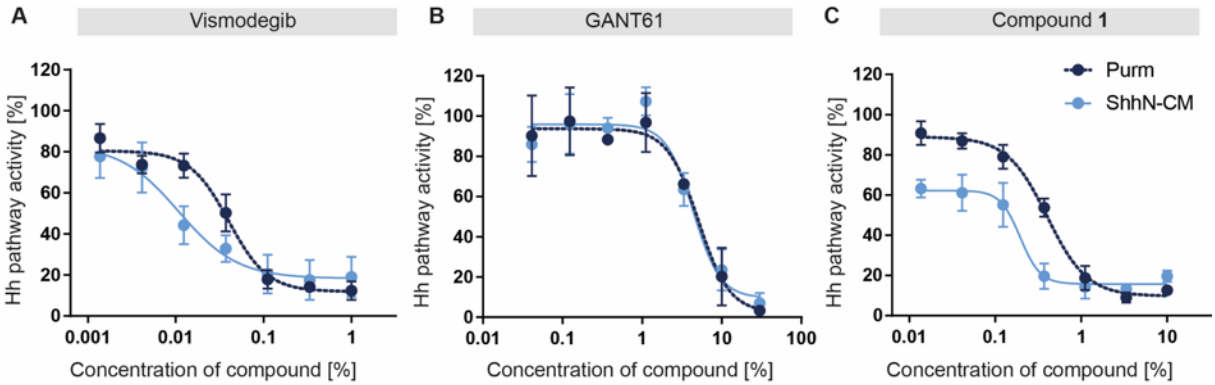

Figure 14: Evaluation of SMO binding using SHH-conditioned medium. Shh-LIGHT2 cells were treated with 2 µM purmorphamine and different concentrations of the compounds or DMSO as a control, or with SHH-conditioned medium (SHH-CM) and different concentrations of the compounds or DMSO as a control for 48 h. Values obtained for the Hh-responsive firefly luciferase were divided by the respective *Renilla* luciferase value and normalized to purmorphamine and DMSO or SHH-CM and DMSO treated samples. **A:** Vismodegib. **B:** GANT61. **C:** Compound **1**. Data are mean values of three biological replicates (N = 3, n = 3) ± SD.

For the known SMO antagonist Vismodegib an IC_{50} value of 38 ± 5 nM was obtained upon Hh pathway activation using the SMO agonist purmorphamine (Figure 14A). For SHH-CM-induced Hh pathway activation, an IC_{50} of 8 ± 6 nM was determined. The non-SMO binder GANT61 (Figure 14B) inhibited GLI2/3-dependent reporter activity with IC_{50} values of 5.0 ± 0.2 µM and 5.3 ± 0.3 µM after activation of Hh signaling with purmorphamine or SHH-CM, respectively. Compound **1** inhibits purmorphamine induced Hh signaling with an IC_{50} of 400 ± 100 nM and SHH-CM induced Hh signaling with an IC_{50} of 135 ± 65 nM (Figure 14C). Consequently, SMO binding of compound **1** could be confirmed by this approach. However, while Vismodegib and GANT61 reach a plateau phase at 100 % pathway activity, compound **1** reaches a plateau phase at 60 % in the presence of SHH-CM.

The results that were presented for compound **1** were included in the publication "Furo[3,2-*b*]pyridine: A Privileged Scaffold for Highly Selective Kinase Inhibitors and Effective Modulators of the Hedgehog Pathway", Nemec *et al.*[93]

5.2 A 4-Arylisoquinolone as Hh pathway inhibitor

During a screening campaign at the COMAS, several 4-arylisoquinolones, which were synthesized by Dr. Gang Shan at the MPI Dortmund, were identified as inhibitors of Hh-induced osteoblast differentiation with **5** (Figure 15A) being the most potent compound with an IC_{50} of 2.3 ± 0.3 µM. To confirm inhibition of Hh signaling, the compound was tested in a GLI2/3-dependent reporter gene assay (Figure 15B).

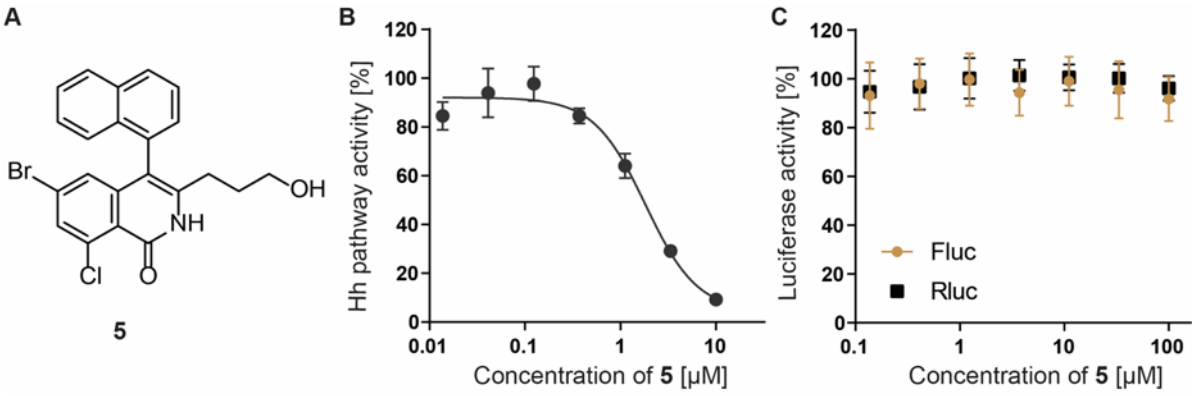

Figure 15: 4-Arylisoquinolone 5 inhibits Hh signaling. A: Chemical structure of **5**. **B:** GLI2/3-dependent reporter gene assay. Shh-LIGHT2 cells were treated with 2 µM purmorphamine and different concentrations of **5** or DMSO as a control for 48 h. Values obtained for firefly luciferase were divided by the respective *Renilla* values and data was normalized to the value of purmorphamine and DMSO treated samples, which was set to 100 %. Data are mean values of three biological replicates (N = 3, n = 3) ± SD. **C:** Luciferase activity assay. Lysates were treated with different concentrations of compound **5** or DMSO as a control for 1 h. Data were normalized to the value of samples that was treated with DMSO, which was set to 100 % and are mean values of three biological replicates (N = 3, n = 3) ± SD.

The GLI2/3-dependent reporter gene assay confirmed that compound **5,** which displayed an IC_{50} of 1.8 ± 0.1 µM, inhibits Hh signaling. The compound did not show any direct influence on firefly and Renilla luciferase activities (Figure 15C). To further validate and characterize **5** as a Hh pathway inhibitor, the influence on Hh target gene expression was evaluated by means of RT-qPCR (Figure 16).

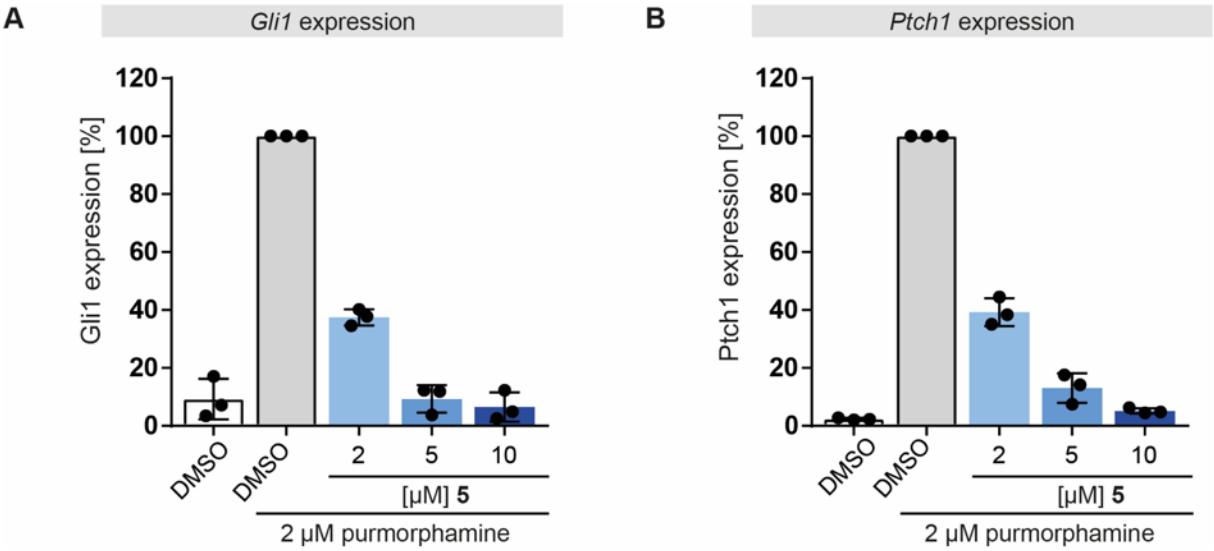

Figure 16: The 4-arylisoquionolone 5 inhibits Hh target gene expression. NIH-3T3 cells were treated with 2 µM purmorphamine and different concentrations of **5** or DMSO as a control for 48 h. For quantification of *Gli1* (**A**) and *Ptch1* (**B**) gene expression levels, RT-qPCR was performed with primers specific for *Gli1* and *Ptch1* as Hh target genes and *Gapdh* as a housekeeping gene. Data were normalized to values of samples that were treated with purmorphamine and DMSO (100 %) and are mean values of three biological replicates (N = 3, n = 3) ± SD.

Compound **5** dose-dependently inhibited *Gli1* (Figure 16A) and Ptch1 (Figure 16B) expression. In line with the result obtained from the GLI2/3-dependent reporter gene assay, the level of both target genes was reduced to a level of 40 % at a concentration of 2 µM. At a concentration of 10 µM the expression of both Hh target genes was reduced to the level of unstimulated cells.

5.2.1 4-Arylisoquinolone derivative does not bind to SMO

The ability of compound **5** to bind to the heptahelical bundle of SMO was evaluated by means of a BODIPY-cyclopamine displacement assay, as described in chapter 5.1.2. The corresponding results are shown in Figure 17. The microscopy images in Figure 17A show that compound 5 was not able to displace cyclopamine at a concentration of 20 µM. Quantification of the BODIPY fluorescence by means of flow cytometry confirmed this observation at a compound concentration of 30 µM. Thus, the 4-arylisoquinolone **5** does not bind to the heptahelical bundle of SMO and acts most likely independent of SMO.

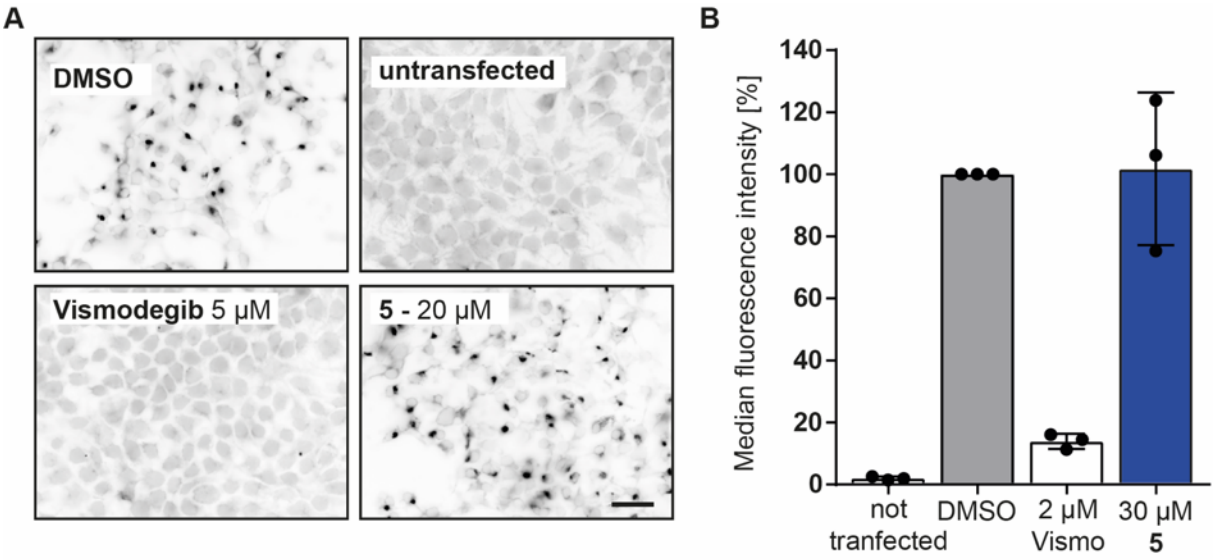

Figure 17: Compounds 5 does not bind to the heptahelical bundle of SMO. **A:** HEK293-T cells transiently transfected with a plasmid encoding for SMO were fixed and treated with 5 nM BODIPY-cyclopamine and 20 µM of compound **5** or 5 µM Vismodegib, or DMSO as a control for 4 h. BODIPY fluorescence was assessed by means of fluorescence microscopy. Images are representative for three biological replicates (n = 3). **B:** HEK293-T cells transiently transfected with a plasmid encoding for BFP-SMO were treated with 5 nM BODIPY-cyclopamine and 30 µM of compound **5**, 2 µM Vismodegib or DMSO as a control for 4 h. Fluorescence signals were detected by means of flow cytometry. Data were normalized to values of DMSO-treated samples (100 %) and are mean values of three biological replicates (n = 3).

Since compound **5** does not bind to the heptahelical bundle of SMO, the structure-activity relationship (SAR) of this compound class was explored to identify a site that would be suitable for attachment of a linker, to design a probe for subsequent target deconvolution. However, screening of a focused library of 20 derivatives in the Hh-dependent osteoblast differentiation assay (screening was done at COMAS) could not give any hints towards an SAR, since all derivatives had very similar IC_{50} values.

The results presented for compound **5** have contributed to the publication “C-H Bond Activation for the Synthesis of Heterocyclic Atropisomers Yields Novel Hedgehog Pathway Inhibitors” Shan *et al.* [94]

5.3 Identification of 8-oxotetrahydroprotoberberines as inhibitors of Hh-dependent osteogenesis

During a screening campaign at COMAS, 8-oxotetrahydroprotoberberine derivative **6** (Figure 18A) was identified as initial hit compound and potent inhibitor of Hh-induced osteoblast differentiation. This substance was synthesized by Dr. Zhijun Jia in the group of Prof. H. Waldmann at the MPI in Dortmund. Since no complete curve for determination of an IC_{50} value was obtained during the screening, the osteogenesis assay was repeated for this substance with more datapoints and higher fold-dilutions, to confirm the observed activity. The corresponding dose-response curve is shown in Figure 18B. Compound **6** inhibits Hh-dependent osteogenesis with an IC_{50} of 1.2 ± 0.4 nM.

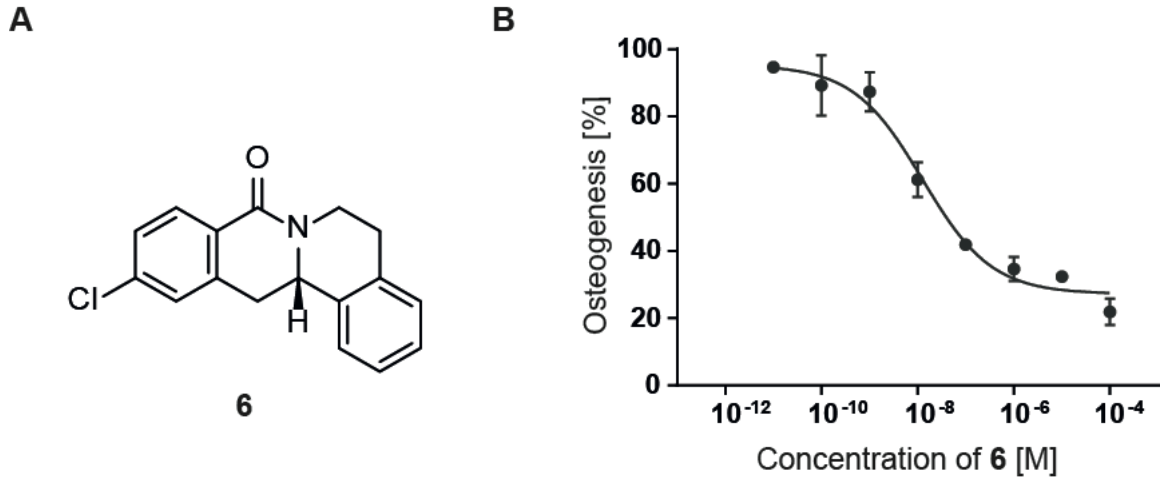

Figure 18: Identification of 8-oxotetrahydroprotoberin 6 as a potent inhibitor of Hh-dependent osteoblast differentiation. A: Chemical structure of compound **6**. **B:** Osteoblast differentiation assay. C3H10T1/2 cells were treated with 1.5 µM purmorphamine and different concentrations of compound **6** or DMSO as a control for 96 h. Data were normalized to values of samples that were treated with 1.5 µM purmorphamine and DMSO, which were set to 100 %. Data are mean values of three biological replicates (N = 3, n = 3) ± SD.

5.3.1 8-oxotetrahydroprotoberberin 6 does not inhibit Hh signaling

To confirm compound **6** as a Hh pathway inhibitor, this substance was evaluated in a GLI2/3-dependent reporter gene assay (Figure 19A). Surprisingly, compound **6** did not show any influence in this experiment. To further evaluate the influence of compound **6** on Hh signaling, RT-qPCR was performed to directly analyze Hh target gene expression. The corresponding results for *Ptch1* and *Gli1* are shown in Figure 19B.

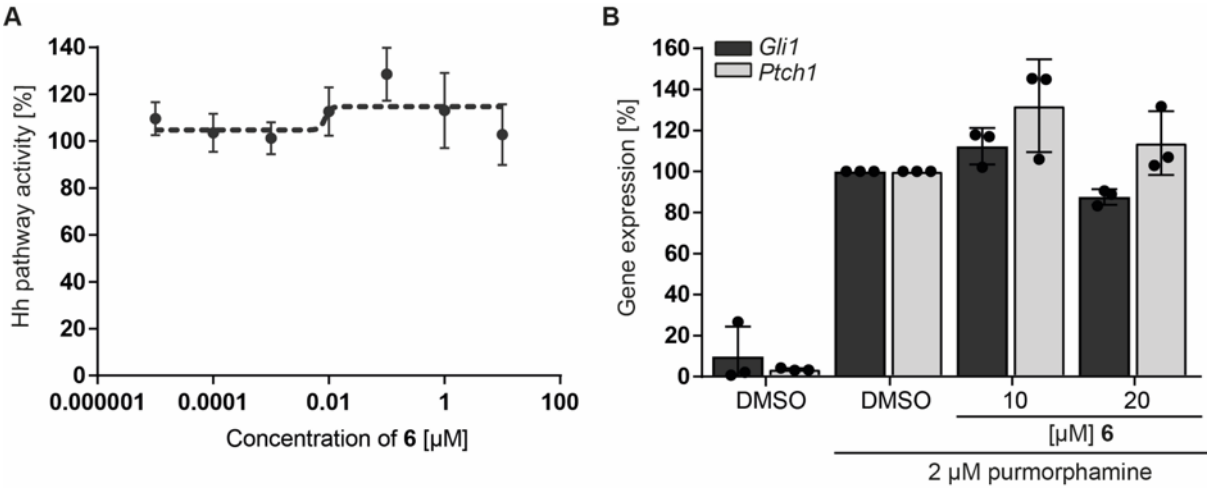

Figure 19: 8-oxotetrahydroprotoberin 6 does not inhibit canonical Hh signaling. A: GLI2/3-dependent reporter gene assay. Shh-LIGHT2 cells were treated with 2 µM purmorphamine and different concentrations of **6** or DMSO as a control for 48 h. Values obtained for firefly luciferase were divided by the respective *Renilla* values and data was normalized to purmorphamine and DMSO treated samples, which were set to 100 %. Data are mean values of three biological replicates (N = 3, n = 3) ± SD. **B:** Influence of **6** on Hh target gene expression. NIH-3T3 cells were treated with 2 µM purmorphamine and different concentrations of **6** or DMSO as a control for 48 h. For quantification of *Gli1* and *Ptch1* gene expression levels, RT-qPCR was performed with primers specific for *Gli1* and *Ptch1* as Hh target genes and *Gapdh* as housekeeping gene. Data were normalized to values of samples that were treated with purmorphamine and DMSO (100 %) and are mean values of three biological replicates (N = 3, n = 3) ± SD.

The gene expression analysis confirmed the results of the GLI2/3-dependent reporter gene assay. Even at a concentration of 20 µM, which is more than 16000-fold higher than the IC_{50} value obtained in the Hh-dependent osteoblast differentiation assay, no reduction of *Ptch1* and *Gli1* expression could be observed. Consequently, compound **6** does not inhibit canonical Hh signaling.

5.3.2 8-oxotetrahydroprotoberin 6 does not inhibit Wnt signaling

As described in chapter 2.4.2, several signaling pathways are involved in osteoblast differentiation besides Hh signaling.[70] Wnt signaling is known to crosstalk with Hh signaling and it acts downstream of Hh signaling during osteoblast differentiation.[75, 78] During Wnt signaling, T-cell factors/lymphoid enhancer factors (TCF/LEF) are the transcription factors that mediate the transcriptional responses of canonical Wnt signaling.[95] For this reason, the influence of compound **6** on canonical Wnt signaling was explored by means of a TCF/LEF-dependent reporter gene assay. The corresponding results in Figure 20A clearly show that compound **6** does not inhibit canonical Wnt signaling. An influence of compound **6** on the reporter gene assay readout was excluded by means of a luciferase activity assay (Figure 20B).

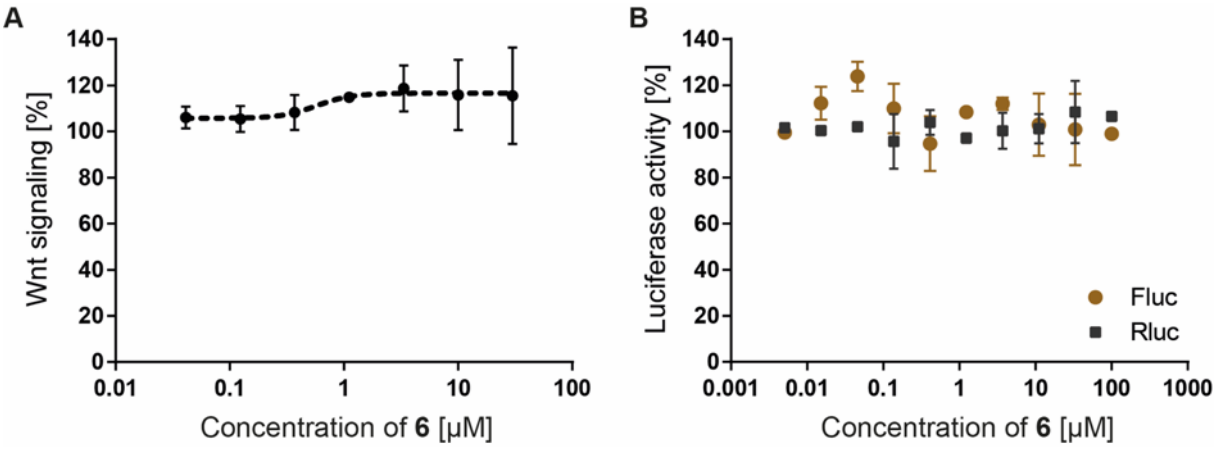

Figure 20: 8-oxotetrahydroprotoberin 6 does not inhibit canonical Wnt signaling. A: TCF/LEF-dependent reporter gene assay. HEK293-T cells were transiently transfected with plasmids encoding for a TCF/LEF-dependent firefly luciferase, constitutively expressed *Renilla* luciferase and Wnt-3A to activate Wnt signaling or an empty vector as a negative control. After 6 h, transfected cells were treated with different concentrations of compound **6** or DMSO as a control, for 24 h. Values obtained for firefly luciferase were divided by the respective *Renilla* values and data was normalized to values of Wnt-3A-expressing cells that were treated with DMSO (100 %). Data are mean values of three biological replicates (N = 3, n = 3) ± SD. **B:** Luciferase activity assay. Lysates of Fluc- or Rluc-expressing cells were treated with different concentrations of the compound **6** or DMSO as a control for 1 h. Data were normalized to values of samples that were treated with DMSO, which was set to 100 % and are mean values of three biological replicates (N = 3, n = 3) ± SD.

Since inhibition of canonical Hh and Wnt signaling was excluded for compound **6**, this compound could either modulate non-canonical Hh or Wnt signaling, or another pathway involved in osteoblast differentiation. Because of the potency of the compound, this natural-product inspired compound class and the molecular mechanisms that result in inhibition of Hh-dependent osteogenesis was explored in more detail.

5.3.3 Structure-activity relationship of 8-oxotetrahydroprotoberberines

Exploration of the structure-activity relationship (SAR) was enabled by Dr. Zhijun Jia and Dr. Saad Shaaban, who synthesized a focused library of 26 analogues of compound **6**. Compound **6**, which was initially synthesized by Dr. Zhijun Jia, was re-synthesized by Dr. Saad Shaaban and a library of derivatives with modifications at R^1 to R^5 was generated (Table 6). To study the SAR, all compounds were first tested at a single concentration of 10 µM in the Hh-dependent osteoblast differentiation assay and a CellTiter-Glo® assay to detect potential cytotoxic effects. 12 analogues inhibited Hh-dependent osteogenesis at least down to a level of 50 % while retaining a cell viability of at least 80 %. For these analogues, IC_{50} values were determined and summarized in Table 6. The corresponding dose-response curves are shown in Figure 21.

Table 6: Structure-activity relationship (SAR) of 8-oxotetrahydroprotoberberines in Hh dependent osteoblast differentiation. Compound activities were assessed via an Hh-dependent osteoblast differentiation assay using C3H10T1/2 cells. Cells were treated with 1.5 µM purmorphamine and different concentrations of the compounds or DMSO as a control for 96 h. Data were normalized to values of samples that were treated with 1.5 µM purmorphamine and DMSO, which were set to 100 %. Data are mean values of three biological replicates (N = 3, n = 3). IC_{50} values were determined for small molecules that inhibited osteogenesis at least down to a level of 50 % at a concentration of 10 µM without showing any toxic effects. Data are mean values ± SD (N = 3, n=3). Cmpd: compound. Via: Viability.

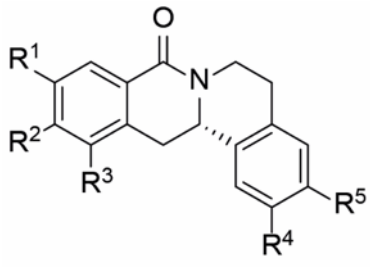

Entry	Cmpd No.	R^1	R^2	R^3	R^4	R^5	Stereo-center	Activity at 10 µM [%]	Via. at 10 µM [%]	IC_{50} ± SEM [nM]
1	**7**	H	H	H	H	H	S	100	103	-
2	**8**	H	*i*Pr	H	H	H	S	90.1	117	-
3	**9**	H	Me	H	H	H	S	93.2	101	-
4	**10**	H	OMe	H	H	H	S	114	92	-
5	**11**	H	F	H	H	H	S	61.2	101	-
6	**6**	H	Cl	H	H	H	S	30.4	96	1.2 ± 0.4
7	**12**	H	Br	H	H	H	S	44.2	91	4.2 ± 1.6
8	**13**	H	I	H	H	H	S	57.8	94	-
9	**14**	H	CF_3	H	H	H	S	33.1	94	0.7 ± 0.2
10	**15**	H	H	Cl	H	H	S	53.0	100	-
11	**16**	Cl	H	Cl	H	H	S	53.2	91	-
12	**17**	Cl	Cl	H	H	H	S	49.9	109	0.010 ± 0.002
13	**18**	Br	Cl	H	H	H	S	29.1	92	0.003 ± 0.001
14	**19**	I	Cl	H	H	H	S	30.7	115	0.004 ± 0.002
15	**20**	H	Cl	F	H	H	S	67.2	110	-
16	**21**	H	Cl	Cl	H	H	S	36.0	99	1.1 ± 0.3
17	**22**	H	Cl	Br	H	H	S	42.7	84	0.016 ± 0.008
18	**23**	H	Cl	I	H	H	S	39.0	97	0.074 ± 0.021
19	**24**	Br	Cl	Br	H	H	S	27.9	102	0.36 ± 0.24
20	**25**	Br	Cl	H	OMe	H	S	67.3	105	-
21	**26**	H	H	H	F	H	S	112	117	-
22	**27**	H	H	H	OMe	F	S	127	99	-
23	**28**	H	H	H	H	Cl	S	87	105	-
24	**29**	H	H	H	OMe	OMe	S	96.5	105	-
25	**30**	OMe	OMe	H	OMe	OMe	S	55.2	104	-
26	**31**	H	Cl	H	H	H	R	27.4	90	850 ± 420
27	**32**	Br	Cl	H	H	H	R	50.1	106	72.0 ± 41.0

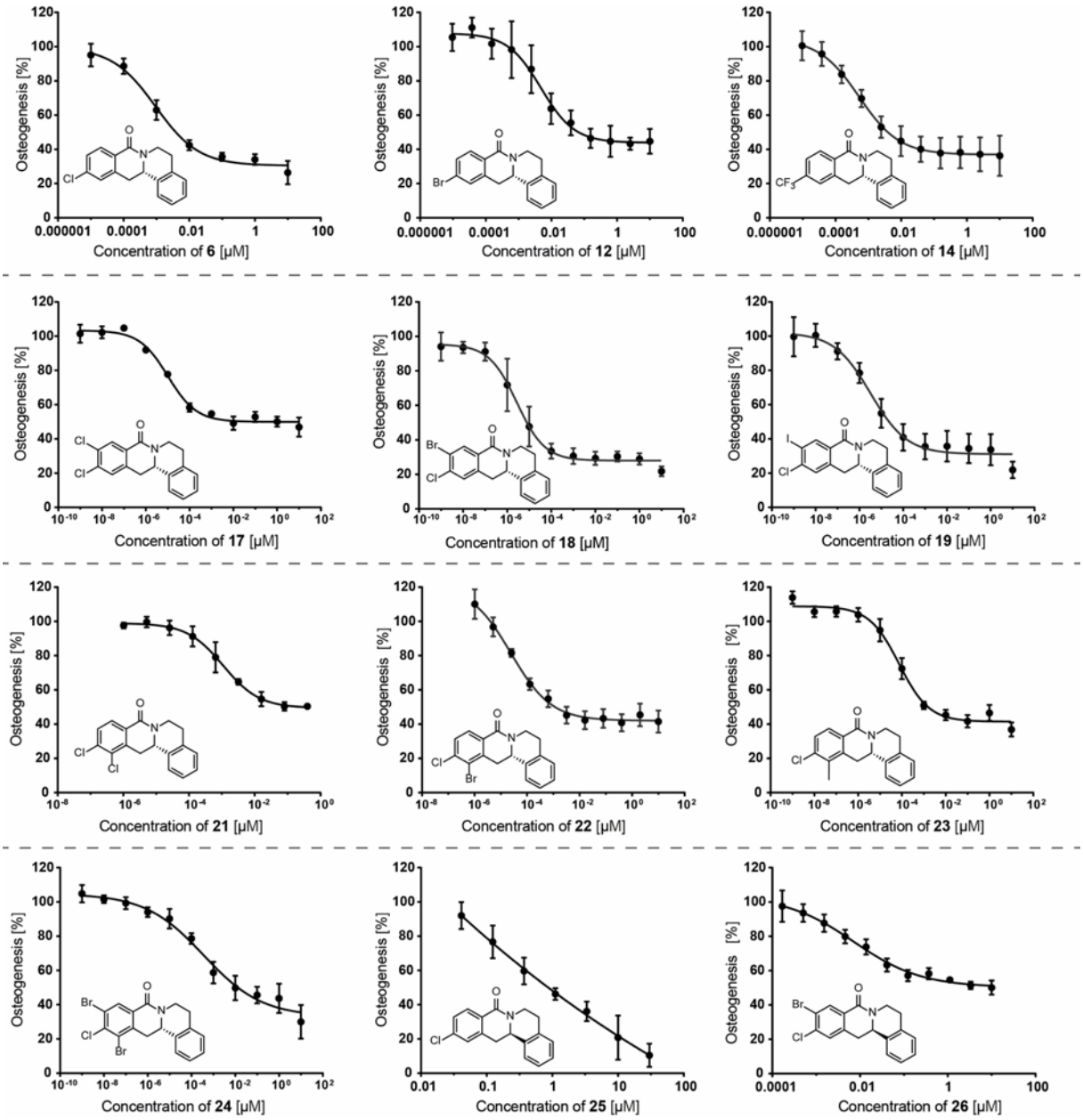

Figure 21: Structure activity relationship of 8-oxotetrahydroprotoberberines for Hh-dependent osteoblast differentiation. C3H10T1/2 cells were treated with 1.5 µM purmorphamine and different concentrations of the compound**s** or DMSO as a control for 96 h. Data were normalized to values of samples that were treated with 1.5 µM purmorphamine and DMSO, which were set to 100 %. Data are mean values of three biological replicates (N = 3, n ≥ 3).

Exploration of the focused library of 27 8-oxotetrahydroprotoberberines in the Hh-dependent osteoblast differentiation assay revealed that the presence of a halogen moiety at R^2 is essential for the biological activity (Table 6, entry 1 – 8). The unsubstituted as well as the iPr-, Me- or OMe-substituted derivatives (Table 6, entry 1 – 4) did not reduce alkaline phosphatase levels at a concentration of 10 µM. In contrast, all analogues with a halogen substitution at R^2 decreased alkaline phosphatase activity (Table 6, entry 5 – 8). While the

fluoro- and iodo-derivatized analogues only weakly inhibited osteogenesis at 10 µM to a level of 61.2 % and 57.3 %, respectively, the bromo-substituted analogue reduced alkaline phosphatase activity down to 44.2 % (Table 6, compare entry 5 and entry 8 to entry 7). Compared to the initial chloro-substituted hit compound **6**, which reduced osteogenesis down to a level of 30.4 % at 10 µM, the bromo-substituted analogue is slightly less potent (Table 6, compare entry 6 and entry 7). In line with this, the IC_{50} value of compound **12** of 4.2 ± 1.6 nM is higher than the IC_{50} value obtained for compound **6**. The CF_3-substituted derivative (Table 6, entry 9) showed similar activity as compound **6**. In summary these data reveal that for position R^2 both, the electronic properties and the size of the halogen moiety are important for biological activity. Addition of a halogen moiety in para-position is preferred over substitutions in the meta- and ortho-positions (Table 6, entry 10 and 11). With exception of fluoro-substitution at R^3, additional halogenation of the monochlorinated compound **6** at R^1 (Table 6, entry 12 – 14) or R^3 (Table 6, entry 15 – 18), strongly improved the potency. Although, additional halogenation at R^1 is preferred over R^3, in both cases IC_{50} values in the picomolar range were determined for all tested analogues. In both cases increasing the size of the substituent increased the compound potency. Compound **24** (Table 6, entry 19) with halogenation at R^1, R^2 and R^3 (Table 6, entry 19) reduced osteogenesis to a level of 27.9 %, with an IC_{50} of 0.36 ± 0.24 nM and was thus more potent than the initial hit compound **6**. However, it was not as potent as the double halogenated analogues. Modifications on the styrene side strongly reduced the biological activity (Table 6, entry 20 – 25). Finally, the configuration of the stereocenter proved to be important for bioactivity, since S enantiomers showed much higher potency compared to the respective *R* enantiomers (Table **6**, compare entry 6 with entry 26, entry 18 and entry 27).

In summary, the SAR study identified compound **18** (Table 6, entry 13) as the most potent analogue within the 8-oxotetrahydroprotoberberine library, with a single digit picomolar IC_{50} value of 3 ± 1 pM in the Hh-dependent osteogenesis assay. This analogue was termed Picoberin and was selected for all further investigations. The SAR study could not identify any position that was suitable for attachment of a linker, without compromising the activity. For this reason, all further investigations for target identification, validation and mode of action deconvolution were dependent on label-free approaches.

5.3.4 Characterization of Picoberin as inhibitor of Hh-dependent osteoblast differentiation

Picoberin (Figure 22A) inhibited both, purmorphamine and SHH-CM induced osteoblast differentiation down to levels of 29.1 % and 35.8 % with single-digit picomolar IC_{50} values of

3 ± 1 pM and 5.3 ± 2.4 pM, respectively (Figure 22B). To exclude any influence of Picoberin on the enzymatic activity of alkaline phosphatases and, thus, on the readout of the osteoblast differentiation assay, the compound was tested for direct inhibition of ALP (Figure 22C). For this purpose, alkaline phosphatase expressing C3H10T1/2 cells were lysed in presence of the compound and the CDP-Star substrate. This allows detection of reduced luminescence signals if the enzymatic activity is directly inhibited by the compound. However, Picoberin did not modulate the alkaline phosphatase enzymatic activity.

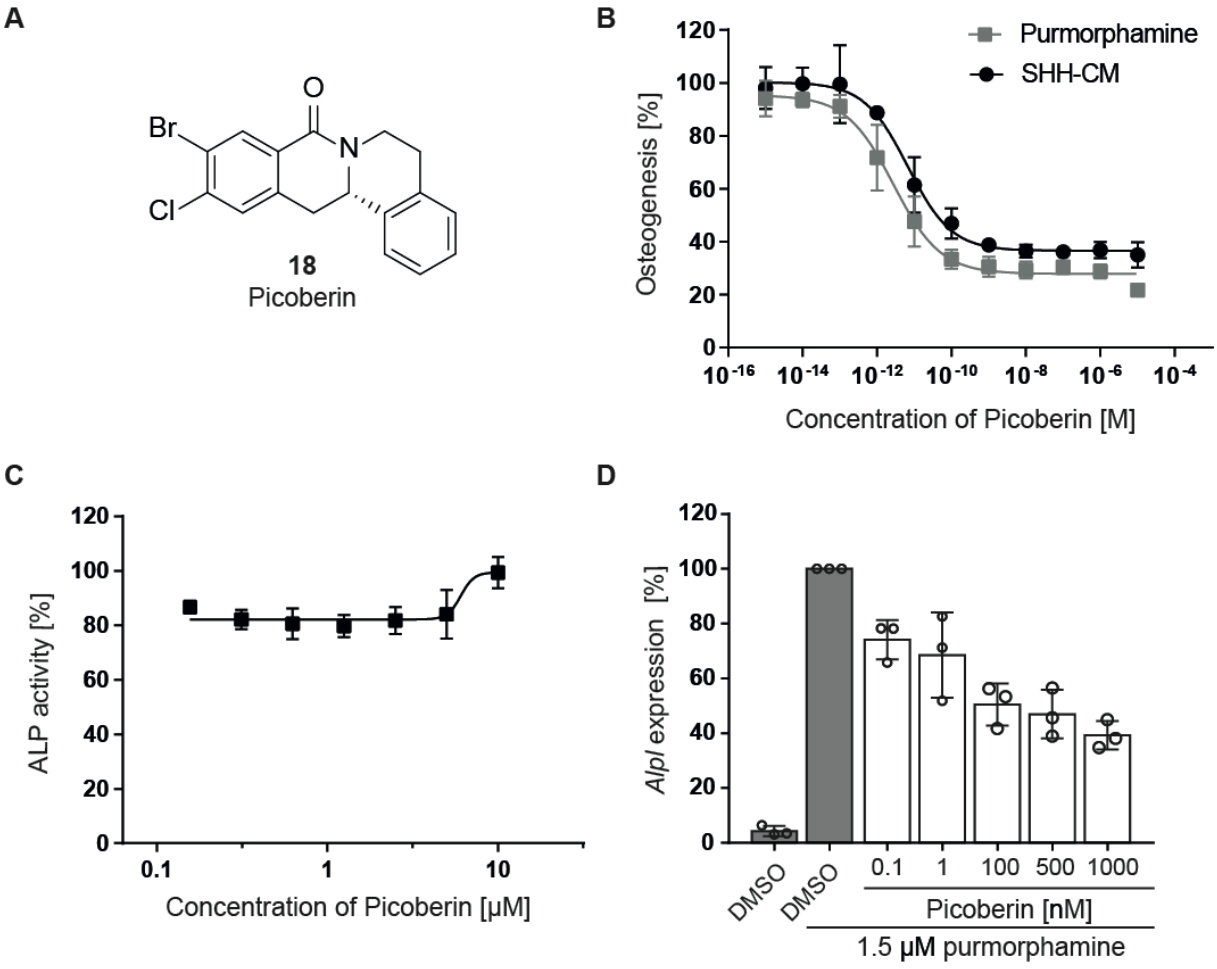

Figure 22: Identification of Picoberin as a highly potent inhibitor of Hh-dependent osteoblast differentiation. A: Chemical structure of compound **18** (Picoberin). **B:** Osteoblast differentiation assay. C3H10T1/2 cells were treated with 1.5 µM purmorphamine and different concentrations of Picoberin or DMSO as a control for 96 h. Data were normalized to values of samples that were treated with 1.5 µM purmorphamine and DMSO (100 %). **C:** Alkaline phosphatase activity assay. C3H10T1/2 cells were treated with 1.5 µM purmorphamine to enable expression of ALP. After 96 h, cells were lysed in presence of different concentrations of Picoberin or DMSO as a control for 1 h prior to assay readout. Data were normalized to values of samples that were treated with DMSO (100 %). **D:** *Alpl* gene expression. C3H10T1/2 cells were treated with 1.5 µM purmorphamine or DMSO and different concentrations of Picoberin or DMSO as a control for 96 h. For quantification of *Alpl* gene expression, RT-qPCR was performed with primers specific for *Alpl* and *Gapdh* and *Ap3d1* as housekeeping genes. Data were normalized to values of samples that were treated with purmorphamine and DMSO (100 %). All data are mean values of three biological replicates (N = 3, n = 3) ± SD.

To further evaluate the influence of Picoberin on osteoblast differentiation, RT-qPCR was performed to directly analyze the effect on *Alpl* gene expression (Figure 22D). Picoberin inhibited *Alpl* gene expression in a dose-dependent manner. In line with the results obtained in the osteoblast differentiation assay, residual *Alpl* expression of 39 ± 4.2 % was observed at a concentration of 1 µM. At a concentration of 100 pM Picoberin inhibited *Alpl* expression down to a level of 74 ± 5.8 %. Although the effect of Picoberin is less pronounced on mRNA level compared to the observations in the Hh-dependent osteoblast differentiation assay, these data clearly show that Picoberin acts at picomolar concentrations. Since ALP is an early marker for osteoblast differentiation[96], these data confirm that Picoberin inhibits early stages of Hh-induced osteogenesis.

A matrix mineralization assay was employed to evaluate the influence of Picoberin on late stages of osteoblast differentiation. In this experiment Alizarin Red S is used to detect calcium deposits which are incorporated into the extracellular matrix of mature osteoblasts. Calcium ions are chelated by Alizarin Red S, resulting in a bright red colored complex. Representative images are shown in Figure 23.

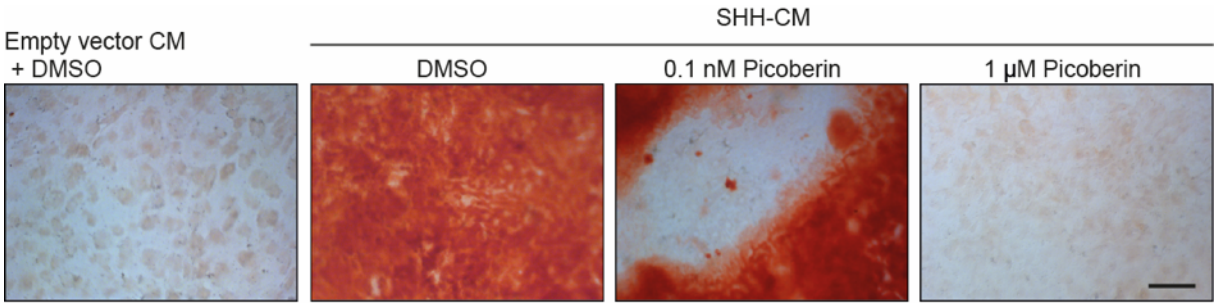

Figure 23: Picoberin inhibits matrix mineralization. C3H10T1/2 cells were treated with SHH-CM containing 10 mM glycerol phosphate and 50 µg/mL L-ascorbic acid-2-phosphate and different concentrations of Picoberin or DMSO as a control. As a negative control, cells were treated with empty vector CM containing 50 mM glycerol phosphate and L-ascorbic acid and DMSO. After 21 days, cells were fixed, and extracellular matrix was stained using Alizarin Red S. Images are representative of three biological replicates (n = 3).

Cultivation of C3H10T1/2 cells in SHH-conditioned medium (SHH-CM) containing 10 mM β-glycerophosphate and 50 µg/mL L-ascorbic acid-2-phosphate clearly induced matrix mineralization after 21 days, as cells clearly displayed a bright red staining upon incubation with Alizarin Red S. In contrast, Alizarin Red S did not stain cells that were treated with empty vector conditioned medium containing β-glycerophosphate and L-ascorbic acid-2-phosphate. For cells that were treated with SHH-CM containing β-glycerophosphate, L-ascorbic acid-2-phosphate and 1 µM Picoberin, no red staining was observed. Picoberin was thus able to completely inhibit matrix mineralization at this concentration. At a concentration of 100 pM

Picoberin only partially inhibited matrix formation. While some areas of the cell monolayer were clearly stained in red, others did not show any staining. These data confirm that Picoberin inhibits also late stages of osteoblast differentiation in a dose-dependent manner.

5.3.4.1 Picoberin does not influence cell growth

The influence of Picoberin on C3H10T1/2 cell growth was explored, to exclude any cytotoxic effects that could potentially cause the reduced ALP activity observed in the Hh-dependent osteoblast differentiation assay. *This experiment was performed by Britta Schulte as part of her master thesis.* The obtained results are shown in Figure 24.

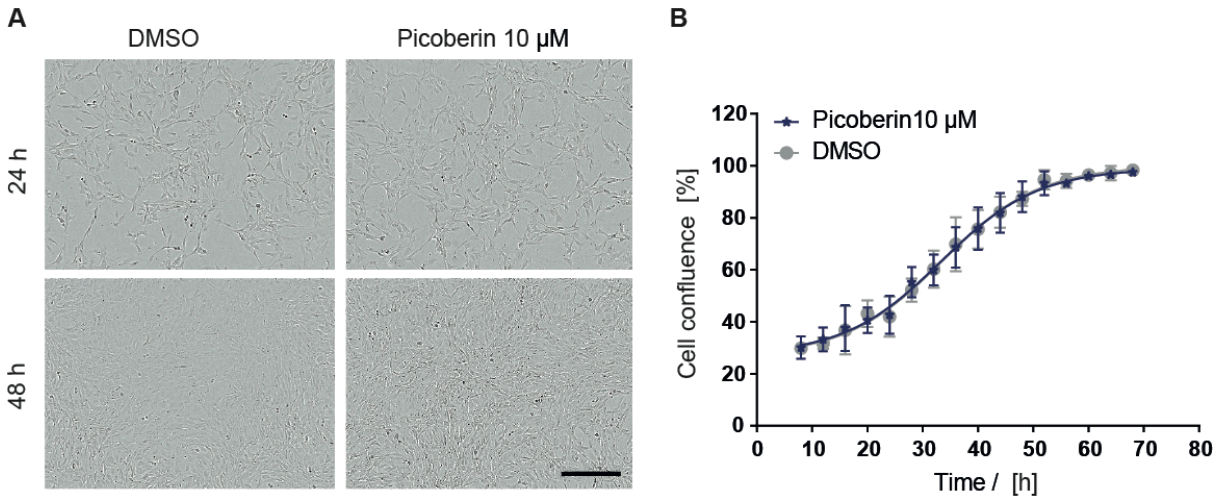

Figure 24: Picoberin does not inhibit cell growth of C3H10T1/2 cells. C3H10T1/2 cells were treated with 10 µM Picoberin of DMSO as a control for 72 h. Cell confluence as a readout for cell growth was monitored over time, using the live cell imaging system IncuCyte Zoom. **A:** Representative images of C3H10T1/2 cells after 24 h and 48 h of Picoberin or DMSO treatment. **B:** Growth curves for DMSO or Picoberin treated cells. Data are mean values of three biological replicates (N = 3, n = 3) ± SD.

Picoberin did not show any obvious effects on C3H10T1/2 cell morphology (Figure 24A). Even at a concentration of 10 µM, which is more than $1x10^6$-times higher than the IC_{50} value obtained in the osteoblast differentiation assay, the compound did not impair C3H10T1/2 cell growth (Figure 24B). Thus, cytotoxic effects of Picoberin during Hh-dependent osteoblast differentiation were excluded.

5.3.4.2 Picoberin does not inhibit canonical Hh signaling

To evaluate if Picoberin is a Hh pathway inhibitor, the influence of this substance was investigated in a GLI2/3-dependent reporter gene assay and a luciferase activity assay as described before. In line with the observations made for the initial hit compound **6**, Picoberin

did not inhibit GLI2/3-dependent reporter activity in Shh-LIGHT2 cells (Figure 25A). Direct effects of Picoberin on the luciferase assay readout were excluded (Figure 25B).

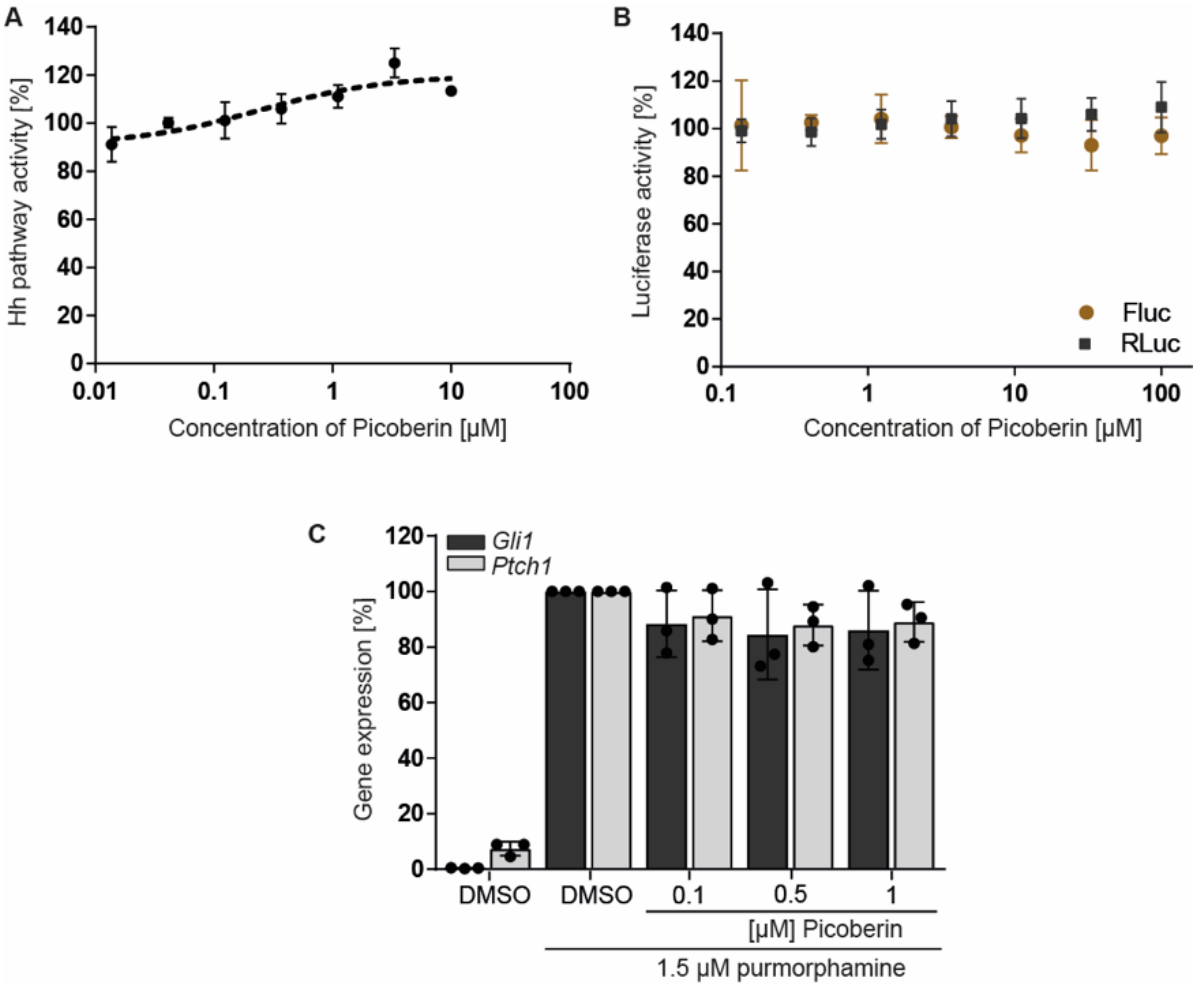

Figure 25: Picoberin does not inhibit Hh signaling. A: GLI2/3-dependent reporter gene assay. Shh-LIGHT2 cells were treated with 2 µM purmorphamine and different concentrations of Picoberin or DMSO as a control for 48 h. Values obtained for firefly luciferase were divided by the respective *Renilla* luciferase values and data was normalized to purmorphamine and DMSO treated samples, which were set to 100 %. Data are mean values of three biological replicates (N = 3, n = 3) ± SD. **B:** Luciferase activity assay. Lysates were treated with different concentrations of Picoberin or DMSO as a control for 1 h. Data were normalized to values of samples that were treated with DMSO, which were set to 100 %. **C:** Influence of Picoberin on Hh target gene expression. C3H10T1/2 cells were treated with 1.5 µM purmorphamine and different concentrations of Picoberin or DMSO as a control for 48 h. For quantification of *Gli1* and *Ptch1* gene expression, RT-qPCR was performed with primers specific for *Gli1* and *Ptch1* as Hh target genes and *Gapdh* and *Ap3d1* as housekeeping genes. Data were normalized to values of samples that were treated with purmorphamine and DMSO (100 %) and are mean values of three biological replicates (N = 3, n = 3) ± SD.

To explore if Picoberin inhibits Hh signaling in C3H10T1/2 cells, the influence on Hh target gene expression was explored in these cells. The corresponding results for *Ptch1* and *Gli1* are shown in Figure 25C. The obtained data confirm the results of the GLI2/3-dependent reporter gene assay: Even at a concentration of 1 µM, which is more than $1x10^5$-fold higher than the

IC_{50} value obtained in the Hh-dependent osteoblast differentiation assay, no reduction of *Ptch1* and *Gli1* expression could be observed in C3H10T1/2 cells. Consequently, Picoberin does not inhibit Hh-induced osteogenesis via suppression of canonical Hh signaling.

5.3.4.3 Picoberin does not inhibit Wnt- and TGFβ signaling

Besides Hh signaling, several other pathways are involved in the regulation of osteoblast differentiation.[70, 76] As described above (see chapter 5.3.2), the influence of Picoberin on canonical Wnt signaling was explored by means of a TCF/LEF-dependent reporter gene assay. The corresponding results show that Picoberin does not inhibit canonical Wnt signaling (Figure 26A).

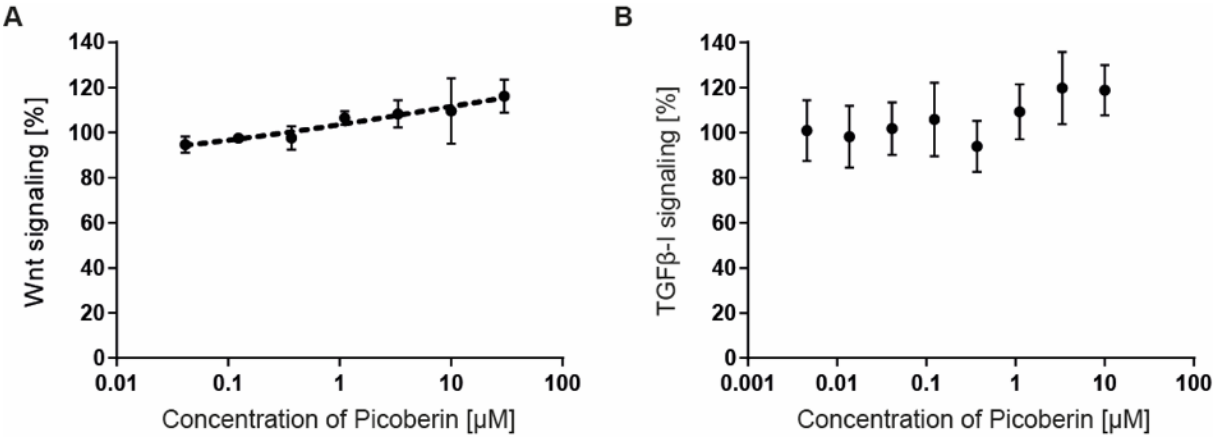

Figure 26: Picoberin does not inhibit Wnt- and TGFβ signaling. A: TCF/LEF-dependent reporter gene assay. HEK293-T cells were transiently transfected with plasmids encoding for a TCF/LEF-dependent firefly luciferase, constitutively expressed *Renilla* luciferase and Wnt-3A to activate Wnt signaling or an empty vector as a negative control. After 6 h, transfected cells were treated with different concentrations of Picoberin or DMSO as a control, for 24 h. Values obtained for firefly luciferase were divided by the respective *Renilla* values and data was normalized to values of Wnt-3A expressing cells that were treated with DMSO (100 %). **B:** SBE4-dependent reporter gene assay. HEK293-T cells were transiently transfected with plasmids encoding for a SBE4-dependent firefly luciferase and constitutively expressed *Renilla* luciferase After 24 h, transfected cells were treated with 20 ng/mL TGFβ-I and different concentrations of Picoberin or DMSO as a control, for 24 h. Values obtained for firefly luciferase were divided by the respective *Renilla* values and data was normalized to values of cells that were treated with TGFβ-I and DMSO (100 %). Data are mean values of three biological replicates (N = 3, n = 3) ± SD.

As described in chapter 2.4.2, also TGFβ signaling influences osteoblast differentiation.[97] A Smad binding element 4 (SBE4)-dependent reporter gene assay was employed to evaluate the effect of Picoberin on Smad-dependent TGFβ signaling. However, the corresponding results show that Picoberin does not modulate canonical TGFβ signaling (Figure 26B).

5.3.4.4 Picoberin inhibits Wnt-3A induced osteogenesis

Although Hh signaling acts upstream of Wnt signaling during osteoblast differentiation, Wnt-3A is reported to induce osteoblast differentiation in C3H10T1/2 cells.[98] To explore this, C3H10T1/2 cells were treated with Wnt-3A conditioned medium and alkaline phosphatase activity was assessed after 4 and 12 days. In line with literature reports, Wnt-3A induced osteoblast differentiation after 12 days (Figure 27A).[98] However, while activation of Hh signaling significantly upregulates alkaline phosphatase activity after 4 days, Wnt-3A conditioned medium did only show a minimal effect at this timepoint. To evaluate whether Picoberin specifically inhibits Hh-induced osteoblast differentiation, or osteoblast differentiation induced by other signaling pathways, the influence of Picoberin on Wnt-3A-induced osteogenesis was explored after 12 days (Figure 27B).

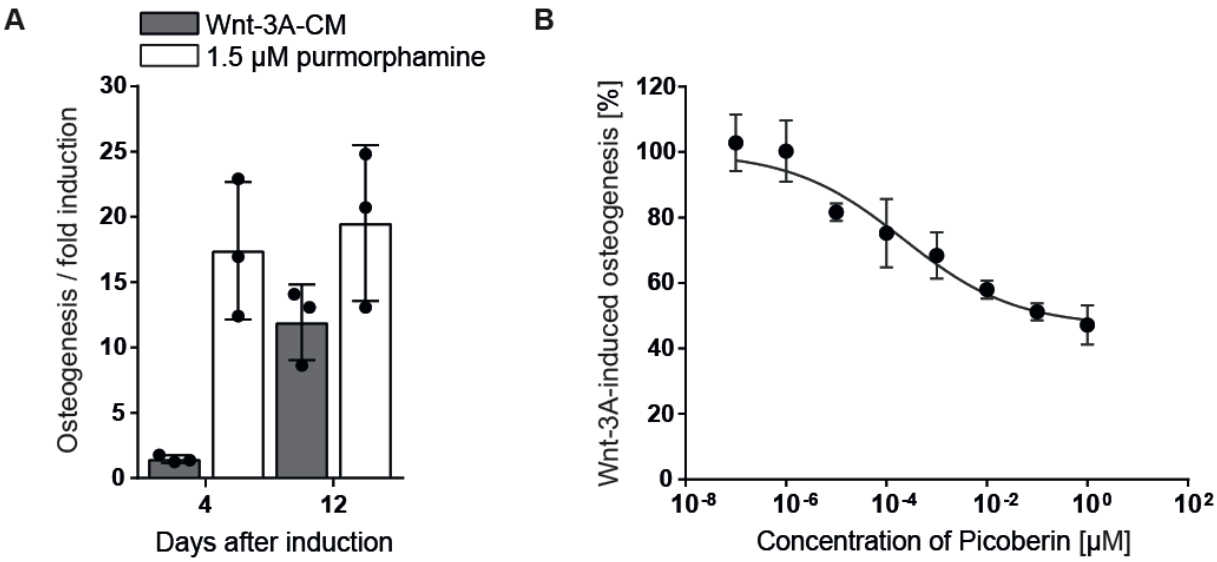

Figure 27: Influence of Picoberin on Wnt-3A-induced osteogenesis. A: C3H10T1/2 cells were treated with Wnt-3A-conditioned medium (Wnt-3A-CM) or control medium, or with 1.5 µM purmorphamine or DMSO for 4 or 12 days. Alkaline phosphatase levels were determined by means of a chemiluminescence measurement and values of all samples were related to the values of samples that were treated with control medium (which were set to 1). **B:** C3H10T1/2 cells were treated with WCM and different concentrations of Picoberin or DMSO as a control for 12 days. The activity of alkaline phosphatase was determined and values of WCM / DMSO-treated samples were set to 100 %.

Picoberin partially inhibited Wnt-3A-induced osteoblast differentiation of C3H10T1/2 cells with an IC_{50} of 890 ± 64 pM and down to a level of 47.2 ± 4.9 % at a concentration of 1 µM. Thus, Picoberin may not exclusively inhibit Hh-dependent osteogenesis. However, since crosstalk between Hh and Wnt signaling is reported, regulation of Hh signaling cannot be excluded in this assay setup.[99]

5.3.4.5 Picoberin does not inhibit BMP4 induced osteogenesis

To explore the effect of Picoberin on BMP4 induced osteoblast differentiation, the compound was tested in a BMP4-dependent osteogenesis assay in C2C12 *cells by Dr. Fabian Wesseler.* C2C12 cells are murine myoblasts that differentiate into osteoblasts upon exposure to BMPs, such as BMP4.[100] Osteogenesis was induced by addition of 10 ng/mL BMP4. In analogy to the Hh-dependent osteoblast differentiation assay with C3H10T1/2 cells, the differentiation status of the C2C12 cells was assessed via detection of alkaline phosphatase activity as osteogenesis marker. The results in Figure 28A show, that Picoberin does not influence BMP4 induced differentiation of C2C12 cells.

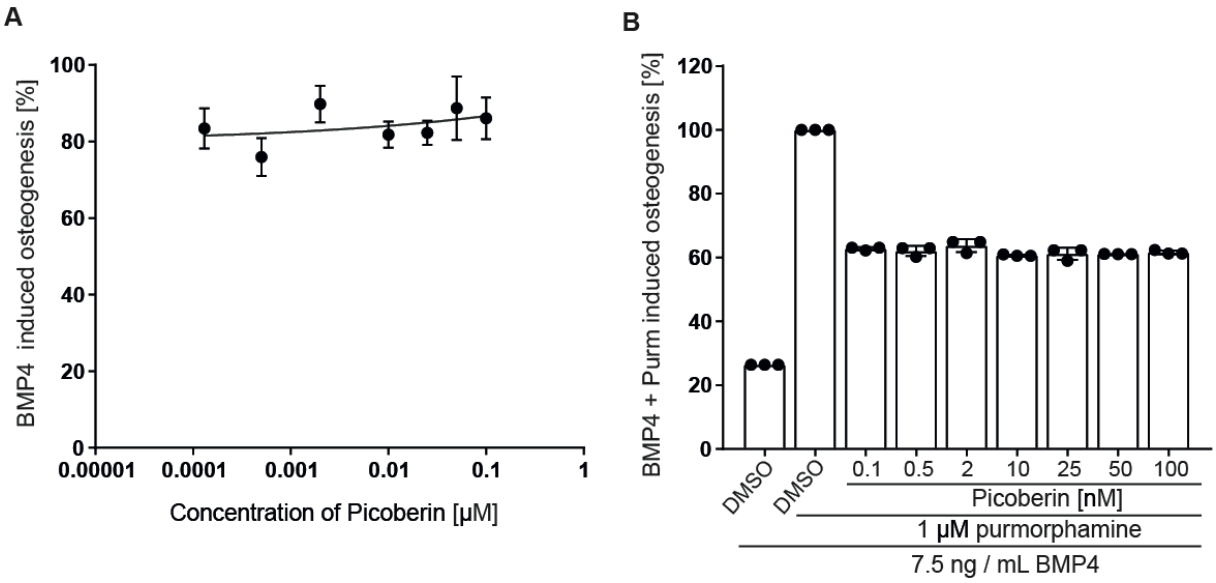

Figure 28: Influence of Picoberin on BMP4 induced osteoblast differentiation of C2C12 cells. A: C2C12 cells were treated with 7.5 ng/mL BMP4 and different concentrations of Picoberin or DMSO as a control. After 72h ALP activities were detected and all values were related to values obtained for cells treated with 7.5 ng/mL BMP4 and DMSO, which were set to 100 %. **B:** C2C12 cells were treated with 7.5 ng/mL BMP4, 1 µM purmorphamine and different concentrations of Picoberin or DMSO as a control for 72h. Values were related to values obtained for cells that were treated with 7.5 ng/mL BMP4, 1 µM purmorphamine and DMSO, which were set to 100 %. All data are mean values of three biological replicates and three technical replicates per biological replicate (N = 3, n = 3).

Interestingly, simultaneous treatment of C2C12 cells with 10 ng/mL BMP4 and 1 µM purmorphamine enhanced osteoblast differentiation compared to treatment with BMP4 only. Moreover, Picoberin partially inhibited alkaline phosphatase activity induced by BMP4 and purmorphamine, to a level of 60 % at concentrations ranging from 100 nM to 100 pM (Figure 28B). These data clearly show, that Picoberin inhibits BMP4 and purmorphamine induced osteogenesis at picomolar concentrations. Furthermore, these data suggest that BMP4 and purmorphamine may act independently during osteogenesis in C2C12 cells, and that Picoberin interferes with purmorphamine-induced signaling cascades but not with BMP4-induced signaling during osteoblast differentiation of C2C12 cells.

5.4 Identification of the molecular target of Picoberin

5.4.1 Target identification via computational target prediction

To obtain an initial hint towards a possible molecular target of Picoberin, computational target prediction was carried out, using the web-based tool *Similarity Ensemble Approach* (SEA).[101] This tool compares the structure of a query compound to the structures of annotated compounds with known molecular targets. Based on structural similarity, the software calculates probabilities for potential target proteins. The top 20 identified potential targets with the highest confidence scores are listed in Table 7.

Table 7: Target identification via similarity ensemble approach (SEA). Top 20 most probable targets that were identified based on the structure of Picoberin.

No.	Target Key	Target name	Description	p-value
1	5HT3B_MOUSE	Htr3b	5-hydroxytryptamine receptor 3B	1.884e-36
2	DRD1_RAT	Drd1	D(1A) dopamine receptor	6.655e-24
3	G9IP65_HCMV	US28	G protein coupled receptor	4.441e-15
4	5HT3B_HUMAN	HTR3B	5-hydroxytryptamine receptor 3B	7.438e-15
5	KEAP1_HUMAN	KEAP1	Kelch-like ECH-associated protein 1	5.588e-13
6	Q962Y6_SCHMA	TGR	Thioredoxin glutathione reductase	8.685e-12
7	RAD51_HUMAN	RAD51	DNA repair protein RAD51 homology 1	1.447e-11
8	US28_HCMVA	US28	G protein coupled receptor homologue US28	1.105e-10
9	DRD1_MOUSE	Drd1	D(1A) dopamine receptor	1.186e-10
10	DRD1_HUMAN	DRD1	D(1A) dopamine receptor	2.968e-10
11	DRD5_HUMAN	DRD5	D(1B) dopamine receptor	1.68e-08
12	SC6A2_MOUSE	Slc6a2	Sodium-dependent noradrenaline transporter	3.996e-08
13	HRH1_RAT	Hrh1	Histamine H1 receptor	6.093e-08
14	5HT2B_HUMAN	HTR2B	5-hydroxytryptamine receptor 2B	1.737e-07
15	TS1R2_HUMAN	TAS1R2	Taste receptor type 1 member 2	3.454e-07
16	OPRX_HUMAN	OPRL1	Nociceptin receptor	9.529e-07
17	DRD2_RAT	Drd2	D(2) dopamine receptor	9.69e-07
18	SC6A3_MOUSE	Slc6a3	Sodium-dependent dopamine transporter	1.451e-06
19	TS1R3_HUMAN	TAS1R3	Taste receptor type 1 member 3	1.572e-06
20	5HT2C_HUMAN	HTR2C	5-hydroxytryptamine receptor 2C	7.87e-06

Examination of the hit list in Table 7 showed that 15 of the 20 most probable identified proteins are G protein-coupled receptors (GPCRs). In particular, dopamine receptors and serotonin receptors were over-represented in the list. Thus, Picoberin could potentially target a dopamine or serotonin receptor or another GPCR.

5.4.1.1 Influence of Picoberin on GPCRs

G protein-coupled receptors build a large family of transmembrane proteins that are involved in numerous biological processes, including bone development and remodeling.[80] They play important roles in both, physiological and pathological processes. Since GPCR ligand binding domains are easily accessible and bind a diverse range of small molecules, they comprise one of the most important class of drug targets.[80] Moreover, several GPCRs are modulated by ligands at ultra-low concentrations in the picomolar to attomolar range.[102] To explore if Picoberin could target a GPCR, the compound was tested at a concentration of 500 nM in a cell-based GPCR panel including 157 different GPCRs in agonist and antagonist mode. The obtained results are summarized in Table 8. GPCRs whose activity was affected at least 30 % in agonist mode or at least 50 % inhibition in antagonist mode were considered as significantly modulated.

Table 8: Influence of Picoberin on GPCR activities. Picoberin was tested at a concentration of 500 nM in a GPCR panel (GPCR MAX panel, Eurofins DiscoverX) by means of a cell-based β-arrestin enzyme fragment complementation (EFC) assays in agonist and antagonist mode. Values calculated for % activity (% Activ.) as the % activity relative to the baseline (0 % activity) and max (100 % activity) values. Values indicated for % inhibition (% Inhib.) were calculated relative to the vehicle treated control (0 % inhibition) and basal (100 % inhibition) values.

GPCR	% Activ.	% Inhib.	GPCR	% Activ.	% Inhib.	GPCR	% Activ.	% Inhib.
ADCYAP1R1	2%	8%	DRD1	-1%	3%	MC4R	-1%	4%
ADORA3	-3%	-10%	DRD2L	1%	-9%	MC5R	-3%	-4%
ADRA1B	-2%	13%	DRD2S	-1%	-5%	MCHR1	-1%	5%
ADRA2A	-1%	8%	DRD3	8%	-3%	MCHR2	-1%	-2%
ADRA2B	-11%	15%	DRD4	-9%	-10%	MLNR	0%	3%
ADRA2C	4%	-13%	DRD5	-1%	-12%	MRGPRX1	0%	12%
ADRB1	-4%	2%	EBI2	1%	-15%	MRGPRX2	0%	-3%
ADRB2	0%	-12%	EDG1	1%	25%	MTNR1A	-3%	9%
AGTR1	1%	4%	EDG3	-2%	6%	NMBR	-4%	8%
AGTRL1	-1%	-4%	EDG4	7%	-13%	NMU1R	1%	-7%
AVPR1A	-1%	1%	EDG5	-1%	-1%	NPBWR1	1%	-17%
AVPR1B	-2%	-3%	EDG6	-7%	-44%	NPBWR2	-1%	8%
AVPR2	0%	3%	EDG7	-2%	19%	NPFFR1	2%	25%
BDKRB1	-2%	-7%	EDNRA	1%	-2%	NPSR1B	-6%	-1%
BDKRB2	0%	6%	EDNRB	0%	0%	NPY1R	5%	3%
BRS3	3%	11%	F2R	-2%	10%	NPY2R	0%	1%
C3AR1	0%	5%	F2RL1	0%	-4%	NTSR1	0%	0%
C5AR1	1%	-8%	F2RL3	-3%	5%	OPRD1	-1%	-1%
C5L2	9%	-20%	FFAR1	14%	15%	OPRK1	-3%	10%
CALCR	-2%	6%	FPR1	-2%	-20%	OPRL1	-1%	1%
CALCRL-RAMP1	0%	5%	FPRL1	0%	6%	OPRM1	1%	-3%
CALCRL-RAMP2	2%	5%	FSHR	0%	6%	OXER1	-4%	4%
CALCRL-RAMP3	1%	1%	GALR1	0%	1%	OXTR	0%	3%
CALCR-RAMP2	0%	9%	GALR2	-1%	4%	P2RY1	0%	-11%
CALCR-RAMP3	0%	-4%	GCGR	1%	15%	P2RY11	-5%	6%
CCKAR	-1%	-6%	GHSR	-3%	3%	P2RY12	2%	-10%
CCKBR	-1%	-10%	GIPR	-2%	0%	P2RY2	2%	-3%
CCR10	-1%	-3%	GLP1R	0%	2%	P2RY4	-4%	7%
CCR1	-3%	9%	GLP2R	0%	-1%	P2RY6	0%	-8%
CCR2	0%	10%	GPR1	0%	-5%	PPYR1	-1%	13%

GPCR	% Activ.	% Inhib.	GPCR	% Activ.	% Inhib.	GPCR	% Activ.	% Inhib.
CCR3	-4%	2%	GPR103	-4%	-18%	PRLHR	1%	26%
CCR4	0%	8%	GPR109A	-3%	6%	PROKR1	0%	8%
CCR5	1%	-1%	GPR109B	-1%	4%	PROKR2	-1%	28%
CCR6	-1%	3%	GPR119	2%	-8%	PTAFR	-2%	11%
CCR7	1%	4%	GPR120	-2%	14%	PTGER2	1%	10%
CCR8	0%	1%	GPR35	0%	17%	PTGER3	-3%	-6%
CCR9	0%	-18%	GPR92	1%	2%	PTGER4	4%	11%
CHRM1	-1%	20%	GRPR	0%	-4%	PTGFR	0%	-11%
CHRM2	0%	3%	HCRTR1	0%	-7%	PTGIR	-5%	-1%
CHRM3	2%	-1%	HCRTR2	0%	1%	PTHR1	0%	9%
CHRM4	-11%	-10%	HRH1	-3%	-8%	PTHR2	0%	6%
CHRM5	5%	-2%	HRH2	-5%	-8%	RXFP3	-3%	21%
CMKLR1	0%	10%	HRH3	-7%	-3%	SCTR	0%	2%
CNR1	0%	-5%	HRH4	-1%	-6%	SSTR1	-12%	6%
CNR2	-28%	24%	HTR1A	-2%	3%	SSTR2	0%	-11%
CRHR1	0%	6%	HTR1B	0%	7%	SSTR3	-1%	2%
CRHR2	0%	2%	HTR1E	2%	-12%	SSTR5	-4%	-2%
CRTH2	-1%	1%	HTR1F	1%	-1%	TACR1	-1%	1%
CX3CR1	-1%	7%	HTR2A	1%	5%	TACR2	0%	17%
CXCR1	0%	2%	HTR2C	2%	-3%	TACR3	0%	11%
CXCR2	-3%	5%	HTR5A	0%	10%	TBXA2R	-3%	8%
CXCR3	-4%	9%	KISS1R	0%	3%	TRHR	-1%	5%
CXCR4	0%	52%	LHCGR	-1%	4%	TSHR(L)	-2%	4%
CXCR5	1%	5%	LTB4R	0%	6%	UTR2	-7%	-3%
CXCR6	1%	-2%	MC1R	-3%	19%	VIPR1	0%	-3%
CXCR7	-1%	-9%	MC3R	-1%	0%	VIPR2	-1%	8%

The results in Table 8 show that only one GPCR, the C-X-C chemokine receptor type 4 (CXCR4) was inhibited by Picoberin at a concentration of 500 nM. To validate this result, Picoberin was dose-dependently tested in a CXCR4 cells-based antagonist mode calcium flux assay at Eurofins DiscoverX. The obtained results are shown in Figure 29. The inhibition of CXCR4 by Picoberin observed in the β-arrestin assay could not be validated.

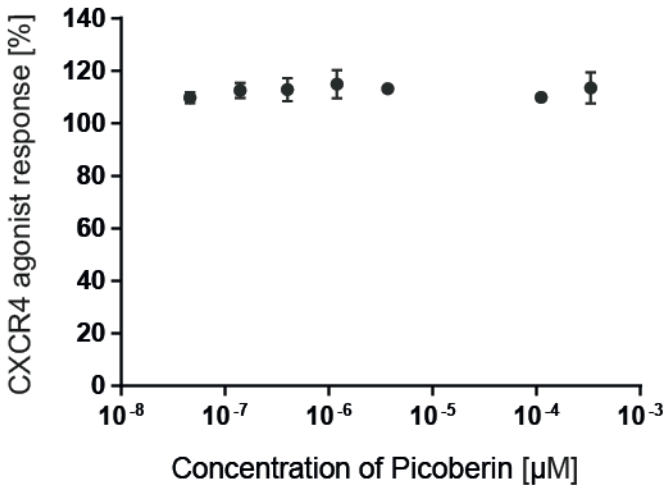

Figure 29: Influence of Picoberin on CXCR4 activity. Human CXCR4 cell-based antagonist calcium flux assay performed by Eurofins DiscoverX. Data are mean values of two biological replicates (n = 2).

5.4.1.2 Influence of Picoberin on nuclear receptors

Several nuclear receptors (NRs), including estrogen receptors and androgen receptors are involved in osteoblast differentiation.[103-105] Highly potent ligands for such receptors are reported in literature[106-108] and, thus, it was guessed that Picoberin may target a nuclear receptor. To explore potential effects of Picoberin on nuclear receptors, the compound was evaluated in a NR panel including 19 different receptors. The corresponding results are shown in Table 9.

Table 9: Influence of Picoberin nuclear receptors. Picoberin was tested at a concentration of 500 nM in a nuclear receptor panel (nhr MAX panel, Eurofins DiscoverX) by means of cell-based nuclear hormone receptor assays in agonist and antagonist mode. Values calculated for % efficacy (agonist) are relative to the baseline (0 % efficacy) and max (100 % efficacy) values. Values indicated for % efficacy (antagonist) were calculated relative to the vehicle treated control (0 % efficacy) and basal (100 % efficacy) values.

Nuclear receptor	% Efficacy Agonist	% Efficacy Antagonist
AR	0.9	13.5
Era	-0.6	-28.2
FXR	1.1	-10.9
GR	-0.1	16.6
LXRa	-0.5	-3.3
LXRb	-2.7	11.6
LXRB-NCOR1	7.7	-4.6
MR	2.1	1.2
PPARa	4	-23
PPARd	2.5	-14.5
PPARg	-2.4	-4.1
Pra	-6	-21.8
PRb	-0.3	-0.4
RARa	-4	19.7
RARb	-14	15.7
RXRa	-2.8	7.2
RXRg	-21 7	34.5
THRa	7.3	-6.9
THRb	4.8	7.8

NRs that were modulated by Picoberin by at least 30 % in agonist mode or at least 50 % in antagonist mode were considered to be modulated. At a concentration of 500 nM Picoberin none of the NRs was modulated to this extent and therefore, Picoberin does not directly target any of these NRs.

5.4.2 Target identification via global transcriptome profiling

Since computational target predictions and scientifically informed guesses did not lead to the identification of the molecular target of Picoberin during Hh-induced osteoblast differentiation, other approaches for target identification were required. However, since no suitable site for attachment of a linker could be identified during the SAR studies, classical approaches such as affinity-based target enrichment was not possible in this case. For this reason, the differential effects of Picoberin on the transcriptome of C3H10T1/2 were investigated in a time-resolved manner, using RNA-Seq. Although this method does not detect direct interactions of Picoberin with potential target proteins, it is a highly powerful approach to explore cellular responses to compound treatment. Consequently, this approach can provide insights into the mode of action of Picoberin and could thereby indirectly hint towards potential molecular targets. To investigate modulation of global gene expression, C3H10T1/2 cells were treated with purmorphamine and DMSO, purmorphamine and 1 nM Picoberin or only with DMSO for 24 h, 48 h, 96 h and 7 days.

5.4.2.1 Purmorphamine treatment activates Hh signaling in C3H10T1/2 cells

To evaluate influences of Picoberin on Hh-dependent osteogenesis, it was first required to explore the gene expression profile of cells that were treated with purmorphamine and DMSO compared to only DMSO (Figure 30). All significantly regulated genes for each timepoint are listed in the appendix (Supplementary Table 1-4).

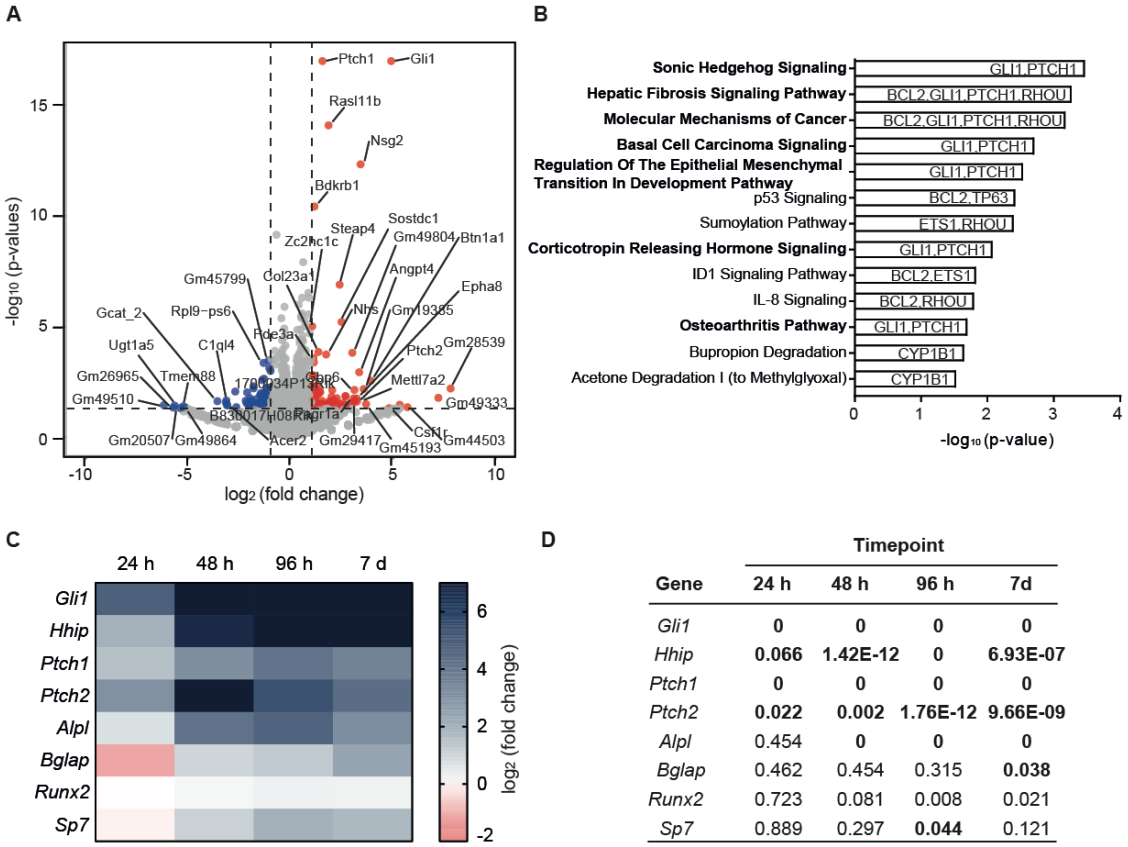

Gene	Timepoint 24 h	48 h	96 h	7d
Gli1	**0**	**0**	**0**	**0**
Hhip	**0.066**	**1.42E-12**	**0**	**6.93E-07**
Ptch1	**0**	**0**	**0**	**0**
Ptch2	**0.022**	**0.002**	**1.76E-12**	**9.66E-09**
Alpl	0.454	**0**	**0**	**0**
Bglap	0.462	0.454	0.315	**0.038**
Runx2	0.723	0.081	0.008	0.021
Sp7	0.889	0.297	**0.044**	0.121

Figure 30: Activation of Hh signaling in C3H10T1/2 cells upon treatment with purmorphamine. C3H10T1/2 cells were treated with 1.5 µM purmorphamine or DMSO as a control. Total RNA was isolated after 24 h, 48 h, 96 h or 7 days and samples were subjected to Illumina sequencing to quantify global gene expression levels. **A:** Volcano plot of samples treated with 1.5 µM purmorphamine and DMSO compared to samples treated with DMSO for 24 h. Blue dots: significantly upregulated genes. Red dots: significantly down-regulated genes. **B:** Pathway over-representation analysis using Ingenuity Pathway Analysis (IPA) for samples that were treated with 1.5 µM purmorphamine compared to samples treated with DMSO for 24 h. Pathways regulated by the Hh signaling are marked in bold. Regulated genes detected in the transcriptome sequencing and assigned to the pathways are displayed in the respective bars. **C** and **D:** Heatmap of fold changes (**C**) and p-values (**D**) of Hh target genes and osteogenesis markers in cells that were treated for the indicated time with 1.5 µM purmorphamine compared to DMSO.

Figure 30A shows a volcano plot for samples that were treated with 1.5 µM purmorphamine and DMSO compared to samples that were treated with only DMSO for 24 h. The Hh target genes *Ptch1* and *Gli1* are the two most significantly upregulated genes and confirm activation of Hh signaling upon treatment of C3H10T1/2 cells with purmorphamine. In line with this, pathway over-representation analysis identified Hh signaling as the most significantly regulated pathway at this timepoint (Figure 30B). The heatmap in Figure 30C and the corresponding p-values listed in Figure 30D clearly show an increase in the expression of the Hh target genes *Gli1*, *Hhip*, *Ptch1* and *Ptch2* as well as the osteogenesis marker genes *Alpl, Sp7* (encoding for osterix, OSX) and *Bglap* (encoding for osteocalcin, OCN) over time. Taken together these data confirm that Hh signaling was activated in C3H10T1/2 cells by treatment with purmorphamine and that this induces osteoblast differentiation.

5.4.2.2 Evaluation of Picoberin during Hh-induced osteogenesis

To explore the influence of Picoberin on global gene expression during osteoblast differentiation, the gene expression profiles of samples that were treated with 1.5 µM purmorphamine and 1 nM Picoberin were compared to the gene expression profiles after treatment of cells with 1.5 µM purmorphamine and DMSO. To obtain an overview about most significantly up- and down regulated genes, volcano plots were generated for each of the four timepoints (see Figure 31).

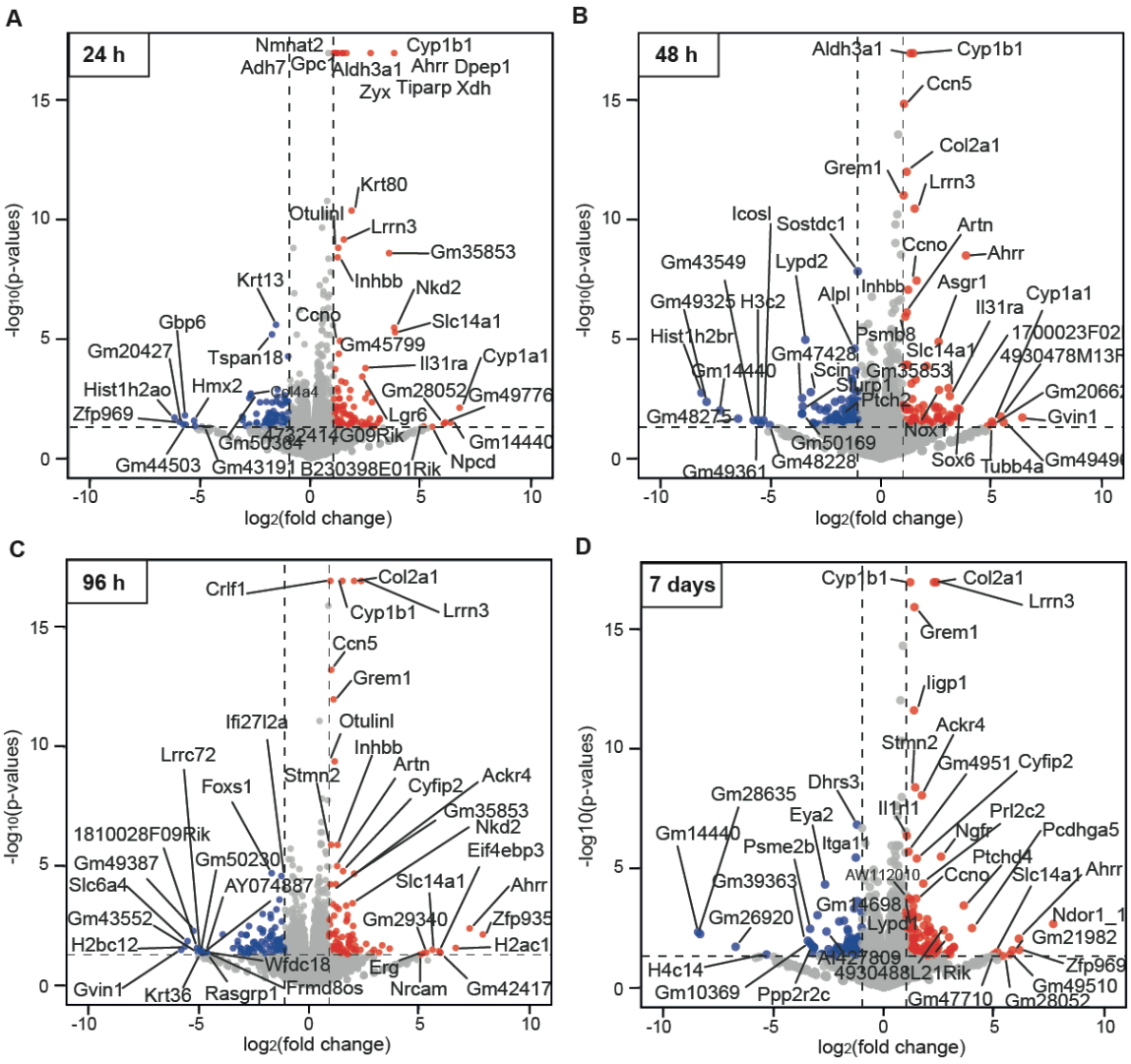

Figure 31: Influence of Picoberin on gene expression in C3H10T1/2 cells. RNA-Seq data. Volcano plots for samples treated with 1.5 µM purmorphamine and 1 nM Picoberin compared to samples treated with 1.5 µM purmorphamine and DMSO. C3H10T1/2 cells were treated with 1.5 µM purmorphamine and 1 nM Picoberin or DMSO as a control. Total mRNA was isolated after 24 h (**A**), 48 h (**B**), 96 h (**C**) or 7 days (**D**) and samples were subjected to Illumina sequencing to quantify global gene expression levels. Values of samples treated with 1.5 µM purmorphamine and 1 nM Picoberin are compared to values of samples treated with 1.5 µM purmorphamine and DMSO. Red dots: significantly upregulated genes. Blue dots: significantly down-regulated genes. The top 40 most significantly regulated genes are labelled in the plots. Complete lists of all significantly regulated genes can be found in the appendix (Supplementary Table 5 - 8). Data are mean values of three biological replicates (n = 3).

After 24 h, 48 h, 96 h and 7 days 175, 163, 117 and 199 genes were identified respectively, to be significantly (p-value < 0.05) up- or down regulated with a fold change of at least 2, upon Picoberin treatment. For a better overview, only the top 40 most significantly regulated genes are labelled in the volcano plots in Figure 31. The complete lists with all significantly regulated genes can be found in the appendix (Supplementary Table 5 - 8).

After 24 h Picoberin most significantly upregulated genes encoding for several phase I and II metabolic enzymes, including *Cyp1b1*, *Aldh3a1*, *Adh7*, *Nqo1*, *Xdh, Cyp1a1* and *Tiparp* (Figure 31A). Interestingly, *Cyp1b1* gene levels remained among the most significantly up-regulated genes at all timepoints. In line with observations made for Picoberin in the Hh-dependent osteogenesis assay and gene expression analysis, *Alpl* was found among the most significantly down-regulated genes after 48 h (Figure 31B). Furthermore, *Sostdc1*, which is regulated by Hh and Wnt signaling during osteoblast differentiation[109, 110], was significantly downregulated at this timepoint. Interestingly, also the mRNA levels of *Ptch2*, an isoform of the Hh target gene *Ptch1* was significantly decreased. However, in line with initial results, other Hh target genes including *Gli1*, *Gli2* and *Ptch1* were not regulated by Picoberin, again confirming that canonical Hh signaling is not regulated by this compound. After 48 h (Figure **31**B), *Ahrr* gene levels were strongly upregulated in cells treated with purmorphamine and 1 nM Picoberin and the level remained significantly higher in these samples compared to purmorphamine and DMSO treated samples after 96 h and 7 days (Figure 31C and D). The same temporal behavior was observed for several other genes, including *Col2a1*, *Lrrn3* and *Grem1*.

To identify signaling pathways that are affected by Picoberin, a pathway-overrepresentation analysis was performed using the Ingenuity Pathway Analysis (IPA) software (QIAGEN Digital Insights). The top 10 most significantly enriched pathways that were identified by the software are summarized in Figure 32.

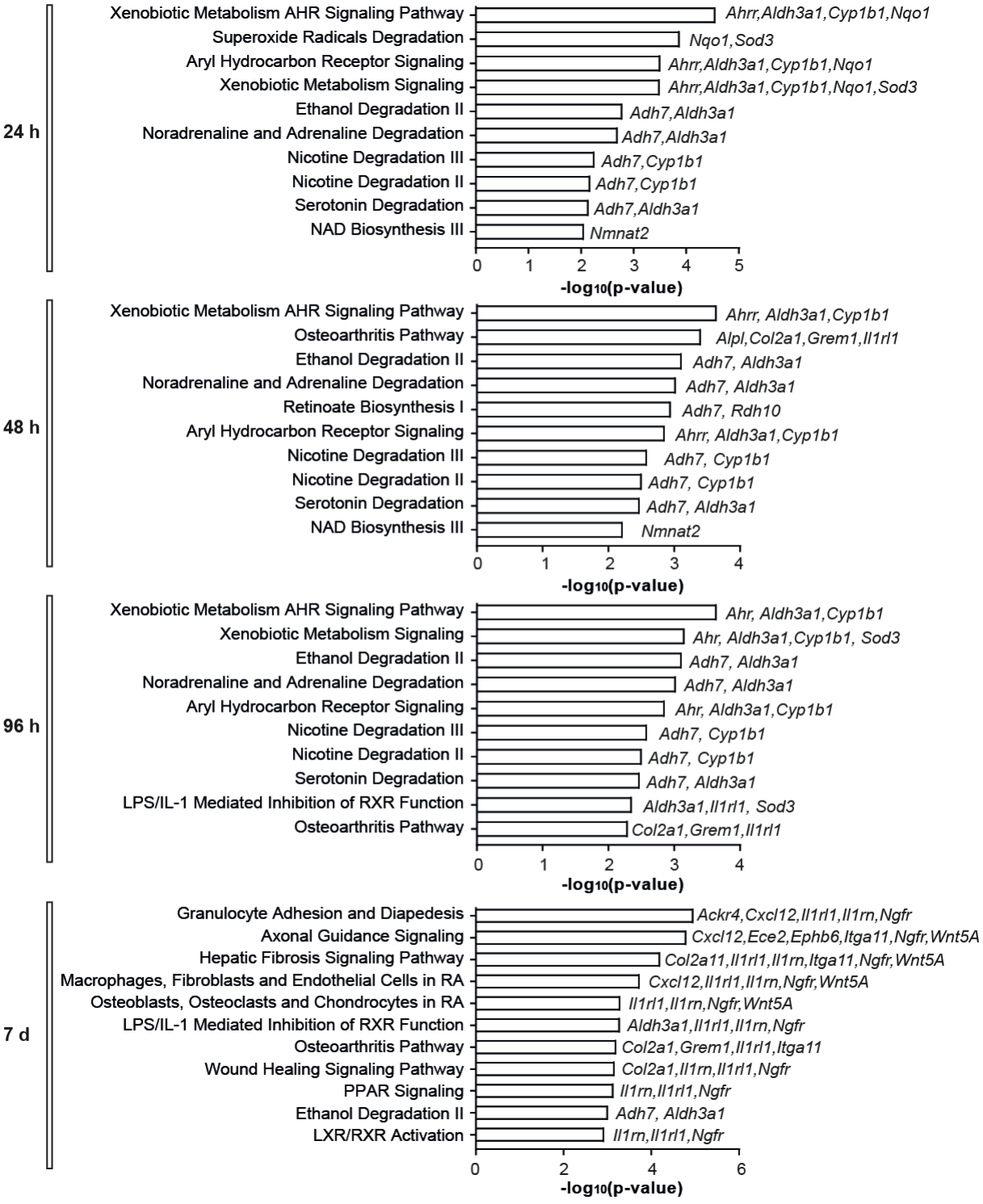

Figure 32: Influence of Picoberin on gene expression during osteoblast differentiation of C3H10T1/2 cells. Pathway over-representation analysis of RNA-Seq data using Ingenuity Pathway Analysis. C3H10T1/2 cells were treated with 1.5 µM purmorphamine and 1 nM Picoberin or DMSO as a control. Total mRNA was isolated after 24 h, 48 h, 96 h or 7 days and samples were subjected to Illumina sequencing to quantify global gene expression levels. Graphs show the top 10 pathways that are over-represented in samples that were treated with 1.5 µM purmorphamine and 1 nM Picoberin compared to samples treated with 1.5 µM purmorphamine and DMSO for the indicated timepoints. Differentially expressed genes that contribute to pathway enrichment are indicated next to the respective bar in the graphs.

Pathway over-representation analysis linked the observed enrichment of phase I and II metabolic enzymes to several cellular degradation processes, such as ethanol and nicotine degradation, and to Aryl hydrocarbon Receptor (AhR) signaling. *Cyp1b1*, *Aldh3a1*, *Adh7*, *Nqo1*, *Xdh, Cyp1a1* and *Tiparp* are AhR target genes, that are upregulated upon activation of this ligand-activated transcription factor.[111, 112] Consequently, AhR is a potential target of Picoberin. To illustrate the influence of Picoberin on AhR and Hh signaling in more detail, a heatmap of samples treated with 1.5 µM purmorphamine and 1 nM Picoberin compared to samples treated with 1.5 µM purmorphamine and DMSO was generated (Figure 33). The corresponding $\log_2$(fold change) values and the p-values are listed in Table 10.

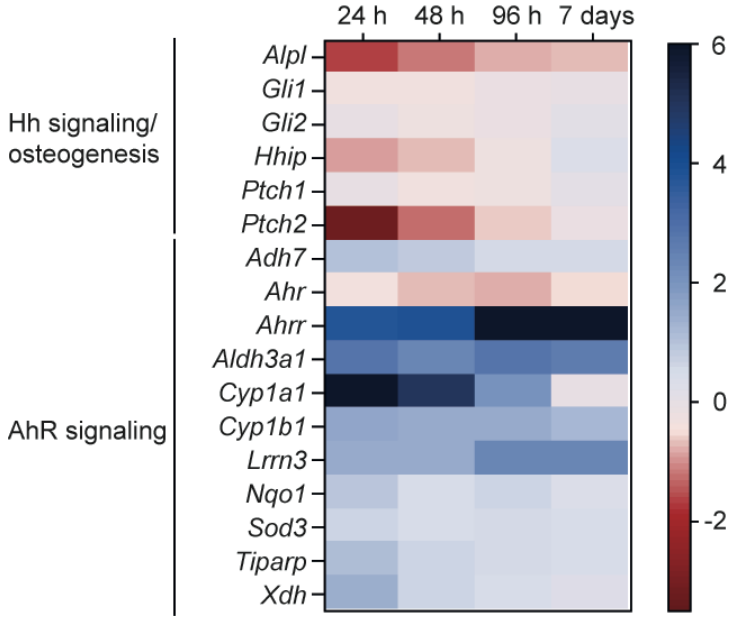

Figure 33: Time-resolved influence of Picoberin on the expression of genes involved in Hh and AhR signaling. RNA-Seq data. Heatmap for samples treated with 1.5 µM purmorphamine and 1 nM Picoberin compared to samples treated with 1.5 µM purmorphamine and DMSO. C3H10T1/2 cells were treated with 1.5 µM purmorphamine and 1 nM Picoberin or DMSO as a control for 24 h, 48 h, 96 h or 7 days. Samples were subjected to Illumina sequencing to quantify global gene expression levels. Values of samples treated with 1.5 µM purmorphamine and 1 nM Picoberin are compared to values of samples treated with 1.5 µM purmorphamine and DMSO. Red color: negative $\log_2$ fold changes (FC). Blue: Positive $\log_2$(FC). Data are mean values of three biological replicates (n = 3).

As observed during the initial experiments, Picoberin did not influence the expression of Hh target genes *Gli1, Gli2* and *Ptch1,* suggesting that this substance does not act as a canonical Hh pathway inhibitor. Interestingly, the expression of the *Ptch1* homologue *Ptch2* was significantly downregulated at early timepoints, e.g., 24 h and 48 h. Moreover, the Hh target gene *Hhip* was slightly reduced after 24 h and 48 h, however this was only significant after 48 h. The effects observed for *Ptch2* expression could hint towards a potential role of non-canonical Hh signaling during Picoberin-mediated inhibition of Hh-induced osteoblast differentiation.[113]

Several AhR target genes, including *Adh7, Cyp1a1, Nqo1, Tiparp* and *Xdh* are upregulated by 1 nM Picoberin after 24 h, however, their expression decreases over time. In contrast, expression of AhR regulated genes *Ahrr*, *Aldh3a1*, *Cyp1b1* and *Lrrn3* are constantly upregulated over time or get even further upregulated after 96 h and 7 days. The expression of *AhR* itself is slightly downregulated in Picoberin treated samples at all explored timepoints. Together with the observed upregulation of the negative regulator *Ahrr*, this could hint towards a negative feedback mechanism in AhR signaling.

Table 10: Time-resolved influence of Picoberin on the expression of genes involved in Hh and AhR signaling. NGS data. Calculated log_2 fold changes (FC) for samples treated with 1.5 µM purmorphamine and 1 nM Picoberin compared to samples treated with 1.5 µM purmorphamine and DMSO for 24 h, 48 h, 96 h or 7 days. Data are mean values of three biological replicates (n = 3). Significant values are depicted in bold.

Gene	24h Log_2 (FC)	24h p-value	48h Log_2 (FC)	48h p-value	96h Log_2 (FC)	96h p-value	7d Log_2 (FC)	7d p-value
Alpl	-1.639	1.45E-01	**-1.191**	**2.55E-05**	**-0.760**	**3.31E-03**	-0.722	7.39E-03
Gli1	-0.334	7.10E-02	-0.356	4.49E-02	-0.129	4.63E-01	-0.050	7.83E-01
Gli2	0.007	9.64E-01	-0.207	1.77E-01	-0.084	5.81E-01	0.157	3.33E-01
Hhip	-0.868	2.89E-01	**-0.678**	**3.33E-03**	-0.200	3.06E-01	0.369	5.90E-02
Ptch1	-0.036	8.27E-01	-0.331	4.15E-02	-0.197	2.23E-01	0.017	9.19E-01
Ptch2	-3.132	1.93E-02	**-1.264**	**4.93E-03**	-0.607	8.58E-02	-0.089	8.17E-01
Adh7	**1.000**	**0**	**0.784**	**2.59E-14**	**0.580**	**1.40E-08**	**0.567**	**2.57E-08**
Ahr	-0.428	1.22E-02	**-0.651**	**2.16E-04**	**-0.749**	**8.79E-06**	-0.488	6.53E-03
Ahrr	**3.752**	**5.62E-13**	**3.862**	**3.11E-09**	**7.278**	**3.94E-03**	6.116	9.32E-03
Aldh3a1	**2.863**	**0**	**2.345**	**0**	**2.809**	**0**	**2.658**	**0**
Cyp1a1	**6.719**	**7.90E-03**	5.037	2.95E-02	2.083	1.35E-01	-0.017	9.96E-01
Cyp1b1	**1.586**	**0**	**1.468**	**0**	**1.505**	**0**	**1.191**	**0**
Lrrn3	**1.467**	**6.77E-10**	**1.534**	**3.36E-11**	**2.362**	**0**	**2.379**	**0**
Nqo1	**0.872**	**1.57E-08**	0.428	5.68E-03	**0.594**	**1.27E-04**	**0.368**	1.69E-02
Sod3	**0.671**	**7.76E-11**	**0.476**	**3.85E-06**	**0.550**	**1.35E-07**	**0.490**	**1.97E-06**
Tiparp	**1.142**	**0**	**0.659**	**9.31E-10**	**0.519**	**1.24E-06**	**0.402**	**1.68E-04**
Xdh	**1.402**	**0**	**0.639**	**5.58E-07**	**0.423**	**4.26E-04**	**0.214**	7.00E-02

In summary, the global transcriptome profiling data led to the identification of AhR as a potential protein target of Picoberin during Hh-induced osteoblast differentiation.

5.4.3 Target identification via global proteome profiling

As a second approach for target identification and to obtain a more holistic view on the effects of Picoberin during Hh-induced osteoblast differentiation, time-resolved global proteome profiling was performed (see 4.2.1.19). For this purpose, C3H10T1/2 cells were treated with

1.5 µM purmorphamine and DMSO, 1.5 µM purmorphamine and 1 nM Picoberin or only with DMSO for 0 h, 24 h, 48 h, 96 h or 7 days. The collected proteins were reduced, alkylated and digested by trypsin. The obtained peptides were labelled with tandem mass tags for subsequent quantification via nanoHPLC-MS/MS analysis. To explore effects that were induced by Picoberin, the protein levels of samples that were treated with 1.5 µM purmorphamine and 1 nM Picoberin were compared to the protein levels of samples that were treated with 1.5 µM purmorphamine and DMSO. To obtain an overview about most significantly up- and down regulated proteins at each timepoint, volcano plots were generated and the top 20 most significantly ($p < 0.05$) regulated proteins were labelled (Figure 34).

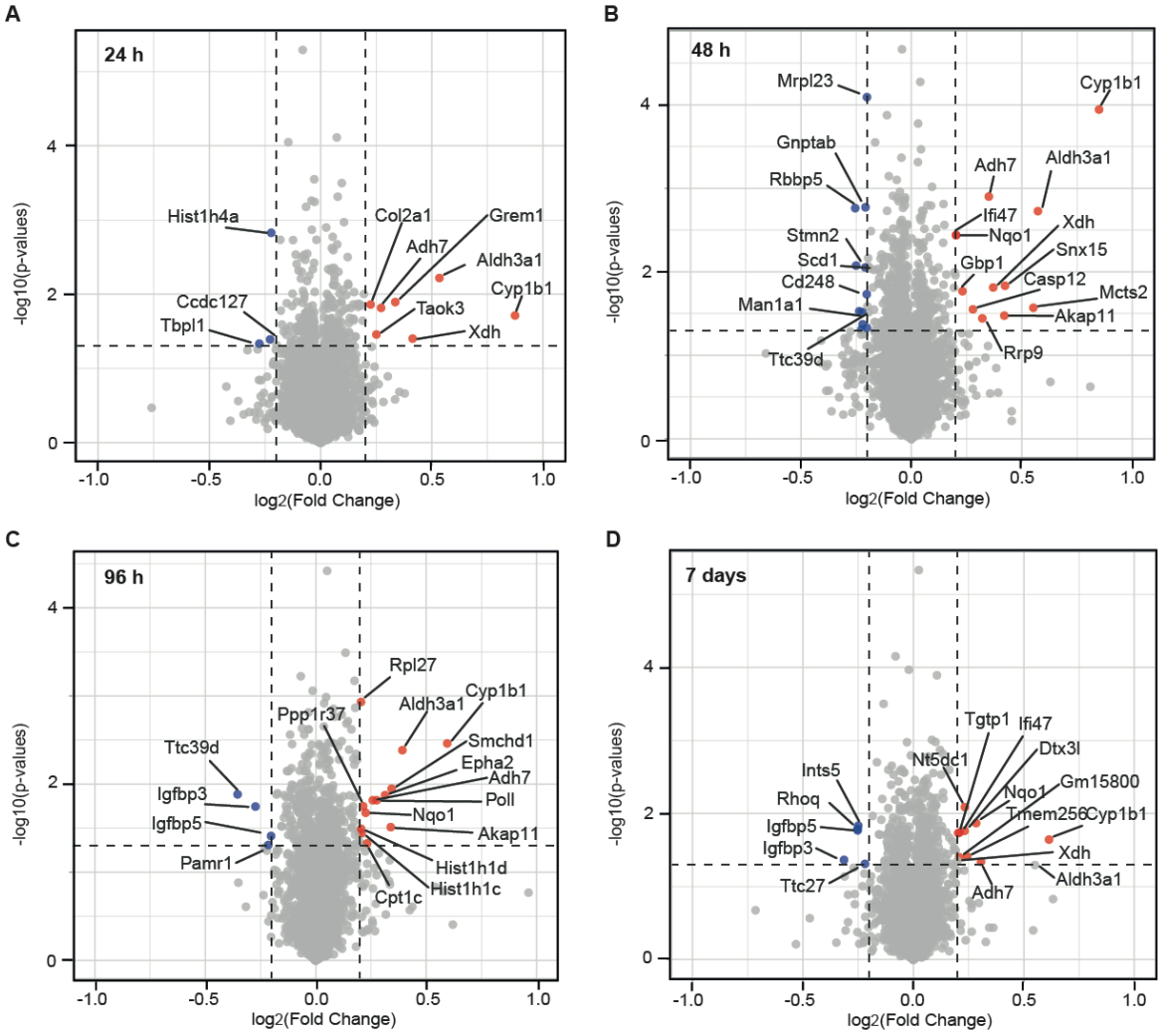

Figure 34: Influence of Picoberin on protein levels. Proteome profiling data. Volcano plots for samples treated with 1.5 µM purmorphamine and 1 nM Picoberin compared to samples treated with 1.5 µM purmorphamine and DMSO. C3H10T1/2 cells were treated with 1.5 µM purmorphamine and 1 nM Picoberin or 1.5 µM purmorphamine and DMSO as a control. Cell lysates were collected after 24 h (**A**), 48 h (**B**), 96 h (**C**) or 7 days (**D**) and subjected to MS/MS analysis to quantify protein abundances. Values of samples treated with 1.5 µM purmorphamine and 1 nM Picoberin are compared to values of samples treated with 1.5 µM purmorphamine and DMSO. Red dots: significantly upregulated proteins. Blue dots: significantly down-regulated proteins.

The complete lists with all significantly regulated proteins can be found in the appendix (Supplementary Table 9 - 12).

At all four timepoints, Picoberin significantly upregulated several phase I and II metabolic enzymes, including cytochrome 1B1 (CYP1B1), aldehyde dehydrogenase 3 family member A1 (ALDH3A1), alcohol dehydrogenase 7 (ADH7), NAD(P)H quinone dehydrogenase 1 (NQO1) and xanthine dehydrogenase (XDH). These proteins are encoded by the genes *Cyp1b1*, *Aldh3a1*, *Adh7*, *Nqo1* and *Xdh,* respectively, which were all significantly regulated by Picoberin in the global transcriptome profiling and whose expression is regulated by AhR.[111, 112] To illustrate the temporal changes in the levels of these proteins in cell treated with 1.5 µM purmorphamine and 1 nM Picoberin compared to cells that were treated with 1.5 µM purmorphamine and DMSO, the log_2(fold change) values of both conditions compared to cells that were only treated with DMSO were plotted for each timepoint in Figure 35.

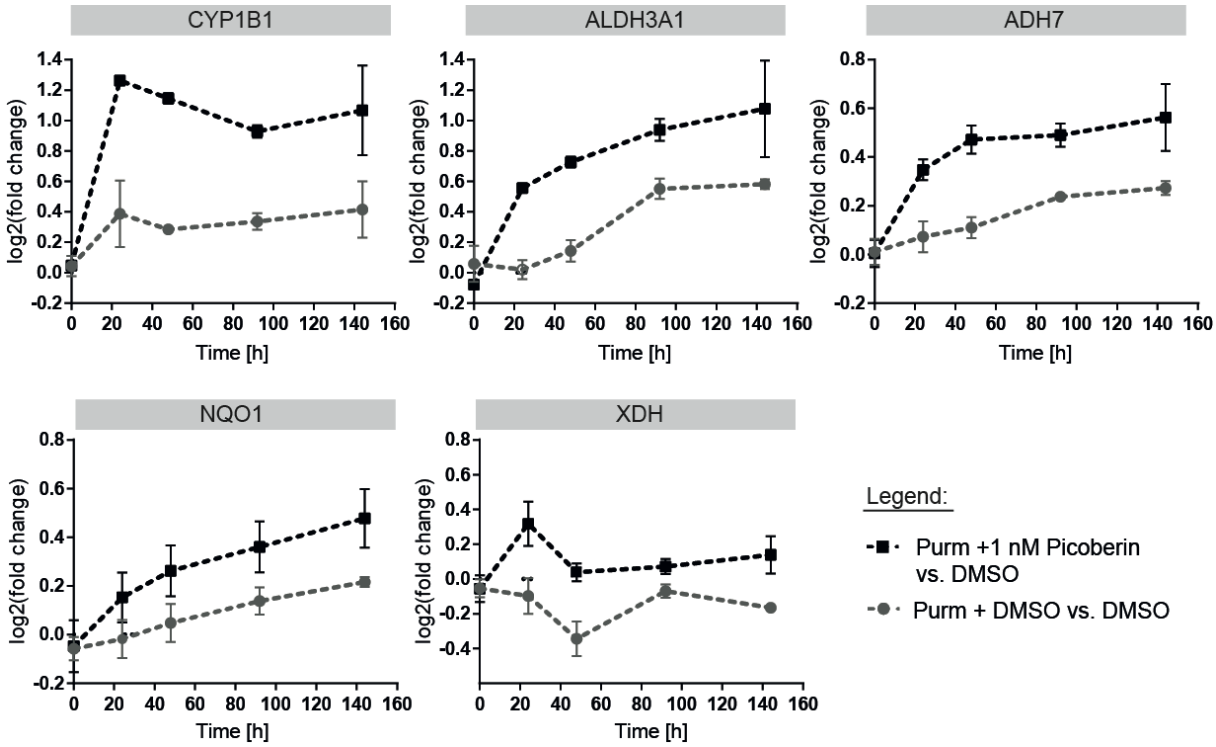

Figure 35: Time-resolved influence of purmorphamine and Picoberin on AhR-regulated proteins compared to cells treated with purmorphamine and DMSO. Proteome profiling data. C3H10T1/2 cells were treated with 1.5 µM purmorphamine and 1 nM Picoberin or 1.5 µM purmorphamine and DMSO as a control. Cell lysates were collected after 24 h, 48 h, 96 h or 7 days and subjected to MS/MS analysis to quantify protein abundances. Levels of the indicated proteins in samples treated with 1.5 µM purmorphamine and 1 nM Picoberin or with 1.5 µM purmorphamine and DMSO were compared to cells that were only treated with DMSO. The obtained log_2(fold change) values were plotted for each timepoint. Data are mean values of three biological replicates (n = 3) ± SD.

Figure 35 demonstrates the upregulation of the indicated metabolic enzymes in cells that were treated with purmorphamine and 1 nM Picoberin compared to cells that were treated with purmorphamine and DMSO over time. A similar trend can also be observed for ALDH3A1, ADH7 and NQO1 in cells that were treated with purmorphamine and DMSO. These trends could hint towards a functional role of AhR signaling during Hh-induced osteogenesis.
Only few proteins were found to be downregulated upon Picoberin treatment and only three of them were significantly reduced at more than one timepoint: Tetratricopeptide repeat domain 39D (TCT39D), Insulin-like growth factor-binding protein 3 (IGFBP3) and Insulin-like growth factor-binding protein 5 (IGFBP5). The osteogenesis markers ALP, OSX and OCN were not identified by the MS/MS analysis. In line with results obtained from the global transcriptome profiling, Picoberin did not regulate RUNX2 protein levels.

To identify pathways that are linked to the global protein profile induced by Picoberin, pathway over-representation analysis was performed using the software IPA (QIAGEN Digital Insights). The top 10 most significantly enriched pathways that were identified by the software are summarized in Figure 36.

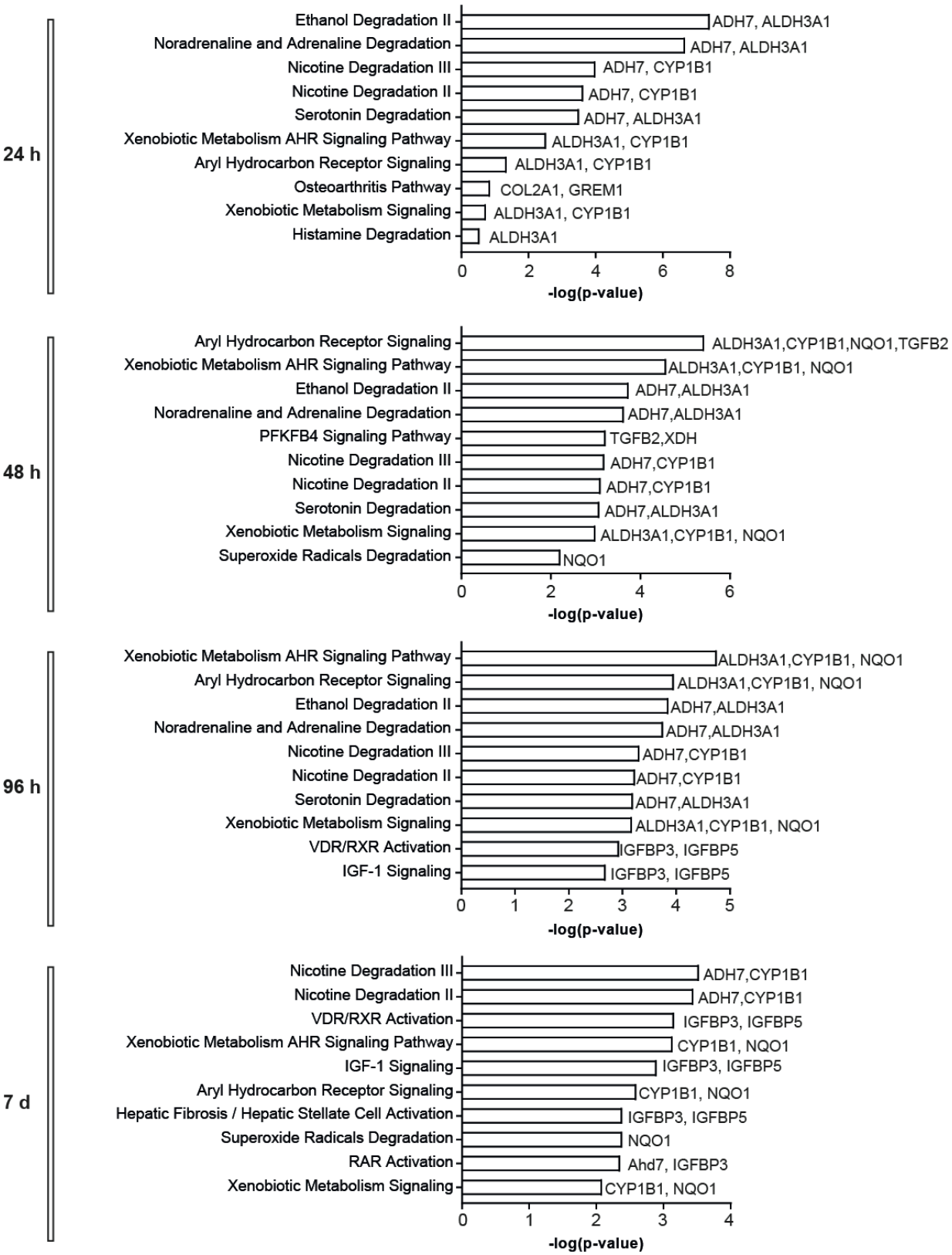

Figure 36: Influence of Picoberin on protein levels. Pathway over-representation analysis of global proteome profiling data using the Ingenuity Pathway Analysis. C3H10T1/2 cells were treated with 1.5 µM purmorphamine and 1 nM Picoberin or DMSO as a control. Cell lysates were generated after 24 h, 48 h, 96 h or 7 days and samples were subjected to nanoHPLC MS/MS analysis to quantify protein levels. Graphs show the top 10 pathways that are over-represented in cells treated with 1.5 µM purmorphamine and 1 nM Picoberin compared to cells treated with 1.5 µM purmorphamine and DMSO for the indicated timepoints.

At all four timepoints, the top 10 pathways that were regulated by Picoberin are mostly related to induction of the metabolic enzymes mentioned before. In line with the results of the global transcriptome profiling, these proteins are linked to several cellular degradation processes, and to AhR signaling. After 96 h and after 7 days, downregulation of IGFBP3 and IGFBP5 was linked to IGF signaling and activation of vitamin D receptor (VDR) and retinoic acid receptor (RXR). Both, the timing of IGFBP3 and IGFBP5 downregulation as well as reported crosstalk of VDR/RXR activity and IGF signaling with AhR signaling suggest that the modulation of these pathways could be a secondary effect caused by activation of AhR.[114, 115]

Since both, global transcriptome and global proteome profiling strongly pointed towards Picoberin-mediated activation of AhR signaling, AhR may be the molecular target of this highly potent inhibitor of Hh-induced osteoblast differentiation.

5.4.4 Target identification via thermal proteome profiling

To detect potential molecular interactions of Picoberin with the AhR or other proteins involved in AhR signaling and to identify other potential protein targets, thermal proteome profiling (TPP) was carried out. Cellular thermal shift assays (CETSA) allow for detection of the thermal stability of proteins, which can be altered upon binding of a ligand.[15] For this purpose, cell lysates are incubated with the compound of interest or vehicle control and are then subjected to heat-treatment in a temperature gradient for 3 min. Precipitated proteins are removed via ultra-centrifugation and the remaining soluble fraction of the proteins can be quantified via SDS-PAGE and immunoblotting. Alternatively, the soluble protein fractions can be labelled with tandem mass tags, which allows analysis of the samples via MS/MS analysis. This approach is called thermal proteome profiling and allows for detection of the thermal stability of many proteins in parallel.[116] TPP can thus serve as an unbiased approach for protein target identification. In this case, C3H10T1/2 cell lysates were treated with 100 nM Picoberin for 10 min, prior to removal of precipitated proteins and MS/MS analysis. *This experiment was performed by Britta Schulte as part of her master thesis.*

Table 11: List of proteins with altered melting temperature after Picoberin treatment. Thermal proteome profiling was performed in C3H10T1/2 cell lysates and 100 nM Picoberin. Proteins with a difference in melting temperature (ΔTm) of at least ≥ 2°C or ≤ -2°C were considered as potential hits. Data are mean values of three biological replicates (n = 3).

Protein name	Gene	ΔTm
UPF0184 protein C9orf16 homolog	*Cunh9orf16*	5.4 ± 1.2
CDK2-associated and cullin domain-containing protein 1	*Cacul1*	2.7 ± 2.1
Biogenesis of lysosome-related organelles complex 1 subunit 5	*Bloc1s5*	2.7 ± 1.7
DNA repair protein RAD50	*Rad50*	2.2 ± 0.7
E3 ubiquitin-protein ligase UBR4	*Ubr4*	-2.4 ± 0.6
Zinc finger protein-like 1	*Zfpl1*	-2.5 ± 0.2
Cyclin-G-associated kinase	*Gak*	-2.7 ± 1.6
Splicing regulatory glutamine/lysine-rich protein 1	*Srek1*	-2.7 ± 0.5
Alpha-1,6-mannosylglycoprotein 6-beta-N-acetylglucosaminyltransferase A	*Mgat5*	-3.1 ± 0.8
HEAT repeat-containing protein 5A	*Heatr5a*	-3.3 ± 2.2
Phosphorylated adapter RNA export protein	*Phax*	-3.4 ± 0.7
Integrin beta-3	*Itgb3*	-3.7 ± 0.9
Terminal uridylyltransferase 4	*Zcchc11*	-3.8 ± 0.3
Na(+)/H(+) exchange regulatory cofactor NHE-RF1	*Slc9a3r1*	-3.9 ± 2.9
TBC1 domain family member 10A	*Tbc1d10a*	-4.7 ± 2.7
Protein CREG1	*Creg1*	-5.1 ± 0.7
Semaphorin-5A	*Sema5a*	-5.2 ± 1.9
Dynamin-binding protein	*Dnmbp*	-6.2 ± 4.0
THUMP domain-containing protein 2	*Thumpd2*	-7.7 ± 3.4

In total 4330 proteins were identified in the TPP experiment. Manual evaluation of the detected melting curves for each protein identified 19 proteins, which displayed a shift of the melting temperature of at least ≥ 2°C or ≤ -2°C (Table 11). For Cyclin-G-associated kinase (GAK), Integrin beta-3 (ITGB3) and Na(+)/H(+) exchange regulatory cofactor NHE-RF1 (SLC9A3R1) hints for an involvement in bone regulation were reported in literature.[117-119] However, none of them could be linked to regulation of AhR signaling. Similar to the global proteome profiling data set, AhR was not identified during the MS/MS analysis of the TPP samples. However, several proteins that directly interact with this receptor were identified, including the Aryl hydrocarbon receptor interacting protein (AIP), Aryl hydrocarbon receptor nuclear translocator (ARNT), Heat Shock protein 90 (HSP90) and SRC. Since interaction of Picoberin with one of these proteins could in theory lead to activation of this receptor, it was of high interest to explore them as potential alternative targets to AhR itself. However, addition of Picoberin did not alter the thermal stability of these proteins and, thus, Picoberin does most likely not directly interact with these proteins (Figure 37).

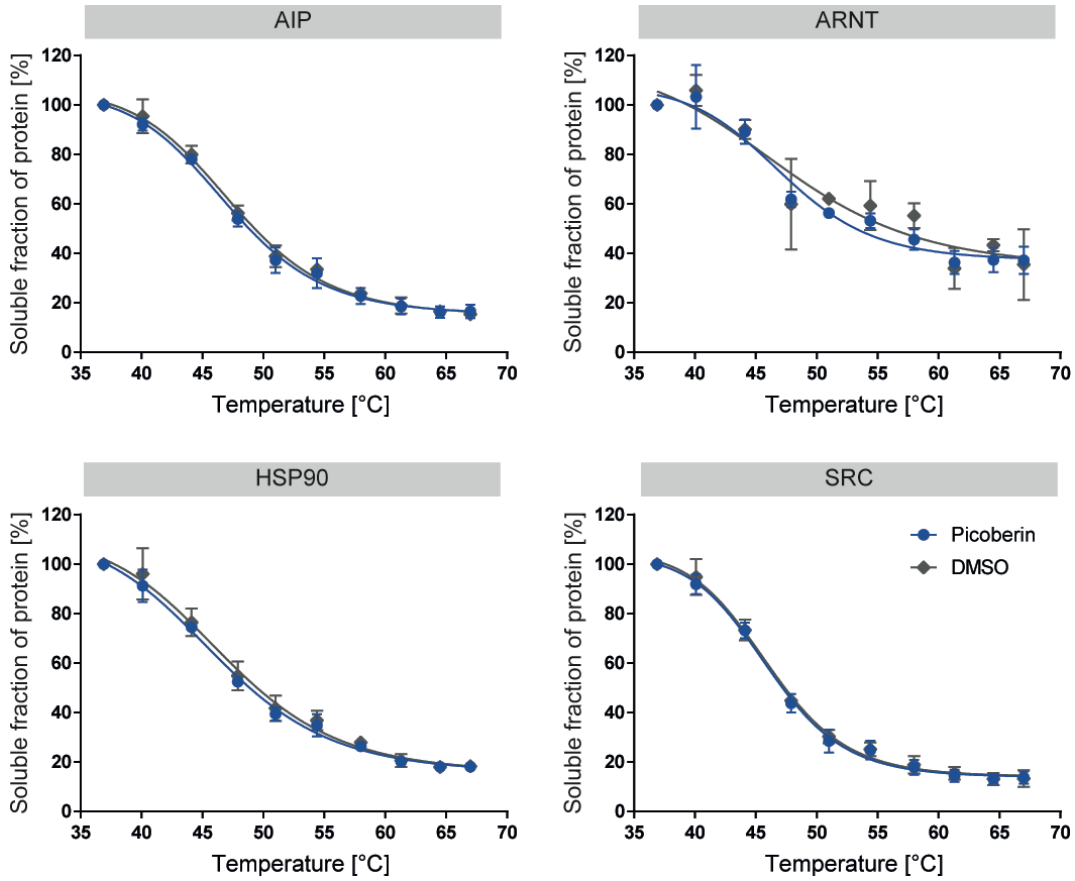

Figure 37: Melting curves of proteins that are linked to AHR signaling. Thermal proteome profiling was performed in C3H10T1/2 cell lysates and 100 nM Picoberin. Proteins were quantified by means of MS/MS analysis and data was normalized to the respective protein abundance at 35.9°C. (n = 3).

Interestingly, the E3 ubiquitin-protein ligase UBR4 and the CDK2-associated and cullin domain-containing protein 1 (CACUL1) were identified as potential target proteins with a thermal shift of -2.4 ± 0.6°C and 2.7 ± 2.1 upon addition of Picoberin, respectively. Also AhR has an intrinsic E3 ubiquitin ligase function.[120] However, no hint for a link between AhR and UBR4 or CACUL1 was found in literature.

In summary, the TPP identified several proteins as potential, possibly additional protein targets for Picoberin, but it could not support AhR as a potential protein target. However, due to the clear hints towards selective activation of AhR signaling in the global transcriptome and proteome analysis, AhR was still selected for target validation studies.

5.5 Target validation

5.5.1 Chemical validation of AhR as the target of Picoberin

To evaluate, if the interaction of Picoberin with AhR is responsible for the inhibition of Hh-induced osteogenesis, chemical validations were carried out. This approach aims exploring if known, structurally unrelated modulators of a putative target induce the same phenotype as observed for a research compound (see 2.1.4).

5.5.1.1 Influence of AhR modulators on Hh-dependent osteogenesis

To explore AhR as a potential protein target of Picoberin, the influence of the known AhR agonists 6-formylindolo[3,2-*b*]carbazole (FICZ), 2,3,7,8-tetrachlorodibenzo-p-dioxin (TCDD), Benzo[*a*]pyrene (B[a]P), YH439 (also referred to as Mivotilate) and Tapinarof on Hh-induced osteoblast differentiation of C3H10T172 cells was investigated. Besides these AhR agonists, also the effect of the known AhR antagonist CH223191 was evaluated. The corresponding results are shown in Figure 38.

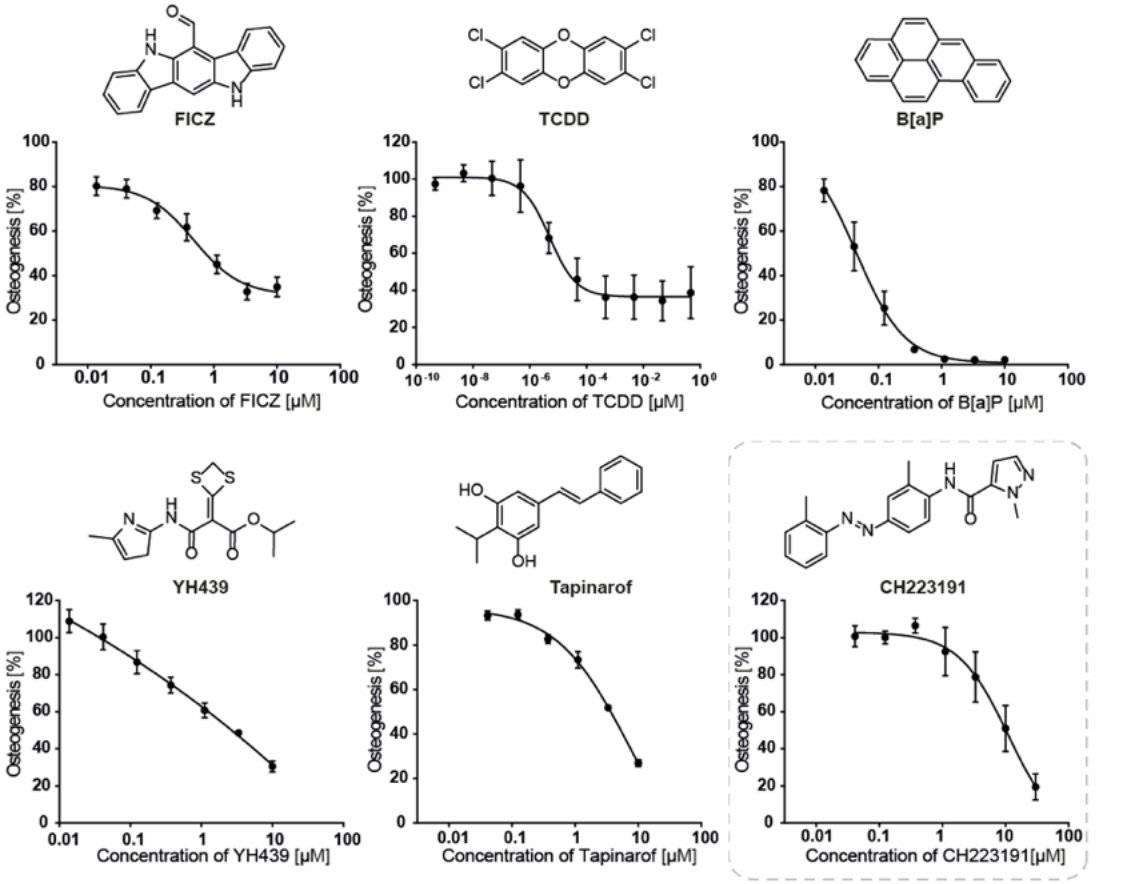

Figure 38: Influence of known AhR modulators on Hh-induced osteoblast differentiation. C3H10T1/2 cells were treated with 1.5 µM purmorphamine to induce Hh signaling and thereby osteoblast differentiation and different concentrations of the compounds or DMSO as a control. After 96 h, alkaline phosphatase activity was determined by chemiluminescence readout. The obtained values of cells that were treated with purmorphamine and compound were related to cells that were treated with purmorphamine and DMSO. Values are mean values of three biological replicates (N = 3, n = 3) ± SD. To calculate IC_{50} values, a non-linear regression was performed using a four-parameter fit.

All tested AhR agonists dose-dependently inhibit Hh-induced osteoblast differentiation of C3H10T1/2 cells and, thus, these data support the hypothesis that AhR could be the target of Picoberin. The IC_{50} values that were determined in the osteogenesis assay for these compounds as well as their reported activities on AhR activity are summarized in Table 12.

Table 12: IC_{50} and EC_{50} values of known AhR modulators. For Hh-dependent osteoblast differentiation assays (Hh ODA), C3H10T1/2 cells were treated with 1.5 µM purmorphamine and different concentrations of the compounds for 96h, prior to assay readout. All values were related to samples treated with 1.5 µM purmorphamine and DMSO (100%). IC_{50} values were determined via a non-linear regression using the GraphPad Prism software. Data are mean values of three biological replicates (N = 3, n = 3) ± SD. Cell-based EC_{50} and IC_{50} values for AhR were retrieved from literature.

No.	AhR (ant-)agonist	IC_{50} Hh ODA	AhR EC_{50} [a]
1	FICZ	510 ± 160 nM	9 – 32 pM[121]
2	TCDD	5.2 ± 1.4 pM	1 – 2400 pM[122]
3	B[a]P	47 ± 16 nM	0.36 – 100 nM[123]
4	YH439	910 ± 250 nM	Not available
5	Tapinarof	≈ 5.9 ± 0.2 µM	160 pM[124, 125]
6	CH223191	≈ 9.4 ± 4.4 µM	30 nM[126]

[a] Depending on the species, cell type and assay time

The AhR activities retrieved from the literature show that all selected AhR agonists are highly potent activators of AhR signaling with EC_{50} values in the picomolar to nanomolar range. For TCDD and B[a]P, the IC_{50} values of 5.2 ± 1.4 pM and 46 ± 16 nM that were obtained in the Hh-dependent osteogenesis assay, respectively, match well to the respective EC_{50} values reported for induction of AhR. However, the IC_{50} values obtained for FICZ and Tapinarof show, that these compounds are less potent in inhibiting Hh-induced osteogenesis compared to AhR induction. Similar to Picoberin, the dose-response curves of FICZ and TCDD reached a lower plateau phase at an osteogenesis level of 34.9 ± 4.5 % and 20.3 ± 1.3 %, respectively. In contrast, B[a]P completely inhibited Hh-induced osteogenesis at concentrations of 1 µM and higher. In case of YH439 and Tapinarof, the lower plateau phase was not reached at a concentration of 10 µM.

Interestingly also the AhR antagonist CH223191 inhibits AhR signaling with an IC_{50} of 30 nM.[125, 126] Also this compound inhibited Hh-induced osteoblast differentiation of C3H10T1/2 cells. Since the IC_{50} of approx. 9.4 ± 4.4 µM, which was obtained in the osteogenesis assay is much weaker compared with the reported activity of CH223191 on AhR, further analyses are needed to investigate whether inhibition of AhR is the reason for inhibition of Hh-dependent osteogenesis. The inhibition of Hh-induced osteogenesis mediated by CH223191 may demonstrate that AhR plays a functional role in this differentiation process and that tight regulation of the activity of this protein may be critical for proper differentiation.

5.5.1.2 Influence of FICZ on gene expression of C3H10T1/2 cells

To explore the effect of a known AhR agonist on Hh-dependent osteoblast differentiation in more detail, FICZ, an AhR agonist that is frequently used as a reference compound during research in AhR biology, was selected for further investigations. Gene expression analysis was performed to evaluate the influence of FICZ on the expression of the osteogenesis marker *Alpl*, the AhR target gene *Cyp1b1* and on *AhR* itself, as well as on the Hh target genes *Gli1*, *Ptch1* and *Ptch2*. *These experiments were performed by Britta Schulte as part of her master thesis.* The obtained results are depicted in Figure 39.

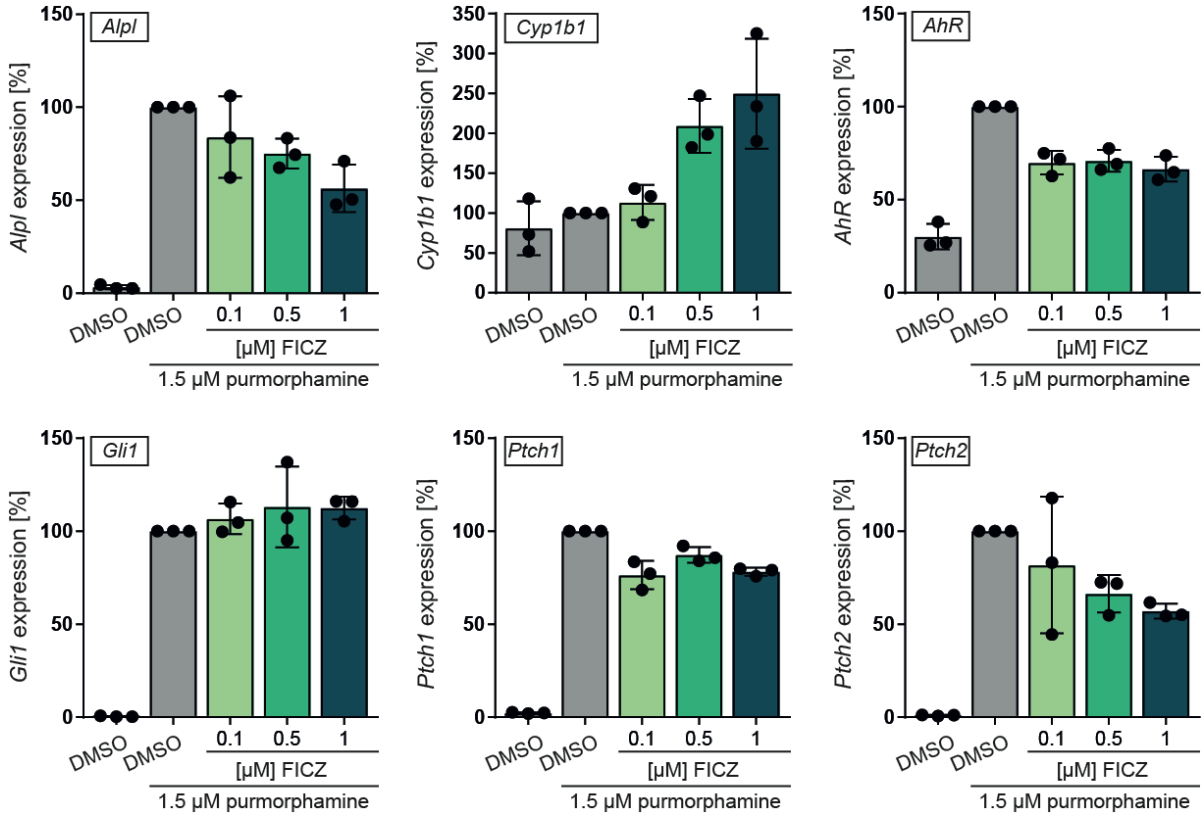

Figure 39: Influence of the AhR agonist FICZ on gene expression in C3H10T1/2 cells. C3H10T1/2 cells were treated with 1.5 µM purmorphamine to induce Hh signaling and thereby osteoblast differentiation and different concentrations of FICZ or DMSO as a control. After 96 h, gene expression levels were quantified by means of RT-qPCR using primers specific for *Alpl, Cyp1b1, AhR, Gli1, Ptch1, Ptch2* and *Gapdh* and *Ap3d1* as housekeeping genes. Data were normalized to values of samples that were treated with purmorphamine and DMSO (100 %) and are mean values of three biological replicates (N = 3, n = 3) ± SD.

In line with the results of the Hh-induced osteoblast differentiation assay, FICZ dose-dependently inhibited the expression of the osteogenesis marker *Alpl* after 96 h, down to a level of 56.4 ± 10.4 % at a concentration of 1 µM. The expression of the AhR target gene *Cyp1b1* was dose-dependently upregulated by FICZ up to a level of 150 ± 56 % at a concentration of 1 µM, which confirms activation of AhR signaling. Purmorphamine alone did

not show any influence on *Cyp1b1* expression. As already observed in the global transcriptome profiling data set, purmorphamine significantly upregulated AhR gene expression after 96 h. Interestingly, purmorphamine-induced AhR expression was partially reduced by FICZ to a level of 65 % at all tested concentrations. FICZ did not modulate the purmorphamine-induced expression of the Hh target genes *Ptch1* and *Gli1,* which confirms, that this AhR agonist does not inhibit Hh-induced osteogenesis via inhibition of canonical Hh signaling. In agreement with the observation made for Picoberin in the global transcriptome profiling, *Ptch2* expression was partially inhibited by FICZ expression down to a level of 57.0 ± 3.3 %.

In summary, the results obtained throughout the chemical validations demonstrate, that modulation of AhR signaling during Hh-induced osteoblast differentiation inhibit this differentiation process. Similar to Picoberin, the known AhR agonist FICZ does not inhibit canonical Hh signaling. Consequently, these data support the hypothesis of AhR as the protein target of Picoberin that causes inhibition of Hh-induced osteoblast differentiation.

5.5.2 Functional validation of AhR as target of Picoberin

Functional validations were carried out to explore the influence of Picoberin on the biological functions of the aryl hydrocarbon receptor. For this purpose, several experiments monitoring different aspects of AhR signaling in different cell lines, were carried out.

5.5.2.1 Picoberin activates the AhR in C3H10T1/2 cells

To validate the target hypothesis made based on the global transcriptome and proteome profiling and to evaluate, if Picoberin activates AhR in C3H10T1/2 cells in a dose-dependent manner and at picomolar concentrations, the influence of different concentrations of Picoberin on *Cyp1b1* gene expression was explored after 48 h and 96 h by means of RT-qPCR. The corresponding results are shown in Figure 40.

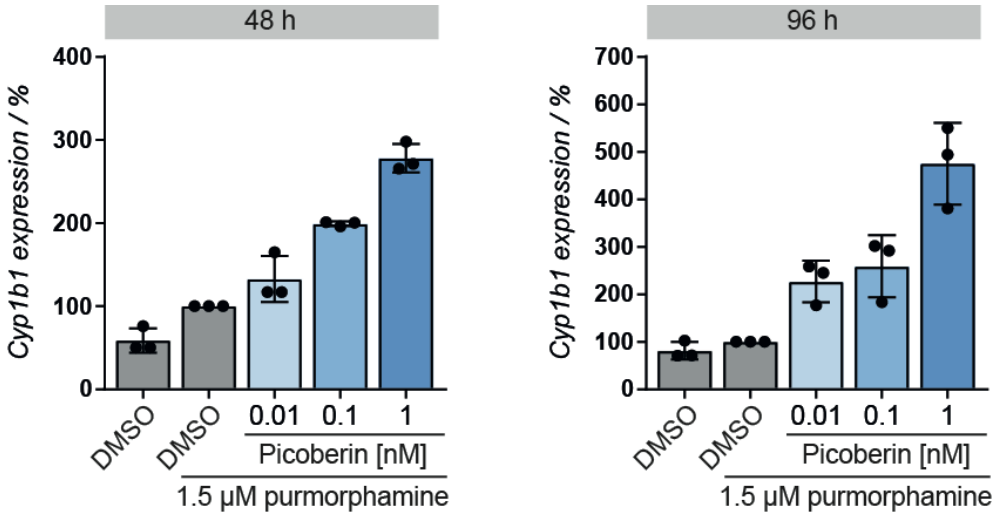

Figure 40: Picoberin induces expression of the AhR target gene *Cyp1b1*. C3H10T1/2 cells were treated with 1.5 µM purmorphamine to induce Hh signaling and thereby osteoblast differentiation and different concentrations of the Picoberin or DMSO as a control. After 48 h and 96 h, gene expression levels were quantified by means of RT-qPCR using primers specific for the AhR target gene *Cyp1b1* and *Gapdh* and *Ap3d1* as housekeeping genes. Data were normalized to values of samples that were treated with purmorphamine and DMSO (100 %) and are mean values of three biological replicates (N = 3, n = 3) ± SD.

Figure 40 demonstrates, that Picoberin dose-dependently upregulated the expression of the AhR target gene *Cyp1b1* after 48 h and 96 h. After 48 h, *Cyp1b1* expression is elevated to a level of 278.3 ± 14.1 % at a concentration of 1 nM Picoberin and already at a concentration of 100 pM a clear increase of *Cyp1b1* levels could be observed. After 96 h, *Cyp1b1* mRNA levels after treatment of cells with 1 nM Picoberin further increased to a level of 475.0 ± 70.4 %. At this timepoint, already a concentration of 10 pM Picoberin clearly upregulated *Cyp1b1* levels up to 226.9 ± 35.7 %.

5.5.2.2 Picoberin induces nuclear localization of the AhR in C3H10T1/2 cells

Activation of AhR signaling induces translocation of cytoplasmic AhR into the nucleus.[127] For this reason, the influence of Picoberin on the cellular localization of AhR was explored by means of immunofluorescence microscopy. Since endogenous AhR levels could not be detected via immunofluorescence in C3H10T1/2 cells, these cells were transiently transfected with a plasmid encoding for mAhR-FLAG for 24 h. Transfected cells were treated with different concentrations of Picoberin or DMSO as a control for 24 h, prior to fixation, permeabilization and antibody staining. To visualize mAhR-FLAG an anti-FLAG antibody was used. Representative images are shown in Figure 41. The images confirm, that Picoberin induces nuclear localization of AhR proteins and thus activates AhR signaling in C3H10T1/2 cells. Consequently, Picoberin activates AhR signaling in C3H10T1/2 cells.

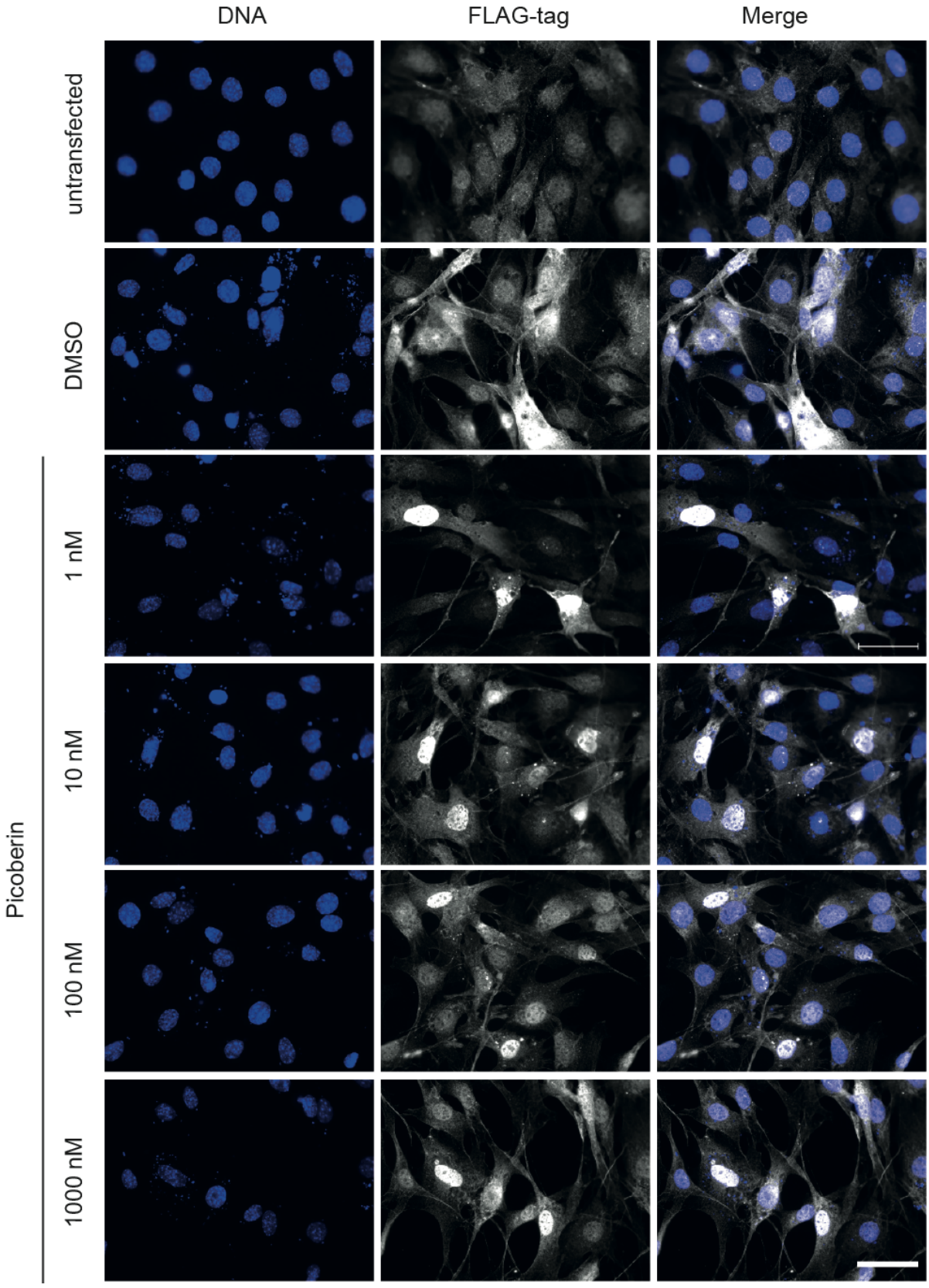

Figure 41: Picoberin induces nuclear translocation of AhR in C3H10T1/2 cells. C3H10T1/2 cells transiently transfected with a plasmid encoding for mAhR-FLAG were treated with different concentrations of Picoberin or DMSO for 24 h. After fixation, permeabilization and blocking cells were incubated with an antibody against FLAG-tag (white) and DAPI (blue) to visualize AhR and the nuclei, respectively. Images are representative of three biological replicates (n = 3). Scale bar: 50 µm.

5.5.2.3 Exploration of Picoberin induced AhR activity in different cell lines

To further explore the activity of Picoberin and to confirm it as an AhR agonist, the effect of Picoberin on xenobiotic responsive element (XRE)-dependent reporter gene activity was investigated in human hepatocellular carcinoma cells (HepG2), immortalized human keratinocytes (HaCaT) and murine embryonic fibroblasts (NIH-3T3). XRE-dependent reporter activities were assessed after 4 h and 24 h of Picoberin or FICZ treatment. The obtained dose-response curves are shown in Figure 42. *These experiments were performed by B.Sc. Anke Flegel as part of her internship at MPI Dortmund.*

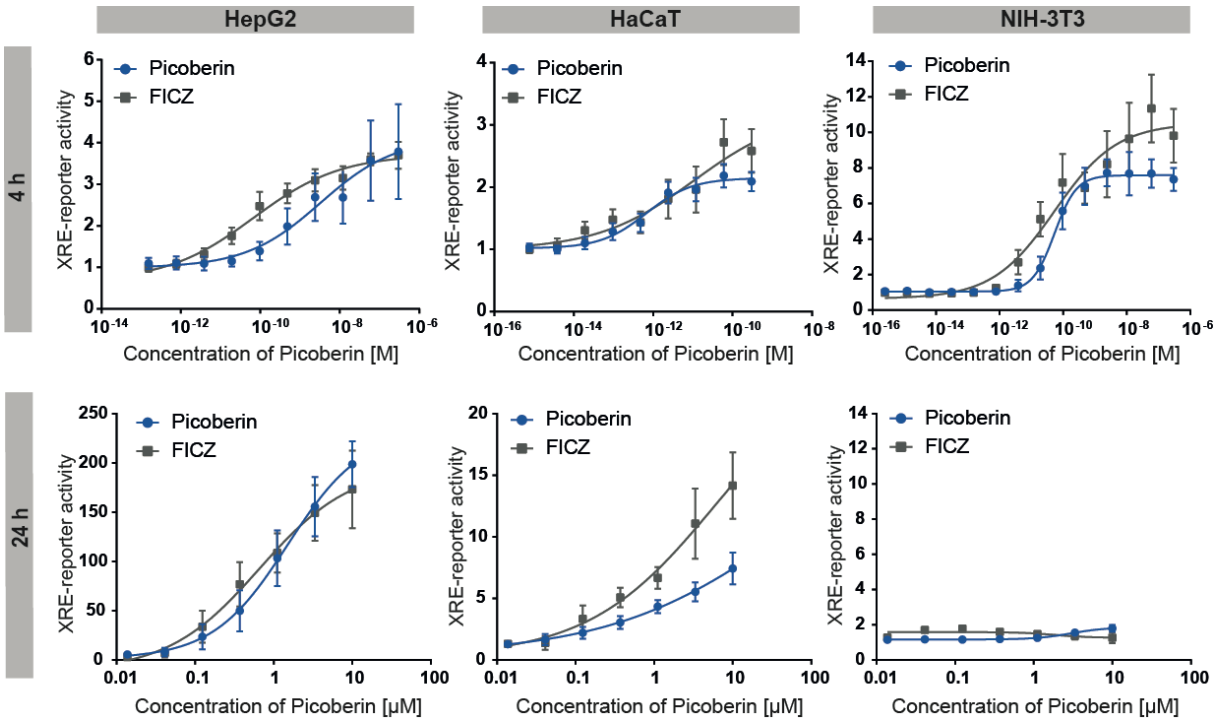

Figure 42: Influence of Picoberin in xenobiotic response element (XRE)-dependent reporter gene assays in different cell lines and comparison to FICZ. HepG2 cells were transiently transfected with plasmids encoding for an XRE-dependent firefly luciferase and a constitutively expressed *Renilla* luciferase. HaCaT cells and NIH-3T3 cells were virally transduced with an XRE-dependent firefly luciferase construct and a construct for constitutively expressed *Renilla* luciferase. All cell lines were treated with different concentrations of Picoberin or FICZ, or DMSO as a control for 4 h and 24 h. Values obtained for firefly luciferase were divided by the respective *Renilla* values. Data were normalized to values of DMSO treated cells, which were set to 1. Data are mean values of three biological replicates (N = 3, n = 3) ± SD.

The dose-response curves in in Figure 42 show, that both, FICZ and Picoberin clearly induced XRE-dependent reporter activity in all three cell lines after 4 h. In HepG2 cells, the response of the reporter activity induced by Picoberin or FICZ treatment strongly increased over time. After 4 h a maximal induction of about 3.5-fold was determined for both compounds, whereas after 24 h a maximal reporter activity increased to ~180-fold. In HaCaT cells a similar trend towards higher responses after 24 h was observed. However, in these cells the XRE-

dependent reporter activities increased only moderately from maximal ~2-fold after 4h for both compounds to a 14-fold for FICZ and 7.5-fold in case of Picoberin, after 24 h. In NIH-3T3 cells maximal XRE-reporter inductions of 7.5-fold (Picoberin) and 10-fold (FICZ) were detected after 4 h. Thus, these cells showed the strongest response to FICZ and Picoberin after 4 h compound treatment compared to the other cell lines. However, in contrast to HepG2 und HaCaT cells, no XRE-dependent reporter activity was observed after 24 h of compound treatment in these cells. The EC_{50} values that were determined for FICZ and Picoberin based on the dose-response curves are summarized in Table 13.

Table 13: EC_{50} values that were determined for Picoberin and FICZ in XRE-dependent reporter gene assays in different cell lines after 4 h and 24 h. EC_{50} values were determined using a non-linear regression four parameter fit with variable slope and are mean values of three biological replicates (N = 3, n = 3) ± SD.

Cell line	EC_{50} at 4 h nM		EC_{50} at 24 h nM	
	Picoberin	FICZ	Picoberin	FICZ
HepG2	6.5 ± 7.3	0.067 ± 0.038	1200 ± 400	660 ± 150
HaCaT	0.7 ± 0.3	2.2 ± 0.8	> 10000	> 5000
NIH-3T3	0.053 ± 0.004	0.054 ± 0.003	n.d.	n.d.

The results in Table 13 show that despite the greater responses of XRE-dependent reporter activities in HepG2 und HaCaT cells after 24 h, significantly lower EC_{50} values were obtained after the shorter treatment time of 4h. Depending on the cell line, the EC_{50} values obtained after 4h were in the single digit nanomolar to picomolar range for both compounds. In HepG2 cells, FICZ and Picoberin showed similar activities with EC_{50} values in the single digit micromolar to nanomolar range. In HaCaT cells, FICZ was more active than Picoberin after 24 h. However, since the upper plateau phase of the dose-response curve was not reached at a concentration of 10 µM for both compounds, no exact EC_{50} values could be determined but were estimated to be in the range of 5 – 10 µM.

To explore, if similar trends for a structure-activity relationship can be found in XRE-dependent reporter gene assay compared to the SAR observed for Hh-dependent osteogenesis, selected Picoberin analogues were tested in NIH-3T3 cells at a concentration of 1 µM after 4 h. The results in Figure 43 and Table 14 show that the activities of the selected 8-oxotetrahydroprotoberines correlated in both assays. The analogues **7**, **8** and **9** were inactive in the Hh-dependent osteoblast differentiation assay and also did not induce XRE-dependent reporter activity in NIH-3T3 cells. The double chlorinated analogues **17** and **21** both significantly induced the XRE-dependent reporter. However, while analogue **17** that is chlorinated at R^1 and R^2 shows similar activity as Picoberin in NIH-3T3 cells, analogue **21** with chloro-substitution at R^2 and R^3 is less potent in both assays. As observed during the SAR

studies using the Hh-dependent osteogenesis assay, the *R*-configured enantiomer of Picoberin (compound **32**) was clearly less potent than Picoberin itself.

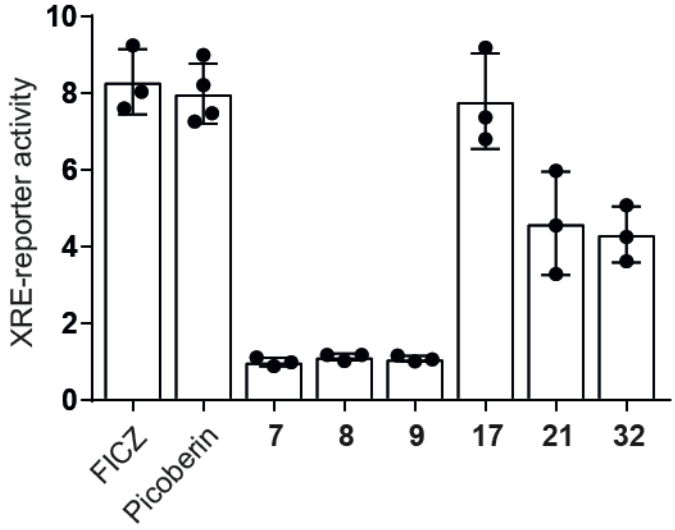

Figure 43: Influence of 8-oxotetrahydroprotoberberines on an XRE-dependent reporter gene assay in NIH-3T3 cells. NIH-3T3 cells were virally transduced with a construct for XRE-dependent firefly luciferase and a constitutively expressed *Renilla* luciferase and were treated with 1 µM of the compounds or DMSO as a control for 4 h. Values obtained for firefly luciferase were divided by the respective *Renilla* values and data was normalized to values of cells treated with DMSO, which were set to 1. Data are mean values of three biological replicates (N = 3, n = 3) ± SD.

Table 14: Comparison of SAR trends of 8-oxotetrahydroprotoberberines in an XRE-dependent reporter gene assay in NIH-3T3 cells and Hh-induced osteogenesis of C3H10T1/2 cells. For the structures of the compounds are specified in Table 6. All data are mean values of three biological replicates (n = 3) ± SD.

Compound	Hh ODA IC_{50} [nM]	XRE-reporter activity (fold-induction)
FICZ	510 ± 160	8.3± 0.7
Picoberin	0.003 ± 0.001	8.0 ± 0.7
7	inactive	1.0 ± 0.1
8	inactive	1.1 ± 0.1
9	inactive	1.1 ± 0.1
17	0.010 ± 0.002	7.8 ± 1.0
21	1.1 ± 0.3	4.6 ± 1.1
32	72.0 ± 41.0	4.3 ± 0.6

Taken together the data presented in this chapter clearly confirm, that Picoberin activates AhR signaling in several human and murine cell lines. Interestingly, the activity of FICZ and Picoberin strongly depends on the cell line that is used and the treatment time. In several conditions, Picoberin shows activities that are comparable to FICZ, which is one of the most potent endogenous AhR agonists reported in the literature.[121, 128] Especially the strong induction of AhR signaling in the murine fibroblast cell line NIH-3T3 with a picomolar EC_{50}

value strongly correlates with the picomolar activity of Picoberin in the murine cell line C3H10T1/2 during Hh-induced osteogenesis. Exploration of selected 8-oxotetrahydroprotoberine analogues provided evidence for overlapping SAR in two different and independent assays using NIH-3T3 or C3H10T1/2 cells. Consequently, these data clearly support the hypothesis of AhR as the protein target of Picoberin during Hh-dependent osteogenesis.

5.5.2.4 Exploration of Picoberin activity in HepG2 cells

To further validate Picoberin as an AhR agonist, the influence of this small molecule on AhR signaling was explored in more detail in the human hepatoblastoma cell line HepG2. These cells express high levels of AhR and are frequently used as an *in vitro* model in AhR biology research. In addition to the induction of the XRE-dependent reporter shown in chapter 5.5.2.3, the influence of Picoberin on AhR signaling was explored by means of a Cytochrome 1A1 (CYP1A1) Glo assay, which was carried out *by Lisa-Marie Pulvermacher during her master thesis at the MPI in Dortmund.* This assay monitors the enzymatic activity of CYP1A1, which is upregulated through activation of AhR signaling in HepG2 cells. To assess the effect of Picoberin on CYP1A1 activity, HepG2 cells were treated with different concentrations of Picoberin for 24 h. The results in Figure 44 show, that Picoberin dose-dependently up-regulated CYP1A1 enzymatic activity and support activation of AhR signaling by Picoberin in HepG2 cells.

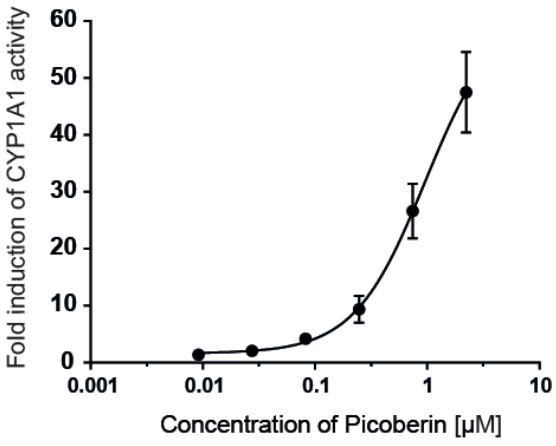

Figure 44: Picoberin activates the AhR in HepG2 cells. CYP1A1 Glo assay. HepG2 cells were treated with different concentrations of Picoberin or DMSO as a control for 24 h. To detect CYP1A1 activity, a CYP1A1 Glo assay was used. Values of samples that were treated with compound were related to values of cells that were treated with DMSO, which were set to 1. Data are mean values of three biological replicates (N = 3, n = 3) ± SD.

However, in line with results obtained from the XRE-dependent reporter gene assay (Figure 42 and Table 13) the potency of Picoberin in HepG2 cells after 24 h of compound treatment is significantly lower that the effects that were observed in C3H10T1/2 cells.

The influence of Picoberin on cellular AhR localization in HepG2 cells was explored by means of immunofluorescence microscopy. For this purpose, HepG2 cells were treated with different concentrations of Picoberin or DMSO as a control for 15 min. Representative images are shown in Figure 45.

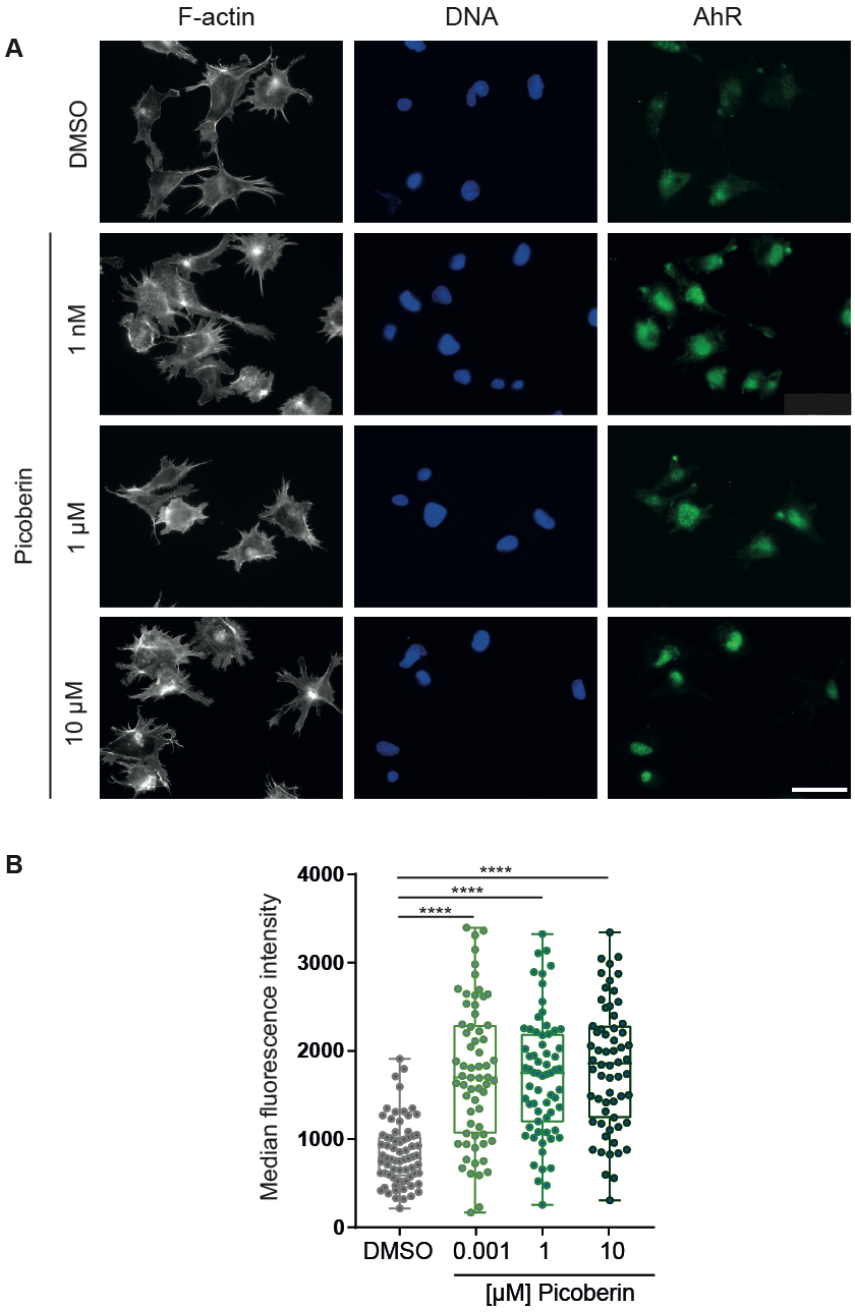

Figure 45: Influence of Picoberin on AhR localization in HepG2 cells. HepG2 cells were treated with different concentration of Picoberin or DMSO as a control for 15 min. After fixation, permeabilization and blocking cells were treated with an antibody against F-actin (white) and AhR (green). DAPI (blue) was used to visualize the nuclei. **A:** Microscopy images are representative of three biological replicates (n = 3). Scale bar: 50 µm. **B:** Quantification of the nuclear AhR staining. Data are representative of three biological replicates (n = 3), Significances were determined by means of a student's t-test ($p \leq 0.0001$).

The microscopy images in Figure 45A demonstrate, that Picoberin induces an enrichment of AhR in the cell nuclei, already after a very short incubation time of 15 min. Even at a Picoberin concentration of 1 nM this effect was clearly observed. Quantification of the AhR fluorescence signal in the nuclei using the software Fiji confirmed this observation (Figure 45B). Consequently, Picoberin induces translocation of AhR into the nucleus after short treatment times and at low nanomolar concentrations.

5.5.2.5 Picoberin reduces the cellular AhR level in HepG2 cells

Activation of AhR by TCDD or FICZ induces a marked reduction in cellular AhR levels, as part of a regulatory negative feedback loop.[129, 130] The influence of Picoberin on cellular AhR levels was explored by means of immunoblotting. For this purpose, HepG2 cells were treated with different concentrations of Picoberin or DMSO for 4 h, prior to cell lysis and protein separation via SDS-PAGE and subsequent transfer to a membrane. The detected protein bands of the AhR, the nuclear protein Lamin A (LMNA) and β-tubulin are shown in Figure 46A. In Figure 46B, the band intensities of the immunoblot were determined densiometrically and values obtained for AhR were normalized to the levels of LMNA and β-tubulin. The AhR protein levels obtained for Picoberin treated samples were related to DMSO treated sample, which was set to 100 %.

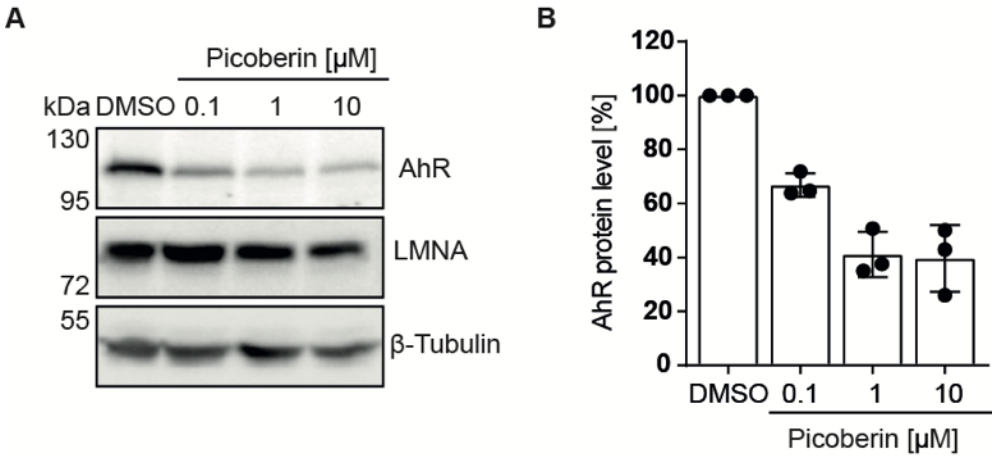

Figure 46: Influence of Picoberin on cellular AhR protein levels in HepG2 cells. HepG2 cells were treated with different concentrations of Picoberin or DMSO as a control for 4 h. A: Protein levels of AhR, the nuclear protein LMNA and β-tubulin were determined by means of immunoblotting. Representative images of three biological replicates (n = 3). **B:** Quantification of AhR protein levels detected in A. AhR levels were normalized to LMNA and β-tubulin protein levels and related to values of samples that were treated with DMSO (100 %). Data are mean values of three biological replicates (n = 3).

The immunoblot (Figure 46A) and the corresponding quantification of the band intensities (Figure 46B) show, that Picoberin reduced AhR protein levels in HepG2 cells after 4 h. These

results are in line with observations reported for the known AhR agonists TCDD and FICZ and further support the hypothesis of AhR as a protein target of Picoberin.

5.5.3 Exploration of the binding of Picoberin to the AhR

The results obtained above provide evidence, that the AhR could be a protein target of Picoberin. To demonstrate target engagement and to confirm direct binding of Picoberin to AhR, several types of cellular thermal shift assays (CETSA) were performed.

5.5.3.1 CETSA with HepG2 cell lysates

To explore the influence of Picoberin on the thermal stability of human AhR, HepG2 cell lysates were treated with 20 µM Picoberin or DMSO as a control, followed by heat treatment, removal of precipitated proteins and detection of the soluble fraction of AhR in the lysates (see 4.2.1.18). A representative blot and the quantification of AhR band intensities are shown in Figure 47.

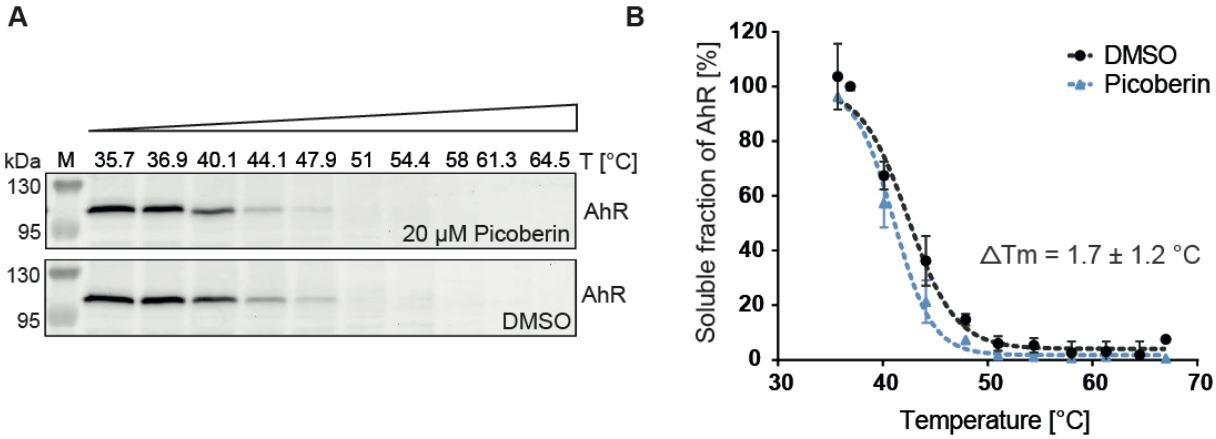

Figure 47: Picoberin treatment leads to thermal destabilization of AhR in HepG2 cell lysates. HepG2 cell lysates were treated with 20 µM Picoberin or DMSO as a control for 10 min. The lysates were then aliquoted into 10 vials and each aliquot was subjected to a heat treatment at different temperatures, prior to ultracentrifugation to remove precipitated proteins. Soluble proteins were separated via SAD-PAGE and transferred to a PVDF membrane. AhR protein levels were detected using an anti-AhR antibody. **A:** Representative western blot. In total three biological replicates were performed (n = 3). **B:** Quantification of AhR band intensities from A. All band intensities were related to the AhR protein level in samples that were heated to 36.9°C. Data are mean values of three biological replicates (n = 3) ± SD.

The immunoblot in Figure 47A shows a temperature-dependent decrease of AhR levels for both samples that were incubated with DMSO or Picoberin. In HepG2 cell lysates that were pre-incubated with DMSO AhR had a melting temperature of 42.4 ± 0.7°C. In samples which were pre-incubated with 20 µM Picoberin the AhR melting temperature slightly decreased to 41.0 ± 0.7°C. For the three biological replicates, a mean temperature shift of -1.7 ± 1.2°C was

detected, indicating a slight destabilization upon Picoberin treatment. To evaluate, if this minor destabilization may be indicative of direct binding of Picoberin to AhR, Picoberin was titrated, and treated lysates were subjected to an isothermal heat-treatment at 41°C. The corresponding results of this isothermal CETSA are shown in Figure 48.

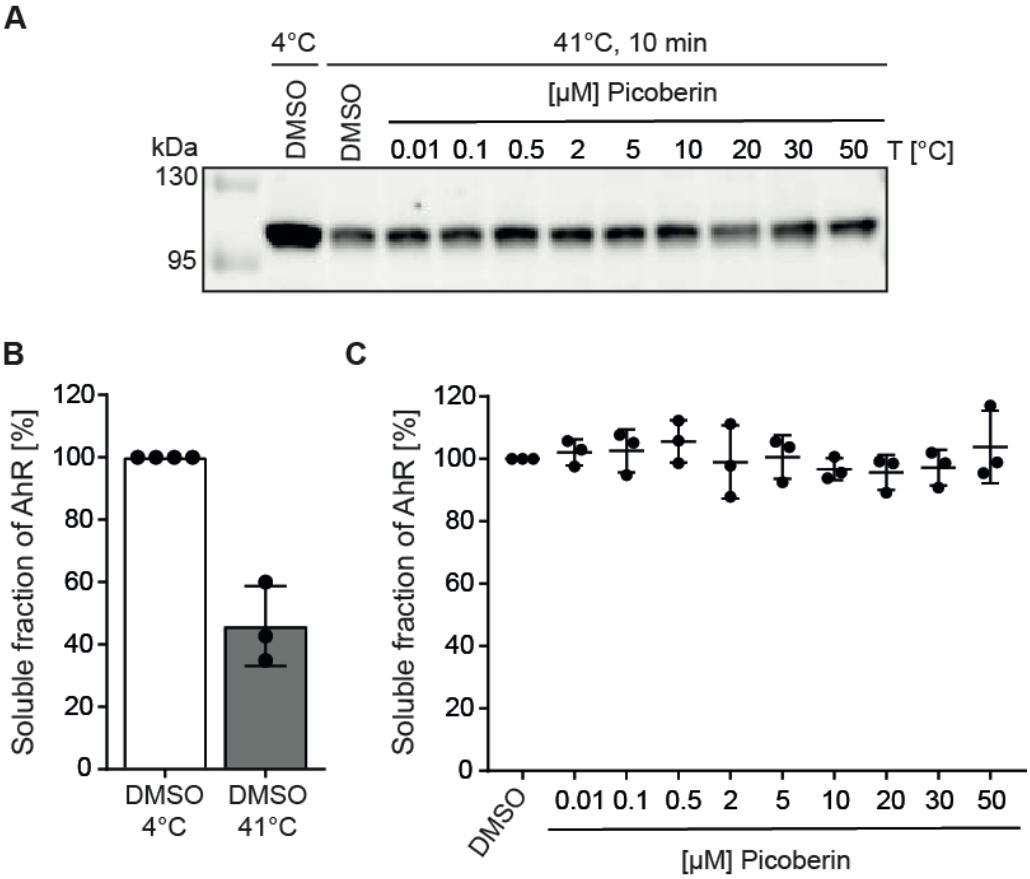

Figure 48: Picoberin has no influence in an isothermal AHR-CETSA with HepG2 cell lysates. HepG2 cell lysates were treated with different concentrations of Picoberin or DMSO as a control for 10 min. The lysates were then subjected to a temperature of 41°C for 10 min, prior to ultracentrifugation to remove precipitated proteins. The soluble proteins were separated by via SAD-PAGE and transferred to a PVDF membrane. AhR protein levels were detected using an anti-AhR antibody. **A:** Image of a representative western blot. In total three biological replicates were performed (n = 3). **B:** Quantification of the melting at 41°C of the DMSO treated sample from A. Band intensities of the DMSO and 4°C treated sample were related to samples that were treated with DMSO but were kept on at 4°C, which was set to 100 %. **C:** Quantification of AhR band intensities from A. All band intensities were related to the AhR protein level in the sample that was treated with DMSO and incubated at 41°C. Data are mean values of three biological replicates (n = 3) ± SD.

Figure 48 shows that the heat treatment led to a clear reduction of AhR protein levels in samples that were treated with DMSO compared to samples that were treated with DMSO and were kept at 4°C (Figure 46A and 46B). However, Picoberin treatment of HepG2 cell lysates did not lead to a dose-dependent destabilization of AhR compared to samples incubated with DMSO after the heat-treatment at 41°C. Consequently, these experiments could not confirm binding of Picoberin to AhR.

To explore the influence of Picoberin on the thermal stability of AhR in a more physiological context, an *in-cell* CETSA was performed. For this approach, living HepG2 cells were treated with 20 µM Picoberin or DMSO as a control for 15 min. After collection of the cells, they were aliquoted and subjected to different temperatures for 3 min. Cells were then lysed, precipitated proteins were removed by ultracentrifugation and the soluble fraction of proteins was separated via SDS-PAGE. AhR protein levels were detected and quantified by means of immunoblotting. Since Picoberin induces translocation of AhR into the nucleus, the levels of the nuclear protein Lamin A (LMNA) were detected to confirm proper lysis of the nuclei. Furthermore, β-actin was detected as a cytosolic control. The corresponding results are shown in Figure 49.

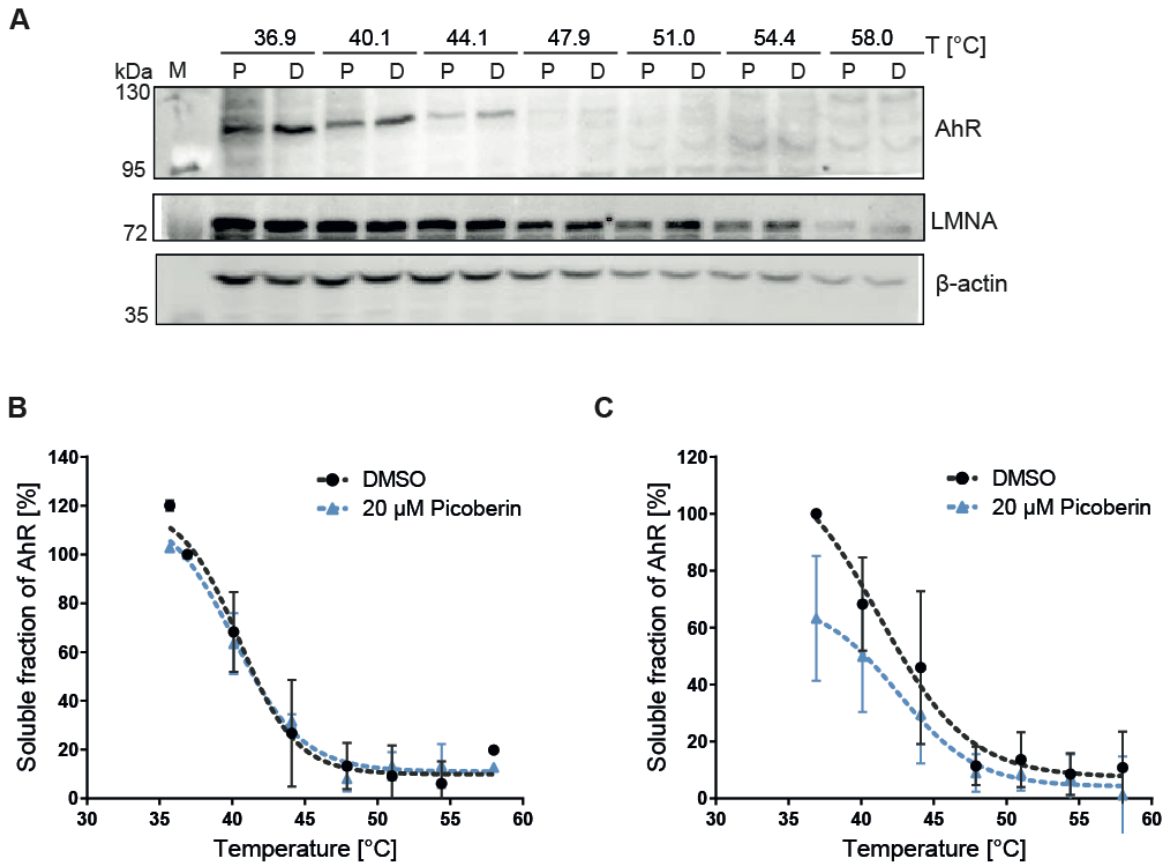

Figure 49: Picoberin does not influence the thermal stability of AhR in HepG2 cells. For in-cell CETSA, HepG2 cells were treated with 20 µM Picoberin or DMSO as a control for 15 min. Cells were then collected, aliquoted and subjected to heat treatment with different temperatures for 3 min. After subsequent cell lysis and removal of precipitated proteins, the soluble protein fractions were separated via an SDS-PAGE and transferred to a PVDF membrane. AhR protein levels were detected using an anti-AhR antibody. In total three biological replicates were performed (n = 3). **A:** Image of a representative western blot. **B:** Quantification of the AhR band intensities from A. Band intensities of DMSO or Picoberin treated samples were related to the AhR protein level in the respective samples that were treated with DMSO or Picoberin and that were heated to 36.9°C. **C:** Quantification of AhR band intensities from A. Band intensities of all samples were related to the AhR protein level in samples that were treated with DMSO and that were heated to 36.9°C. Data are mean values of three biological replicates (n = 3) ± SD.

The immunoblot in Figure 49A shows, that AhR protein levels were reduced in samples that were treated with Picoberin compared to the respective DMSO-treated sample. The band intensities were quantified, and the obtained data were plotted in Figure 49B and C. In Figure 49B, band intensities obtained for DMSO or Picoberin treated samples were related to the respective sample that was subjected to 36.9°C during the heat-treatment step. The curves clearly demonstrate, that Picoberin did not alter the melting temperature of AhR in this assay setup. For samples that were pre-incubated with DMSO a mean melting temperature of 40.7 ± 0.9°C was determined for AhR. Pre-incubation of cells with 20 µM Picoberin led to the detection of a mean AhR melting temperature of 40.6 ± 0.8°C. However, the melting curves in Figure 49B do not reflect the observed differences in the AhR band intensities. For this reason, the band intensities of all samples were related to the sample that was treated with DMSO and heated to 36.9°C (Figure 49C). Despite the large error bars obtained after quantification, these data show that Picoberin reduces cellular AhR levels already after 15 min. Reduction of AhR protein levels are in line with the reduced AhR levels in HepG2 cells that was observed after 4 h of compound treatment and described in chapter 5.5.2.5. However, in view of the very short treatment time during the in-cell CTESA, this reduction could hint towards a direct effect of Picoberin of the AhR.

All CETSA experiments presented above were conducted either with HepG2 cell lysates or HepG2 cells and thus, with human AhR. To evaluate binding of Picoberin to murine AhR, HEK293-T cells were transfected with a plasmid encoding for mAhR-FLAG. After 48 h, cell lysates were generated and treated with 40 µM Picoberin, 40 µM FICZ or DMSO prior to heat-treatment, removal of precipitated proteins and quantification of mAhR protein levels as described above. The obtained immunoblots and the corresponding quantifications are shown in Figure 50. For samples that were pre-incubated with DMSO, an AhR melting temperature of 42.3 ± 2.1°C was detected. However, in this approach neither the known AhR agonist FICZ (Figure 50C, Tm = 43.8 ± 1.2°C), nor Picoberin (Figure 50B, Tm = 42.9 ± 1.1°C) altered the thermal stability of AhR.

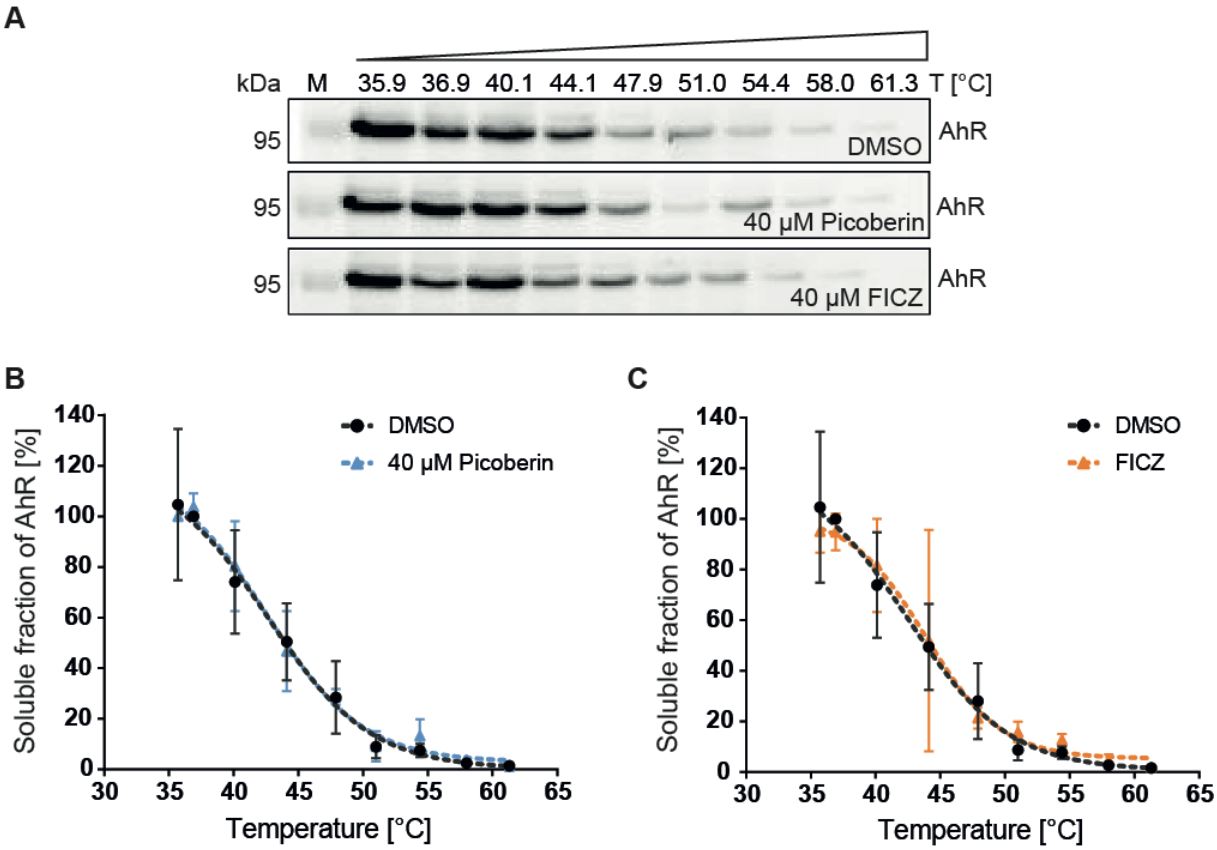

Figure 50: Picoberin does not influence the thermal stability of mAhR-FLAG. HEK293-T cells were transiently transfected with a plasmid encoding mAhR-FLAG for 48 h prior to cell lysis. Lysates were treated with 40 µM Picoberin, 40 µM FICZ or DMSO as a control for 10 min. The lysates were then aliquoted into 10 vials and each aliquot was subjected to a heat treatment at different temperatures, prior to ultracentrifugation to remove precipitated proteins. The soluble proteins were separated by via SDS-PAGE and transferred to a PVDF membrane. AhR protein levels were detected using an anti-AhR antibody. **A:** Representative western blot. In total three biological replicates were performed (n = 3). **B:** Treatment with Picoberin. Quantification of the AhR band intensities from **A** for samples treated with DMSO or Picoberin. **C:** Treatment with FICZ. Quantification of the AhR band intensities from A for DMSO and FICZ treated samples. All band intensities were related to the AhR protein level in DMSO treated samples that were heated to 36.9°C. Data are mean values of three biological replicates (n = 3) ± SD.

In summary, several types of CETSA were carried out to demonstrate direct binding of Picoberin to AhR. However, these experiments could not provide a clear proof for a direct molecular interaction and could thus not further support the target hypothesis.

5.5.4 Genetic validation of AhR as target of Picoberin

5.5.4.1 siRNA-mediated AhR depletion

To evaluate, if the influence of Picoberin on AhR is responsible for the picomolar inhibition of Hh-induced osteogenesis, AhR expression was downregulated via RNA interference (RNAi), prior to induction of Hh-dependent osteogenesis and Picoberin treatment of C3H10T1/2 cells. Small interfering RNA (siRNA) specifically binds to complementary oligonucleotides on mRNA and induces its degradation. Since mRNA levels are reduced, less mRNA gets translated, and therefore, the corresponding protein levels decrease over time. Here, C3H10T1/2 cells were transfected with 30 nM non-targeting (NT)-siRNA or AhR siRNA for 24 h, prior to induction of Hh-dependent osteogenesis and Picoberin treatment. After 48 h, an *AhR* knockdown efficiency of 72.2 ± 6.5 % was achieved (Figure 51A) on mRNA level. C3H10T1/2 cells with reduced *AhR* levels showed lower induction of *Alpl* levels upon treatment with 1.5 µM purmorphamine, suggesting that AhR is required during Hh-induced osteogenesis (Figure 51B). Furthermore, AhR-depletion mitigated the effect of 100 pM and 1 nM Picoberin on Hh-dependent osteogenesis (Figure 51C). While after 48 h *Alpl* levels were reduced to a level of 29.3 ± 7.9 % and 27.8 ± 14.4 % in C3H10T1/2 cells transfected with NT siRNA, *Alpl* levels were only reduced to 62.4 ± 7.9 % and 66.5 ± 14.2 % in AhR-depleted cells, that were treated with 100 pM and 1 nM Picoberin, respectively.

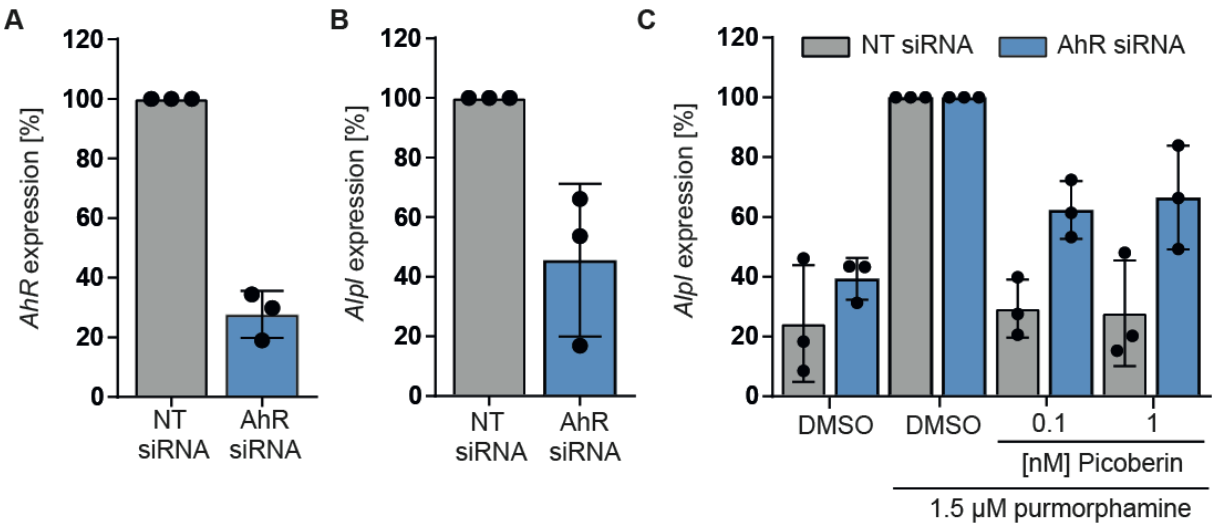

Figure 51: Influence of siRNA-mediated AhR depletion on osteoblast differentiation and Picoberin treatment after 48 h. C3H10T1/2 cells were bulk-transfected with 30 nM AhR siRNA or non-targeting (NT)-siRNA for 24 h, prior to re-seeding and treatment with 1.5 µM purmorphamine and DMSO, 1.5 µM purmorphamine and 100 pM or 1 nM Picoberin or only DMSO. After 48 h, total RNA was isolated and expression level of *AhR* and *Alpl* were determined by means of RT-qPCR. **A:** Knockdown efficiency was determined by means of RT-qPCR. **B:** Effect of AhR knockdown on osteoblast differentiation based on *Alpl* expression. **C:** Influence of AhR depletion on Picoberin-mediated inhibition of Hh-induced osteoblast differentiation after 48 h. Data of NT- and AhR siRNA treated samples were related to the respective samples that were treated with purmorphamine and DMSO. Data are mean values of three biological replicates (n = 3).

To further explore the effect of AhR depletion on Hh-dependent osteogenesis of C3H10T1/2 cells, the influence of the siRNA-mediated AhR knockdown was investigated after 96 h, on mRNA level and by means of the osteoblast differentiation assay. The corresponding results are shown in Figure 52.

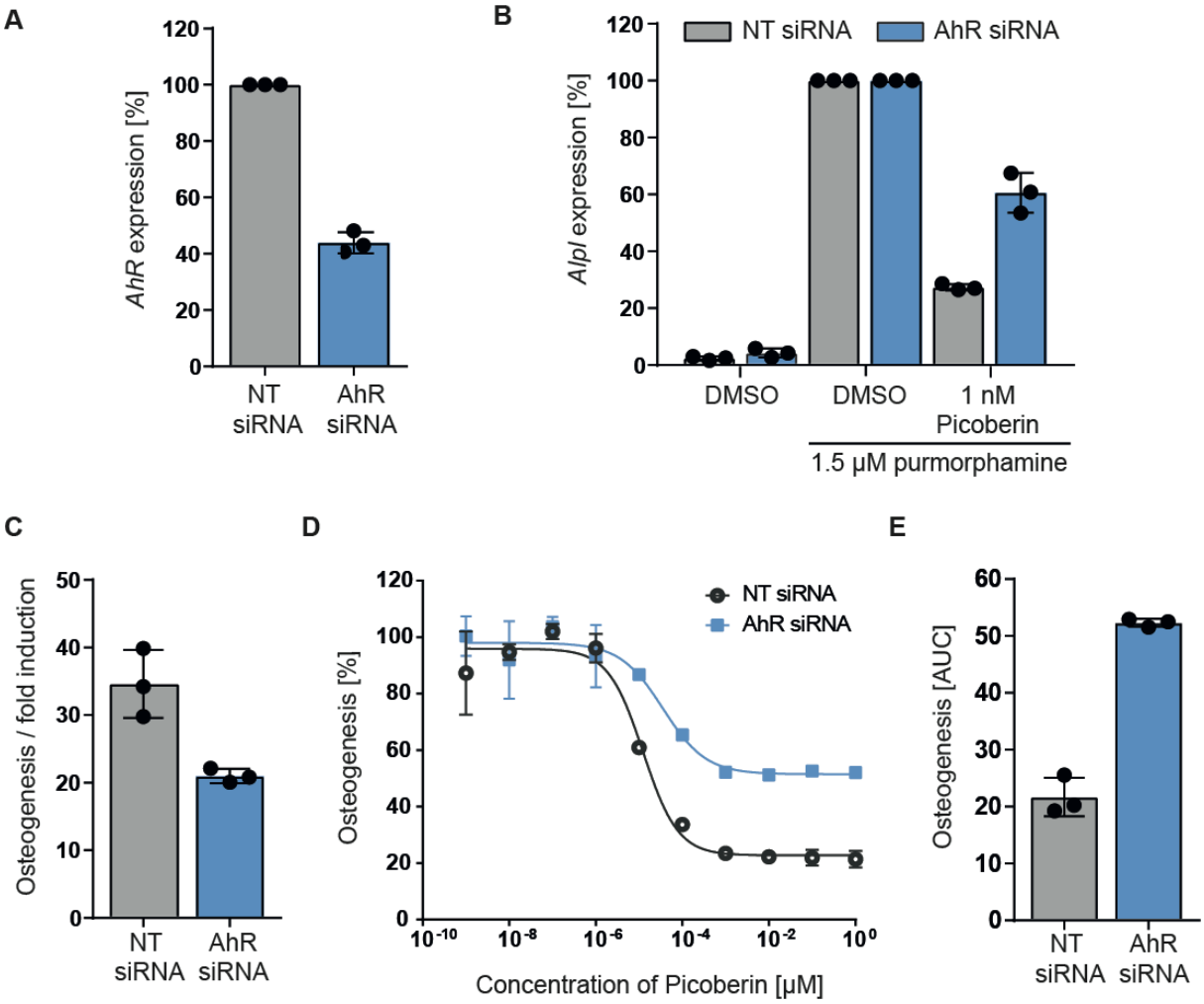

Figure 52: Influence of siRNA-mediated AhR depletion on osteoblast differentiation and Picoberin treatment after 96 h. C3H10T1/2 cells were bulk-transfected with 30 nM AhR siRNA or non-targeting (NT)-siRNA for 24 h, prior to re-seeding and treatment with 1.5 µM purmorphamine and DMSO, 1.5 µM purmorphamine and 100 pM Picoberin or only DMSO for 96 h. **A:** AhR knockdown efficiency was determined by means of RT-qPCR. **B:** Influence of AhR depletion on Picoberin-mediated inhibition of Hh-induced osteoblast differentiation after 96 h. Values of samples treated with NT siRNA or AhR siRNA were related to the respective sample that was treated with purmorphamine and DMSO. **C-E:** Osteoblast differentiation assay. **C:** Influence of AhR-depletion on Hh-induced osteogenesis. **D** and **E:** Influence of AhR-depletion on Picoberin-mediated inhibition of Hh-induced osteogenesis. **E:** Area under curve (AUC) values that were obtained for each biological replicate of the data shown in **D**. Data are mean values of three biological replicates (n = 3).

After 96 h an AhR knockdown efficiency of 56.1 ± 3.1 % was achieved (Figure 52A). In line with the results obtained after 48 h and despite the only partial AhR knockdown, the influence of 1nM Picoberin on the *Alpl* expression was mitigated in AhR-depleted cells on mRNA level

(Figure 52B). In cells transfected with NT siRNA, the level of *Alpl* mRNA was reduced by 1 nM Picoberin to a level of 27.4 ± 0.9 % compared to 60.6 ± 5.6 % in AhR-depleted cells. Induction of Hh-dependent osteogenesis was reduced in AhR-depleted cells (Figure 52C) and this observation is in line with the results obtained after 48 h (Figure 51A). The dose-response curves in Figure 52D demonstrate that AhR knockdown reduces Picoberin's influence on Hh-dependent osteogenesis. For cells that were transfected with NT siRNA or AhR siRNA, IC_{50} values of 12.4 ± 3.5 pM and 35.6 ± 14.3 pM were determined, respectively. Over all three biological replicates, a mean shift in IC_{50} of 14.2 ± 6.1 pM was calculated. The influence of AhR-depletion on Picoberin mediated inhibition of osteogenesis becomes even more clear, when considering the maximal inhibition that is reached by Picoberin. While the dose-response curve has a lower plateau phase at 20 – 25 % in case of NT siRNA, a maximal inhibition to a level of only 50 % is reached in AhR-depleted cells. To demonstrate this more clearly, the area under curve (AUC) was determined for each biological replicate (Figure 52E). For NT siRNA and AhR siRNA-transfected cells AUCs of 21.7 ± 2.7 and 52.3 ± 0.6 were determined, respectively. Both, the shift of the IC_{50} value as well as the AUC reveal a reduced potency of Picoberin in AhR-depleted cells and, thus, these data support the AhR target hypothesis.

In summary, the AhR knockdown suggests that Picoberin mediated activation of AhR activity perturbs Hh-dependent osteoblast differentiation. Consequently, these data strongly support the hypothesis of AhR as the protein target of Picoberin. The data furthermore indicate, that AhR knockdown itself negatively influences Hh-induced osteogenesis, suggesting a functional role of this receptor during normal osteoblast differentiation. This finding is in line with the observed inhibition of Hh-dependent osteogenesis through the AhR antagonist CH233191 (see 5.5.1.1). However, also aberrant AhR activation inhibits osteoblast differentiation, suggesting that tight regulation of AhR signaling is crucial during this differentiation process.

5.5.4.2 Overexpression of AhR

As a complementary approach to genetic knockdown of AhR levels in C3H10T1/2 cells, the influence of plasmid-mediated AhR overexpression was explored. In theory, AhR overexpression should have an opposite effect on Hh-induced osteogenesis compared to *AhR*-depletion. To assess the effect of AhR overexpression, C3H10T1/2 cells were transiently transfected with a plasmid encoding for mAhR-FLAG for 24 h and treated with 1.5 µM purmorphamine and DMSO or 1.5 µM purmorphamine and 10 pM or 100 pM Picoberin or only DMSO as a control for 48 h. Afterwards, total RNA was isolated and the effect of *AhR* overexpression was evaluated by means of RT-qPCR (Figure 53). The graph in Figure 53A shows, that *AhR* levels were 4.1 ± 0.6–fold upregulated in cells transfected with the mAhR-FLAG construct after 72 h. However, this overexpression did not alter Hh-induced osteoblast

differentiation as determined by quantification of the *Alpl* mRNA levels 48 h after treatment of transfected cells with 1.5 µM purmorphamine (Figure 53B).

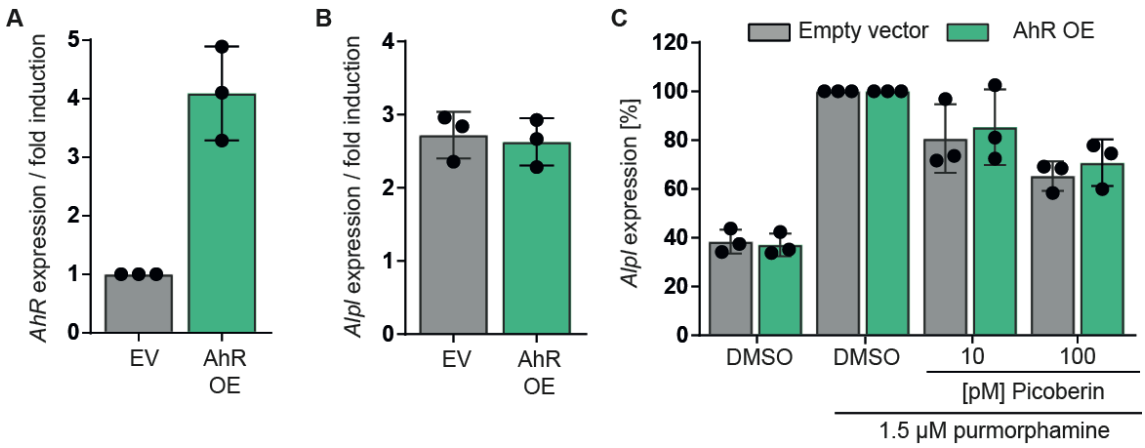

Figure 53: Influence of AhR overexpression (OE) on Hh-dependent osteogenesis and Picoberin-mediated inhibition. C3H10T1/2 cells were transfected with a mAhR-FLAG plasmid or an empty vector (EV) for 24 h, prior to compound treatment. After another 48 h, total RNA was isolated and expression levels of *AhR* and *Alpl* were determined by means of RT-qPCR. **A:** Fold overexpression of *AhR* mRNA. **B:** Influence of AhR overexpression on Hh-induced osteogenesis of C3H10T1/2 cells. **C:** Influence of AhR overexpression on Picoberin-mediated inhibition of osteoblast differentiation. Data of cells that were transfected with mAhR-FLAG or EV were related to the respective sample treated with 1.5 µM purmorphamine and DMSO (100 %). All data are mean values of three biological replicates (n = 3).

Figure 53C demonstrates, that also Picoberin mediated inhibition was not altered by AhR overexpression. To explore the AhR overexpression in more detail, *AhR* and *Cyp1b1* gene levels were determined. The corresponding results are shown in Figure 54.

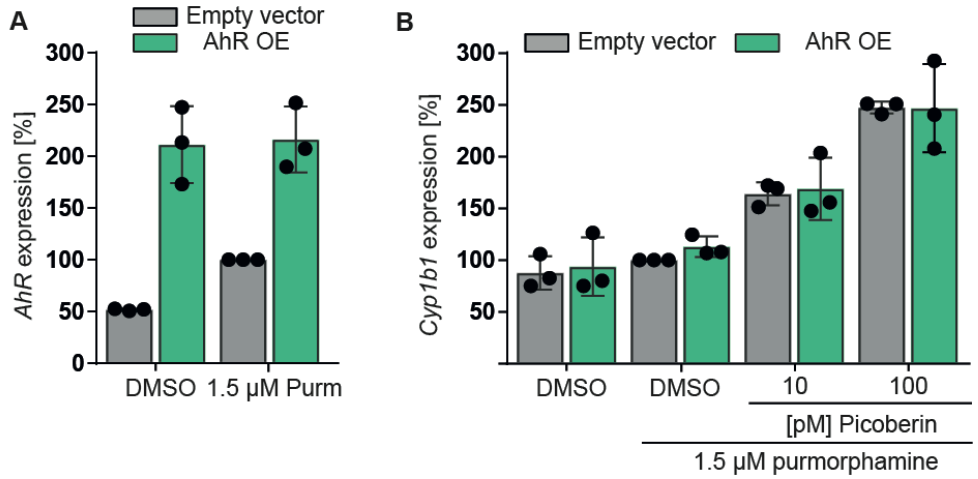

Figure 54: Influence of Picoberin on *AhR* and *Cyp1b1* expression in C3H10T1/2 cells overexpressing AhR. C3H10T1/2 cells were transiently transfected with a mAhR-FLAG plasmid or an empty vector for 24 h, prior to treatment with compounds. After another 48 h, total RNA was isolated and expression level of *AhR* and *Alpl* were determined by means of RT-qPCR. **A:** Influence of purmorphamine on *AhR* expression. **B:** Influence of Picoberin on *Cyp1b1* expression. Values were normalized to the values of samples transfected with empty vector and treated with 1.5 µM purmorphamine and DMSO, which were set to 100 %. All data are mean values of three biological replicates (n = 3).

The results in Figure 54A show that 1.5 µM purmorphamine upregulated AhR expression in cells that were transfected with the empty vector. In cells overexpressing mAhR-FLAG, purmorphamine was not able to further upregulate *AhR* gene levels. In line with observation during the global transcriptome profiling and subsequent RT-qPCR based experiments, *Cyp1b1* levels were dose-dependently upregulated by Picoberin in both, empty vector and mAhR-FLAG transfected cells (Figure 54B). Interestingly, *Cyp1b1* expression levels were not changed in AhR overexpressing cells. These data could indicate that upregulation of *AhR* mRNA levels may not have led to enhanced translation and thus upregulation of AhR protein levels. Detection of mAhR-FLAG protein levels in transfected C3H10T1/2 cells was not successful at any timepoint after transfection in C3H10T1/2 cells.

In summary, AhR overexpression experiments could not further support the hypothesis of AhR as the protein target of Picoberin during osteoblast differentiation. Although C3H10T1/2 cells were successfully transfected as indicated by a significant upregulation of *AhR* mRNA levels it remains unclear if AhR protein levels were changed throughout these experiments.

5.6 Mechanistic considerations

5.6.1 *Ptch2* expression in Picoberin-mediated inhibition of Hh-induced osteogenesis

During the investigation of Picoberin-mediated effects on the global transcriptome (see chapter 5.4.2.2), the expression of *Ptch2* was found significantly down-regulated in cells that were treated with 1.5 µM purmorphamine and 1 nM Picoberin compared to cells that were treated with 1.5 µM purmorphamine and DMSO for 24 h and 48 h. Since *Ptch2* is an homologue of *Ptch1* and a Hh target gene, this effect was explored in more detail.[131] The results in Figure 55A show the influence of the known Hh pathway inhibitor Vismodegib on *Ptch2* expression. Vismodegib completely inhibited purmorphamine-induced upregulation of *Ptch2* after 48 h. Picoberin inhibited purmorphamine-induced *Ptch2* expression in a dose-dependent manner and down to a level of 45.4 ± 7.4 % at a concentration of 1 nM (Figure 55B). The known AhR agonist FICZ showed a similar behavior and inhibited purmorphamine-induced upregulation of *Ptch2* down to a level of 46.0 ± 2.5 % at a concentration of 1 µM (Figure 55B). These data hint towards a potential crosstalk between AhR and Hh signaling.

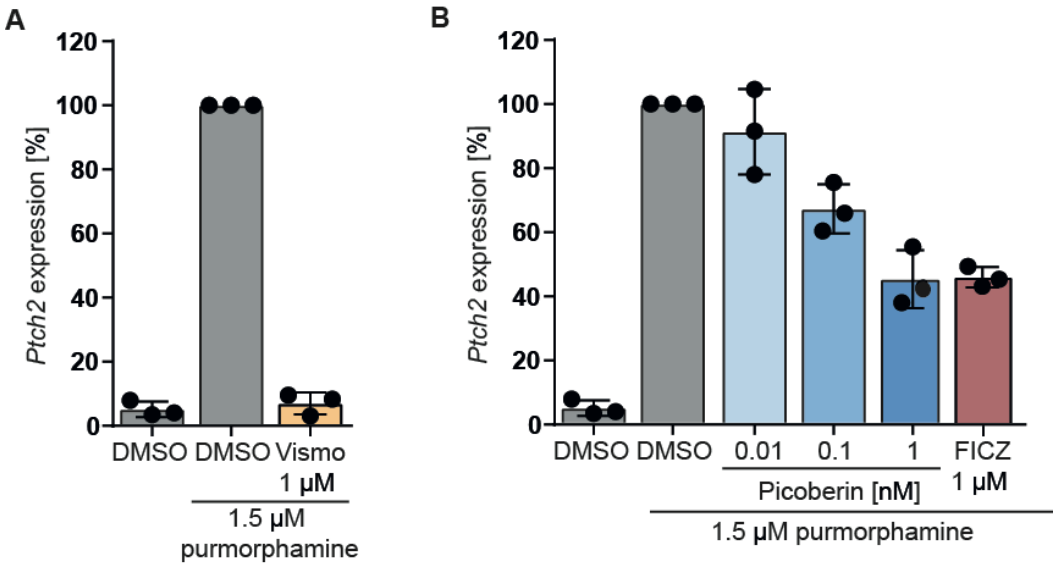

Figure 55: Vismodegib, Picoberin and FICZ inhibit Hh-induced upregulation of *Ptch2*. C3H10T1/2 cells were treated with 1.5 µM purmorphamine and 1 µM Vismodegib (Vismo), different concentrations of Picoberin, 1 µM FICZ or DMSO as a control. After 48 h, *Ptch2* expression levels were quantified by means of RT-qPCR using primers specific for *Ptch2* and *Gapdh* and *Ap3d1* as housekeeping genes. Data obtained for *Ptch2* were normalized to the respective *Gapdh* and *Ap3d1* values. All values were related to values of samples that were treated with purmorphamine and DMSO (100 %) and are mean values of three biological replicates (N = 3, n = 3) ± SD.

To further investigate a potential influence on Hh signaling via regulation of *Ptch2*, *Ptch2* expression levels were explored in AhR-depleted cells compared to NT siRNA treated cells

after 48 h of compound treatment. For these studies, the same samples that were described in chapter 5.5.4.1 were used. The quantification of the AhR knockdown efficiency is shown in Figure 51A. The graph in Figure 56 demonstrates, that the inhibition by 100 pM Picoberin is mitigated in AhR-depleted cells compared to control cells.

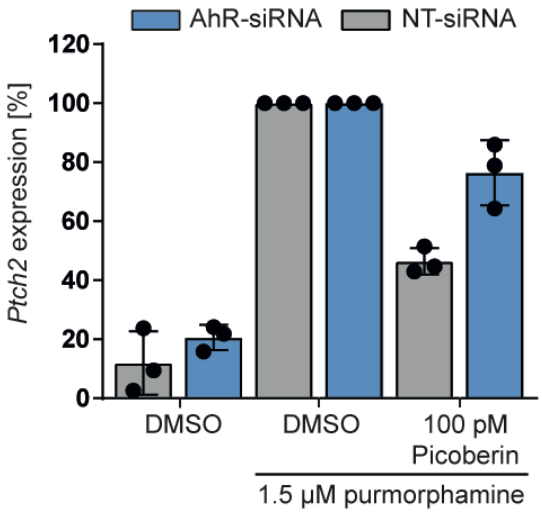

Figure 56: Influence of siRNA mediated AhR depletion and Picoberin on *Ptch2* expression. C3H10T1/2 cells were bulk-transfected with 30 nM AhR siRNA or non-targeting (NT)-siRNA for 24 h, prior to re-seeding and treatment with 1.5 µM purmorphamine and DMSO, 1.5 µM purmorphamine and 100 pM Picoberin or only DMSO. After 48 h, total RNA was isolated and expression level of *Ptch2* and *Gapdh* and *Ap3d1* as housekeeping genes were determined by means of RT-qPCR. Data of NT- and AhR siRNA treated samples were related to the respective values of cells treated with purmorphamine and DMSO. Data are mean values of three biological replicates (n = 3).

In C3H10T1/2 cells transfected with NT siRNA, 100 pM Picoberin reduced *Ptch2* mRNA levels down to 46.4 ± 6.7 % compared to the respective purmorphamine and DMSO treated samples. In AhR siRNA treated cells, *Ptch2* expression was downregulated by Picoberin to a level of 76.4 ± 9.0 %.

In summary, the data presented in this chapter hint towards crosstalk between AhR and Hh signaling.

5.6.2 Influence of Hh signaling on AhR expression and signaling

During the investigation of Picoberin-mediated effects on the global transcriptome (see chapter 5.4.2.2) the AhR was identified as a potential target protein of this small molecule and several findings described above clearly support this target hypothesis. Several experiments provide evidence for a potential crosstalk of AhR and Hh signaling during Hh-dependent osteoblast differentiation. For this reason, the impact of Hh signaling on AhR signaling was explored using

global transcriptome profiling data set. The heatmap in Figure 57 illustrates the changes in cells that were treated with purmorphamine and DMSO or purmorphamine and 1 nM Picoberin, both compared to only DMSO treatment of C3H10T1/2 cells for selected genes that ware involved in AhR signaling. The corresponding log_2 fold change values as well as the respective p-values are summarized in Table 15.

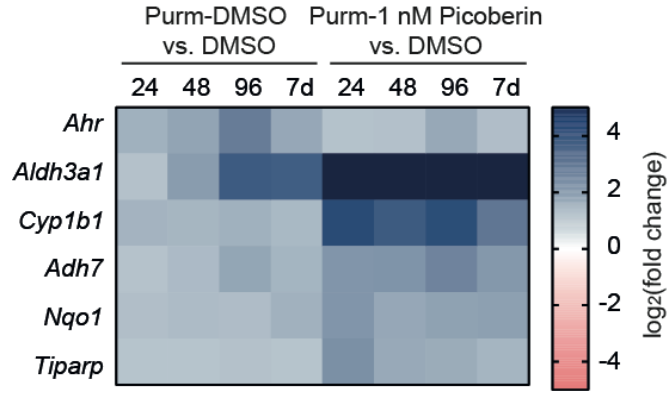

Figure 57: Time-resolved influence of Hh signaling and Picoberin on genes involved in AhR signaling. RNA-Seq. Heatmap for samples treated with 1.5 µM purmorphamine and DMSO or 1.5 µM purmorphamine and 1 nM Picoberin compared to samples treated with only DMSO. Differential gene expression was explored after 24 h, 48 h, 96 h or 7 days of compound treatment. Red color: negative log_2 fold changes. Blue: Positive log_2 fold changes. Data are mean values of three biological replicates (n = 3).

Table 15: Time-resolved influence of Picoberin on genes involved in Hh and AhR signaling. RNA-Seq data. Calculated log_2 fold changes (FC) for samples treated with 1.5 µM purmorphamine and DMSO compared to samples treated with only DMSO for 24 h, 48 h, 96 h or 7 days. Data are mean values of three biological replicates (n = 3). Significant changes are marked in bold.

Gen	24h log_2 (FC)	24 h p-value	48 h log_2 (FC)	48 h p-value	96 h log_2 (FC)	96 h p-value	7 days log_2 (FC)	7 days p-value
Ahr	**0.571**	**9.34E-04**	**0.856**	**1.84E-06**	**1.519**	**0.00E+00**	**0.780**	**1.54E-05**
Aldh3a1	0.179	2.05E-01	**1.005**	**0.00E+00**	**1.941**	**0.00E+00**	**1.914**	**0.00E+00**
Adh7	0.140	1.81E-01	**0.363**	**5.19E-04**	**0.823**	**2.89E-15**	**0.515**	**5.22E-07**
Cyp1b1	0.515	3.14E-06	**0.480**	**1.39E-05**	**0.577**	**1.74E-07**	**0.411**	**1.93E-04**
Nqo1	0.262	9.13E-02	0.360	2.06E-02	0.314	4.46E-02	**0.567**	**2.52E-04**
Tiparp	0.095	4.04E-01	0.091	4.10E-01	0.174	1.12E-01	0.091	3.97E-01

The results in Figure 57 and Table 15 show, that several AhR target genes are upregulated over time upon treatment of C3H10T1/2 cells with 1.5 µM purmorphamine. Especially *Aldh3a1* levels show a strong increase after 96 h and 7 days of differentiation. Furthermore, also *AhR* mRNA levels are upregulated by purmorphamine at all four timepoints, suggesting that *AhR*

may be regulated by Hh signaling and may have a functional role during Hh-induced osteoblast differentiation. To explore, if induction of AhR gene expression is a purmorphamine-specific or a Hh-dependent effect, further gene expression analysis was carried out. Figure 58A demonstrates the influence of SHH-conditioned medium on the expression of the osteogenesis marker *Alpl* and on *AhR* after 96 h. SHH treatment led to a 4-fold induction of *AhR* expression. In line with the results obtained in the global transcriptome profiling, 1.5 µM purmorphamine clearly upregulated *AhR* expression after 96 h and this effect was completely inhibited by the Hh pathway inhibitor Vismodegib (Figure 58B).

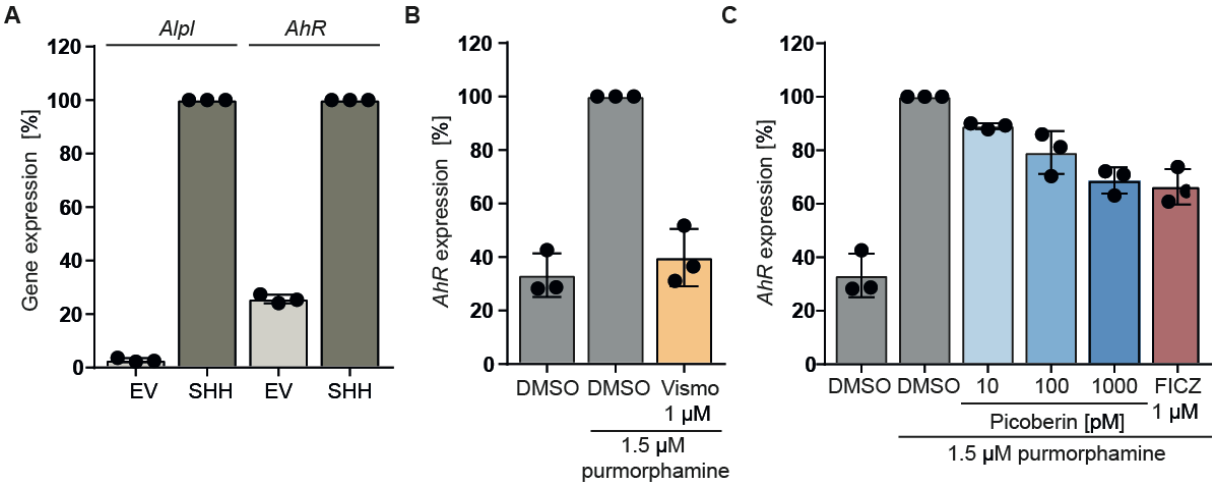

Figure 58: Vismodegib, Picoberin and FICZ inhibit Hh-induced AhR expression. A: C3H10T1/2 cells were treated with SHH-conditioned medium, or empty vector conditioned medium (EV) for 96 h. *AhR* expression levels were quantified by means of RT-qPCR using primers specific for *AhR* and *Gapdh* and *Ap3d1* as housekeeping genes. Data obtained for *AhR* were normalized to the respective *Gapdh* and *Ap3d1* values. All data were related to samples that were treated with SHH-conditioned medium, (100 %). **B** and **C:** C3H10T1/2 cells were treated with 1.5 µM purmorphamine and 1 µM Vismodegib (Vismo), different concentrations of Picoberin, 1 µM FICZ or DMSO as a control. After 96 h, *AhR* expression levels were quantified. Data obtained for *AhR* were normalized to the respective *Gapdh* and *Ap3d1* values. All data were related to samples that were treated with purmorphamine and DMSO (100 %) and are mean values of three biological replicates (N = 3, n = 3) ± SD.

In line with the results obtained in the global transcriptome profiling, Picoberin slightly but dose-dependently inhibited purmorphamine induced expression of AhR, down to a level of 68.7 ± 4.0 % at a concentration of 1 nM (Figure 58C). The known AhR agonist FICZ showed a similar effect at a concentration of 1 µM. Regulation of the *AhR* expression could thus be part of the mode of action of AhR agonists that results in inhibition of Hh-induced osteogenesis.

6 DISCUSSION

6.1 Furo[3,2-b]pyridine, quinoline, pyrroloquinoline and 20-membered macrocycle derivatives inhibit Hh signaling via binding to SMO

A Furo[3,2-b]pyridine (compound **1**), a quinoline (compound **2**), a pyrroloquinoline (compound **3**) and a 20-membered macrocycle (compound **4**) were identified as inhibitors of Hh-dependent osteoblast differentiation with IC_{50} values in the micromolar and sub-micromolar range (Figure 59).

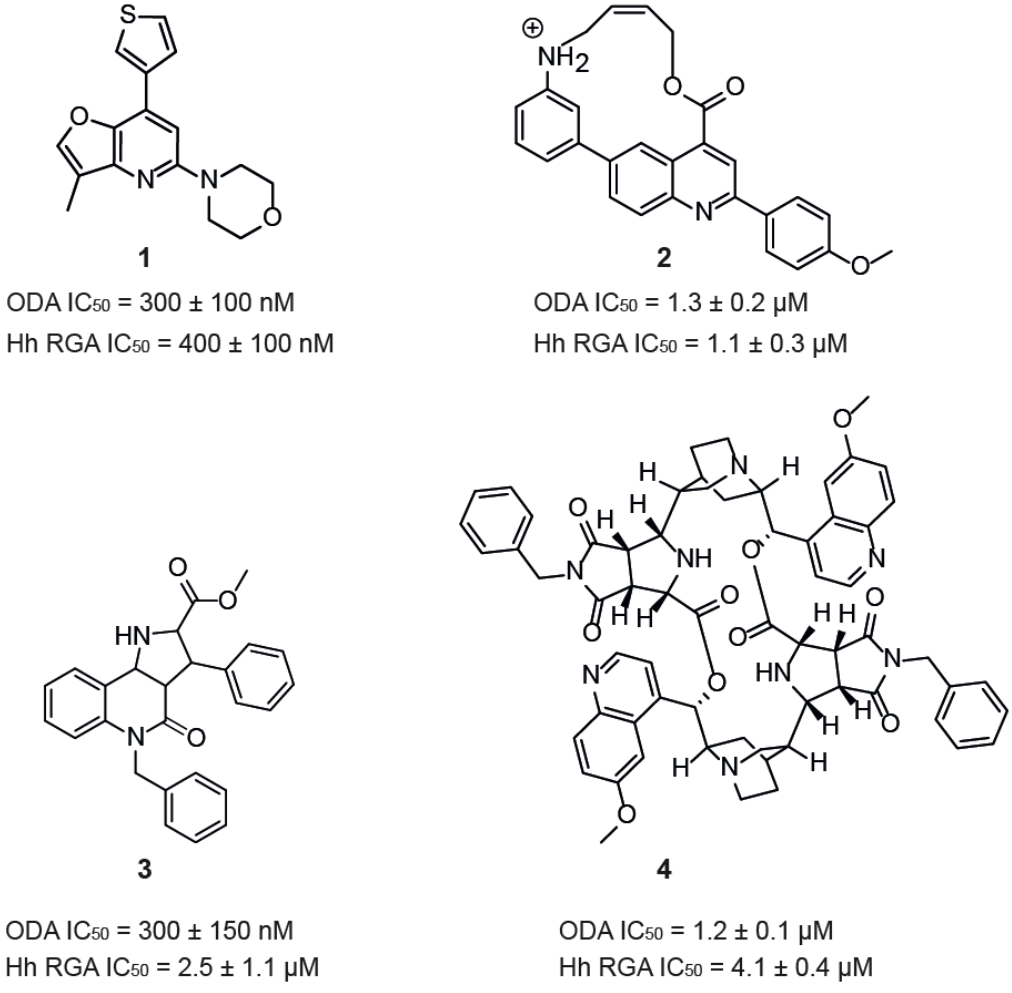

Figure 59: Overview on novel Hh pathway inhibitors. The obtained IC_{50} values in the osteogenesis assay (ODA) are 300 ± 100 nM (compound **1**), 1.3 ± 0.2 µM (compound **2**), 300 ± 150 nM (compound **3**) and 1.2 ± 0.1 µM (compound **4**). IC_{50} values obtained in the GLI2/3-depndent reporter gene assay in (Hh RGA): 400 ± 100 nM (compound **1**), 1.1 ± 0.3 µM (compound **2**), 2.5 ± 1.1 µM (compound **3**) and 4.1 ± 0.4 µM (compound **4**).

While the IC_{50} values obtained for compounds **1** and **2** are in the same concentration range in both assays, the potency of compounds **3** and **4** is markedly reduced in the GLI2/3-dependent reporter gene assay. Such a drop in compound activity in the GLI2/3-dependent reporter gene assay has been observed in the group for several other compound classes before. A direct influence of the compounds on the reporter gene assay readout, which could explain this reduced compound potency, was excluded by means of luciferase activity assays. The differences in potency could be explained by the different types of assays that were used to monitor the activities of the compounds. While the reporter gene assay monitors a GLI2/3- and, thus, a directly Hh-dependent reporter activity, the osteogenesis assay detects alkaline phosphatase activity as a measure for the differentiation status and as an indirect measure for Hh signaling. Osteogenesis is a highly complex process that is tightly regulated by several signaling pathways, such as Wnt, Notch and TGFβ signaling.[72, 132] The higher potencies of compounds **3** and **4** in the Hh-dependent osteogenesis assay could thus hint towards additional interference of these compounds with other signaling pathways during this differentiation process. Strikingly, compound **3** was inactive in other cellular signaling pathways and biological processes monitored at COMAS, including Wnt and BMP signaling, indoleamine 2,3-dioxygenase (IDO) activity, and autophagy. However, a comparison of the dose-response curves obtained in the osteogenesis assay and the GLI2/3-dependent reporter gene assay supports possible additional activities of compound **3**. While Hh-induced osteogenesis was inhibited to basal levels at a concentration of 3 µM, significant residual activity was retained in the GLI2/3-dependent reporter gene assay even at 30 µM. Examination of the influence of compounds **1**, **2** and **3** on expression of the Hh target genes *Gli1* and *Ptch1* further support this hypothesis. While the inhibition of *Gli1* and *Ptch1* expression mediated by compound **1** and **2** matches well to the respective activities in the osteogenesis and the GLI2/3-dependent reporter gene assay, compound **3** only partially reduced *Gli1* and *Ptch1* expression at a concentration of 10 µM. These results are in line with the corresponding results of the GLI2/3-dependent reporter gene assay, but not with complete inhibition of Hh-dependent osteogenesis. Therefore, alterations of other pathways may contribute to compound **3** induced inhibition of Hh-dependent osteogenesis.

In case of compound **4**, an autophagy assay revealed substantial upregulation of LC3-lipidation in addition to inhibition of Hh signaling.[92] Dysregulation of autophagy disturbs the balance between bone formation and resorption and is involved in multiple bone-diseases, including osteoporosis.[133] Thus, compound **4** mediated changes in LC3-lipidation and autophagy may contribute to the observed inhibition of Hh-dependent osteoblast differentiation.

All four compounds displaced BODIPY-cyclopamine. Consequently, all four compounds bind to the heptahelical bundle of SMO and can thus be characterized as SMO binders. For the

most potent compound **1** the influence on SHH-induced Hh signaling was explored via a GLI2/3-dependent reporter gene assay, as a second approach to show binding of this compound to the heptahelical bundle of SMO. The SMO agonist purmorphamine, which was used in the osteogenesis assay and the GLI2/3-dependent reporter gene assay to activate Hh signaling, binds to the same heptahelical bundle of SMO as cyclopamine.[134] Consequently, small molecules that act via binding to the same binding pocket, need to compete with purmorphamine to inhibit Hh signaling. SHH activates Hh signaling upstream of SMO, via binding to the 12-pass transmembrane protein PTC1[135] and thus no competition for binding at the heptahelical bundle of SMO is required. For this reason, SMO-binding Hh inhibitors should in theory be more potent in inhibiting SHH-induced Hh signaling compared to purmorphamine-induced Hh signaling. Indeed, the known SMO antagonist Vismodegib, as well as compound **1** more potently inhibited GLI2/3-dependent reporter activity when SHH-CM was used to activate Hh signaling compared to purmorphamine. In contrast, the known non-SMO binder GANT61 showed the same activity in both assay setups.

Pyrrolo[3,2-c]quinoline-4-one derivatives were reported as Hh pathways inhibitors by the group of Tomohiro Ohashi *et al*.[136] with IC_{50} values in the single digit nanomolar range (compound **33**, IC_{50} = 5.1 nM, Figure 60). It was thus not surprising, that pyrroloquinoline **3** was identified as a Hh pathway inhibitor. However, the reported compounds were not characterized regarding their ability to bind to the heptahelical bundle of SMO.

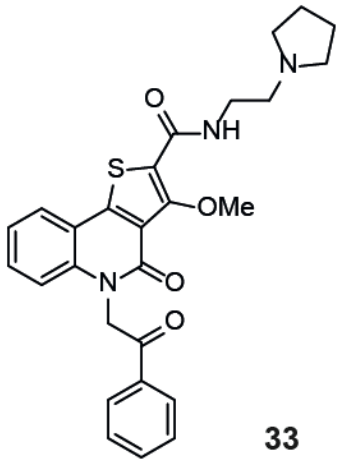

33

Figure 60: Chemical structure of a pyrrolo[3,2-c]quinoline-4-one derivative that was reported as a Hh pathway inhibitor by the group of Tomohiro Ohashi *et al*.[136] Compound 33 inhibits GLI2/3-dependent reporter activity with an IC_{50} of 5.2 nM.

In summary, compounds **1** – **4** were identified and successfully validated as novel Hh pathway inhibitors. All four compounds target the heptahelical bundle of SMO. While compound **1** and **2** seem to specifically inhibit Hh signaling, the presented data hints towards potential additional biological effects of compounds **3** and **4** during Hh-dependent osteoblast differentiation.

6.2 4-Arylisoquinolones inhibit Hh signaling and do not bind to SMO

Compound **5** was identified as an inhibitor of Hh-dependent osteoblast differentiation with an IC_{50} value of 2.3 ± 0.3 µM. Inhibition of Hh signaling could be confirmed by means of the GLI2/3-dependent reporter gene assay in SHH-LIGHT2 cells, which was inhibited by compound **5** with an IC_{50} value of 1.8 ± 0.1 µM. Furthermore, compound **5** reduced the expression of the Hh target genes *Gli1* and *Ptch1* to a level of 40 % at a concentration of 2 µM, which matched to the obtained activities in the osteogenesis and the reporter gene assay. Compound **5** did not displace BODIPY-cyclopamine, suggesting that this compound does not bind to the heptahelical bundle of SMO. Thus, compound **5** may most likely inhibit Hh signaling independently of SMO and identification of its molecular target would be highly interesting. However, although this compound does not bind to the heptahelical bundle of SMO, it could still target another binding site of this protein. Figure 61 gives a schematic overview of the structure and the known and potential binding sites of SMO.[134] Although most SMO-ligands, including Vismodegib, cyclopamine and purmorphamine bind to the heptahelical bundle of SMO, binding to other regions is also reported. Oxysterols and cholesterol bind to the extracellular cysteine-rich domain of SMO.[134] Furthermore, the extracellular linker domain as well as the extracellular loops and the cytosolic tail of SMO could potentially be targeted by small molecules.

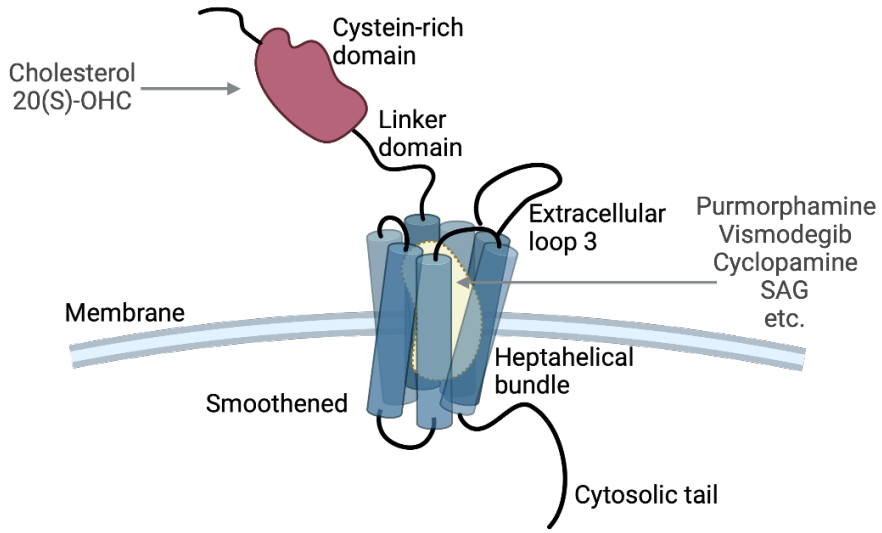

Figure 61: Schematic overview of the structure of SMO and its known ligand binding sites. The 7-pass transmembrane domain, also referred to as heptahelical bundle is the ligand binding domain that is targeted by most of the currently known SMO ligands. The extracellular cysteine-rich domain is known to bind oxysterols, such as 20(S)-OHC and cholesterol. The linker domain as well as the extracellular loop 3 and the cytosolic tail could potentially be targeted by small molecules. Structure was adopted from Eamon FX Byrne *et al.*[134]

To evaluate potential binding of compound **5** to other SMO binding sites, further experiments could be carried out. These include biophysical experiments with purified SMO protein, as for example fluorescence polarization (FP) or surface plasmon resonance (SPR). Furthermore, CETSA could be performed to explore binding of compound **5** to SMO in lysates or even in living cells. Mutational analysis, including the D473H mutant of SMO conferring resistance to Vismodegib treatment, could be performed to investigate whether compound **5** is able to overcome resistance mutations in SMO.[137] However, since no clear structure-activity relationship was observed for this compound class and even more potent compound classes were identified during the screening campaign at COMAS, this compound class was not investigated in more detail during this thesis.

6.3 8-oxotetrahydroprotoberberines inhibit Hh-dependent osteogenesis but not canonical Hh signaling

Initially, compound **6** was identified as a potent inhibitor of Hh-dependent osteoblast differentiation, with an IC_{50} value of 1.2 ± 0.4 nM. Evaluation of this compound in a GLI2/3-dependent reporter gene assay in SHH-LIGHT2 cells, as well as evaluation of the influence on the expression of the Hh target genes *Gli1* and *Ptch1* in NIH-3T3 cells revealed that this compound does not inhibit canonical Hh signaling, even at concentrations up to 30 µM. Due to the high potency in the osteogenesis assay, it was decided to explore this compound class in more detail and to perform target identification and mode of action studies to characterize the inhibition of Hh-dependent osteoblast differentiation in detail.

The structure-activity relationship was explored to identify a position on the molecule that is suitable for attachment of a linker and, thus, design of probe molecules. For this purpose, a focused library with 26 analogues of compound **6** was synthesized by Dr. Saad Shaaban and Dr. Zhijun Jia at the MPI in Dortmund. Besides compound **6**, eleven analogues inhibited Hh-induced osteogenesis at least down to a level of 50 % while retaining a cell viability of at least 80 %. Figure 62 gives a graphical overview of the structure-activity relations that were observed.

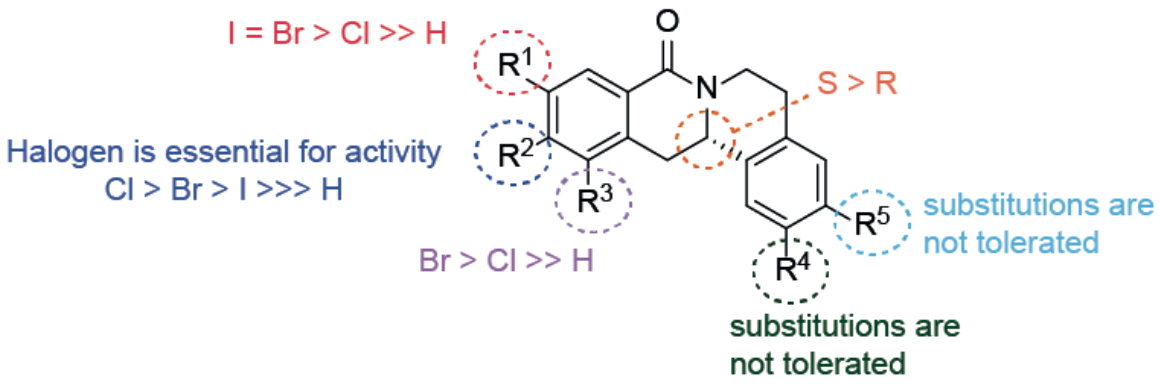

Figure 62: Structure-activity relationship of 8-oxotetrahydroprotoberberines as inhibitors of Hh-dependent osteogenesis of C3H10T1/2 cells. The activity of in total 27 8-oxotetrahydro-protoberberines was explored in the Hh-dependent osteoblast differentiation assay.

The SAR-study revealed that a halogen moiety at position R^2 is essential for the biological activity. Increasing size of the halogen moiety however decreases the potency of the compound. Additional halogenation of R^1 or R^3 both increased the potency compared to the mono-chlorinated analogue **6**, however additional substitution at R^1 is preferred over R^3. In both cases, bromo and iodo substituted analogues are more potent than the chloro- substituted analogues. Modifications at R^4 and R^5 were not tolerated. Furthermore, *S*-configurated analogues were more potent than the respective *R*-configurated compounds.

Since all evaluated modifications either increased compound potency or led to an almost complete loss of biological activity, the SAR-study did not lead to the identification of a position suitable for attachment of a linker and, thus, modifications for the design of probe molecules. Further extension of the SAR study could be carried out e.g., to explore the relevance of the *carbonyl* moiety and the influence of the ring size and ring opening at the nitrogen. In addition, modifications at the so far not modified positions at the aromatic rings could be investigated.

The SAR-study led to the identification of analogue **18**, termed Picoberin, which inhibits Hh-dependent osteogenesis with an IC_{50} value of 3 ± 1 pM and is thus 400-fold more potent than the initial hit compound **6**. Such an ultrapotent activity of a small molecule in a cell-based phenotypic assay is not usual and rarely reported in the literature. To validate this result and to exclude potential effects of Picoberin that could interfere with the assay readout and lead to distorted results, additional experiments were carried out to validate this activity.

The osteoblast differentiation assay is based on the expression of alkaline phosphatase, which is an early marker for osteoblast differentiation.[138] Alkaline phosphatase is an enzyme, that catalyzes the hydrolysis of phosphoric acid monoesters.[139] During osteoblast differentiation, this activity is important to supply cells with inorganic phosphate that is required for mineralization.[139] Since alkaline phosphatase protein levels correlate with the osteogenic differentiation status of cells, its enzymatic activity is exploited for assay readout. Small molecules that interfere with the enzymatic activity of the alkaline phosphatase would distort the readout of the osteoblast differentiation assay. However, Picoberin does not influence the enzymatic activity of alkaline phosphatase, reinforcing the significance of the result obtained in the osteoblast differentiation assay. Moreover, Picoberin dose-dependently reduces *Alpl* mRNA levels in C3H10T1/2 cells at picomolar concentrations. However, a residual *Alpl* expression was detected that matches the results from the Hh-dependent osteoblast differentiation assay. The reduction in alkaline phosphatase at picomolar Picoberin concentrations was substantially greater on protein level. One possible explanation for this difference could be that mRNA and protein expression are decoupled in time.[140] Such timely uncoupled correlation is reported in the literature, e.g., for cells treated with Rapamycin, where mRNA expression profiles after 1 h or 2 h of treatment correlated best with protein expression after 6 h.[141] In addition, other levels of regulation may override the transcriptional level and provide biological fine-tuning to the specific conditions to which cells are exposed.[140] Consequently, despite the different magnitude of the inhibition, the results confirm that Picoberin inhibits Hh signaling-induced expression of alkaline phosphatase and, thus, early stages of Hh-induced osteoblast differentiation at picomolar concentrations.

Picoberin reduced incorporation of calcium-deposits into the extracellular matrix of osteoblasts. This confirms that Picoberin suppresses matrix mineralization and, thus, also late stages of osteoblast differentiation. However, complete inhibition was only observed at a concentration

of 1 µM. At picomolar concentrations matrix mineralization was reduced compared to control cells. Interestingly, this reduction was not manifested by a uniform reduction in calcium deposits, but by an inhomogeneous phenotype. While some areas of the cell monolayer clearly exhibited a bright red staining comparable to that of control cells, other parts were completely unstained. This suggests that low concentrations of Picoberin are not sufficient to completely block Hh-induced osteogenesis in all cells over long incubation periods and may indicate that individual mesenchymal stem cells respond differently to Picoberin treatment. To further investigate these observations and to assess whether the reason for the inhomogeneous formation of calcium deposits is due to an inhomogeneous initial differentiation status of the mesenchymal cells used, quantification of stem cell markers, such as CD44, CD90 or CD105[142] could be carried out for individual cells.

Microscopic monitoring of the influence on C3H10T1/2 cells growth clearly showed that Picoberin has no cytotoxic effects up to a concentration of 10 µM. Also in other cell lines that were testes at COMAS, no influence of Picoberin on cell viability was observed (Table 16).

Table 16: Picoberin has no influence on cell viability of different cell lines. Cell viability was explored at COMAS using a CellTiterGlo® assay.

Cell line	Viability at 10 µM
A549	98 %
C2C12	91 %
HEK293-T	99 %
SHH-LIGHT2	92 %
U2OS	92 %

Considering the high potency of Picoberin, the absence of any cytotoxic effects is very remarkable and may indicate that this small molecule acts in a highly specific manner.[143]

Osteoblast differentiation is a highly complex and tightly regulated process that requires sequential and carefully timed activation or suppression of a variety of signaling pathways. Besides Hh signaling, these include e.g. Wnt, BMP, TGFβ and FGF signaling.[70, 76] Each of these pathways is on its own tightly regulated by a plethora of biomolecules and in addition to canonical signaling cascades, many signaling pathways have multiple non-canonical branches. Moreover, crosstalk among signaling pathways further increases the complexity, resulting in an extended network that controls osteoblast differentiation.[144] As Picoberin does not inhibit canonical Hh signaling, modulation of other pathways, which are involved in osteogenesis, was very likely. To investigate, whether Picoberin exclusively inhibits osteoblast differentiation induced by activation of pathways other than Hh signaling, different stimuli were used to induce osteogenesis. In line with literature reports, Wnt-3A induced osteoblast

differentiation of C3H10T1/2 cells.[145] However, while Hh signaling led to a 20-fold upregulation of alkaline phosphatase activity after four days, Wnt-3A induced osteogenesis by only 1.6-fold. Only after 12 days of incubation, alkaline phosphatase was 13-fold upregulated in cells treated with Wnt-3A. This timely delayed upregulation of the early osteogenesis marker upon treatment of cells with Wnt-3A is consistent with reports, showing that Hh signaling acts upstream of Wnt signaling during osteoblast differentiation and is important for osteoblastic commitment of mesenchymal stem cells.[146] An influence of Picoberin on canonical Wnt signaling was excluded. However, Picoberin inhibited Wnt-3A induced osteoblast differentiation with an IC_{50} of 890 ± 64 pM and down to a level of 47.2 ± 4.9 %, indicating that its activity may not be limited to Hh-induced differentiation processes. Since positive crosstalk between Hh and Wnt signaling is reported and the status of the Hh pathway upon treatment of C3H10T1/2 cells with Wnt-3A was not explored, a Hh-dependent mechanism could not be excluded entirely.[99]

Picoberin did not modulate BMP4 induced osteogenesis of C2C12 cells, nor inhibit TGFβ signaling. Interestingly, Picoberin partially inhibited osteoblast differentiation that was induced by co-treatment of C2C12 cells with BMP4 and purmorphamine at picomolar concentrations. Upregulation of the osteogenesis marker alkaline phosphatase in C2C12 cells that were treated with purmorphamine and BMP4 may thus occur via two independent mechanisms. Since Picoberin inhibits only osteogenesis that is induced via activation of Hh signaling, these data hint to a Hh-dependent mode of action of Picoberin that ultimately results in inhibition of osteogenesis.

6.4 Target identification

During the course of the investigations for this thesis, various approaches to identify the molecular target of Picoberin responsible for inhibition of Hh-dependent osteogenesis were employed. Since no suitable position for attachment of a linker was found, only label-free approaches could be applied. These include computational target prediction, thermal proteome profiling as well as global transcriptome and proteome profiling, which are discussed in detail in the following chapters.

6.4.1 Target identification via computational target prediction

Computational target prediction is a powerful approach that is often used in early drug discovery to gain initial information about the most probable targets of a research compound.[147] Besides identification of potential ‘on-targets’, such methods provide insights into potential ‘off-targets’ and thereby potential adverse effects of a ligand.[147] Moreover, computational target predictions can aid to repurpose already approved drugs if they are found

to interact with protein targets involved in other disease mechanisms.[147] In contrast to wet lab experiments, computational target prediction is cheap and can quickly return target hypotheses that can guide subsequent lab work.[147] Depending on the research context and available data, target-based or ligand-based prediction methods can be applied. However, in both cases computational prediction methods rely on the general assumption that similar molecular structures will interact with similar interaction partners.[147]

Target prediction using *Similarity Ensemble Approach* (SEA)[101] based on the structure of Picoberin identified 15 GPCRs among the top 20 most probable targets. In contrast to classical similarity search, SEA identifies targets based on a group of known compounds for a respective target and not based on a single compound. Thereby this approach allows for calculation of statistical measures that can score the relevance of an identified target.[147] In particular, dopamine receptors and serotonin receptors were over-represented with high relevance scores in the SEA analysis.

Although detailed mode of actions remain largely unknown, multiple GPCRs are involved in regulation of osteoblast differentiation.[148] Moreover, several GPCRs are modulated at picomolar or even sub-picomolar concentrations of ligands. These include β-adrenoreceptors, adenosine receptors and 5-hydroxytryptamine receptors.[102] In a GPCR panel covering 157 different GPCRs, Picoberin inhibited only the CXC chemokine receptor type 4 (CXCR4) as a hit that was inhibited to 52 % at a compound concentration of 500 nM. Picoberin did not activate any of the 157 GPCRs. Indeed, conditional inactivation of CXCR4 inhibits BMP2-induced osteogenic differentiation of mesenchymal progenitor cells.[149]

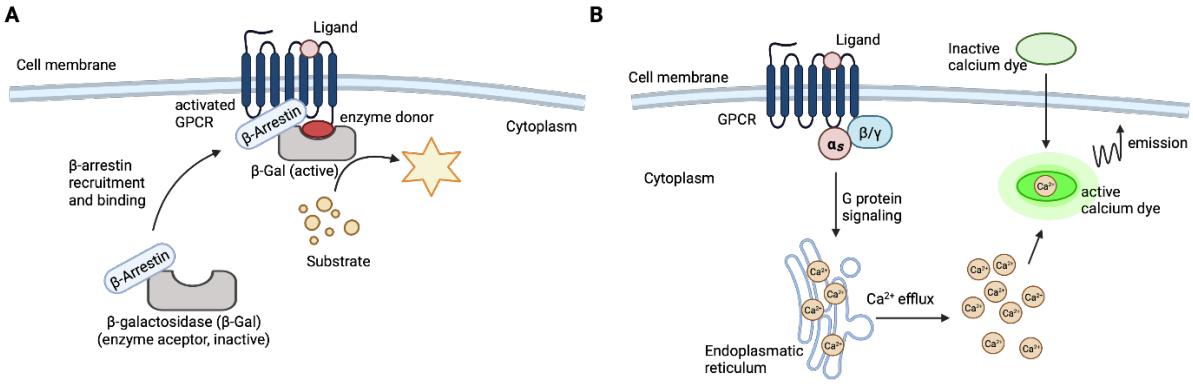

Figure 63: Illustration of the employed cell-based GPCR assay technologies. A: β-Arrestin enzyme fragment complementation assay. β-Galactosidase that serves as a functional reporter is split into two inactive complementary fragments: enzyme acceptor and enzyme donor. The enzyme acceptor is fused to β-arrestin, the enzyme donor is fused to the GPCR of interest. Upon activation of the GPCR, β-arrestin is recruited to the receptor. This leads to fragment complementation of the β-galactosidase, which catalyzes a chemiluminescent reaction for assay readout. **B:** Calcium flux assay. GPCR activation results in the release of calcium ions from intracellular stores and an increase in Ca^{2+}-dependent dye fluorescence that is measured in real time.

Dose-dependent evaluation of Picoberin in an orthogonal cell-based CXCR4 calcium flux assay (Figure 63B) could not confirm inhibition of CXCR4. One reason for these different results could lie in the different assay technologies that were used to detect the CXCR4 activity. While the initial GPCR panel monitored recruitment of β-arrestin to the activated CXCR4 receptor, the calcium flux assay measures direct mobilization of calcium ions upon activation of CXCR4. Compounds that specifically modulate only β-arrestin recruitment but not G-protein signaling activity of a GPCR could show such an activity profile.[148, 150] For this reason, CXCR4 was not entirely excluded as a potential target protein.

However, GPCRs represent one of the major protein families commonly used as drug targets.[151] Databases that are used by target prediction tools are therefore generally biased towards this protein class.[152] The overrepresentation of GPCRs in the hit list was thus not surprising. Only proteins for which similar ligands are annotated in the database can be identified as potential hit candidates. Moreover, even highly similar ligands may target different proteins.[147] Target predictions are therefore not able to predict all possible interactions and thus all molecular targets. Although computational target predictions are helpful to obtain an initial idea about potential protein targets, predictions alone are not suitable to evaluate the totality of all molecular targets. Picoberin was therefore explored further in unbiased, experimental approaches. These could provide both, further evidence towards CXCR4 modulation but also more insights into the mode of action and hints towards other potential molecular targets.

6.4.2 Target identification via global transcriptome and proteome profiling

Quantification of differentially expressed genes and proteins in cells upon treatment with a compound via RNA-Seq or mass spectrometry is a highly powerful approach to gain mechanistic insights into the mode of action and potential molecular targets of a compound. In this thesis, Picoberin-mediated effects were dose- and time-dependently analyzed using global transcriptome and proteome profiling.

Analysis of differentially expressed genes upon treatment of cells with purmorphamine and DMSO clearly showed a significant upregulation of Hh-target genes including *Gli1*, *Gli2*, *Ptch1*, *Ptch2* and *Hhip*, thus proving successful activation of canonical Hh signaling. Furthermore, *Alpl* expression levels were upregulated after 48 h, 96 h and 7 days, which confirmed induction of osteoblast differentiation. Interestingly, *Runx2*, which is an essential master regulator of osteoblast differentiation,[153] was not upregulated at any of the explored timepoints. However, the osteoblast-specific transcription factor *Sp7* (encoding for the protein osterix, OSX), was 4-fold induced after 96 h. *Bglap,* which encodes for the late-stage osteogenesis marker osteocalcin (OCN), was 5.5-fold increased after 7 days. Taken together, these data clearly

confirmed, that purmorphamine induced osteoblast differentiation during this experiment. Since *Runx2* was not regulated, purmorphamine seems to induce osteogenesis in a *Sp7*-dependent but *Runx2*-independent manner. Although OSX has been suggested as a downstream target of RUNX2, the regulatory mechanisms of OSX expression are only poorly understood.[154, 155] In line with observations made in this thesis, several other groups have shown RUNX2-independent regulation of OSX during osteoblast differentiation. Hojo *et al.* has reported that GLI1 overexpression induced expression of the osteogenesis markers *Alpl* and *Bsp* in *Runx2*$^{-/-}$ cells.[156] Matsubara *et al.* observed BMP-2 induced OSX overexpression and upregulation of alkaline phosphatase activity in *Runx2*-deficient mesenchymal stem cells.[79]

Treatment of C3H10T1/2 cells with 1 nM Picoberin reduced expression of the osteogenic marker *Alpl*, which confirmed inhibition of osteoblast differentiation. However, expression levels of *Runx2*, *Sp7* and *Bglap* were not significantly altered by Picoberin at any timepoint. In line with initial gene expression analysis, Hh target-genes *Gli1* and *Ptch1* were not significantly altered, confirming that canonical Hh signaling is not modulated by this compound. Transcriptome profiling revealed Picoberin-mediated upregulation of genes encoding for several phase I and II metabolic enzymes, including *Cyp1b1*, *Aldh3a1*, *Adh7*, *Nqo1*, *Xdh, Cyp1a1* and *Tiparp*. Pathway-overrepresentation analysis linked the increased expression of these genes to activation of several metabolic and degradation pathways and to aryl hydrocarbon receptor (AhR) signaling. Indeed, the above-mentioned genes are known AhR target genes that are upregulated upon activation of AhR signaling.[111] In line with the transcriptome profiles, the metabolic enzymes CYP1B1, ALDH3A1, ADH7, NQO1 and XDH were most significantly upregulated on the protein level upon Picoberin treatment at all four timepoints. Consistent with the transcriptome profiling data, global proteome profiling identified mainly cellular degradation processes, and regulation of AhR signaling among the top 10 most significantly enriched pathways on protein level. Hence, both, global transcriptome and proteome profiling suggested activation of AhR signaling in C3H10T1/2 cells upon as mode of action (MoA) for Picoberin.

The AhR is a ligand-activated transcription factor that binds a diverse set of ligands, which often activate AhR signaling at low picomolar concentrations. These include several environmental toxins, such as polycyclic aryl hydrocarbons (PAHs) and halogenated aryl hydrocarbons (HAHs), but also tryptophan and microbial metabolites.[157] The AhR functions as a master regulator of drug metabolism and establishes functional interactions with signaling pathways governing cell proliferation, cell cycle, cell morphology, cell adhesion and cell migration.[127, 158] AhR is involved in several biological processes, including immune responses, cell differentiation and the control of cell pluripotency and stemness.[158] Furthermore, AhR signaling influences bone remodeling by altering the interplay between bone-forming

osteoblasts and bone-resorbing osteoclasts.[159] Lee T.D. Watson *et al.* showed that activation of AhR signaling using the AhR agonist 2,3,7,8-tetrachlorodibenzo-*p*-dioxin (TCDD) disrupts osteogenic differentiation of human mesenchymal stem cells.[160] Merja Korkalainen and co-workers reported TCDD-mediated inhibition of osteoblast differentiation in murine and rat cells.[161] Similar to observations made in this thesis, picomolar concentrations of TCDD were sufficient to significantly inhibit the expression of osteogenesis markers including alkaline phosphatase.[161] Even at a concentration of 1 nM TCDD, residual levels of 50 % *Alpl* compared to control cells were observed in these studies[161], which is in agreement with results obtained for Picoberin. A time-resolved gene expression analysis showed that TCDD did not alter *Runx2* expression in murine cells.[161] This indicates that AhR agonists may inhibit osteogenesis via a Runx2-independent mechanism, which would fit to the observation that also Hh signaling and Picoberin treatment did not influence *Runx2* expression.
Besides its activity as a ligand activated transcription factor, AhR also possess an intrinsic E3 ubiquitin ligase function.[120, 162] The ubiquitin-proteasome system regulates degradation of cellular proteins.[162] Therefore the observed downregulation of IGFBP3 and IGFBP5 after 96 h and 7 days may occur through this function of AhR. IGF signaling has been linked to AhR signaling[163]. Moreover, IGFBP5 is increased in osteoblasts and positively regulates osteoblast differentiation.[164] Reduced IGFBP3 and IGFBP5 levels may thus contribute to AhR-mediated inhibition of Hh-induced osteogenesis. Further experiments e.g., overexpression of IGFBPs could be carried out to explore this in more detail.

In summary, global transcriptome and proteome profiling strongly point towards Picoberin-mediated activation of AhR signaling and AhR as the protein target of Picoberin.

6.4.3 Target identification via thermal transcriptome profiling

Thermal proteome profiling (TPP) was employed to detect potential molecular interactions of Picoberin with the AhR or other proteins involved in AhR signaling and to identify other potential protein targets. As described in chapter 2.1.3, this approach is based on alterations of the thermal stability of a protein upon direct binding of a ligand, which results in a shift of the melting temperature of this protein. These shifts are either detected via immunoblotting for one protein of interest (CETSA) or for many proteins in parallel via MS/MS analysis (TPP). In total, 19 proteins showed a shift of the melting temperature of at least ≥ 2°C or ≤ -2°C in presence of Picoberin. Similar to the global proteome profiling data, AhR was not identified at all in the data set. Melting curves were obtained for several proteins that are known to directly interact with AhR, such as AIP, HSP90, ARNT and SRC.[165] However, no alterations of the thermal stability upon addition of Picoberin was observed. Thus, Picoberin does most likely not directly interact with any of these proteins.

Only for a few of the 19 proteins, including Cyclin-G-associated kinase (GAK), Integrin beta-3 (ITGB3) and Na(+)/H(+) exchange regulatory cofactor NHE-RF1 (SLC9A3R1) hints for an involvement in bone regulation were found. None of them could be linked to regulation of AhR signaling.[117-119] These 19 proteins should still be considered as potential, additional protein targets of Picoberin.

6.5 Validation of AhR as molecular target of Picoberin

6.5.1 Chemical validation

Chemical validations are carried out to explore, if structurally unrelated ligands of a putative target induce the same phenotype as the corresponding research compound, which can strongly support a target hypothesis.[22] Several AhR agonists including TCDD, FICZ and B[a]P impair osteoblast differentiation.[160, 161, 166] This effect was mainly studied for β-glycerophosphate and ascorbate induced osteogenesis of already committed murine preosteoblasts or human mesenchymal cells or *in vivo* models. All tested AhR agonists suppressed Hh-dependent osteoblast differentiation, which clearly supports AhR as the potential target of Picoberin. Although picomolar EC_{50} values for activation of AhR signaling were reported for the known AhR agonists TCDD, FICZ, B[a]P and Tapinarof, only TCDD inhibited Hh-dependent osteogenesis at picomolar concentrations. Since the differentiation state is determined after 96 h of compound treatment, one possible explanation for the different potencies could be different metabolic stability of the compounds. Since TCDD is resistant to AhR-induced metabolism and has a long half-life, this compound induces sustained activation of AhR signaling.[167, 168] In contrast, FICZ is rapidly metabolized and, thus, AhR activation is only transient.[168] If sustained activation is necessary to effectively inhibit osteoblast differentiation, fast metabolic degradation could explain the comparably low potency of FICZ in the Hh-dependent osteogenesis assay. Another possible explanation for the discrepancy of potencies could be the high diversity in ligand-dependent activation of the AhR. Michael S. Denison *et al.* reported an extremely diverse spectrum of biological and toxic effects of AhR activation that occur in a ligand-, species- and tissue-specific manner.[169] While several genes are consistently altered in different cell lines, exploration of different AhR agonists in gene expression arrays has also revealed huge differences in gene expression profiles.[169] It is thus possible that some AhR ligands modulate genes that are important for osteoblast differentiation, while other AhR agonists may confer completely different effects.

Gene expression analysis of C3H10T1/2 cells after treatment with purmorphamine and different concentrations of FICZ confirmed a dose-dependent reduction of alkaline phosphatase expression on mRNA level and upregulation of the AhR target gene *Cyp1b1*. Furthermore, FICZ partially inhibits purmorphamine-induced AhR expression. However, in line

with Picoberin, FICZ does not modulate purmorphamine induced expression of the Hh target genes *Gli1* and *Ptch1*. Thus, FICZ does not modulate canonical Hh signaling. Despite the differences in Picoberin and FICZ potencies as inhibitors of Hh-dependent osteogenesis, the parallels in biological activities strongly support AhR as the molecular target of Picoberin.

6.5.2 Biological validation

The AhR is a ligand-activated transcription factor and part of a cytosolic multi-protein complex consisting of two heat-shock protein 90 (HSP90), AhR interacting protein (AIP), prostaglandin E synthase 3 (P23) and SRC, in its inactive state (Figure 64).[165] Upon binding of a ligand AhR is released from this complex and translocates into the nucleus. Upon heterodimerization with Aryl hydrocarbon nuclear translocator (ARNT), AhR binds to xenobiotic responsive elements (XRE), which induces expression of AhR target genes, such as *Cyp1a1*, *Cyp1b1* and *Aldh3a1*.[165, 170] Since AhR contains a nuclear export sequence, it gets exported again from the nucleus, followed by proteasomal degradation.[170]

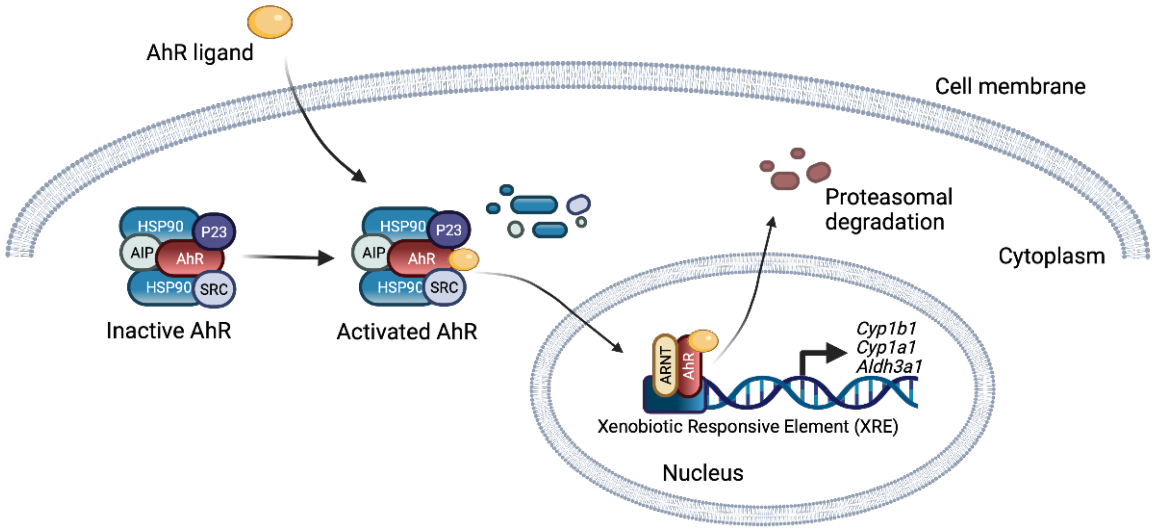

Figure 64: Canonical AhR signaling. Inactive AhR is located as part of a multi-protein complex consisting of two heat-shock protein 90 (HSP90), AhR interacting protein (AIP), prostaglandin E synthase 3 (P23) and SRC, in the cytoplasm of the cell. Upon binding of a ligand this complex dissociates and AhR translocates into the nucleus, where it forms a heterodimer with the Aryl hydrocarbon receptor nuclear translocator (ARNT). The AhR-ARNT heterodimer binds to xenobiotic responsive elements (XRE) and induces transcription of AhR target genes. Due to a nuclear export sequence, AhR is exported from the nucleus and undergoes proteasomal degradation.[165]

Dose-dependent upregulation of *Cyp1b1* expression levels in C3H10T1/2 cells upon treatment with different concentrations of Picoberin confirmed activation of AhR signaling at picomolar concentrations after 48 h and 96 h. Interestingly, *Cyp1b1* levels at a specific Picoberin concentration increased over time, which suggests continuously active AhR signaling. Furthermore, Picoberin induced nuclear localization of mAhR-FLAG in C3H10T1/2 cells, after

24 h at a concentration of 1 nM, supporting the very high potency of this small molecule. Picoberin induced AhR signaling already after 4 h in different AhR-responsive cell lines, such as in human hepatocarcinoma cells (HepG2), human fibroblasts (HaCaT) and murine fibroblasts (NIH-3T3), with EC_{50} values in the single digit nanomolar to picomolar range. Consequently, these data clearly confirm Picoberin as a highly potent AhR agonist and this activity is not restricted to the C3H10T1/2 cell line. Moreover, Picoberin shows bioactivity at similar concentrations as FICZ, which is one of the most potent naturally-occurring AhR agonists reported to date.[128] Interestingly, the EC_{50} values that were obtained suggested a higher potency of Picoberin and FICZ after 4 h compared to 24 h of compound treatment. However, in case of the human hepatocarcinoma cells and to lesser extent also in human fibroblasts, the activation of the XRE-dependent reporter was markedly higher after 24 h. At this time point, EC_{50} values in the micromolar range were determined for these cell lines. Murine fibroblasts showed a stronger induction after 4 h compared to the human cell lines. However, after 24 h no XRE-dependent reporter activity could be observed in these cells. One possible explanation could be routed in species specific differences of drug metabolism. AhR activation leads to increased expression of genes in a ligand-, species-, and cell-type specific manner.[169] While diverse types of human cells express high levels of *Cyp1a1*, murine cells have low *Cyp1a1* but higher *Cyp1b1* expression levels.[171] Thus, AhR ligands may be metabolized faster in murine cells compared to human cells.

Evaluation of a small set of active and inactive 8-oxotetrahydroprotoberberine analogues in the XRE-dependent reporter gene assay in NIH-3T3 cells revealed overlaps in the structure-activity relationship that was observed for inhibition of Hh-induced osteogenesis in C3H10T1/2 cells. Analogues that were inactive in the osteogenesis assay did also not induce AhR signaling. These parallels strongly point towards AhR as the functional target of Picoberin during Hh-induced osteogenesis of C3H10T1/2 cells.

The human hepatocarcinoma cell line HepG2 is frequently used as a model system for research in AhR biology. In contrast to C3H10T1/2 cells, these cells have higher AhR protein levels and were thus selected for further characterization of Picoberin. In HepG2 cells, Picoberin led to translocation of AhR to the nucleus, activation of AhR response and upregulation of the activity of the metabolic enzyme and AhR target CYP1A1 at low nanomolar concentrations. Nuclear AhR localization was already apparent after 15 min of treatment, indicating that Picoberin-mediated AhR activation occurs very fast. Picoberin furthermore reduced AhR protein levels in HepG2 cells after 4 h of compound treatment. Since AhR has both, a nuclear import as well as a nuclear export sequence and undergoes proteasomal degradation upon nuclear export, this finding is a further proof for AhR as the molecular target of Picoberin.[170] In summary, these findings confirmed that Picoberin is a highly potent activator of AhR signaling and, thus, these studies strongly supported the AhR target hypothesis.

6.5.3 Evaluation of AhR binding

The AhR is a very unstable protein that binds to a molecular chaperone complex for stabilization in the cytoplasm.[172] Due to the low protein stability, expression of full-length AhR is highly challenging and most *in vitro* AhR studies are based on the expression of AhR domains.[172, 173] However, even purification of AhR domains is highly challenging and thus, only few groups have explored ligand binding with purified protein.[173] Throughout this thesis, no purified AhR was available for biophysical binding studies.

CETSA can prove binding and target engagement in lysates or in cells without the need of recombinant protein.[15] However, AhR was not detected by means of mass spectrometry in the thermal proteome profiling and also detection of endogenous AhR protein levels using commercially available AhR antibodies was not successful in C3H10T1/2 cells. Explanations for this could be very low expression levels and stability of AhR[173] in these cells, or failure of binding to the used antibodies to the AhR due to species or cell type specific characteristics of the AhR protein. For this reason, CETSA was performed in HepG2 cell lysates. An AhR melting temperature of 42.4 ± 0.7°C was determined in the presence of DMSO. In the ProteomicsDB, a melting temperature (T_m) of 44 ± 0.4°C is reported for AhR in HepG2 cells.[174, 175] Even though these values are in a similar temperature range, the differences may be explained by the usage of different lysis conditions, incubation times and devices. Treatment of HepG2 cell lysates with Picoberin induced a slight de-stabilization of AhR, resulting in a ΔT_m of -1.7±1.2°C. In literature, no studies that report lysate based CETSA for AhR with AhR agonists could be found. It is therefore difficult to judge, if this small change in melting temperature can be considered as a meaningful shift and, thus, as a proof of binding. Additional isothermal dose-response fingerprinting (ITDRF) could not confirm the binding either. Since binding of a ligand to AhR results in the release of this receptor from a multiprotein complex,[165, 170] it was assumed that ligand binding to AhR in cells may lead to higher differences in the thermal protein stability. However, also the *in cell* CETSA did not show any significant alterations of the AhR melting behavior. Moreover, Picoberin had no influence on the thermal stability of murine AhR.

Picoberin reduced cellular AhR protein levels in HepG2 cells after 4 h of compound treatment and this reduction was linked to nuclear export followed by proteasomal degradation of the AhR. Even after 10 min of treatment, Picoberin reduced AhR levels. Proteasomal AhR degradation may occur very fast, which could explain the observed reduction of AhR protein levels after this short treatment time. Furthermore, binding of Picoberin may potentially lead to conformational change of AhR that may influence the binding of the used AhR antibody. Thus, the fast reduction of detectable AhR protein levels could potentially hint towards binding of Picoberin. Interestingly also FICZ, which was evaluated as a control for a known AhR binder, did not alter the thermal stability of murine AhR and, thus, it may be possible that binding of a ligand to AhR in lysate may not influence the thermal stability. A second possible explanation

for the absence of a thermal shift could be binding of DMSO to AhR, which may alter thermal AhR stability in the vehicle control. DMSO binds and induces AhR activation at concentrations of 50 mM to 100 mM.[176, 177] During these experiments the DMSO concentration was 0.5 % in all samples, which corresponds to a concentration of 70 mM DMSO. To evaluate if DMSO alters the melting behavior of AhR, melting curves after a CETSA with wild type lysates could be generated as an additional control.

Taken together, the cellular thermal shift assays did not provide an ultimate proof for direct binding of Picoberin to AhR. The effects observed in the *in cell* CETSA hint towards very fast changes in AhR protein levels, which could carefully be interpreted as a hint to a direct interaction. Cellular thermal shift assays for confirmation of ligand binding to AhR are not reported in the literature. Thus, other label-free approaches for target engagement, such as limited proteolysis or a microscale-thermophoresis may be more suitable.[178] However, AhR expression and purification would be required, which is highly challenging due to the low stability of this protein.[173] Limited proteolysis-coupled mass spectrometry (LiP-MS) could be another option to target engagement.[179] LiP-MS is performed with cell lysates and provides information on protein regions involved in the structural rearrangement on a proteome level.[179] Besides ligand binding, also conformational changes in the protein of interest, protein aggregation, or altered protein–protein interactions can induce structural changes of proteins.[179] For this reason, the low AhR protein stability could be problematic also for this approach.

6.5.4 Genetic validations

Genetic validations examine whether a phenotype can be associated to a particular genotype.[17, 22] They can be used to link Picoberin-mediated activation of AhR signaling to the observed modulation of Hh-induced osteoblast differentiation. One approach to genetic validation is to reduce the cellular level of a protein of interest via RNAi mediated mRNA degradation. A knockdown of AhR was achieved in C3H10T1/2 cells, which were subsequently used for the osteoblast differentiation assay and gene expression analysis. Despite the only moderate AhR knockdown efficiency of 72.2 ± 6.5 % and 56.1 ± 3.1 % after 48 h and 96 h of compound treatment, respectively, clear effects on Hh-induced osteogenesis became apparent. Alkaline phosphatase levels were reduced in AhR-depleted cells, suggesting a positive regulatory function of AhR in this differentiation process. This observation is in line with inhibition of Hh-dependent osteogenesis that was observed upon treatment of cells with the AhR antagonist CH322191. However, since the inhibition only occurred at concentrations substantially higher than the reported inhibition of AhR, further studies would be required to

explore whether C322191-mediated inhibition of Hh-dependent osteogenesis occurs through inhibition of AhR.

Certainly and in agreement with literature reports, activation of AhR signaling inhibits Hh-induced osteogenesis.[160, 161] If AhR is the functional target of Picoberin during inhibition of Hh-dependent osteogenesis, AhR depletion should thus reduce the potency of this compound (Figure 65).

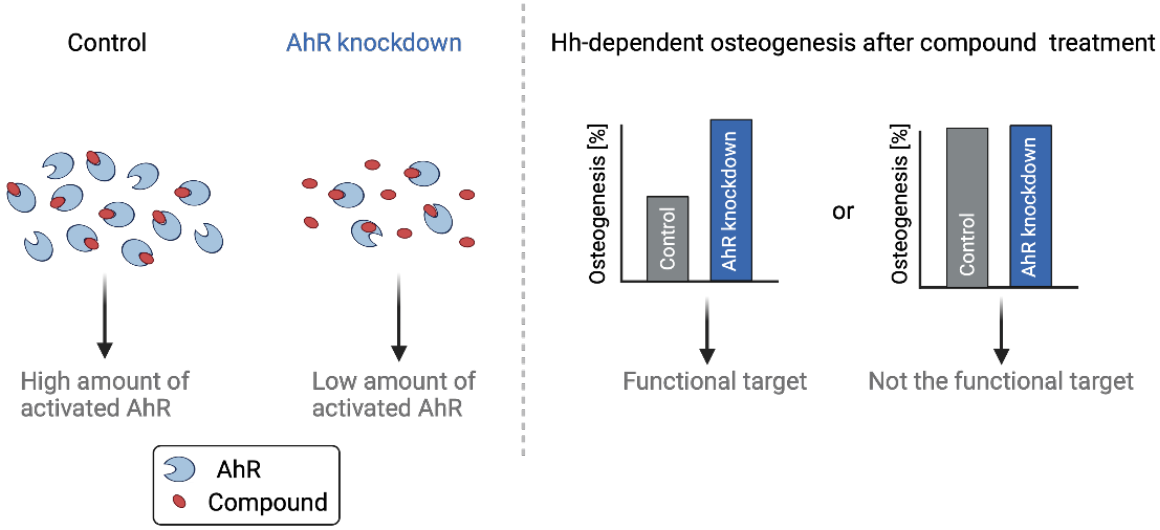

Figure 65: Possible influences of AhR knockdown on Picoberin-mediated inhibition of Hh-dependent osteogenesis. In control cells, high amount of AhR get activated upon agonist treatment and this causes inhibition of osteogenesis. In AhR knockdown cells, less AhR is activated at the same concentration of agonist. If AhR is the functional target of Picoberin, less inhibition of osteogenesis should be observed in AhR-depleted cells.

Reduced potency of Picoberin in AhR-depleted cells was detected with a shift in the IC_{50} value from 12.4 ± 3.5 pM in control cells to 35.6 ± 14.3 pM in AhR-depleted cells. Moreover, while Picoberin reduces Hh-dependent osteogenesis down to a level of approx. 20 % in control cells, only a maximal inhibition down to a level of 50 % was reached at reduced AhR levels. When less AhR is present in cells, a threshold is reached when all available AhR molecules are activated by Picoberin. At this stage, increasing the concentration of Picoberin does not have any further impact on the osteogenesis level. Consequently, AhR is the functional molecular target of Picoberin during Hh-dependent osteogenesis.

A complementary approach to RNAi-mediated reduction of cellular AhR levels, is evaluation of the influence of AhR overexpression on Picoberin-mediated inhibition of Hh-induced osteogenesis. In theory, AhR overexpression should show opposite effects compared to AhR-depletion. However, this assumption only applies, if the overexpressed AhR protein is fully functional in the cells. In case of an agonist, this hypothesis would furthermore depend on the assumption, that effects that are observed in cells are limited by the amount of available protein

and not the available number of compound molecules. If this would be the case, increasing the protein amount of AhR would in theory lead to an even higher potency of Picoberin, if AhR is the functional target. Regarding the high number of biological variables that are unknown, the outcome of this experiment can hardly be predicted, and results may be difficult to interpret. Quantification of the *AhR* mRNA level clearly confirmed successful transfection of C3H10T1/2 cells with FLAG-mAhR encoding plasmids. However, no differences for Hh-induced osteogenesis and Picoberin-mediated inhibition of this process were observed in mAhR-FLAG transfected cells compared to control cells. Thus, these experiments could not provide further proof for target validation.

6.6 Mechanistic considerations

Activation of AhR impairs bone development. This was not only observed for Hh-dependent osteogenesis throughout this thesis, but also by other groups who explored osteogenesis in different species and cell types, upon induction with different stimuli and also in animal models.[160] During the course of these studies several results indicated a functional role of AhR during Hh-dependent osteoblast differentiation of C3H10T1/2 cells. Besides several AhR agonists, also the known AhR antagonist CH322191 inhibited Hh-dependent osteogenesis. Consistently, AhR knockdown reduced osteoblast differentiation. Moreover, *AhR* mRNA levels were upregulated in C3H10T1/2 cells upon activation of Hh signaling and the AhR target genes *Aldh3a1* and to lesser extent *Adh7* were increased over time during Hh-induced osteogenesis. These observations are in line with Ryan *et al.,* who reported upregulation of *AhR* gene and protein levels in rat calvaria cells upon induction of mineralization via treatment of cells with β-glycerophosphate and ascorbate.[180] In addition, bone mineralization was reduced by 70 % in AhR knockout cells compared to control cells.[180] Taken together, this provides evidence for a positive regulatory function of AhR during osteogenesis and tight regulation of AhR signaling seems essential for this process. Interestingly, purmorphamine and SHH increase *AhR* mRNA levels. In case of purmorphamine, *AhR* upregulation was already present after 24 h of treatment and remained throughout differentiation. Furthermore, Hh-induced expression of *AhR* is inhibited down to the level of unstimulated cells upon addition of the known Hh pathway inhibitor Vismodegib. Thus, AhR could be a Hh target gene. Evaluation of the AhR promoter activity upon activation of Hh signaling could prove this hypothesis and may potentially establish a direct link between these pathways.

Taken together, these data confirm that the observed increase of the AhR expression is caused by and dependent on Hh pathway activity and, thus, provide evidence for crosstalk of AhR and Hh signaling. This hypothesis was supported by reduced *Ptch2* expression levels upon co-treatment of cells with purmorphamine and Picoberin (Figure 66). The gene *Ptch2* is a close homologue of the Hh target gene *Ptch1,* and both are upregulated upon activation of Hh

signaling.[181] *Protein patched homolog* 2 (PTC2) is a functional receptor for SHH and regulates SMO localization and activity *in vitro*.[181] However, besides these overlapping functions, PTC1 and PTC2 may differently regulate downstream signaling.[113] While PTC1 is well characterized, PTC2 is only poorly explored so far.[181] However, unlike PTC1, PTC2-mediated Hh signaling induces phosphorylation of SRC.[113] This tyrosine kinase is part of the cytosolic AHR-multiprotein complex and may thus link PTC2 to AhR signaling. [165] Picoberin-mediated reduction of *Ptch2* expression is dose dependent and, also FICZ shows a similar effect. Furthermore, Picoberin-mediated inhibition of *Ptch2* expression was mitigated in AhR-depleted cells, suggesting an AhR-dependent regulation of *Ptch2* expression. Interestingly, hints towards binding of AhR to the *Ptch2* promoter and reduction of *Ptch2* expression in response to TCDD treatment were found in published chromatin immunoprecipitation (ChiP) and global gene expression data sets, which support this hypothesis.[182, 183] Thus AhR-mediated regulation of *Ptch2* may link AhR and Hh signaling and may contribute to Picoberin-mediated inhibition of Hh-dependent osteogenesis.

Picoberin and the known AhR agonist FICZ partially reduce Hh-induced *AhR* expression (Figure 66). This could be part of a negative feedback mechanism to reduce AhR levels in cells upon activation of signaling. Besides Hh signaling and in contrast to BMP, also activation of canonical Wnt signaling, which acts downstream of Hh signaling during osteogenesis upregulates AhR expression in many cell lines.[98, 184] If upregulation of *AhR* expression is required for Hh-dependent and WNT-3A-induced osteogenesis, AhR agonist-mediated reduction of *AhR* mRNA levels could contribute to inhibition of the differentiation. Whereas Picoberin inhibits osteogenesis that is induced by WNT-3A or by co-treatment of BMP4 and purmorphamine, it has no influence on osteogenesis that is induced by BMP4 alone.

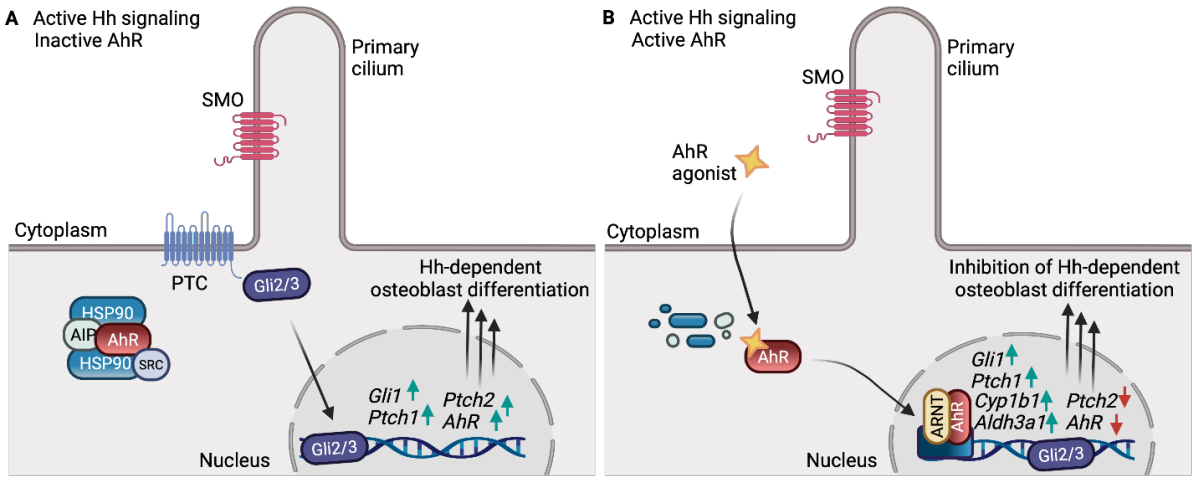

Figure 66: Schematic summary. A: Active Hh signaling and inactive AhR signaling. **B:** Active Hh signaling and active AhR signaling.

While the levels of *AhR* mRNA were reduced when cells were treated with purmorphamine and Picoberin, high levels of *Aldh3a1* and, to a much lesser extent, *Cyp1b1* were persistent throughout differentiation. Aldehyde dehydrogenases (ALDHs) such as ALDH3A1 are detoxifying enzymes that oxidize exogenous but also endogenous aldehydes and that are involved in the biosynthesis of molecules that are important for cell homeostasis, such as retinoic acid, gamma-aminobutyric acid betaine.[185] Moreover, ALDHs have non-enzymatic functions, including anti-oxidant, structural and regulatory mechanisms.[185] Several ALDHs positively or negatively modulate osteogenesis, depending on the isoform, cell type and stimulus. ALDH2 activity increases osteoblast differentiation via positive regulation of BMP-2 expression.[186, 187] However, high ALDH activity is linked to a less differentiated osteogenic state compared to cells with low ALDH activity.[186, 187] The Picoberin-mediated increase in *Aldh3a1* expression leads to a constantly high level of ALDH3A1, which may thus contribute to inhibition of osteoblast differentiation.

In summary, this thesis demonstrates crosstalk of AhR and Hh signaling during Hh-dependent osteogenesis. Since Picoberin inhibits expression of the Hh target gene *Ptch2* and Hh signaling-induced upregulation of *AhR* mRNA levels, AhR may regulate osteoblast differentiation via a Hh-dependent mechanism. In agreement with this, Picoberin did not modulate BMP4 induced osteogenesis. However, other factors including sustained upregulation of *Aldh3a1* and *Cyp1b1* levels may also contribute to Picoberin-mediated inhibition of Hh-dependent osteogenesis.

6.7 Therapeutic potential of AhR agonists

The aryl hydrocarbon receptor was confirmed as a protein target of Picoberin and, thus, evaluation of potential applications of this small molecule are of high interest. Historically, the aryl hydrocarbon receptor was identified as the molecular target and mediator of toxic effects of TCDD and other halogenated aromatic environmental contaminants.[188] This stigma and the link to several human poisonings, including those in Italy (Seveso, 1976)[189], Japan (Yusho, 1968)[190] and Taiwan (Yusheng, 1979)[190] are the reason why potential modulation of AhR as a drug target was not explored.[188] However, in the last two decades many endogenous AhR ligands were uncovered, including tryptophan metabolites like kynurenine and FICZ, or microbial metabolites. It is evident that different AhR modulators induce cellular responses that are highly ligand-, species- and cell type-dependent and these contribute to several physiological and pathological functions.[191] Besides the activity as environmental sensor, AhR is involved in regulation of stem cell differentiation and immune cell responses.[158] Moreover, recent studies provide evidence that AhR is involved in carcinogenesis and exhibits both, pro-oncogenic and tumor suppressor-like functions.[188, 192] While *AhR* expression is upregulated and linked to poor prognosis in various types of cancer, tumor suppressive functions were

observed in cancers associated with brain, central nervous system, liver, digestive system, and skin.[192] Yunxia Fan *et al.* reported increased liver tumor formation, repression of tumor suppressor genes and increased expression of proliferative markers in $AhR^{-/-}$ mouse models.[193] Garcia-Villatoro *et al.* reported that the expression of AhR in intestinal epithelial cells is required to reduce the formation of premalignant colon cancer lesions.[194] Moreover, Sarić *et. al* reported that reduced AhR pathway activity promotes progression of SHH-dependent medulloblastoma.[195] Therapeutic modulation of AhR signaling could thus have great potential for personalized medicine in cancer therapies.[192] However, this will require extensive investigation of cancer- and patient-specific AhR expression and function as well as careful and precise characterization of AhR agonists and antagonists, to exclude highly toxic side-effects.

Besides its functions in cancer, AhR signaling is involved in cardiovascular physiology and the development of chronic inflammatory cardiac diseases, e.g. atherosclerosis and cardiac hypertrophy.[196] In addition, AhR is involved in inflammatory skin diseases, including atopic dermatitis and psoriasis. Only recently, the AhR agonist Tapinarof was approved as the first-in-class small-molecule therapeutic AhR-modulating agent for topical treatment of these common inflammatory skin diseases.[124, 197]

Taken together, there is accumulating evidence reported in the literature, about physiological functions of AhR signaling and both, aberrant activation but also loss-of-function seem to be involved in several diseases. Thus, it will be of high interest and important to move away from the AhR as the mediator of only toxic effects of TCDD and explore other ligands in cell type and disease context to objectively examine the potential of the AhR as a drug target. AhR agonists like Picoberin will be of high importance not only as tool compounds for AhR research, but also as potential starting points for the development of therapeutic AhR modulating agents.

7 CONCLUSION & PERSPECTIVES

Hh signaling is essential for embryonic differentiation, stem cell homeostasis and tissue regeneration. However, aberrant activation of Hh signaling is involved in the development and progression of different types of cancer, including basal cell carcinoma and medulloblastoma. Thus, identification of Hh pathway inhibitors is in high demand for the development of novel therapeutic approaches for treatment of Hh-dependent types of cancer. Especially identification of small molecules that inhibit Hh signaling independently of SMO is of high interest to overcome acquired drug resistances upon treatment of patients with SMO antagonists and for treatment of SMO-independent miss-regulation of Hh signaling.

For identification of potential Hh pathway inhibitors, a Hh-dependent osteoblast differentiation assay was employed for primary screening. However, besides Hh signaling several other cellular pathways are involved in osteoblast differentiation. For this reason, compounds that were identified as inhibitors of Hh-dependent osteogenesis were subsequently evaluated in orthogonal assays, including a GLI2/3-dependent reporter gene assay and Hh target gene analysis to verify inhibition of Hh signaling.

Throughout this thesis five novel Hh pathway inhibitors were identified and characterized. Furo[3,2-b]pyridine, quinoline, pyrroloquinoline and 20-membered macrocycle derivatives inhibit Hh signaling with IC_{50} values in the micromolar or even sub-micromolar range. Compound **5** inhibited Hh signaling independently of SMO, with an IC_{50} value of 1.8 ± 0.1 µM. Since the molecular target was not investigated in this thesis, future studies may aim at identifying the molecular target of this small molecule. This may provide novel insights into the molecular basics of the Hh pathway and may lead to the identification of potentially new therapeutic approaches for treatment of Hh-dependent types of cancer.

Compound **6** was identified as inhibitor of Hh-dependent osteogenesis with an IC_{50} value of 1.2 ± 0.4 nM. Surprisingly, this small molecule did not influence canonical Hh signaling or Wnt signaling. Exploration of the structure activity relationship led to the identification of Picoberin, which is even more potent than compound **6** and inhibits Hh-dependent osteogenesis with an IC_{50} value of 3 ± 1 pM but has no influence on canonical Hh signaling. Global transcriptome and proteome profiling led to the identification of the aryl hydrocarbon receptor as the molecular protein target of Picoberin. Chemical validation confirmed that several known AhR agonists inhibit Hh-dependent osteogenesis but not canonical Hh signaling and could thus support the target hypothesis. Picoberin dose-dependently upregulates expression of the AhR target gene *Cyp1b1* and induces nuclear localization of AhR in C3H10T1/2 cells. Furthermore, Picoberin activates XRE-dependent reporter activity in several human and murine cell lines with EC_{50} values in the single digit nanomolar to picomolar range after 4 h of compound treatment. In HepG2 cells, Picoberin upregulated CYP1A1 enzymatic activity. Interestingly, nuclear localization of AhR was observed already after 15 min of Picoberin treatment,

indicating a fast activation of this receptor upon addition of this small molecule. Moreover, AhR protein levels were dose-dependently reduced in HepG2 cells after 4 h of compound treatment, which is in line with reported proteasomal degradation of this ligand-activated transcription factor upon nuclear export. In summary, these findings confirmed that Picoberin mediates activation of AhR signaling. Picoberin reduces cellular AhR levels already after 10 min of compound treatment, which could be interpreted as a hint towards a direct molecular interaction. Further approaches, including limited proteolysis and microscale thermophoresis could be carried out in future to prove this hypothesis. Genetic knockdown of cellular AHR levels mitigated Picoberin-mediated inhibition of Hh-dependent osteogenesis and this confirmed AhR as the functional molecular target of Picoberin during this differentiation process. Furthermore, AhR-depletion as well as inhibition of AhR signaling reduced Hh-dependent osteogenesis of C3H10T1/2 cells, suggesting a positive functional role of the AhR. This hypothesis is further supported by Hh-dependent upregulation of AhR gene expression during osteogenesis. Moreover, Picoberin and FICZ inhibited *Ptch2* and AhR-depletion mitigated Picoberin mediated inhibition of *Ptch2* expression. Taken together, these data indicate crosstalk between Hh and AhR signaling, potentially via PTC2. Future studies may explore the underlying molecular mechanisms in more detail.

Although initially identified and characterized as the cellular receptor mediating the toxic effects of TCDD and other xenobiotic compounds, AhR is involved in numerous physiological processes. Both, aberrant activation but also loss of AhR function has been linked to several pathological processes, including development of different types of cancer, atherosclerosis, and inflammatory skin diseases. Only recently an AhR agonist was approved for treatment of plaque psoriasis and is currently evaluated for treatment of atopic dermatitis. Exploration of potential further clinical applications of AhR as a drug target as well as the identification and detailed characterization of specific AhR modulators is of high interest. Thus, Picoberin could not only serve as a tool compound in the field of AhR research, but also provide a starting point for the development of further therapeutic AhR modulators.

8 REFERENCES

1. Bucci, M., C. Goodman, and T.L. Sheppard, *A decade of chemical biology.* Nature Chemical Biology, 2010. **6**(12): p. 847-854.
2. Schenone, M., et al., *Target identification and mechanism of action in chemical biology and drug discovery.* Nat Chem Biol, 2013. **9**(4): p. 232-40.
3. Schneidewind, T., et al., *Combined morphological and proteome profiling reveals target-independent impairment of cholesterol homeostasis.* Cell Chem Biol, 2021. **28**(12): p. 1780-1794 e5.
4. Kawasumi, M. and P. Nghiem, *Chemical genetics: elucidating biological systems with small-molecule compounds.* J Invest Dermatol, 2007. **127**(7): p. 1577-84.
5. Funato, H., *Forward genetic approach for behavioral neuroscience using animal models.* Proc Jpn Acad Ser B Phys Biol Sci, 2020. **96**(1): p. 10-31.
6. Shim, J.S. and H.J. Kwon, *Chemical genetics for therapeutic target mining.* Expert Opin Ther Targets, 2004. **8**(6): p. 653-61.
7. Lawson, N.D. and S.A. Wolfe, *Forward and reverse genetic approaches for the analysis of vertebrate development in the zebrafish.* Dev Cell, 2011. **21**(1): p. 48-64.
8. Stockwell, B.R., *Chemical genetics: ligand-based discovery of gene function.* Nat Rev Genet, 2000. **1**(2): p. 116-25.
9. Spring, D.R., *Chemical genetics to chemical genomics: small molecules offer big insights.* Chem Soc Rev, 2005. **34**(6): p. 472-82.
10. Ziegler, S., et al., *Target identification for small bioactive molecules: finding the needle in the haystack.* Angew Chem Int Ed Engl, 2013. **52**(10): p. 2744-92.
11. Knight, Z.A. and K.M. Shokat, *Chemical genetics: where genetics and pharmacology meet.* Cell, 2007. **128**(3): p. 425-30.
12. Karageorgis, G. and H. Waldmann, *Guided by Evolution: Biology-Oriented Synthesis of Bioactive Compound Classes.* Synthesis, 2018. **51**(01): p. 55-66.
13. Chen, X., et al., *Target identification of natural medicine with chemical proteomics approach: probe synthesis, target fishing and protein identification.* Signal Transduction and Targeted Therapy, 2020. **5**(1).
14. Cravatt, B.F., A.T. Wright, and J.W. Kozarich, *Activity-based protein profiling: from enzyme chemistry to proteomic chemistry.* Annu Rev Biochem, 2008. **77**: p. 383-414.
15. Martinez Molina, D. and P. Nordlund, *The Cellular Thermal Shift Assay: A Novel Biophysical Assay for In Situ Drug Target Engagement and Mechanistic Biomarker Studies.* Annu Rev Pharmacol Toxicol, 2016. **56**: p. 141-61.
16. Franken, H., et al., *Thermal proteome profiling for unbiased identification of direct and indirect drug targets using multiplexed quantitative mass spectrometry.* Nature Protocols, 2015. **10**(10): p. 1567-1593.
17. Titov, D.V. and J.O. Liu, *Identification and validation of protein targets of bioactive small molecules.* Bioorg Med Chem, 2012. **20**(6): p. 1902-9.
18. Du, X., et al., *Insights into Protein-Ligand Interactions: Mechanisms, Models, and Methods.* Int J Mol Sci, 2016. **17**(2).
19. Lea, W.A. and A. Simeonov, *Fluorescence polarization assays in small molecule screening.* Expert Opin Drug Discov, 2011. **6**(1): p. 17-32.
20. Robers, M.B., et al., *Target engagement and drug residence time can be observed in living cells with BRET.* Nat Commun, 2015. **6**: p. 10091.
21. Nowak, R.P. and L.H. Jones, *Target Validation Using PROTACs: Applying the Four Pillars Framework.* SLAS DISCOVERY: Advancing the Science of Drug Discovery, 2021. **26**(4): p. 474-483.
22. Wyatt, P.G., et al., *Target Validation: Linking Target and Chemical Properties to Desired Product Profile.* Current Topics in Medicinal Chemistry, 2011. **11**(10): p. 1275-1283.
23. in *Evolution of Translational Omics: Lessons Learned and the Path Forward*, C.M. Micheel, S.J. Nass, and G.S. Omenn, Editors. 2012: Washington (DC).

24. Misra, B.B., et al., *Integrated Omics: Tools, Advances, and Future Approaches.* J Mol Endocrinol, 2018.
25. Hasin, Y., M. Seldin, and A. Lusis, *Multi-omics approaches to disease.* Genome Biology, 2017. **18**(1): p. 83.
26. Paananen, J. and V. Fortino, *An omics perspective on drug target discovery platforms.* Brief Bioinform, 2020. **21**(6): p. 1937-1953.
27. Kukurba, K.R. and S.B. Montgomery, *RNA Sequencing and Analysis.* Cold Spring Harb Protoc, 2015. **2015**(11): p. 951-69.
28. Subramanian, I., et al., *Multi-omics Data Integration, Interpretation, and Its Application.* Bioinform Biol Insights, 2020. **14**: p. 1177932219899051.
29. Perez-Riverol, Y., et al., *Quantifying the impact of public omics data.* Nat Commun, 2019. **10**(1): p. 3512.
30. Edgar, R., M. Domrachev, and A.E. Lash, *Gene Expression Omnibus: NCBI gene expression and hybridization array data repository.* Nucleic Acids Research, 2002. **30**(1): p. 207-210.
31. Barrett, T., et al., *NCBI GEO: archive for functional genomics data sets-update.* Nucleic Acids Research, 2013. **41**(D1): p. D991-D995.
32. Giani, A.M., et al., *Long walk to genomics: History and current approaches to genome sequencing and assembly.* Comput Struct Biotechnol J, 2020. **18**: p. 9-19.
33. Shendure, J., et al., *DNA sequencing at 40: past, present and future.* Nature, 2017. **550**(7676): p. 345-353.
34. Wang, B., et al., *Reviving the Transcriptome Studies: An Insight Into the Emergence of Single-Molecule Transcriptome Sequencing.* Frontiers in Genetics, 2019. **10**.
35. Yang, X., et al., *High-Throughput Transcriptome Profiling in Drug and Biomarker Discovery.* Front Genet, 2020. **11**: p. 19.
36. Anamika, K., et al., *Transcriptomic Profiling Using Next Generation Sequencing - Advances, Advantages, and Challenges*, in *Next Generation Sequencing - Advances, Applications and Challenges*. 2016.
37. Chavan, P., K. Joshi, and B. Patwardhan, *DNA microarrays in herbal drug research.* Evid Based Complement Alternat Med, 2006. **3**(4): p. 447-57.
38. Ozsolak, F. and P.M. Milos, *RNA sequencing: advances, challenges and opportunities.* Nat Rev Genet, 2011. **12**(2): p. 87-98.
39. Bentley, D.R., et al., *Accurate whole human genome sequencing using reversible terminator chemistry.* Nature, 2008. **456**(7218): p. 53-59.
40. Agrawal, N., et al., *RNA interference: biology, mechanism, and applications.* Microbiology and molecular biology reviews : MMBR, 2003. **67**(4): p. 657-685.
41. Peng, Z.P., et al., *The Effects of Hedgehog Signaling Pathway on the Proliferation and Apoptosis of Melanoma Cells.* J Oncol, 2022. **2022**: p. 4984866.
42. Briscoe, J. and P.P. Therond, *The mechanisms of Hedgehog signalling and its roles in development and disease.* Nat Rev Mol Cell Biol, 2013. **14**(7): p. 416-29.
43. Carballo, G.B., et al., *A highlight on Sonic hedgehog pathway.* Cell Commun Signal, 2018. **16**(1): p. 11.
44. Sari, I.N., et al., *Hedgehog Signaling in Cancer: A Prospective Therapeutic Target for Eradicating Cancer Stem Cells.* Cells, 2018. **7**(11).
45. Zhou, H., et al., *Research progress on the hedgehog signalling pathway in regulating bone formation and homeostasis.* Cell Prolif, 2022. **55**(1): p. e13162.
46. Teglund, S. and R. Toftgård, *Hedgehog beyond medulloblastoma and basal cell carcinoma.* Biochim Biophys Acta, 2010. **1805**(2): p. 181-208.
47. Merchant, A.A. and W. Matsui, *Targeting Hedgehog — a Cancer Stem Cell Pathway.* Clinical Cancer Research, 2010. **16**(12): p. 3130-3140.
48. Skoda, A.M., et al., *The role of the Hedgehog signaling pathway in cancer: A comprehensive review.* Bosn J Basic Med Sci, 2018. **18**(1): p. 8-20.
49. Gupta, S., N. Takebe, and P. Lorusso, *Targeting the Hedgehog pathway in cancer.* Ther Adv Med Oncol, 2010. **2**(4): p. 237-50.

50. Jamieson, C., et al., *Hedgehog Pathway Inhibitors: A New Therapeutic Class for the Treatment of Acute Myeloid Leukemia.* Blood Cancer Discovery, 2020. **1**(2): p. 134-145.
51. Gutzmer, R. and J.A. Solomon, *Hedgehog Pathway Inhibition for the Treatment of Basal Cell Carcinoma.* Targeted Oncology, 2019. **14**(3): p. 253-267.
52. Chen, J.K., et al., *Inhibition of Hedgehog signaling by direct binding of cyclopamine to Smoothened.* Genes Dev, 2002. **16**(21): p. 2743-8.
53. Wu, T.M., et al., *Synthesis and biological evaluation of novel benzamide derivatives as potent smoothened antagonists.* Bioorg Med Chem Lett, 2014. **24**(5): p. 1426-31.
54. Pan, S., et al., *Discovery of NVP-LDE225, a Potent and Selective Smoothened Antagonist.* ACS Med Chem Lett, 2010. **1**(3): p. 130-4.
55. Norsworthy, K.J., et al., *FDA Approval Summary: Glasdegib for Newly Diagnosed Acute Myeloid Leukemia.* Clin Cancer Res, 2019. **25**(20): p. 6021-6025.
56. Ghirga, F., M. Mori, and P. Infante, *Current trends in Hedgehog signaling pathway inhibition by small molecules.* Bioorg Med Chem Lett, 2018. **28**(19): p. 3131-3140.
57. Axelson, M., et al., *U.S. Food and Drug Administration Approval: Vismodegib for Recurrent, Locally Advanced, or Metastatic Basal Cell Carcinoma.* Clinical Cancer Research, 2013. **19**(9): p. 2289-2293.
58. Brancaccio, G., et al., *Sonidegib for the Treatment of Advanced Basal Cell Carcinoma.* Frontiers in Oncology, 2020. **10**.
59. Lacroix, C., et al., *Identification of Novel Smoothened Ligands Using Structure-Based Docking.* Plos One, 2016. **11**(8).
60. Stanton, B.Z., et al., *A small molecule that binds Hedgehog and blocks its signaling in human cells.* Nat Chem Biol, 2009. **5**(3): p. 154-6.
61. Lauth, M., et al., *Inhibition of GLI-mediated transcription and tumor cell growth by small-molecule antagonists.* Proc Natl Acad Sci U S A, 2007. **104**(20): p. 8455-60.
62. Hyman, J.M., et al., *Small-molecule inhibitors reveal multiple strategies for Hedgehog pathway blockade.* Proc Natl Acad Sci U S A, 2009. **106**(33): p. 14132-7.
63. Sinha, S. and J.K. Chen, *Purmorphamine activates the Hedgehog pathway by targeting Smoothened.* Nature Chemical Biology, 2006. **2**(1): p. 29-30.
64. Chen, J.K., et al., *Small molecule modulation of Smoothened activity.* Proc Natl Acad Sci U S A, 2002. **99**(22): p. 14071-6.
65. Wu, X., et al., *Purmorphamine induces osteogenesis by activation of the hedgehog signaling pathway.* Chem Biol, 2004. **11**(9): p. 1229-38.
66. Chen, G., C. Deng, and Y.P. Li, *TGF-β and BMP signaling in osteoblast differentiation and bone formation.* Int J Biol Sci, 2012. **8**(2): p. 272-88.
67. Ponzetti, M. and N. Rucci, *Osteoblast Differentiation and Signaling: Established Concepts and Emerging Topics.* International Journal of Molecular Sciences, 2021. **22**(13).
68. Rutkovskiy, A., K.O. Stensløkken, and I.J. Vaage, *Osteoblast Differentiation at a Glance.* Med Sci Monit Basic Res, 2016. **22**: p. 95-106.
69. Amarasekara, D.S., S. Kim, and J. Rho, *Regulation of Osteoblast Differentiation by Cytokine Networks.* International Journal of Molecular Sciences, 2021. **22**(6).
70. Huang, W., et al., *Signaling and transcriptional regulation in osteoblast commitment and differentiation.* Frontiers in Bioscience-Landmark, 2007. **12**: p. 3068-3092.
71. Arboleya, L. and S. Castañeda, *Osteoimmunology: The Study of the Relationship Between the Immune System and Bone Tissue.* Reumatología Clínica (English Edition), 2013. **9**(5): p. 303-315.
72. Lin, G.L. and K.D. Hankenson, *Integration of BMP, Wnt, and notch signaling pathways in osteoblast differentiation.* J Cell Biochem, 2011. **112**(12): p. 3491-501.
73. Yang, J., et al., *The Hedgehog signalling pathway in bone formation.* International Journal of Oral Science, 2015. **7**(2): p. 73-79.
74. Rawadi, G., et al., *BMP-2 controls alkaline phosphatase expression and osteoblast mineralization by a Wnt autocrine loop.* Journal of Bone and Mineral Research, 2003. **18**(10): p. 1842-1853.

75. Hu, H., et al., *Sequential roles of Hedgehog and Wnt signaling in osteoblast development.* Development, 2005. **132**(1): p. 49-60.
76. Amarasekara, D.S., S. Kim, and J. Rho, *Regulation of Osteoblast Differentiation by Cytokine Networks.* International Journal of Molecular Sciences, 2021. **22**(6): p. 2851.
77. Lojk, J. and J. Marc, *Roles of Non-Canonical Wnt Signalling Pathways in Bone Biology.* Int J Mol Sci, 2021. **22**(19).
78. Houschyar, K.S., et al., *Wnt Pathway in Bone Repair and Regeneration - What Do We Know So Far.* Front Cell Dev Biol, 2018. **6**: p. 170.
79. Matsubara, T., et al., *BMP2 regulates Osterix through Msx2 and Runx2 during osteoblast differentiation.* J Biol Chem, 2008. **283**(43): p. 29119-25.
80. Luo, J., et al., *The role of GPCRs in bone diseases and dysfunctions.* Bone Res, 2019. **7**: p. 19.
81. Imai, Y., et al., *Nuclear Receptors in Bone Physiology and Diseases.* Physiological Reviews, 2013. **93**(2): p. 481-523.
82. Kremer, L., et al., *Discovery of a Novel Inhibitor of the Hedgehog Signaling Pathway through Cell-based Compound Discovery and Target Prediction.* Angewandte Chemie-International Edition, 2017. **56**(42): p. 13021-13025.
83. Cox, J. and M. Mann, *MaxQuant enables high peptide identification rates, individualized p.p.b.-range mass accuracies and proteome-wide protein quantification.* Nature Biotechnology, 2008. **26**(12): p. 1367-1372.
84. Tyanova, S., et al., *The Perseus computational platform for comprehensive analysis of (prote)omics data.* Nature Methods, 2016. **13**(9): p. 731-740.
85. Goedhart, J. and M.S. Luijsterburg, *VolcaNoseR – a web app for creating, exploring, labeling and sharing volcano plots.* bioRxiv, 2020: p. 2020.05.07.082263.
86. Friese, A., et al., *Chemical Genetics Reveals a Role of dCTP Pyrophosphatase 1 in Wnt Signaling.* Angewandte Chemie-International Edition, 2019. **58**(37): p. 13009-13013.
87. Kremer, L., et al., *Discovery of the Hedgehog Pathway Inhibitor Pipinib that Targets PI4KIII beta.* Angewandte Chemie-International Edition, 2019. **58**(46): p. 16617-16628.
88. Livak, K.J. and T.D. Schmittgen, *Analysis of relative gene expression data using real-time quantitative PCR and the 2(-Delta Delta C(T)) Method.* Methods, 2001. **25**(4): p. 402-8.
89. Laemmli, U.K., *Cleavage of Structural Proteins during the Assembly of the Head of Bacteriophage T4.* Nature, 1970. **227**(5259): p. 680-685.
90. Cox, J. and M. Mann, *MaxQuant enables high peptide identification rates, individualized p.p.b.-range mass accuracies and proteome-wide protein quantification.* Nat Biotechnol, 2008. **26**(12): p. 1367-72.
91. Tyanova, S. and J. Cox, *Perseus: A Bioinformatics Platform for Integrative Analysis of Proteomics Data in Cancer Research.* Methods Mol Biol, 2018. **1711**: p. 133-148.
92. Niggemeyer, G., et al., *Synthesis of 20-Membered Macrocyclic Pseudo-Natural Products Yields Inducers of LC3 Lipidation.* Angew Chem Int Ed Engl, 2022. **61**(11): p. e202114328.
93. Nemec, V., et al., *Furo[3,2-b]pyridine: A Privileged Scaffold for Highly Selective Kinase Inhibitors and Effective Modulators of the Hedgehog Pathway.* Angewandte Chemie-International Edition, 2019. **58**(4): p. 1062-1066.
94. Shan, G., et al., *C-H Bond Activation for the Synthesis of Heterocyclic Atropisomers Yields Hedgehog Pathway Inhibitors.* Angew Chem Int Ed Engl, 2018. **57**(43): p. 14250-14254.
95. Cadigan, K.M. and M.L. Waterman, *TCF/LEFs and Wnt signaling in the nucleus.* Cold Spring Harb Perspect Biol, 2012. **4**(11).
96. Zernik, J., K. Twarog, and W.B. Upholt, *Regulation of alkaline phosphatase and alpha 2(I) procollagen synthesis during early intramembranous bone formation in the rat mandible.* Differentiation, 1990. **44**(3): p. 207-15.
97. Wu, M., G. Chen, and Y.-P. Li, *TGF-β and BMP signaling in osteoblast, skeletal development, and bone formation, homeostasis and disease.* Bone Research, 2016. **4**(1): p. 16009.

98. Winkler, D.G., et al., *Sclerostin inhibition of Wnt-3a-induced C3H10T1/2 cell differentiation is indirect and mediated by bone morphogenetic proteins.* J Biol Chem, 2005. **280**(4): p. 2498-502.
99. Wang, Y., et al., *Wnt3a-regulated TCF4/β-catenin complex directly activates the key Hedgehog signalling genes Smo and Gli1.* Experimental and therapeutic medicine, 2018. **16**(3): p. 2101-2107.
100. Li, G., et al., *Differential effect of BMP4 on NIH/3T3 and C2C12 cells: implications for endochondral bone formation.* J Bone Miner Res, 2005. **20**(9): p. 1611-23.
101. Keiser, M.J., et al., *Relating protein pharmacology by ligand chemistry.* Nat Biotechnol, 2007. **25**(2): p. 197-206.
102. Civciristov, S. and M.L. Halls, *Signalling in response to sub-picomolar concentrations of active compounds: Pushing the boundaries of GPCR sensitivity.* Br J Pharmacol, 2019. **176**(14): p. 2382-2401.
103. Imai, Y., et al., *Nuclear receptors in bone physiology and diseases.* Physiological reviews, 2013. **93**(2): p. 481-523.
104. Roforth, M.M., et al., *Examination of nuclear receptor expression in osteoblasts reveals Rorβ as an important regulator of osteogenesis.* J Bone Miner Res, 2012. **27**(4): p. 891-901.
105. Jeong, B.-C., et al., *The Orphan Nuclear Receptor Estrogen Receptor-related Receptor γ Negatively Regulates BMP2-induced Osteoblast Differentiation and Bone Formation *.* Journal of Biological Chemistry, 2009. **284**(21): p. 14211-14218.
106. Shen, J., et al., *Discovery of Potent Ligands for Estrogen Receptor β by Structure-Based Virtual Screening.* Journal of Medicinal Chemistry, 2010. **53**(14): p. 5361-5365.
107. Germain, P., et al., *Rational design of RAR-selective ligands revealed by RARβ crystal stucture.* EMBO reports, 2004. **5**(9): p. 877-882.
108. He, Y., et al., *Novel nonsteroidal ligands with high binding affinity and potent functional activity for the androgen receptor.* Eur J Med Chem, 2002. **37**(8): p. 619-34.
109. Faraahi, Z., et al., *Sostdc1: A soluble BMP and Wnt antagonist that is induced by the interaction between myeloma cells and osteoblast lineage cells.* Bone, 2019. **122**: p. 82-92.
110. Collette, N.M., et al., *Sost and its paralog Sostdc1 coordinate digit number in a Gli3-dependent manner.* Dev Biol, 2013. **383**(1): p. 90-105.
111. Lo, R. and J. Matthews, *High-Resolution Genome-wide Mapping of AHR and ARNT Binding Sites by ChIP-Seq.* Toxicological Sciences, 2012. **130**(2): p. 349-361.
112. Franchini, A.M., et al., *Genome-Wide Transcriptional Analysis Reveals Novel AhR Targets That Regulate Dendritic Cell Function during Influenza A Virus Infection.* Immunohorizons, 2019. **3**(6): p. 219-235.
113. Kim, Y., et al., *Ptch2/Gas1 and Ptch1/Boc differentially regulate Hedgehog signalling in murine primordial germ cell migration.* Nature Communications, 2020. **11**(1): p. 1994.
114. Slominski, A.T., et al., *Differential and Overlapping Effects of 20,23(OH)$_2$D3 and 1,25(OH)$_2$D3 on Gene Expression in Human Epidermal Keratinocytes: Identification of AhR as an Alternative Receptor for 20,23(OH)$_2$D3.* Int J Mol Sci, 2018. **19**(10).
115. Talia, C., L. Connolly, and P.A. Fowler, *The insulin-like growth factor system: A target for endocrine disruptors?* Environment International, 2021. **147**: p. 106311.
116. Mateus, A., et al., *Thermal proteome profiling for interrogating protein interactions.* Molecular Systems Biology, 2020. **16**(3): p. e9232.
117. Susa, M., et al., *Cyclin G-associated kinase is necessary for osteosarcoma cell proliferation and receptor trafficking.* Mol Cancer Ther, 2010. **9**(12): p. 3342-50.
118. Peng, Y., et al., *Regulation of the integrin αVβ3- actin filaments axis in early osteogenesis of human fibroblasts under cyclic tensile stress.* Stem Cell Research & Therapy, 2021. **12**(1): p. 523.
119. Liu, L., et al., *Na+/H+ exchanger regulatory factor 1 (NHERF1) directly regulates osteogenesis.* The Journal of biological chemistry, 2012. **287**(52): p. 43312-43321.
120. Luecke-Johansson, S., et al., *A Molecular Mechanism To Switch the Aryl Hydrocarbon Receptor from a Transcription Factor to an E3 Ubiquitin Ligase.* Mol Cell Biol, 2017. **37**(13).

121. Kim, I.S., et al., *In vitro and in silico evaluation of transactivation potencies of avian AHR1 and AHR2 by endogenous ligands: Implications for the physiological role of avian AHR2.* Comp Biochem Physiol C Toxicol Pharmacol, 2016. **187**: p. 1-9.
122. Dere, E., et al., *In vivo-in vitro toxicogenomic comparison of TCDD-elicited gene expression in Hepa1c1c7 mouse hepatoma cells and C57BL/6 hepatic tissue.* BMC Genomics, 2006. **7**: p. 80.
123. Milner, J.A. and D.F. Romagnolo, *Bioactive Compounds and Cancer*. 2010: Humana Press.
124. Smith, S.H., et al., *Tapinarof Is a Natural AhR Agonist that Resolves Skin Inflammation in Mice and Humans.* Journal of Investigative Dermatology, 2017. **137**(10): p. 2110-2119.
125. Kim, S.H., et al., *Novel compound 2-methyl-2H-pyrazole-3-carboxylic acid (2-methyl-4-o-tolylazo-phenyl)-amide (CH-223191) prevents 2,3,7,8-TCDD-induced toxicity by antagonizing the aryl hydrocarbon receptor.* Mol Pharmacol, 2006. **69**(6): p. 1871-8.
126. Zhao, B., et al., *CH223191 is a ligand-selective antagonist of the Ah (Dioxin) receptor.* Toxicol Sci, 2010. **117**(2): p. 393-403.
127. Zhu, K., et al., *Aryl hydrocarbon receptor pathway: Role, regulation and intervention in atherosclerosis therapy (Review).* Mol Med Rep, 2019. **20**(6): p. 4763-4773.
128. Zhang, C., et al., *Gram-scale synthesis of FICZ, a photoreactive endogenous ligand of the aryl hydrocarbon receptor.* Scientific Reports, 2019. **9**(1): p. 9982.
129. Ma, Q. and K.T. Baldwin, *2,3,7,8-tetrachlorodibenzo-p-dioxin-induced degradation of aryl hydrocarbon receptor (AhR) by the ubiquitin-proteasome pathway. Role of the transcription activaton and DNA binding of AhR.* J Biol Chem, 2000. **275**(12): p. 8432-8.
130. Wincent, E., et al., *Biological effects of 6-formylindolo[3,2-b]carbazole (FICZ) in vivo are enhanced by loss of CYP1A function in an Ahr2-dependent manner.* Biochemical Pharmacology, 2016. **110-111**: p. 117-129.
131. Rahnama, F., R. Toftgård, and P.G. Zaphiropoulos, *Distinct roles of PTCH2 splice variants in Hedgehog signalling.* Biochem J, 2004. **378**(Pt 2): p. 325-34.
132. Chen, G., C. Deng, and Y.-P. Li, *TGF-β and BMP signaling in osteoblast differentiation and bone formation.* International journal of biological sciences, 2012. **8**(2): p. 272-288.
133. Yin, X., et al., *Autophagy in bone homeostasis and the onset of osteoporosis.* Bone Research, 2019. **7**(1): p. 28.
134. Byrne, E.F., et al., *Multiple ligand binding sites regulate the Hedgehog signal transducer Smoothened in vertebrates.* Curr Opin Cell Biol, 2018. **51**: p. 81-88.
135. Carballo, G.B., et al., *A highlight on Sonic hedgehog pathway.* Cell Communication and Signaling, 2018. **16**(1): p. 11.
136. Ohashi, T., et al., *Discovery of pyrrolo[3,2-c]quinoline-4-one derivatives as novel hedgehog signaling inhibitors.* Bioorg Med Chem, 2012. **20**(18): p. 5496-506.
137. Yauch, R.L., et al., *Smoothened mutation confers resistance to a Hedgehog pathway inhibitor in medulloblastoma.* Science (New York, N.Y.), 2009. **326**(5952): p. 572-574.
138. Huang, W., et al., *Signaling and transcriptional regulation in osteoblast commitment and differentiation.* Frontiers in bioscience : a journal and virtual library, 2007. **12**: p. 3068-3092.
139. Vimalraj, S., *Alkaline phosphatase: Structure, expression and its function in bone mineralization.* Gene, 2020. **754**: p. 144855.
140. Koussounadis, A., et al., *Relationship between differentially expressed mRNA and mRNA-protein correlations in a xenograft model system.* Scientific Reports, 2015. **5**(1): p. 10775.
141. Fournier, M.L., et al., *Delayed Correlation of mRNA and Protein Expression in Rapamycin-treated Cells and a Role for Ggc1 in Cellular Sensitivity to Rapamycin*.* Molecular & Cellular Proteomics, 2010. **9**(2): p. 271-284.
142. Maleki, M., et al., *Comparison of mesenchymal stem cell markers in multiple human adult stem cells.* International journal of stem cells, 2014. **7**(2): p. 118-126.
143. Judson, R., et al., *Editor's Highlight: Analysis of the Effects of Cell Stress and Cytotoxicity on In Vitro Assay Activity Across a Diverse Chemical and Assay Space.*

Toxicological sciences : an official journal of the Society of Toxicology, 2016. **152**(2): p. 323-339.
144. Weng, G., U.S. Bhalla, and R. Iyengar, *Complexity in biological signaling systems.* Science (New York, N.Y.), 1999. **284**(5411): p. 92-96.
145. Winkler, D.G., et al., *Sclerostin Inhibition of Wnt-3a-induced C3H10T1/2 Cell Differentiation Is Indirect and Mediated by Bone Morphogenetic Proteins*.* Journal of Biological Chemistry, 2005. **280**(4): p. 2498-2502.
146. Oliveira, F.S., et al., *Hedgehog signaling and osteoblast gene expression are regulated by purmorphamine in human mesenchymal stem cells.* J Cell Biochem, 2012. **113**(1): p. 204-8.
147. Sydow, D., et al., *Advances and Challenges in Computational Target Prediction.* J Chem Inf Model, 2019. **59**(5): p. 1728-1742.
148. Luo, J., et al., *The role of GPCRs in bone diseases and dysfunctions.* Bone Research, 2019. **7**(1): p. 19.
149. Zhu, W., et al., *Conditional inactivation of the CXCR4 receptor in osteoprecursors reduces postnatal bone formation due to impaired osteoblast development.* J Biol Chem, 2011. **286**(30): p. 26794-805.
150. Campbell, A.P. and A.V. Smrcka, *Targeting G protein-coupled receptor signalling by blocking G proteins.* Nature reviews. Drug discovery, 2018. **17**(11): p. 789-803.
151. Santos, R., et al., *A comprehensive map of molecular drug targets.* Nature Reviews Drug Discovery, 2017. **16**(1): p. 19-34.
152. Ezzat, A., et al., *Drug-target interaction prediction via class imbalance-aware ensemble learning.* BMC Bioinformatics, 2016. **17**(19): p. 509.
153. Komori, T., *Regulation of osteoblast differentiation by Runx2.* Adv Exp Med Biol, 2010. **658**: p. 43-9.
154. Nakashima, K., et al., *The Novel Zinc Finger-Containing Transcription Factor Osterix Is Required for Osteoblast Differentiation and Bone Formation.* Cell, 2002. **108**(1): p. 17-29.
155. Zhang, C., *Transcriptional regulation of bone formation by the osteoblast-specific transcription factor Osx.* Journal of Orthopaedic Surgery and Research, 2010. **5**(1): p. 37.
156. Hojo, H., et al., *Gli1 Protein Participates in Hedgehog-mediated Specification of Osteoblast Lineage during Endochondral Ossification *.* Journal of Biological Chemistry, 2012. **287**(21): p. 17860-17869.
157. Murray, I.A., A.D. Patterson, and G.H. Perdew, *Aryl hydrocarbon receptor ligands in cancer: friend and foe.* Nature reviews. Cancer, 2014. **14**(12): p. 801-814.
158. Mulero-Navarro, S. and P.M. Fernandez-Salguero, *New Trends in Aryl Hydrocarbon Receptor Biology.* Frontiers in Cell and Developmental Biology, 2016. **4**.
159. Park, R., S. Madhavaram, and J.D. Ji, *The Role of Aryl-Hydrocarbon Receptor (AhR) in Osteoclast Differentiation and Function.* Cells, 2020. **9**(10): p. 2294.
160. Watson, A.T.D., et al., *Evidence for Aryl hydrocarbon Receptor-Mediated Inhibition of Osteoblast Differentiation in Human Mesenchymal Stem Cells.* Toxicological sciences : an official journal of the Society of Toxicology, 2019. **167**(1): p. 145-156.
161. Korkalainen, M., et al., *Dioxins interfere with differentiation of osteoblasts and osteoclasts.* Bone, 2009. **44**(6): p. 1134-42.
162. Ohtake, F., Y. Fujii-Kuriyama, and S. Kato, *AhR acts as an E3 ubiquitin ligase to modulate steroid receptor functions.* Biochemical Pharmacology, 2009. **77**(4): p. 474-484.
163. Tomblin, J.K. and T.B. Salisbury, *Insulin like growth factor 2 regulation of aryl hydrocarbon receptor in MCF-7 breast cancer cells.* Biochemical and biophysical research communications, 2014. **443**(3): p. 1092-1096.
164. Zhang, Z.M., et al., *Insulin-Like Growth Factor Binding Protein 5: an Important Regulator of Early Osteogenic Differentiation of hMSCs.* Folia Biol (Praha), 2021. **67**(3): p. 118-125.
165. Wright, E.J., et al., *Canonical and non-canonical aryl hydrocarbon receptor signaling pathways.* Current opinion in toxicology, 2017. **2**: p. 87-92.

166. Yoshikawa, Y., et al., *Roles for B[a]P and FICZ in subchondral bone metabolism and experimental temporomandibular joint osteoarthritis via the AhR/Cyp1a1 signaling axis.* Scientific Reports, 2021. **11**(1): p. 14927.
167. Miniero, R., et al., *An overview of TCDD half-life in mammals and its correlation to body weight.* Chemosphere, 2001. **43**(4): p. 839-844.
168. Ehrlich, A.K., et al., *TCDD, FICZ, and Other High Affinity AhR Ligands Dose-Dependently Determine the Fate of CD4+ T Cell Differentiation.* Toxicological sciences : an official journal of the Society of Toxicology, 2018. **161**(2): p. 310-320.
169. Denison, M.S. and S.C. Faber, *And Now for Something Completely Different: Diversity in Ligand-Dependent Activation of Ah Receptor Responses.* Current opinion in toxicology, 2017. **2**: p. 124-131.
170. Tkachenko, A., et al., *The Q-rich/PST domain of the AHR regulates both ligand-induced nuclear transport and nucleocytoplasmic shuttling.* Scientific Reports, 2016. **6**(1): p. 32009.
171. Martignoni, M., G.M.M. Groothuis, and R. de Kanter, *Species differences between mouse, rat, dog, monkey and human CYP-mediated drug metabolism, inhibition and induction.* Expert Opinion on Drug Metabolism & Toxicology, 2006. **2**(6): p. 875-894.
172. Uemura, S., et al., *Biochemical properties of human full-length aryl hydrocarbon receptor (AhR).* The Journal of Biochemistry, 2020. **168**(3): p. 285-294.
173. Tsuji, N., et al., *The activation mechanism of the aryl hydrocarbon receptor (AhR) by molecular chaperone HSP90.* FEBS open bio, 2014. **4**: p. 796-803.
174. Samaras, P., et al., *ProteomicsDB: a multi-omics and multi-organism resource for life science research.* Nucleic Acids Research, 2019. **48**(D1): p. D1153-D1163.
175. Schmidt, T., et al., *ProteomicsDB.* Nucleic Acids Research, 2017. **46**(D1): p. D1271-D1281.
176. Zhang, H.F., et al., *Regulation of the activity and expression of aryl hydrocarbon receptor by ethanol in mouse hepatic stellate cells.* Alcoholism, clinical and experimental research, 2012. **36**(11): p. 1873-1881.
177. Henry, E.C. and T.A. Gasiewicz, *Agonist but not antagonist ligands induce conformational change in the mouse aryl hydrocarbon receptor as detected by partial proteolysis.* Mol Pharmacol, 2003. **63**(2): p. 392-400.
178. Stinn, A., et al., *Novel Method for Quantifying AhR-Ligand Binding Affinities Using Microscale Thermophoresis.* Biosensors (Basel), 2021. **11**(3).
179. Schopper, S., et al., *Measuring protein structural changes on a proteome-wide scale using limited proteolysis-coupled mass spectrometry.* Nature Protocols, 2017. **12**(11): p. 2391-2410.
180. Ryan, E.P., et al., *Environmental toxicants may modulate osteoblast differentiation by a mechanism involving the aryl hydrocarbon receptor.* J Bone Miner Res, 2007. **22**(10): p. 1571-80.
181. Zhulyn, O., et al., *Ptch2 shares overlapping functions with Ptch1 in Smo regulation and limb development.* Dev Biol, 2015. **397**(2): p. 191-202.
182. Thornley, J.A., et al., *Differential regulation of polysome mRNA levels in mouse Hepa-1C1C7 cells exposed to dioxin.* Toxicology in Vitro, 2011. **25**(7): p. 1457-1467.
183. Sartor, M.A., et al., *Genomewide analysis of aryl hydrocarbon receptor binding targets reveals an extensive array of gene clusters that control morphogenetic and developmental programs.* Environ Health Perspect, 2009. **117**(7): p. 1139-46.
184. Schneider, A.J., A.M. Branam, and R.E. Peterson, *Intersection of AHR and Wnt signaling in development, health, and disease.* International journal of molecular sciences, 2014. **15**(10): p. 17852-17885.
185. Shortall, K., et al., *Insights into Aldehyde Dehydrogenase Enzymes: A Structural Perspective.* Frontiers in Molecular Biosciences, 2021. **8**.
186. Vella, J.B., et al., *Murine and human myogenic cells identified by elevated aldehyde dehydrogenase activity: implications for muscle regeneration and repair.* PLoS One, 2011. **6**(12): p. e29226.

187. Mittal, M., et al., *Pharmacological activation of aldehyde dehydrogenase 2 promotes osteoblast differentiation via bone morphogenetic protein-2 and induces bone anabolic effect.* Toxicol Appl Pharmacol, 2017. **316**: p. 63-73.
188. Kolluri, S.K., U.-H. Jin, and S. Safe, *Role of the aryl hydrocarbon receptor in carcinogenesis and potential as an anti-cancer drug target.* Archives of toxicology, 2017. **91**(7): p. 2497-2513.
189. Eskenazi, B., et al., *The Seveso accident: A look at 40 years of health research and beyond.* Environment international, 2018. **121**(Pt 1): p. 71-84.
190. Woolf, A.D., *Chapter 1.10 - Japan "Yusho" poisoning, 1968 and Taiwan "Yucheng" poisoning, 1979*, in *History of Modern Clinical Toxicology*, A.D. Woolf, Editor. 2022, Academic Press. p. 121-135.
191. Safe, S., et al., *Aryl Hydrocarbon Receptor (AhR) Ligands as Selective AhR Modulators: Genomic Studies.* Current opinion in toxicology, 2018. **11-12**: p. 10-20.
192. Paris, A., et al., *AhR and Cancer: From Gene Profiling to Targeted Therapy.* Int J Mol Sci, 2021. **22**(2).
193. Fan, Y., et al., *The aryl hydrocarbon receptor functions as a tumor suppressor of liver carcinogenesis.* Cancer Res, 2010. **70**(1): p. 212-20.
194. Garcia-Villatoro, E.L., et al., *Effects of high-fat diet and intestinal aryl hydrocarbon receptor deletion on colon carcinogenesis.* Am J Physiol Gastrointest Liver Physiol, 2020. **318**(3): p. G451-g463.
195. Sarić, N., et al., *The AHR pathway represses TGFβ-SMAD3 signalling and has a potent tumour suppressive role in SHH medulloblastoma.* Sci Rep, 2020. **10**(1): p. 148.
196. Zhu, K., et al., *Aryl hydrocarbon receptor pathway: Role, regulation and intervention in atherosclerosis therapy (Review).* Molecular medicine reports, 2019. **20**(6): p. 4763-4773.
197. Bissonnette, R., et al., *Tapinarof in the treatment of psoriasis: A review of the unique mechanism of action of a novel therapeutic aryl hydrocarbon receptor–modulating agent.* Journal of the American Academy of Dermatology, 2021. **84**(4): p. 1059-1067.
198. Veeman, M.T., et al., *Zebrafish prickle, a modulator of noncanonical Wnt/Fz signaling, regulates gastrulation movements.* Curr Biol, 2003. **13**(8): p. 680-5.
199. Taipale, J., et al., *Effects of oncogenic mutations in Smoothened and Patched can be reversed by cyclopamine.* Nature, 2000. **406**(6799): p. 1005-9.
200. Zawel, L., et al., *Human Smad3 and Smad4 are sequence-specific transcription activators.* Mol Cell, 1998. **1**(4): p. 611-7.
201. Najdi, R., et al., *A uniform human Wnt expression library reveals a shared secretory pathway and unique signaling activities.* Differentiation, 2012. **84**(2): p. 203-13.

9 ABBREVIATIONS

Abbreviation	Description
ABP	Affinity-based chemical proteomics
ABPP	Activity-based proteome profiling
ADH7 / *Adh7*	Alcohol dehydrogenase 7
AhR/ *AhR*	Aryl hydrocarbon receptor
Ahrr	Aryl hydrocarbon receptor repressor
AIP	Aryl hydrocarbon receptor-interacting protein
AKT	Protein kinase B
ALDH3A1/ Aldh3a1	Aldehyde dehydrogenase family 3 member A1
ALP/ *Alpl*	Alkaline phosphatase
Amp	Ampicillin
Ap3d1	AP-3 complex subunit delta-1
APS	Ammonium persulfate
ARNT	Aryl hydrocarbon receptor nuclear translocator
AUC	Area under curve
B[a]P	Benzo(a)pyrene
BFP	Blue fluorescent protein
BGP	β-glycerophosphate
BMP	Bone morphogenic protein
BODIPY	Dipyrrometheneboron difluoride
BSA	Bovine serum albumin
cDNA	Complementary DNA
CETSA	Cellular thermal shift assay
ChiP	Chromatin immunoprecipitation
CK1	Casein kinase 1
CM	Conditioned medium
Cmpd	Compound
CMV	Cytomegalovirus
COL2A1/ *Col2a1*	Collagen type 2 alpha-1
COMAS	Compound Management and Screening Center
CSC	Cancer stem cell
CYP1A1/ *Cyp1a1*	Cytochrome P450 1A1
CYP1B1/*Cyp1b1*	Cytochrome P450 1B1
DAPI	4′,6-diamidino-2-phenylindole
ddNTPs	Dideoxynucleoside triphosphate
DHH	Desert Hedgehog
DMEM	Gibco Dulbecco’s Modified Eagle Medium
DMSO	Dimethyl sulfoxide
DNA	Deoxyribonucleic acid
Drd1	D(1A) dopamine receptor
Drd2	D(2) dopamine receptor
DRD5	D(1B) dopamine receptor
DTE	Dithioerythritol
DTT	Dithiothreitol
EDTA	Ethylenediaminetetraacetic acid
EMA	European Medicines Agency

ERK	Extracellular signal-regulated kinase
EtOH	Ethanol
FACS	Fluorescence assisted cell sorting
FBS	Fetal bovine serum
FC	Fold change
FCS	Fetal calf serum
FDA	Food and Drug Administration
FGF	Fibroblast growth factor
FICZ	6-formylindolo[3,2-*b*]carbazole
Fluc	Firefly luciferase
FP	Fluorescence polarization
fw	forward
G418	Geneticin
GAK	Cyclin-G-associated kinase
Gapdh	Glyceraldehyde 3-phosphate dehydrogenase
gDNA	Genomic DNA
GEO	Gene Expression Omnibus
GLI1/ *Gli1*	Glioma-associated oncogene 1
GLI2 / *Gli2*	Glioma-associated oncogene 2
GLI2/3	Glioma-associated oncogene 2 and 3
GLI2/3-R	repressor form of GLI2/3
GPCR	G-protein coupled receptor
Grem1	Gremlin-1
GSK3β	Glycogen synthase kinase 3β
HAH	Halogenated aryl hydrocarbons
HCD	High energy collision dissociation
HCl	Hydrochloric acid
HEPES	2-(4-(2-Hydroxyethyl)-1-piperazinyl)-ethansulfonic acid
Hh	Hedgehog
Hh RGA	Hh reporter gene assay
HHIP/ *Hhip*	Hedgehog-interacting protein
HPLC	High pressure liquid phase chromatography
Hrh1	Histamine H1 receptor
HSP90	HSP90 co-chaperone
HTR2B	5-hydroxytryptamine receptor 2B
HTR2C	5-hydroxytryptamine receptor 2C
HTR3B	5-hydroxytryptamine receptor 3B
HTS	High-throughput screening
IHH	Indian Hedgehog
IPA	Ingenuity Pathway Analysis
ITC	isothermal titration calorimetry
ITDRF	Isothermal dose-response fingerprinting
ITGB3	Integrin beta-3
JNK	Stress-activated protein kinase JNK
KCl	Potassium chloride
KEAP1	Kelch-like ECH-associated protein 1
LB	Lysogeny broth
LC	Liquid chromatography
LEF	Lymphoid enhancer-binding factor 1

LiP-MS	Limited proteolysis-coupled mass spectrometry
LMNA	Lamin A
lncRNA	Long non-coding RNA
LRP5	Low-density lipoprotein receptor-related protein 5
Lrrn3	Leucine-rich repeat neuronal protein 3
MAPK	Mitogen-activated protein kinase
MeOH	Methanol
$MgCl_2$	Magnesiumchloride
miRNA	MicroRNA
MoA	Mode of action
mRNA	Messenger RNA
MS	Mass spectrometry
MS/MS	Tandem mass spectrometry
MSC	Mesenchymal stem cells
NaOH	Sodium hydroxide
ncRNA	Non-conding RNA
NGS	Next generation sequencing
NP-40	Nondiet P-40
NQO1/ *Nqo1*	NAD(P)H dehydrogenase [quinone] 1
NR	Nuclear receptor
NT	Non-targeting
OCN/ *Bglap*	Osteocalcin
ODA	Osteoblast differentiation assay
OmicsDI	Omics Discovery Index
OPN/ *Spp1*	Osteopontin
OPRL1	Nociceptin receptor
OSX/ *Sp7*	Osterix / Transcription factor Sp7
P23	Prostaglandin E synthase 3
PAH	Polycyclic aryl hydrocarbons
PBS	Phosphate buffered saline
PCR	Polymerase chain reaction
PKA	Protein kinase A
PLC	Phospholipase
POI	Protein of interest
PROTAC	Proteolysis targeting chimera
PTC1/ *Ptch1*	Patched 1
PTC2/ *Ptch2*	Patched 2
PTH	Parathyroid hormone
PTHR	PTH receptor
Purm	purmorphamine
PVDF	Polyvinyldiene difluoride
RAD51	DNA repair protein RAD51 homology 1
RGA	Reporter gene assay
Rluc	*Renilla* luciferase
RNA	Ribonucleic acid
RNA-Seq	RNA Sequencing
RNAi	RNA interference
RT-qPCR	Reverse transcription quantitative PCR
RUNX2/ *Runx2*	Runt-related transcription factor 2

rv	reverse
RXR	Retinoic acid receptor
SAG1.3	SMO Agonist 1.3
SAR	Structure-activity relationship
SBE4	Smad-binding element 4
SD	Standard deviation
SDS	Sodium dodecyl sulfate
SDS-PAGE	SDS-polyacrylamide gel electrophoresis
SEA	Similarity Ensemble Approach
SEM	Standard error of the mean
SHH	Sonic Hedgehog
siRNA	Small-interferring RNA
Slc6a2	Sodium-dependent noradrenaline transporter
Slc6a3	Sodium-dependent dopamine transporter
SLC9A3R1	Na(+)/H(+) exchange regulatory cofactor NHE- RF1
Smad	Mothers against decapentaplegic
SMO	Smoothened
SOX9	SRY-Box transcription factor 9
SPR	Surface plasmon resonance
SRC	Tyrosinkinase SRC (from sarcoma)
STF	SuperTop-Flash luciferase
SUFU	Suppressor of Fused
TAE	TRIS-Acetate-EDTA
TAS1R2	Taste receptor type 1 member 2
TAS1R3	Taste receptor type 1 member 3
TCDD	2,3,7,8-Tetrachlorodibenzo-*p*-dioxin
TCEP	TRIS(2-carboxyethyl)phosphine hydrochloride
TCF	T-cell factor
TCGA	The Cancer Genome Atlas
TEAB	Triethylammonium bicarbonate buffer
TEMED	Tetramethylethylendiamin
TFA	Trifluoric acid
TGFβ	Transforming growth factor β
TGR	Thioredoxin glutathione reductase
TGS	Third generation sequencing
Tiparp	Mono ADP-ribosyltransferase TIPARP
TK	Thymidine kinase
TMT	Tandem mass tag
TPP	Thermal proteome profiling
tRNA	Transfer RNA
US28	G protein coupled receptor homologue US28
VDR	Vitamin D receptor
Via.	Viability
Vismo	Vismodegib
WB	Western blot
Wnt-3A	Protein Wnt-3A
XDH/ *Xdh*	Xanthine dehydrogenase
XRE	Xenobiotic responsive element

10 Appendix

10.1 Vector maps

pcDNA3.1

The pcDNA3.1 plasmid was obtained from Thermo Fisher (V79020).

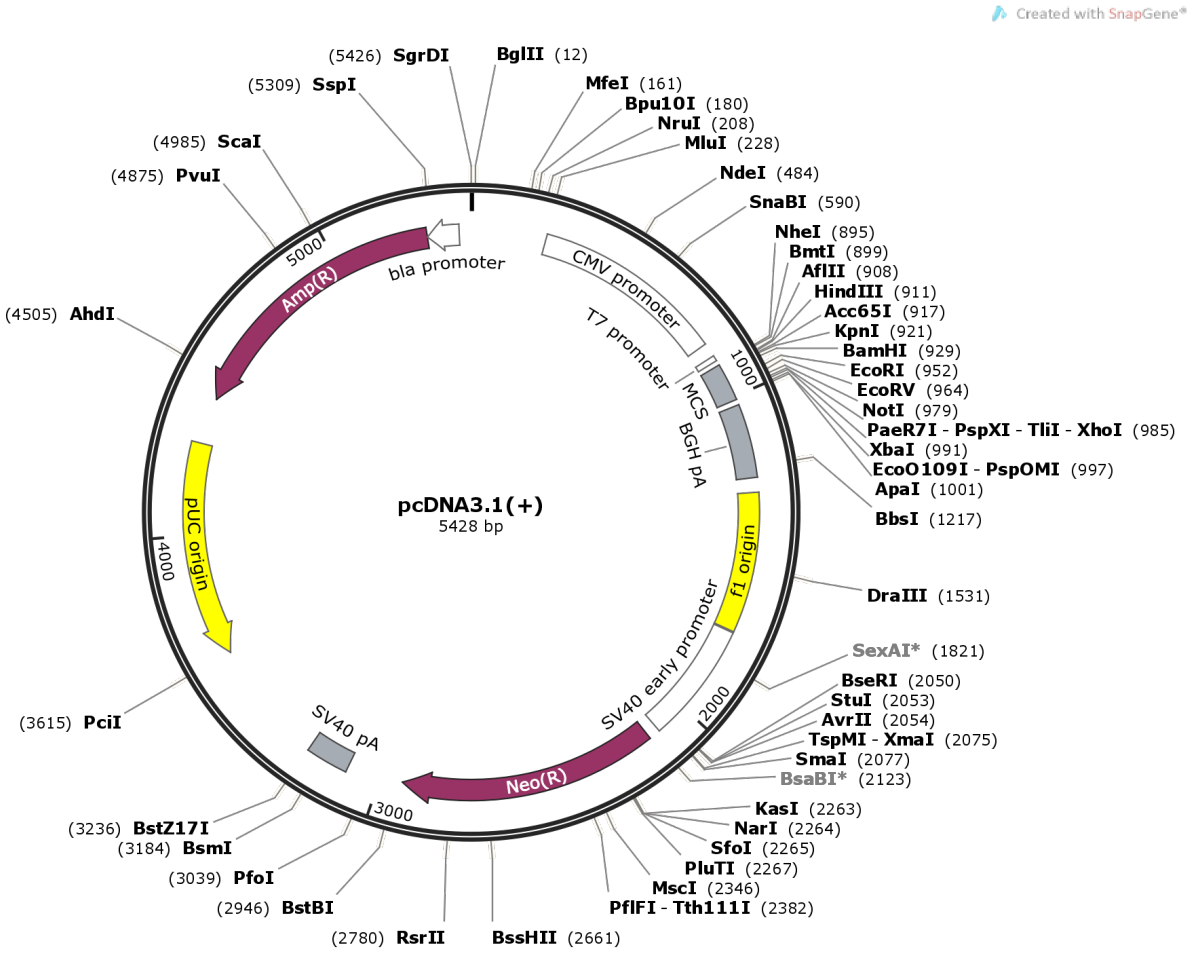

Vector map of pcDNA3.1.

M50 Super 8x TOPFlash

The M50 Super 8x TOPFlash plasmid was obtained from Addgene (12456), where it was deposited by M. T. Veemann.[198]

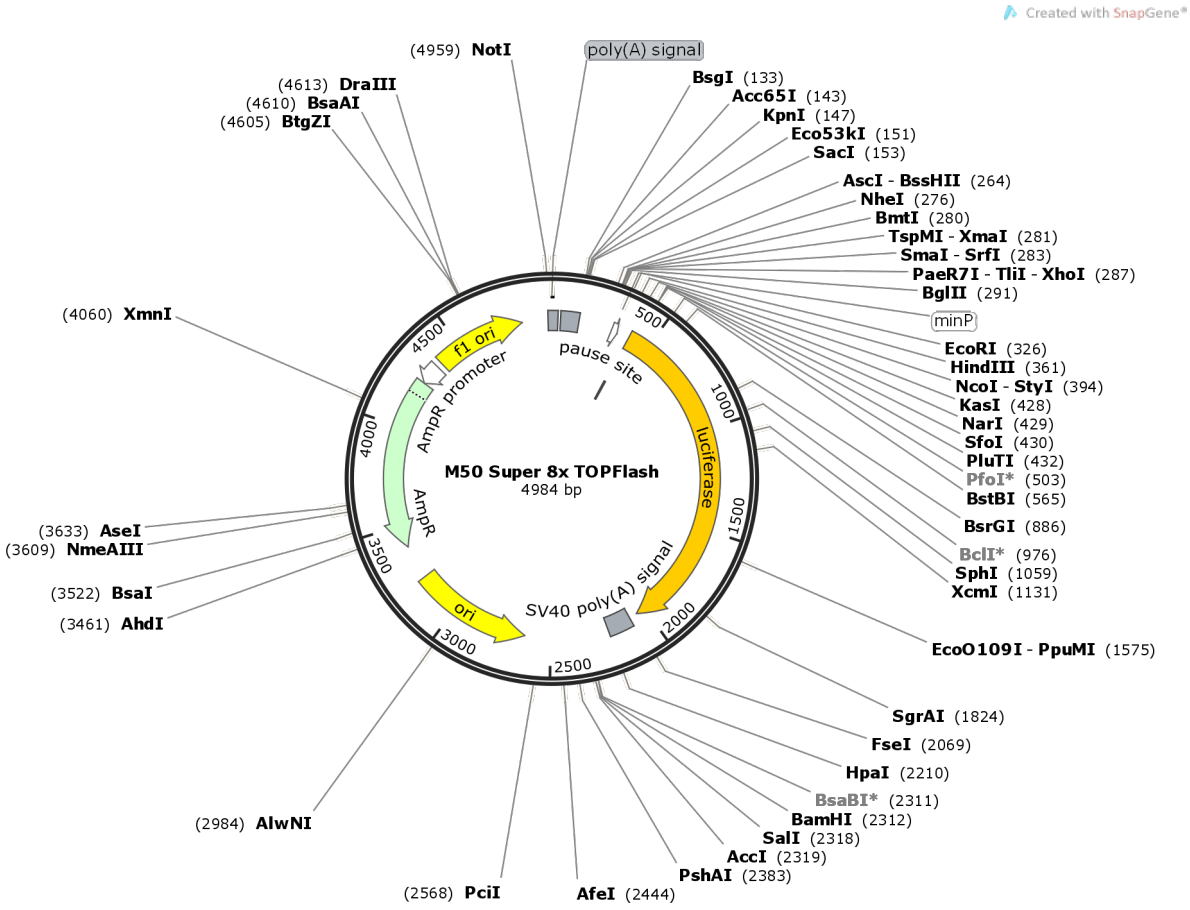

Vector map of M50 Super 8x TOPFlash.

pcDNA3.1-mAhR-FLAG

The pcDNA3.1-mAhR-FLAG plasmid was purchased from GeneScript (OMu19221).

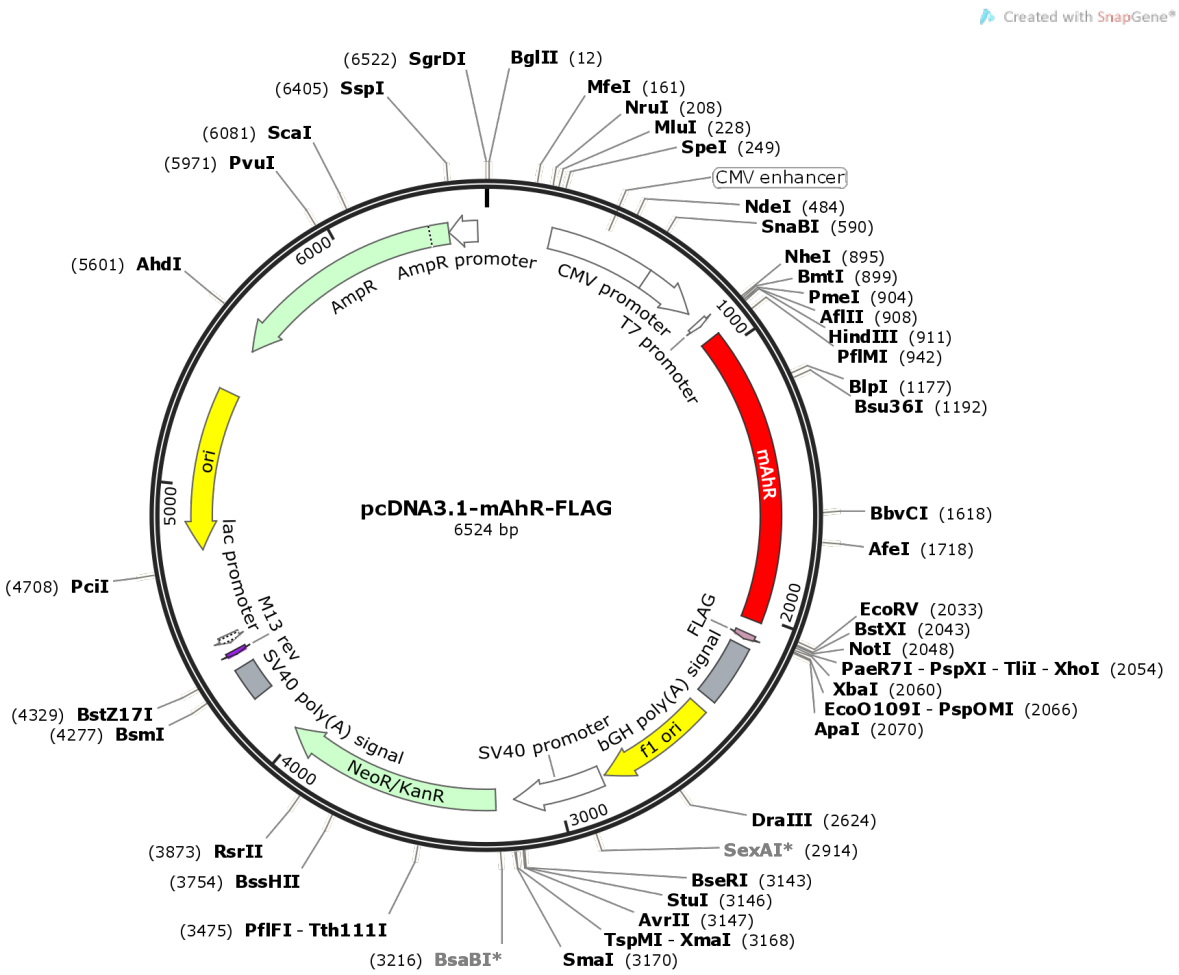

Vector map of pcDNA3.1-mAhR-FLAG.

pcDNA3.1-ShhN

The pcDNA3.1-ShhN plasmid was obtained from Addgene (37680) and was a gift from Phillip Beachy.

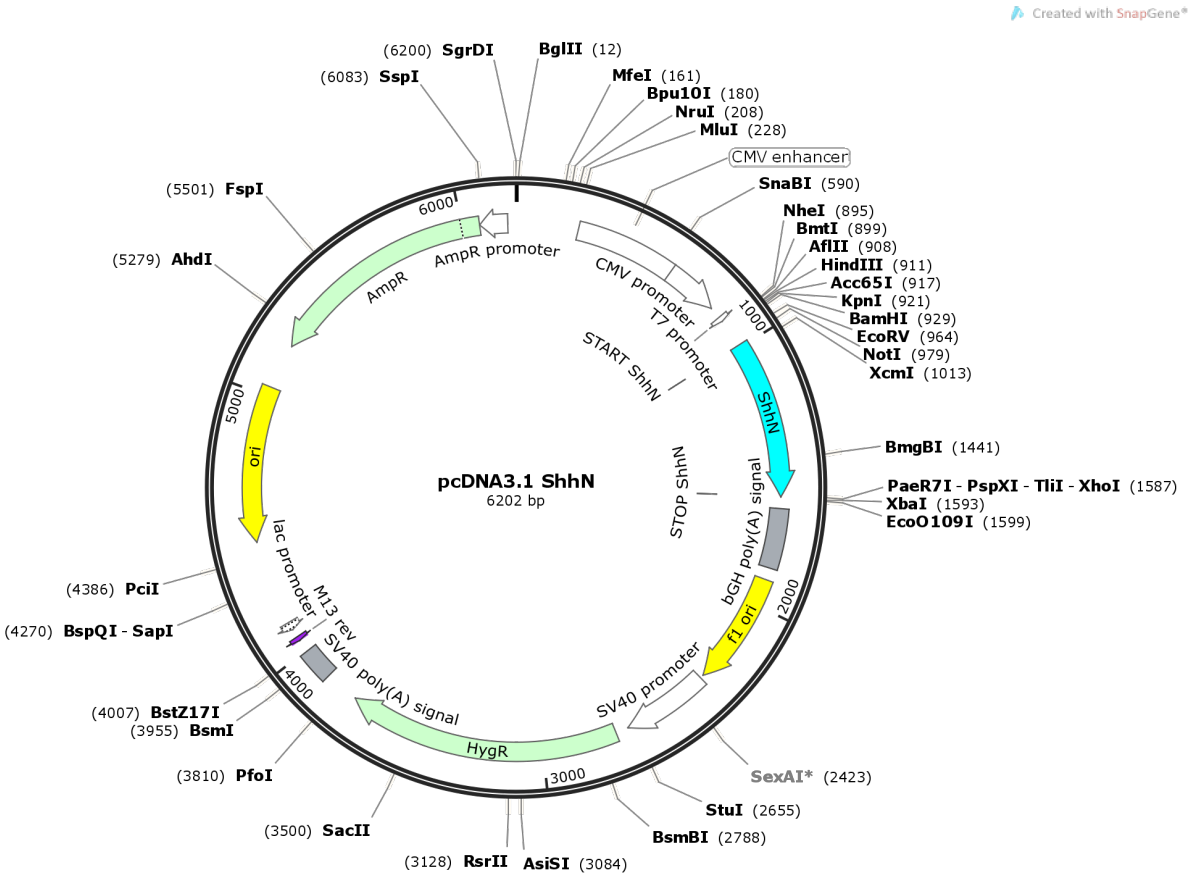

Vector map of pcDNA3.1-ShhN.

pGen-mSMO

The pGen-mSMO plasmid was obtained from Addgene (37673), where it was deposited from P. Beachy.[199]

Vector map of pGen-mSMO.

pGL4.54[luc2/TK]

The pGL4.54[luc2/TK] plasmid was purchased from Promega (9PIE412).

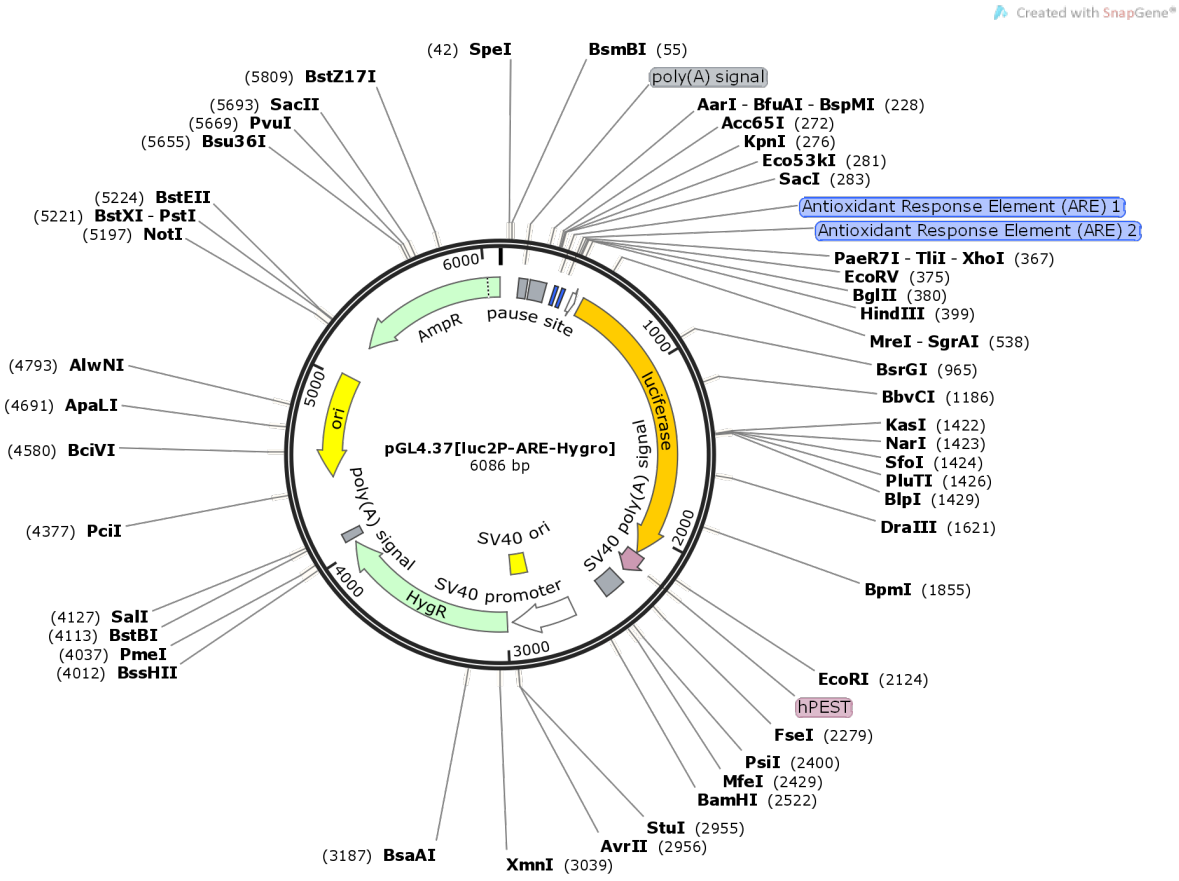

Vector map of pGL4.54[luc2/TK].

pRL-TK-Rluc

The pRL-TK-Rluc plasmid was purchased from Promega (E2241).

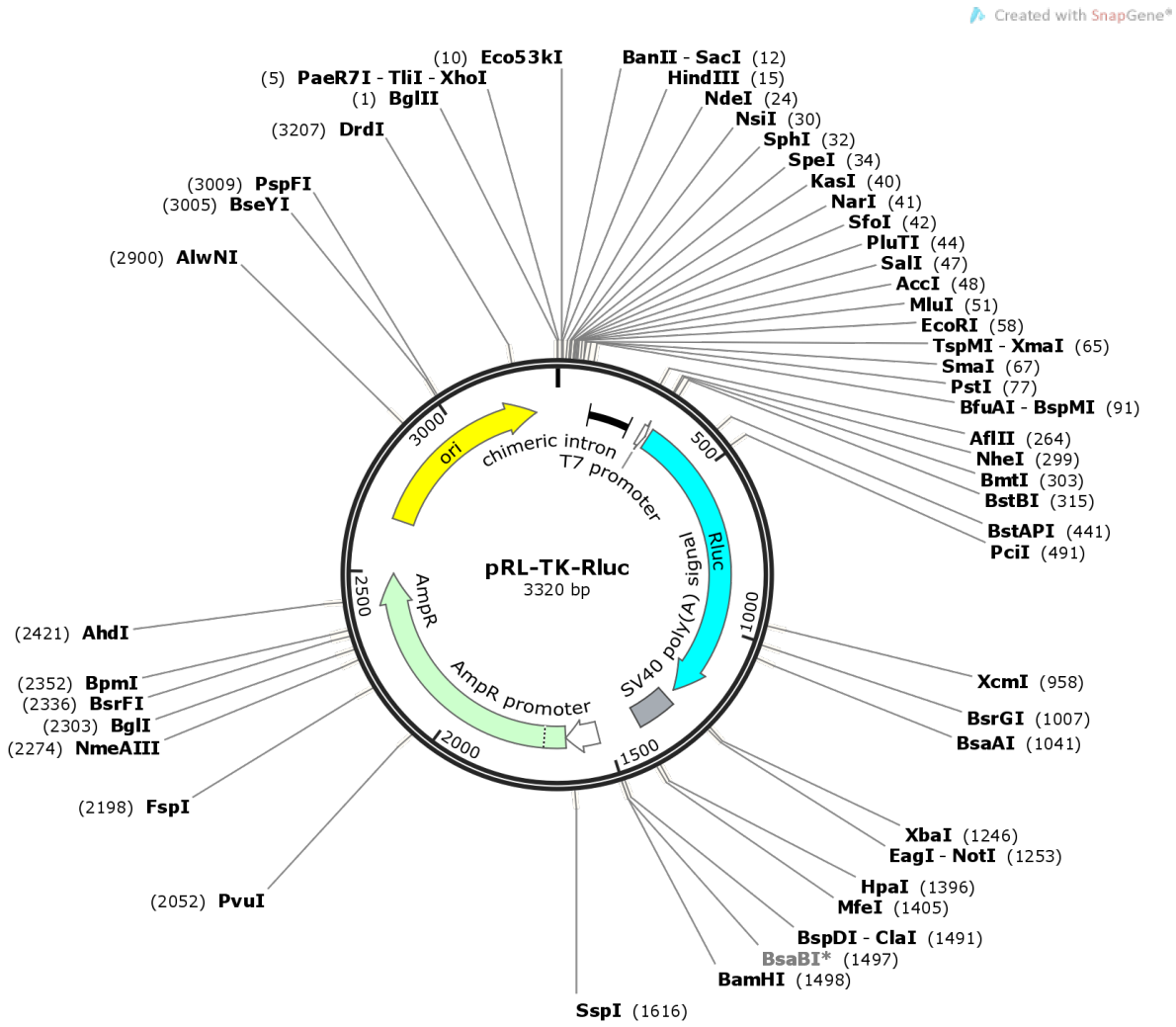

Vector map of pRL-TK-Rluc.

pBV-SBE4-Luc

The pBV-SBA4-Luc plasmid was obtained from Addgene (16495), where it was deposited by L. Zawel et al.[200]

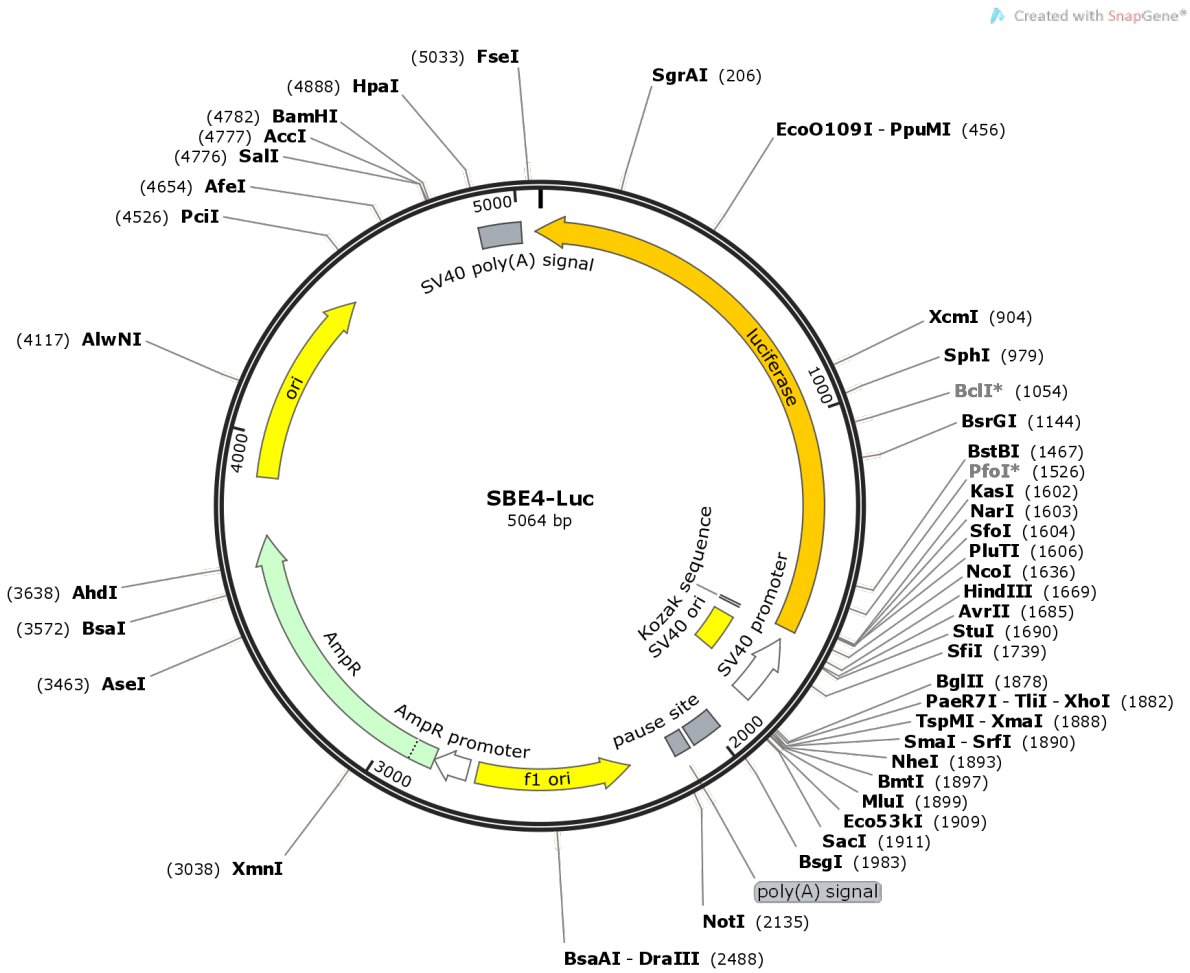

Vector map of pBV-SBE4-Luc.

SMO-BFP

The SMO-BFP plasmid was created by Lea Kremer at the MPI in Dortmund.[82]

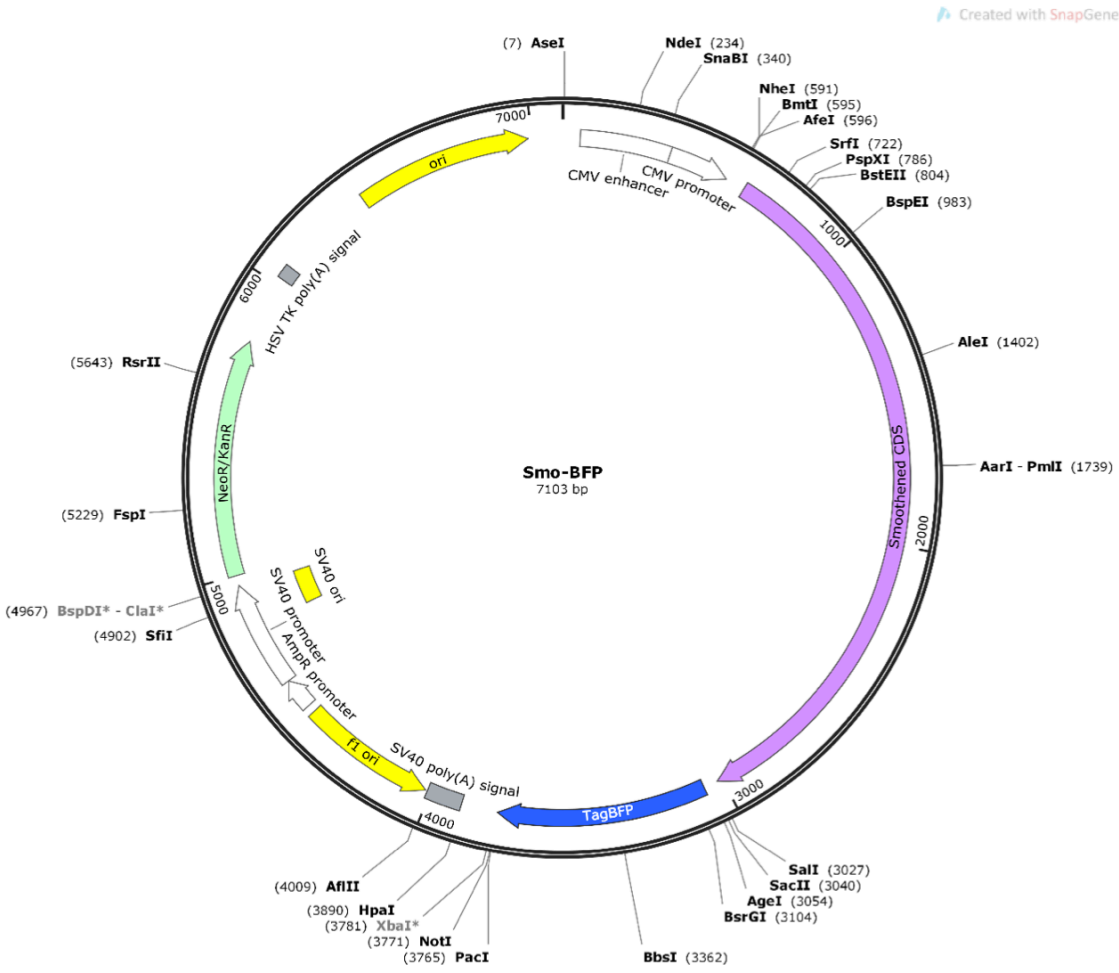

Vector map of the SMO-BFP plasmid.

pcDNA-Wnt3A

The pcDNA3.1-Wnt3A plasmid was obtained from Addgene (35908), where it was deposited by R. Najdi *et al*.[201]

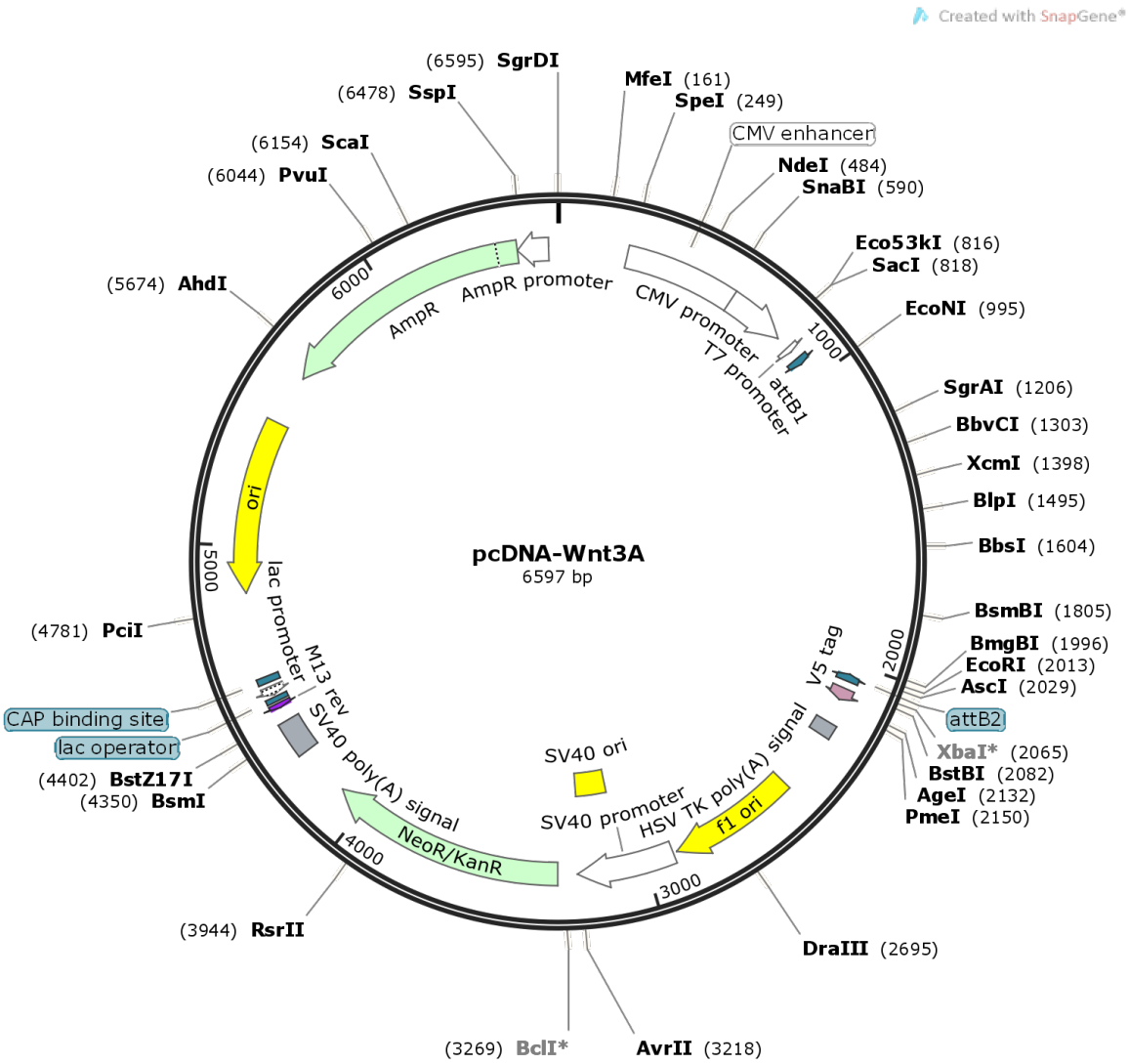

Vector map of pcDNA-Wnt3A.

10.2 RNA-Seq Results

10.2.1 Genes differentially regulated by purmorphamine

Supplementary Table 1: Genes that were differentially expressed upon activation of Hh signaling after 24 h. RNA-Seq data. C3H10T1/2 cells were treated with 1.5 µM purmorphamine and DMSO and were compared to samples that were treated with DMSO. Log_2 fold changes of at least ± 1 with a p-value ≤ 0.05 were considered as significantly up or down regulated.

Gene	Log_2 fold change	Fold change	p-value	FDR p-value
1700034P13Rik	-2.73	-6.64	0.008649	0.9994704
1700094D03Rik	1.48	2.79	0.04575959	0.9994704
4833419F23Rik	1.37	2.59	0.03491335	0.9994704
4930426L09Rik	-1.23	-2.35	0.01901673	0.9994704
4930517E14Rik	-1.33	-2.51	0.002283	0.70070902
8430436N08Rik	-1.01	-2.02	0.02788123	0.9994704
9530052C20Rik	2.03	4.10	0.04977626	0.9994704
A230060F14Rik	-1.69	-3.24	0.03319412	0.9994704
A930024E05Rik	1.04	2.05	0.02302713	0.9994704
Acer2	-3.13	-8.75	0.03421405	0.9994704
Acvrl1	2.66	6.33	0.0140532	0.9994704
Adamts18	5.31	39.61	0.03435722	0.9994704
Angpt4	3.33	10.04	0.001158	0.46945505
Atp8b3	2.14	4.40	0.03358983	0.9994704
B3gnt4	1.15	2.22	0.02699494	0.9994704
B830017H08Rik	-3.19	-9.11	0.02687114	0.9994704
BC067074	-1.69	-3.22	0.01899119	0.9994704
Bdkrb1	1.14	2.20	3.741E-11	3.123E-07
Bdkrb2	2.65	6.29	0.01392222	0.9994704
Bmp5	-1.19	-2.27	0.01155405	0.9994704
Btn1a1	3.90	14.92	0.002795	0.77495316
C1ql4	-3.16	-8.94	0.02192317	0.9994704
Camk2b	-1.59	-3.01	0.02818059	0.9994704
Cd93	1.97	3.93	0.01473934	0.9994704
Cerkl	-1.14	-2.20	0.03340424	0.9994704
Ces1a	-2.15	-4.43	0.009462	0.9994704
Cfb	1.24	2.37	0.01035942	0.9994704
Clcn1	2.54	5.82	0.02854753	0.9994704
Cldn1	1.11	2.16	0.0004166	0.25574787
Clgn	-1.92	-3.78	0.0256145	0.9994704
Col23a1	1.33	2.52	0.0001409	0.14349849
Col4a4	2.01	4.03	0.007497	0.9994704
Comp	1.25	2.38	0.03048561	0.9994704
Creb3l4	-1.47	-2.78	0.01018606	0.9994704
Creld1	1.48	2.79	0.03540646	0.9994704
Csf1r	4.79	27.64	0.04863119	0.9994704
CT010467.1	-1.52	-2.86	0.01270129	0.9994704
Cyp2j12	1.72	3.30	0.04755823	0.9994704
D730003I15Rik	1.11	2.16	0.03412335	0.9994704
Ddx25	2.41	5.32	0.04412264	0.9994704
Depp1	1.04	2.06	0.001622	0.55972599
Disp2	1.51	2.85	0.02279315	0.9994704
Dlx6os1_1	-1.41	-2.65	0.002589	0.76297546
Dmp1	-1.34	-2.53	0.02253094	0.9994704
Dnah10	2.66	6.33	0.03409217	0.9994704
Dnaic2	-1.51	-2.84	0.02662484	0.9994704
E130102H24Rik	1.88	3.67	0.02817798	0.9994704
Endou	1.88	3.67	0.03037271	0.9994704
Epha8	3.21	9.22	0.01774834	0.9994704
Fn3k	1.91	3.76	0.04225383	0.9994704
Fyb2	-1.38	-2.61	0.02392971	0.9994704
Gbp11	2.76	6.79	0.04053671	0.9994704
Gbp6	3.09	8.54	0.007292	0.9994704
Gcat_2	-3.60	-12.12	0.02349862	0.9994704
Gdf6	-1.62	-3.07	0.03347714	0.9994704
Gipc2	1.19	2.28	0.01855242	0.9994704

Gli1	4.89	29.62	0	0
Gm12023	-1.51	-2.85	0.03212422	0.9994704
Gm13781	1.28	2.43	0.04276653	0.9994704
Gm13889	1.84	3.58	0.02885731	0.9994704
Gm16364_2	1.40	2.63	0.007961	0.9994704
Gm16499_1	-1.23	-2.34	0.03053922	0.9994704
Gm19385	3.54	11.67	0.006676	0.9994704
Gm20507	-5.42	-42.79	0.04803768	0.9994704
Gm26651	1.52	2.87	0.0359189	0.9994704
Gm26797	1.15	2.21	0.03345278	0.9994704
Gm26965	-5.76	-54.06	0.04584929	0.9994704
Gm28042	2.38	5.19	0.03192939	0.9994704
Gm28539	7.79	221.74	0.006286	0.9994704
Gm29054	-2.22	-4.65	0.02239864	0.9994704
Gm29100	-1.10	-2.14	0.01222852	0.9994704
Gm29417	3.07	8.41	0.02709226	0.9994704
Gm29609	-2.09	-4.24	0.03622992	0.9994704
Gm3417	2.21	4.62	0.03137652	0.9994704
Gm37584	2.24	4.71	0.01720604	0.9994704
Gm3854	2.07	4.19	0.02197559	0.9994704
Gm38910	2.04	4.10	0.04228982	0.9994704
Gm43549	-2.67	-6.39	0.04400742	0.9994704
Gm44503	5.69	51.49	0.04401855	0.9994704
Gm45193	3.66	12.67	0.03194217	0.9994704
Gm45799	-1.09	-2.13	0.0003367	0.23040881
Gm48623	1.05	2.08	0.004685	0.9994704
Gm49333	7.20	146.53	0.01660627	0.9994704
Gm49510	-6.22	-74.59	0.03602615	0.9994704
Gm49804	2.99	7.93	0.000153	0.14883942
Gm49864	-5.16	-35.80	0.04572192	0.9994704
Gm5144	-1.96	-3.88	0.03374125	0.9994704
Gm8066	-1.84	-3.57	0.004983	0.9994704
H3f3aos	1.24	2.37	0.02752897	0.9994704
Hey1	1.20	2.29	0.01032969	0.9994704
Hey2	1.18	2.27	0.01398223	0.9994704
Hk1os	-1.06	-2.09	0.000754	0.34970887
Il1rapl1	-1.92	-3.78	0.02260901	0.9994704
Il34	2.15	4.43	0.02306925	0.9994704
Lancl3	-1.84	-3.57	0.006132	0.9994704
Lmx1b	-1.84	-3.58	0.03791029	0.9994704
Lncenc1	1.52	2.87	0.03032151	0.9994704
Loxl2	1.13	2.19	0.005248	0.9994704
Lrrc36	1.88	3.67	0.02286259	0.9994704
M1ap	-2.01	-4.03	0.01720284	0.9994704
Mdfi	1.48	2.79	0.03327528	0.9994704
Mettl7a2	3.22	9.31	0.0242626	0.9994704
Mkln1os	1.28	2.43	0.03711317	0.9994704
Myrfl	-2.04	-4.11	0.03280735	0.9994704
Ndrg2	-1.31	-2.49	0.02079731	0.9994704
Nhs	1.71	3.28	0.0001831	0.16616158
Nsg2	3.39	10.51	4.626E-13	4.828E-09
Pagr1a	3.06	8.33	0.01755661	0.9994704
Pcp4l1	1.22	2.33	0.008712	0.9994704
Pde3a	1.09	2.13	0.0002641	0.21577219
Pip5k1b	-3.12	-8.72	0.03655655	0.9994704
Ppp1r14c	-1.40	-2.63	0.0135897	0.9994704
Prex1	-1.03	-2.04	0.02816512	0.9994704
Prtn3	-1.41	-2.66	0.03030376	0.9994704
Ptch1	1.53	2.89	0	0
Ptch2	3.08	8.44	0.02222706	0.9994704
Ptchd4	-1.21	-2.32	0.00566	0.9994704
Ptprz1	-1.00	-2.01	0.001011	0.43042717
Rad9b	1.12	2.17	0.00161	0.55972599
Rasl11b	1.83	3.55	7.994E-15	1.112E-10
Rassf4	1.22	2.33	0.02693697	0.9994704
Rpl9-ps6	-1.35	-2.54	0.0004395	0.2607394
Rpp25	1.43	2.69	0.009421	0.9994704
Sfrp4	-1.19	-2.28	0.02175261	0.9994704
Slc16a2	-1.11	-2.16	0.005836	0.9994704

Smoc1	1.14	2.21	0.04235675	0.9994704
Sostdc1	2.47	5.52	6.188E-06	0.0123006
Sprr3	2.92	7.58	0.03214466	0.9994704
Steap4	2.37	5.16	1.28E-07	0.000668
Strip2	1.30	2.46	0.004324	0.99813626
Syt4	-2.18	-4.54	0.02874396	0.9994704
Tafa2	-1.83	-3.55	0.03685741	0.9994704
Tmem88	-5.27	-38.47	0.04021307	0.9994704
Ttll13	-1.01	-2.01	0.0443979	0.9994704
Ugt1a5	-5.69	-51.69	0.03746893	0.9994704
Wfdc12	1.32	2.49	0.01127808	0.9994704
Wfdc18	-1.28	-2.43	0.009326	0.9994704
Zc2hc1c	1.03	2.04	9.767E-06	0.0177261
Zmynd12	-1.33	-2.51	0.01030212	0.9994704

Supplementary Table 2: Genes that were differentially expressed upon activation of Hh signaling after 48 h. RNA-Seq data. C3H10T1/2 cells were treated with 1.5 µM purmorphamine and DMSO and were compared to samples that were treated with DMSO. Log_2 fold changes of at least ± 1 with a p-value ≤ 0.05 were considered as significantly up- or down regulated.

Gene	Log_2 fold change	Fold change	p-value	FDR p-value
38231	-1.68	-3.20	0.02693002	0.62004395
1520401A03Rik	1.45	2.73	0.01159368	0.36215825
2410080I02Rik	-2.97	-7.85	0.03306649	0.70279756
2500002B13Rik	-1.13	-2.19	0.010611	0.33837644
2810404M03Rik	-1.58	-2.99	0.0250945	0.59383199
2810454H06Rik	1.08	2.11	0.04292941	0.82277433
3110082J24Rik	-2.50	-5.68	0.04350532	0.82735416
4921525O09Rik	2.13	4.39	0.03699967	0.75409308
4930547M16Rik	-1.29	-2.44	0.0484471	0.88234176
5730405O15Rik	-3.37	-10.37	0.01032639	0.33132537
9230116L04Rik	-3.12	-8.69	0.02295333	0.56031638
9230116N13Rik	-1.77	-3.40	0.02737119	0.62708872
9630013D21Rik	1.09	2.13	0.003545	0.15241146
9930111J21Rik2	1.37	2.59	1.113E-11	3.938E-09
A230065N10Rik	1.96	3.89	0.04234823	0.81688643
A830052D11Rik	1.96	3.89	0.04322444	0.82539704
Abca4	1.19	2.28	0.00001717	0.001871
Abcb9	-1.23	-2.35	0.03439257	0.72070729
Abcc3	-1.67	-3.18	0.005718	0.21865954
Abcc9	3.60	12.15	0.005399	0.20982696
Abcg4	-3.37	-10.37	0.01041805	0.3340097
Ace	2.24	4.72	0.00003562	0.003507
Acox2	-1.07	-2.09	0.002377	0.11222714
Acp6	1.23	2.34	0.03203016	0.68980888
Acpp	-1.04	-2.06	0.04835368	0.8814094
Acsbg1	1.31	2.47	0.000399	0.02647139
Adam8	1.20	2.30	0.02724173	0.62514597
Adamts15	1.70	3.24	3.658E-11	1.193E-08
Adap1	1.76	3.38	0.01095914	0.34656617
Adgrv1	-1.98	-3.94	0.02997127	0.66231106
Adipoq	-1.65	-3.14	0.01541611	0.43592709
Adrb1	-2.97	-7.85	0.02871996	0.64717673
Agtr2	-1.27	-2.42	0.03047914	0.66962678
Aldh1a3	2.83	7.12	0.03818961	0.7678945
Aldh3a1	1.00	2.01	0	0
Alpl	4.25	19.01	0	0
Als2cl	1.14	2.21	0.01542223	0.43592709
Angpt2	1.48	2.80	0.00005004	0.004652
Angpt4	3.62	12.33	4.051E-12	1.551E-09
Ano1	1.06	2.08	0.01031669	0.33132537
Apln	-1.25	-2.37	5.662E-15	3.376E-12
Apob	-2.08	-4.23	0.007935	0.27765466

Apoc1	-3.60	-12.15	0.01050171	0.33643355
Apod	1.28	2.42	1.146E-08	2.531E-06
Apol9b	1.65	3.13	1.11E-16	8.912E-14
Arhgap26_2	2.52	5.75	0.0005061	0.0319597
Artn	-1.13	-2.19	2.192E-06	0.0002896
Asic1	1.31	2.48	0	0
Atp8b4	-2.81	-7.01	0.04262972	0.81918106
Avil	1.31	2.48	0.02094745	0.52866347
B230216N24Rik	-1.84	-3.58	0.04625968	0.85937599
B3galt1	-1.02	-2.03	6.656E-06	0.0007849
B930059L03Rik	2.27	4.82	0.04327676	0.82569897
Bace2	-1.16	-2.23	2.081E-11	6.95E-09
Bambi	-1.36	-2.56	3.3E-11	1.085E-08
BC025920	-1.21	-2.32	0.001829	0.09143477
BC034090	1.33	2.51	0.002368	0.11196359
Bcl11b	1.42	2.68	0.03877922	0.77675675
Bdh1	-2.41	-5.33	0.008721	0.29595973
Bmp6	2.12	4.35	0.007418	0.26464638
Btn1a1	3.78	13.72	8.042E-10	2.18E-07
Btn2a2	2.45	5.45	0.001255	0.06639649
C1qtnf3	-1.39	-2.63	0.02921925	0.6532936
Camk2b	2.62	6.16	0.003454	0.14989316
Casq1	-1.84	-3.58	0.03346452	0.70729583
Ccbe1	1.18	2.27	8.956E-12	3.251E-09
Ccdc142	-2.23	-4.68	0.0444532	0.83812544
Ccdc3	3.42	10.68	2.226E-13	9.885E-11
Ccl6	-1.14	-2.20	0.006709	0.24589192
Ccl9	-1.52	-2.88	0	0
Cd68	1.17	2.26	0.0349547	0.72737486
Cd93	2.29	4.90	1.476E-06	0.000206
Cdh1	1.15	2.22	0.00006388	0.005722
Cdh17	1.70	3.26	5.44E-15	3.291E-12
Cdh5	3.36	10.29	2.784E-06	0.0003598
Cdhr1	-1.07	-2.11	0.008433	0.29020798
Ceacam1	2.57	5.93	0.009218	0.30634888
Cela1	-1.45	-2.72	0.0002149	0.01593046
Chrdl1	1.13	2.19	9.914E-07	0.0001447
Chst8	3.70	13.02	4.016E-08	7.783E-06
Cldn1	2.08	4.24	3.442E-15	2.177E-12
Cldn2	2.87	7.32	2.665E-15	1.765E-12
Clic6	3.20	9.17	0.02639296	0.61261493
Clvs1	-2.81	-7.01	0.04598126	0.85687316
Cmpk2	1.64	3.12	0.02870111	0.64717673
Cnmd	-2.15	-4.45	0.0006505	0.03946655
Col15a1	-1.17	-2.24	0.003462	0.15006786
Col23a1	2.86	7.24	0	0
Col28a1	-1.01	-2.02	0.03516498	0.73029442
Col4a4	3.93	15.24	0.00008983	0.0077
Col8a1	1.35	2.55	1.441E-06	0.0002019
Colec10	-1.24	-2.35	0.00009443	0.007963
Cpvl	-1.83	-3.57	0.006623	0.24356367
Crispld2	1.43	2.70	0.01294127	0.38947893
Cyfip2	1.64	3.12	0.0203599	0.51918758
Cyp2c23	-2.04	-4.12	0.02258452	0.55423015
Cys1	1.44	2.71	2.173E-06	0.0002879
Cystm1	1.07	2.10	8.829E-06	0.001013
D430019H16Rik	1.37	2.58	0.03724354	0.75547276
D630033O11Rik	-2.81	-7.01	0.04850841	0.88304743
D930007J09Rik	1.13	2.19	0.004274	0.17697325
Dchs2	-1.28	-2.43	0.00001416	0.001572
Dgki	-1.07	-2.11	0.004447	0.18199552
Dkk2	-1.11	-2.16	2.399E-06	0.0003139
Dlg2	1.42	2.68	0.001084	0.05882069
Dnah2	1.19	2.28	0.00001756	0.001904
Dpt	-1.15	-2.22	0.0002058	0.01539524
E130310I04Rik	-2.68	-6.39	0.008599	0.29343857
E2f2	1.19	2.29	0.01631732	0.45152712
Efnb3	2.19	4.55	0.009751	0.31922907
Egfr	1.09	2.13	4.154E-12	1.562E-09

Eldr	1.28	2.44	0.000928	0.05206757
Emb	-1.04	-2.06	0	0
Eml2	1.83	3.56	0.001053	0.05758974
Enpp2	-1.11	-2.16	1.51E-14	8.634E-12
Entpd2	2.41	5.31	2.238E-09	5.696E-07
Ermap	-2.48	-5.57	0.02858517	0.64638718
Esr2	1.13	2.19	0.0007166	0.04284555
Etl4	1.17	2.25	4.108E-15	2.559E-12
Faim2	1.17	2.26	0.0006778	0.0408281
Fam53b	1.01	2.02	4.763E-14	2.425E-11
Fam81a	1.23	2.34	0.02355197	0.56828311
Fat2	2.02	4.05	0.02015406	0.51553661
Fbxo48	2.11	4.33	0.003588	0.15362964
Fbxw10	1.01	2.01	0.01243901	0.38042625
Fcrlb	-4.49	-22.40	0.0009013	0.05098166
Fibcd1	-1.78	-3.43	0.002809	0.12759645
Filip1l	1.13	2.19	4.341E-14	2.237E-11
Fkbp5	1.34	2.54	0	0
Fmo1	1.49	2.81	7.361E-13	3.168E-10
Foxd1	1.41	2.65	0	0
Foxo6	1.65	3.15	0.00007563	0.00655
Frmpd4	-1.13	-2.19	0.006455	0.238899
Fry	3.75	13.45	0.0003572	0.02428482
Fxyd7	2.07	4.18	0.02866983	0.64717673
G0s2	-1.11	-2.16	0.0001591	0.01243389
Galnt12	-1.23	-2.34	0.0001888	0.01430172
Galnt2	1.14	2.21	1.598E-06	0.0002201
Gas7	1.77	3.41	2.198E-09	5.628E-07
Gdf6	-2.39	-5.23	0.0005267	0.03306302
Gfap	-1.60	-3.04	0.02159332	0.53776182
Gipc2	2.95	7.75	2.932E-06	0.0003765
Gli1	8.23	300.47	0	0
Gm10425	-1.26	-2.40	0.01675028	0.45925854
Gm13411	-1.52	-2.86	0.0294981	0.65723245
Gm14167	-2.21	-4.63	0.02725395	0.62514597
Gm15527	1.29	2.44	0.002868	0.12914149
Gm15834	-4.76	-27.04	0.04335813	0.82606036
Gm16499_1	-1.13	-2.19	0.03389696	0.71271699
Gm16677	2.96	7.76	0.02410966	0.57839618
Gm17455	1.04	2.05	0.001863	0.09258008
Gm2000	-1.28	-2.44	0.00004265	0.004084
Gm20517	-1.45	-2.73	0.04766251	0.87530229
Gm20544	-1.95	-3.85	0.03138079	0.68154436
Gm20695	1.62	3.06	0.02046082	0.5207903
Gm21986	-1.58	-2.99	0.04647486	0.86183921
Gm21992	-1.25	-2.38	0.03500609	0.72808124
Gm28052	6.97	125.09	0.01322173	0.39478889
Gm28710_1	-1.24	-2.36	0.0004083	0.02685317
Gm29674	-5.47	-44.39	0.01798411	0.48184255
Gm30122	1.49	2.81	0.03104416	0.67763487
Gm34376	-2.20	-4.61	0.03682069	0.7512249
Gm37240	3.04	8.25	0.001955	0.09634295
Gm38190	1.52	2.88	0.01532933	0.4355972
Gm38708	-1.70	-3.25	0.0292803	0.65360822
Gm38910	-2.17	-4.50	0.006213	0.23280544
Gm42901	5.26	38.31	0.04318562	0.82517541
Gm42918	1.10	2.14	0.01236127	0.37906486
Gm45890	-1.92	-3.79	0.02290487	0.5594606
Gm47223	1.40	2.64	0.04588761	0.85550975
Gm47547	-2.02	-4.06	0.03667461	0.74939593
Gm48275	6.45	87.67	0.02604142	0.60864908
Gm48882	-2.21	-4.63	0.02991194	0.66169263
Gm48972	-2.35	-5.08	0.03745581	0.75751829
Gm49361	5.42	42.69	0.0411921	0.80424786
Gm49380	2.05	4.14	0.04140926	0.8063218
Gm49417	2.95	7.73	0.009419	0.31156445
Gm4951	1.04	2.05	0.01351353	0.400427
Gm50139	-5.85	-57.52	0.02470996	0.58739628
Gm50241	-6.28	-77.78	2.571E-08	5.356E-06

Gm5662	-2.14	-4.42	0.03270469	0.69805106
Gm7324	-2.58	-6.00	0.009556	0.31458303
Gm765	1.15	2.21	3.238E-06	0.0004084
Gm7694	1.06	2.09	0.03242887	0.69428311
Gm8797	-1.58	-3.00	0.0002019	0.0151563
Gm973	1.70	3.25	0.02222625	0.5487737
Gm9908	-1.91	-3.76	0.0165048	0.45460893
Gpm6b	-1.13	-2.19	3.11E-09	7.82E-07
Gpr135	-1.06	-2.08	0.03716437	0.75491602
Gpr155	1.15	2.22	0	0
Gpr160	1.49	2.81	0.01969696	0.50879337
Gpr179	2.70	6.51	0.04152347	0.80694336
Gpr39	-1.14	-2.20	6.068E-07	0.00009631
Gpx7	-1.58	-3.00	0.006768	0.24703896
H19	1.59	3.01	6.613E-07	0.000103
Has2os	1.48	2.78	0.006233	0.23293498
Hcls1	1.06	2.08	0.01827309	0.48615269
Hdc	1.02	2.03	0.01950365	0.50705666
Hebp2	1.05	2.07	1.248E-13	5.853E-11
Hes1	1.76	3.39	0	0
Hey1	2.08	4.23	0.00001513	0.001667
Hhip	6.82	112.78	1.454E-12	6.008E-10
Hist1h4m	-3.48	-11.17	0.03091098	0.67555869
Hmcn2	-1.89	-3.71	0.01308764	0.39275163
Hmgcs2	2.25	4.75	0.001063	0.05797926
Homer2	1.32	2.49	0.007803	0.27446711
Hr	1.42	2.68	2.331E-14	1.298E-11
Hsd11b2	-1.21	-2.31	0.03034476	0.66737694
Hspa12a	1.01	2.02	0.01068286	0.34040809
Icam1	1.33	2.52	0.000208	0.01549472
Icosl	5.31	39.56	0.03194591	0.6889805
Ifitm1	1.01	2.01	0.0003995	0.02647139
Igdcc3	6.15	71.12	0.01516011	0.43344416
Igf2	1.76	3.39	3.142E-14	1.681E-11
Igfbp3	2.87	7.33	0	0
Igfbp6	1.17	2.24	0.01625155	0.45152712
Igsf23	2.29	4.90	0.009117	0.30349171
Il17re	-1.96	-3.89	0.003279	0.14347907
Il1rn	-1.76	-3.39	0	0
Il31ra	-2.71	-6.57	0.01022164	0.33050487
Inhba	1.13	2.19	3.653E-09	8.901E-07
Insyn2a	1.66	3.16	0.04074813	0.79894276
Islr2	-2.20	-4.59	0.04782943	0.87606146
Itgb2	-1.64	-3.11	0.008105	0.28287825
Itgb6	1.84	3.58	0.03660848	0.74872512
Jag1	1.19	2.28	9.23E-09	2.117E-06
Kcne2	1.23	2.34	0.0458618	0.85541062
Kcnf1	-1.75	-3.36	0.03075914	0.67354356
Kcnj8	6.05	66.16	0.01381435	0.40609321
Kif26a	2.90	7.44	1.354E-11	4.751E-09
Klf4	1.52	2.86	0	0
Kng1	-1.24	-2.36	0.005363	0.20887628
Lama5	1.55	2.92	0.0001233	0.009958
Lcp1	1.51	2.84	0.007116	0.25668311
Lgr4	1.28	2.42	0	0
Lifr	-1.11	-2.17	3.331E-16	2.528E-13
Lims2	1.15	2.22	8.252E-07	0.0001239
Lin7a	-3.49	-11.21	0.007693	0.27211111
Lpar3	-1.75	-3.36	0.003576	0.15340468
Lrr1	1.01	2.02	0.03150743	0.68358344
Lrrn3	-1.01	-2.02	0.00001289	0.001447
Lrrtm2	2.15	4.45	0	0
Ly6f	1.29	2.45	0.001894	0.09365755
Ly6g2	2.81	7.02	4.874E-07	0.00007947
Lypd1	-1.62	-3.07	4.01E-08	7.783E-06
Lypd2	6.95	123.91	0.004767	0.19152975
Magi1	1.73	3.31	0	0
Mal2	-3.12	-8.69	0.02244322	0.55173577
Mamstr	2.56	5.88	1.391E-11	4.84E-09

Megf10	-1.12	-2.18	1.231E-09	3.251E-07
Megf6	1.76	3.38	0.01615653	0.45051583
Meox1	-2.21	-4.63	0.01840786	0.48880359
Mettl7a3	2.65	6.26	0.01543493	0.43592709
Mfap3l	1.12	2.18	1.156E-12	4.825E-10
Mfsd7a	1.10	2.14	0.01825363	0.48615269
Mkln1os	1.16	2.23	0.04432395	0.8378337
Mlph	1.95	3.86	0.008897	0.2994996
Mpeg1	3.44	10.88	0.01028613	0.33132537
Mrc1	-2.81	-7.01	0.04147461	0.80674493
Mtss1	1.70	3.26	1.312E-08	0.00000286
N4bp3	1.06	2.08	0.004789	0.19202382
Nalcn	1.76	3.38	0.03293668	0.70146724
Nap1l3	-1.22	-2.33	0.03485431	0.7271229
Nat8f5	-1.32	-2.49	0.01229875	0.37860379
Ndnf	2.54	5.82	0	0
Ndst4	-1.71	-3.28	0.005533	0.2134409
Nhs	1.38	2.60	0.0002948	0.02068169
Nkain3	-1.09	-2.13	0.0000283	0.002867
Nnmt	-1.38	-2.61	0.01026843	0.33124815
Nox1	-2.13	-4.39	0.01214332	0.37548041
Npr3	-1.44	-2.72	0	0
Nr1h3	-1.24	-2.36	0.04674035	0.86484158
Nrcam	-2.20	-4.59	0.04780998	0.87606146
Nrtn	1.62	3.08	0.00677	0.24703896
Nsg2	4.09	17.01	0	0
Ntn4	1.00	2.00	3.254E-07	0.00005433
Ntn5	1.76	3.38	0.005976	0.2255438
Oas2	1.15	2.22	0.02000569	0.51345398
Olfml2a	2.68	6.43	0.0002753	0.01952835
Optc	-1.49	-2.81	0.01971927	0.50905481
Osmr	-1.01	-2.01	9.825E-14	4.769E-11
Panx3	1.64	3.11	5.007E-06	0.0006073
Pcp4l1	1.60	3.04	0.0001301	0.01040333
Pcsk6	-1.02	-2.03	4.004E-06	0.0004974
Pde1a	-1.01	-2.02	0	0
Pde3a	1.36	2.56	1.717E-08	3.676E-06
Pdzd2	2.08	4.22	0	0
Pdzk1ip1	1.06	2.08	0.04691884	0.86737511
Penk	2.54	5.83	0	0
Pgf	1.33	2.51	0.001833	0.09150784
Pi16	1.74	3.34	0	0
Pigz	4.90	29.91	0.04754035	0.87397586
Pik3r6	2.70	6.51	0.04624647	0.85937599
Pla2g4e	2.96	7.80	0.03609631	0.74281324
Plvap	1.08	2.11	0.02626023	0.61097286
Plxdc1	1.90	3.74	6.003E-08	0.00001139
Plxna4	1.01	2.01	0.004925	0.19635539
Pmaip1	2.47	5.54	0.02725644	0.62514597
Podn	1.37	2.59	4.444E-09	0.00000106
Podnl1	-1.16	-2.23	0.000129	0.01033672
Pou2af1	-1.52	-2.86	0.01945107	0.50651657
Pram1	2.84	7.14	0.04888056	0.88868518
Prickle1	1.10	2.14	6.677E-10	1.822E-07
Prrt2	-3.18	-9.05	0.03930518	0.78149309
Prx	1.38	2.60	1.042E-13	5.002E-11
Ptch1	3.10	8.60	0	0
Ptch2	7.46	176.53	0.002439	0.11426213
Ptchd1	-1.32	-2.50	1.304E-08	0.00000286
Ptchd4	-1.56	-2.96	0.0002008	0.0151276
Ptger4	4.11	17.30	2.195E-13	9.852E-11
Pthlh	1.10	2.14	0.01694772	0.46330333
Ptprv	1.04	2.06	0.0006202	0.03795947
Pygm	2.22	4.64	0.02059782	0.52332003
Rag1	1.24	2.37	0.03364325	0.71035423
Rasgef1a	2.05	4.14	0.02396646	0.57695034
Rasgrp1	-1.94	-3.85	0.04768314	0.87530229
Rasgrp3	-1.48	-2.78	0.001021	0.05606946
Rasl11b	3.27	9.64	0	0

Rassf9	-1.26	-2.40	1.279E-13	5.867E-11
Rbp1	-1.93	-3.82	0.003048	0.13520344
Rgcc	-1.05	-2.08	3.921E-07	0.00006495
Rgs4	-1.55	-2.93	0	0
Rhou	-1.59	-3.01	0	0
Rhpn2	1.15	2.23	0.00002682	0.002744
Ripor2	1.23	2.35	4.594E-08	8.796E-06
Ripply1	1.62	3.08	0.01762799	0.47657656
Rnf112	1.04	2.05	0.04096742	0.80109497
Rpl36a-ps1	2.47	5.55	0.01631971	0.45152712
Rtl3	1.67	3.19	0	0
Rtl9	1.96	3.90	0.0001596	0.01245362
Rtn4r	2.61	6.10	0.0006179	0.03795947
Rtn4rl1	2.16	4.46	3.331E-15	2.139E-12
Sap30	-1.11	-2.15	1.93E-09	4.974E-07
Sbsn	1.25	2.38	0.04261729	0.81918106
Scara5	1.29	2.45	1.473E-12	6.029E-10
Scin	3.87	14.65	0.00291	0.13032801
Scrg1	-1.52	-2.88	0.00005737	0.005184
Scube3	-1.15	-2.22	0.00004173	0.004005
Sdcbp2	3.27	9.64	0.01848939	0.48991755
Serpinb6c	2.16	4.48	0.04413265	0.83623668
Sfrp2	-1.84	-3.57	4.441E-16	3.252E-13
Sgms2	1.45	2.73	0	0
Slc10a6	-2.05	-4.13	0.0002605	0.01868068
Slc16a14	1.26	2.39	0.02174065	0.54051206
Slc1a4	-1.01	-2.01	0	0
Slc25a34	-1.10	-2.14	0.004801	0.19232564
Slc27a3	1.01	2.01	1.096E-10	3.341E-08
Slc2a6	1.63	3.11	0.00005163	0.004757
Slc6a6	1.13	2.19	1.11E-16	8.912E-14
Slc8a1	-1.29	-2.45	9.14E-12	3.289E-09
Slurp1	5.39	41.97	0.02953712	0.65723245
Smim5	1.01	2.02	0.002645	0.12157861
Sncaip	-1.43	-2.70	9.729E-08	0.00001805
Sorbs2	1.02	2.02	0.001403	0.07339682
Sostdc1	9.44	694.77	0	0
Sprr2k	2.36	5.13	0.009888	0.32187642
Sprr3	7.13	139.59	0.003928	0.16588157
Sptbn5	3.45	10.89	0.009778	0.31961392
St8sia2	1.37	2.58	2.825E-08	5.774E-06
Steap4	3.02	8.11	0	0
Stk32b	1.71	3.26	0.0003769	0.02525114
Ston2	1.25	2.38	1.565E-06	0.0002178
Strip2	1.01	2.01	0.002437	0.11426213
Stxbp6	1.26	2.39	0.0001282	0.01028929
Sult1a1	1.40	2.63	1.011E-11	3.607E-09
Sytl4	1.13	2.18	0.001879	0.09315076
Tbc1d8	1.76	3.38	0.01842561	0.48883739
Tbx2	2.50	5.66	6.587E-08	0.00001244
Tdrd9	1.90	3.72	0.00004728	0.004435
Tec	2.92	7.58	0	0
Tek	1.06	2.08	0.00002492	0.002588
Tgfa	1.84	3.58	1.752E-11	5.898E-09
Thbd	1.13	2.19	0	0
Thbs2	-1.09	-2.14	3.401E-09	8.401E-07
Tm6sf2	-2.97	-7.85	0.02886749	0.64907977
Tmem119	1.04	2.06	3.464E-14	1.83E-11
Tmem151a	1.20	2.30	3.313E-10	9.537E-08
Tmem184a	1.20	2.30	0.0144026	0.41845476
Tmem221	5.02	32.55	0.04569509	0.85328421
Tmem253	2.84	7.14	0.04016079	0.79263926
Tmem74	-1.22	-2.33	0.00001918	0.002064
Tmem95	-1.22	-2.33	0.03055614	0.67096531
Tnfrsf19	-2.01	-4.04	0.01843255	0.48883739
Tnmd	1.04	2.06	0.0002189	0.01614675
Tnnt3	1.07	2.10	0.01968735	0.50879337
Tom1l1	1.19	2.28	2.918E-12	1.16E-09
Tpd52	1.53	2.88	0	0

Tprg	1.10	2.14	0.03591421	0.74108712
Trabd2b	2.41	5.33	0	0
Trf	-1.83	-3.57	0.005792	0.22039783
Trim36	-1.84	-3.58	0.03327859	0.70597092
Trp63	1.07	2.10	6.297E-11	1.991E-08
Trpm5	2.13	4.38	0.01302154	0.39133058
Tsc22d3	1.39	2.62	0	0
Tspan11	2.06	4.18	0	0
Tspan13	1.14	2.20	0.002424	0.11393966
Tspan18	1.09	2.13	0.001583	0.08128426
Tst	1.13	2.18	6.187E-07	0.00009782
Twist2	1.09	2.12	5.551E-16	3.995E-13
Tymp	-1.01	-2.02	0.02345352	0.56689081
Ucma	-2.81	-7.01	0.04254057	0.81908252
Ucp2	2.30	4.92	1.605E-08	3.454E-06
Upk3b	1.84	3.58	0.00002088	0.00222
Vit	2.18	4.53	3.269E-09	8.124E-07
Wfdc1	4.90	29.91	0.04920584	0.89149277
Wfdc12	1.44	2.72	0.002613	0.12064793
Wfdc18	-2.69	-6.44	9.814E-08	0.00001813
Wfdc21	-2.23	-4.70	0.04223026	0.81536442
Wnt6	2.96	7.77	0.03271162	0.69805106
Wnt9a	1.12	2.18	3.549E-09	8.713E-07
Zc2hc1c	1.43	2.70	3.963E-10	1.125E-07

Supplementary Table 3: Genes that were differentially expressed upon activation of Hh signaling after 96 h. RNA-Seq data. C3H10T1/2 cells were treated with 1.5 µM purmorphamine and DMSO and were compared to samples that were treated with DMSO. Log_2 fold changes of at least ± 1.5 with a p-value ≤ 0.05 were considered as significantly up- or down regulated.

Gen	**Log_2 fold change**	**Fold change**	**p-value**	**FDR p-value**
1500009L16Rik	-2.23	-4.69	0	0
1600027J07Rik	-5.21	-36.93	0.03996683	0.41418451
1700019D03Rik	-2.84	-7.14	0.04421631	0.44315036
1700125H20Rik	-5.41	-42.46	0.03527831	0.37788623
1810012K08Rik	5.59	48.29	0.02530083	0.29889088
1810028F09Rik	2.38	5.21	0.0423752	0.43143116
2310040G24Rik	-1.95	-3.85	0.0007298	0.01733905
2310047D07Rik	-5.21	-36.97	0.0439047	0.44151069
2310069B03Rik	-3.09	-8.52	0.02224605	0.27112899
2810404M03Rik	-4.15	-17.76	0.00237	0.04603653
2900026A02Rik	1.67	3.17	8.413E-10	7.226E-08
3110083C13Rik	-2.13	-4.37	0.006077	0.10095081
4833417C18Rik	3.04	8.20	0.02649031	0.30818985
4921516A02Rik	3.04	8.20	0.02794341	0.31946615
4921536K21Rik	2.61	6.10	0.01934704	0.24614556
5033417F24Rik	2.16	4.47	0.0005649	0.01392953
6820426E19Rik	-1.88	-3.67	0.0417752	0.42728682
A230065N10Rik	-1.82	-3.52	0.02631029	0.30643708
A530020G20Rik	-3.19	-9.15	0.03132548	0.3476264
AB124611	-2.57	-5.93	0.0001048	0.003231
Abcc3	-2.43	-5.37	0.004938	0.08528599
Abcc9	3.96	15.54	3.051E-13	4.245E-11
Ackr4	-2.53	-5.77	0	0
Acox2	-1.90	-3.74	0.00006708	0.002174
Acpp	-2.44	-5.44	2.606E-06	0.0001242
Acss3	-1.63	-3.09	0	0
Adam23	-1.85	-3.60	0	0
Adamts15	2.55	5.85	0	0
Adamts18	5.65	50.20	0.0248509	0.29486961
Adamts6	1.74	3.33	6.048E-12	7.112E-10
Adamts8	5.17	35.88	0.03259685	0.35769983
Adap1	2.53	5.77	0.00002805	0.00101
Adcy10	-2.69	-6.46	0.04917148	0.48049153
Adipoq	-2.42	-5.34	0.009112	0.13973126

Agt	-2.17	-4.51	0.02404746	0.28824761
Agtr2	-2.32	-4.99	8.33E-11	8.279E-09
Ahr	1.52	2.87	0	0
AI662270	-1.61	-3.06	0.0007581	0.01788925
AI838599	1.57	2.96	0.03931031	0.40900557
AI854703	-2.81	-7.03	0.01352619	0.1885577
Akr1c14	1.54	2.90	0	0
Akr1c18	2.48	5.59	0.00001281	0.0005166
Aldh1l1	-2.22	-4.65	0.01120137	0.16343189
Aldh3a1	1.94	3.84	0	0
Aloxe3	1.50	2.83	0.008675	0.13437485
Alpl	4.77	27.29	0	0
Angpt2	2.08	4.24	0.00001153	0.0004713
Angpt4	6.01	64.52	2.345E-06	0.0001129
Angptl7	1.67	3.18	0.01153568	0.16740415
Ankrd33b	1.98	3.95	4.441E-16	8.095E-14
Anxa8	1.55	2.94	3.296E-07	0.00001869
Aoc3	-1.77	-3.42	0	0
Aox3	1.72	3.30	0.0001454	0.004302
Apln	-1.66	-3.16	0	0
Aplp1	-1.58	-3.00	8.882E-16	1.558E-13
Apoc1	-5.56	-47.03	0.03248522	0.35703806
Apol8	1.81	3.50	0.001826	0.03692964
Apol9b	2.15	4.43	0	0
Arap2	-2.17	-4.51	0.01772313	0.23104828
Arhgap15	3.17	8.99	0.02456752	0.29267184
Arhgap27	4.64	24.86	0.0003902	0.01017402
Arhgap27os2	3.09	8.51	0.001284	0.02776274
Arhgap45	1.99	3.99	0.04137734	0.42437695
Artn	-1.90	-3.73	1.763E-11	1.989E-09
Arxes1	-1.82	-3.53	0.04417578	0.44285053
Asgr1	3.29	9.76	0.01480128	0.2022422
Asic1	1.55	2.93	0	0
Asphd2	-2.17	-4.52	0.02054939	0.25674738
Atp6v0e2	1.58	2.98	8.904E-14	1.332E-11
Awat2	1.84	3.57	0.03557526	0.38018898
Bace2	-1.73	-3.31	0	0
Baiap3	3.17	8.99	0.01895919	0.24261647
Bambi	-2.57	-5.92	0	0
BC067074	1.63	3.09	0.02552048	0.30050969
Bcl11b	2.18	4.52	0.006025	0.10023771
Bcl6b	1.93	3.82	0.01032167	0.15289473
Bdh1	-2.40	-5.26	0.02552346	0.30050969
Bdkrb1	1.90	3.72	0	0
Bend5	-5.97	-62.61	0.02201537	0.26891861
Bmp3	1.87	3.66	0.03690157	0.38987147
Bmp5	-2.36	-5.13	4.339E-08	2.955E-06
Btn1a1	4.57	23.68	8.091E-08	5.275E-06
Btn2a2	3.80	13.89	0.0002453	0.006853
C530008M17Rik	1.54	2.91	0	0
Calr4	-5.41	-42.47	0.03462696	0.37330406
Camk2b	1.59	3.01	0.02245023	0.27282094
Car9	-1.88	-3.67	0.00001096	0.0004518
Card10	5.66	50.55	0.01894348	0.24261647
Card14	2.39	5.23	0.002514	0.04845123
Carmil3	1.81	3.50	0.0001602	0.004697
Cav1	-1.52	-2.87	0	0
Cbfa2t3	3.93	15.27	0.003636	0.06591325
Cbln1	-2.36	-5.14	9.575E-10	8.157E-08
Ccdc106	-1.56	-2.95	0.03217009	0.35435118
Ccdc142	2.39	5.25	0.03019279	0.33916508
Ccdc162	-1.70	-3.25	0.03655928	0.38733354
Ccdc3	4.55	23.47	0	0
Ccl8	5.05	33.05	0.03660429	0.38750726
Ccr7	2.79	6.89	0.001813	0.03672095
Cd53	2.40	5.27	1.443E-06	0.00007312
Cdh1	2.24	4.72	1.365E-12	1.721E-10
Cdh5	5.00	32.11	1.304E-06	0.00006688
Ceacam1	2.75	6.74	0.0005974	0.01458272
Cela1	-2.22	-4.65	0.00006729	0.002179
Cerkl	-2.22	-4.66	0.0006191	0.01502557

Cerox1	2.72	6.59	0.01615772	0.21555508
Ch25h	-1.65	-3.15	3.089E-06	0.0001444
Chst8	7.66	202.13	0.001259	0.02731863
Ciita	2.22	4.67	0.003991	0.07144748
Cited1	-2.18	-4.54	0.003469	0.06342223
Clca2	-3.24	-9.46	0.0002905	0.00789
Cldn1	3.67	12.76	0	0
Cldn2	4.00	15.99	0	0
Cmbl	-1.80	-3.47	0.002647	0.05036404
Cmpk2	1.78	3.43	0.009945	0.14926952
Cngb1	2.82	7.04	0.01015115	0.15138953
Cnmd	-3.12	-8.68	0.001059	0.02364833
Cntnap5b	-2.30	-4.93	1.539E-06	0.00007684
Cobl	2.38	5.22	4.321E-06	0.000195
Coch	2.79	6.89	0.003813	0.06860433
Col15a1	-2.26	-4.79	1.689E-08	1.222E-06
Col23a1	3.77	13.66	0	0
Col26a1	-3.33	-10.09	0.002147	0.04229108
Col4a3	6.03	65.12	0.01262436	0.17912253
Col4a4	4.04	16.46	8.882E-16	1.558E-13
Col9a1	-2.56	-5.90	0.01001654	0.15002525
Colec10	-2.07	-4.20	1.06E-12	1.37E-10
Cpvl	-2.30	-4.92	0.0001936	0.005544
Cpz	2.52	5.74	3.956E-07	0.00002223
Cracr2a	1.57	2.98	0.0000996	0.003089
Cracr2b	1.55	2.92	0.001528	0.03207607
Crispld2	1.98	3.94	0.001107	0.02450194
Crxos	5.73	53.05	0.01906324	0.24364879
Ctsh	1.86	3.62	0	0
Ctxn3	-1.66	-3.16	0.03600365	0.38329514
Cxadr	-1.54	-2.90	0	0
Cxcl9	-2.39	-5.24	0.03736325	0.39305797
Cyp2b10	3.29	9.79	0.001949	0.03894811
Cyp2j12	-3.39	-10.50	0.01693747	0.22331672
Cyp2s1	3.41	10.65	0.01634963	0.21755904
Cyp3a13	2.72	6.58	0.009777	0.14755659
Cytl1	1.88	3.68	0.00007266	0.002335
D430019H16Rik	1.65	3.13	0.0001357	0.004038
Dchs2	-2.24	-4.73	2.22E-16	4.175E-14
Dcn	1.85	3.61	0	0
Dgki	-1.79	-3.45	0.0002568	0.007123
Dkk2	-2.47	-5.52	0	0
Duoxa1	-1.64	-3.12	0.001874	0.03775596
Dusp27	-2.84	-7.15	0.0379719	0.39735796
E230016K23Rik	-1.67	-3.19	0.01458616	0.19976057
Ear2	-3.00	-8.01	0.008144	0.12765405
Ecrg4	-1.68	-3.21	5.755E-11	5.888E-09
Ecscr	1.77	3.41	0.0143721	0.19806357
Eda2r	1.85	3.61	0	0
Edar	-3.30	-9.88	0.01591015	0.2130694
Egfl6	-3.06	-8.36	0.001214	0.02638586
Egfr	1.77	3.42	0	0
Eln	-2.00	-4.01	4.485E-07	0.00002493
Entpd2	3.75	13.49	0	0
Ephx2	-1.70	-3.25	0.0006081	0.01477642
Erg	-5.74	-53.48	0.02405183	0.28824761
Esm1	1.73	3.31	0	0
Esrrg	-2.03	-4.08	0.01546376	0.20903618
Etl4	1.66	3.17	0	0
Faim2	1.88	3.68	1.205E-06	0.00006212
Fam131c	-1.58	-2.99	0.04395525	0.44180687
Fat2	4.76	27.19	0.0004938	0.01245477
Fcrlb	-3.29	-9.76	0.003354	0.06171063
Fer1l6	-4.40	-21.09	0.0012	0.0261326
Fgd2	1.56	2.95	0.000239	0.006714
Fgd5	-2.11	-4.31	0.02204203	0.2691139
Fgf1	2.47	5.56	0.006409	0.10548813
Fibcd1	-4.49	-22.43	1.491E-06	0.00007491
Fkbp5	2.20	4.59	0	0
Fmnl1	3.29	9.80	0.01724881	0.22655876
Fmo1	1.99	3.97	0	0

Fndc1	-1.58	-2.99	0.00004598	0.001563
Foxd1	1.72	3.29	0	0
Foxo6	2.71	6.56	2.717E-11	2.923E-09
Frmd3	2.11	4.31	0.03686615	0.38959587
Frmd5	2.25	4.76	0	0
Fry	3.50	11.30	0.00002414	0.0008917
Fstl4	-2.16	-4.47	0.02544803	0.29999359
G0s2	-1.60	-3.03	6.003E-08	0.00000399
Gabra3	2.67	6.35	2.941E-11	3.131E-09
Galnt15	1.87	3.65	0.00000108	0.00005638
Galr2	5.28	38.88	0.03067367	0.34235584
Gas7	2.26	4.80	3.209E-14	5.016E-12
Gbp4	1.56	2.94	0.0116838	0.16891733
Gbp5	1.60	3.04	0.01508038	0.2053835
Gcat_2	6.53	92.62	0.02134463	0.26352821
Gdf6	-4.42	-21.40	2.487E-14	3.947E-12
Gfpt2	2.77	6.83	0	0
Gipc2	3.67	12.71	0.00002479	0.0009135
Gja6	-2.64	-6.25	0.0223139	0.27159724
Gli1	9.20	588.29	0	0
Glul	1.59	3.01	0	0
Gm10369	1.54	2.91	0.03190891	0.35209457
Gm11944	2.72	6.61	0.04911962	0.48041247
Gm12022	2.38	5.20	0.04869865	0.47741373
Gm12108	-1.79	-3.47	0.03288897	0.35986483
Gm12185	1.59	3.00	0.001172	0.02561734
Gm12764	3.40	10.58	0.01287074	0.18150781
Gm13272	-2.06	-4.17	0.035739	0.38121107
Gm13293	-3.59	-12.04	0.00007861	0.002505
Gm13411	-3.31	-9.90	0.01491084	0.20340623
Gm14002	-2.18	-4.54	0.0001686	0.004922
Gm14139	-1.78	-3.42	0.01589623	0.21295138
Gm14440	8.08	270.04	0.004481	0.07871576
Gm15408	-1.67	-3.19	0.002521	0.04852269
Gm15608	-1.74	-3.34	0.03536924	0.37856875
Gm16211	-1.59	-3.01	0.02177277	0.26727511
Gm16263	-2.26	-4.78	0.01414648	0.19579462
Gm16268	-2.39	-5.26	0.02717971	0.31393544
Gm17382	-1.70	-3.24	0.02532989	0.29902304
Gm17552	-2.04	-4.10	0.01786408	0.23187193
Gm19385	3.17	8.99	0.01666401	0.22082721
Gm21411	1.85	3.61	0.02499811	0.29636357
Gm21663	2.70	6.49	0.02586719	0.30300512
Gm2629	5.05	33.01	0.04014143	0.41578749
Gm26682	-5.21	-36.92	0.04222631	0.43044027
Gm26744	-2.96	-7.80	0.03512023	0.37648276
Gm26771	-2.84	-7.18	2.604E-06	0.0001242
Gm26902	-2.22	-4.67	0.009831	0.14819818
Gm2694	-1.86	-3.62	0.002821	0.05304593
Gm29157	-2.03	-4.08	0.001079	0.02398314
Gm29674	-3.28	-9.74	0.000269	0.007388
Gm30122	2.67	6.36	0.0003804	0.00998
Gm31045	-2.55	-5.86	0.03054273	0.34144225
Gm31378	-1.54	-2.90	0.003167	0.05860178
Gm31793	-2.18	-4.53	0.01021651	0.15182197
Gm32098	5.58	47.80	0.02247435	0.27303459
Gm32461	-2.31	-4.97	0.01512706	0.20588486
Gm34006	-2.39	-5.23	0.03680995	0.38915932
Gm36107	-2.26	-4.79	0.006851	0.11131678
Gm36377	-1.86	-3.63	0.0128886	0.18163705
Gm36995	2.93	7.62	0.01496824	0.20405592
Gm39302	-2.43	-5.37	0.00273	0.05168601
Gm42109	-1.65	-3.14	0.0249458	0.29591149
Gm42743	-1.55	-2.94	0.02153986	0.2651036
Gm42788	-2.28	-4.85	0.01757188	0.2292913
Gm43549	-4.05	-16.52	0.01448138	0.19871676
Gm44081	-1.88	-3.68	0.01477704	0.20197711
Gm44503	6.03	65.52	0.03337529	0.36306436
Gm45022	2.89	7.41	0.03320052	0.36207328
Gm45234	2.23	4.68	0.009516	0.14429752
Gm45650	2.57	5.92	0.005719	0.09618174

Gm4767	-1.89	-3.70	0.01203919	0.17252043
Gm47920	1.52	2.86	0.02544676	0.29999359
Gm47939	6.37	82.95	0.01187942	0.17075848
Gm48073	5.17	35.96	0.03388546	0.36739757
Gm48791	-3.30	-9.87	0.0164926	0.21876414
Gm49333	-7.50	-180.46	0.01646769	0.21864211
Gm49387	6.99	126.91	0.01194572	0.17153429
Gm49392	-2.57	-5.92	0.01019662	0.15178195
Gm49510	7.19	145.90	0.01165921	0.16869687
Gm49767	2.30	4.91	0.02598351	0.30398811
Gm50203	-2.28	-4.87	0.03934866	0.40930254
Gm50315	2.19	4.57	0.00953	0.1444125
Gm5144	-3.42	-10.73	0.01439633	0.19808903
Gm5431	1.65	3.13	0.02299897	0.27811292
Gm5662	-2.50	-5.68	0.009191	0.14068762
Gm765	1.57	2.96	1.054E-09	8.927E-08
Gng13	3.29	9.80	0.0003549	0.009382
Gpc3	1.72	3.30	0.02066429	0.25772025
Gpm6b	-1.60	-3.04	0	0
Gpr135	-1.52	-2.87	0.009603	0.1452423
Gpr155	1.62	3.07	0	0
Gpr39	-2.23	-4.69	0	0
Grem2	-1.90	-3.73	0.0008172	0.01904581
Grp	2.16	4.47	0.001596	0.03324912
H19	1.54	2.91	1.188E-06	0.00006132
Hapln1	-2.34	-5.06	0.0197404	0.24932637
Has1	2.28	4.87	0.0001384	0.004115
Has2os	1.90	3.73	0.0002647	0.007311
Hbb-bs	2.04	4.12	0.01051337	0.15523863
Hbb-y	4.85	28.82	0.0002406	0.006755
Hecw1	-1.71	-3.28	0.002574	0.04923805
Hes1	2.33	5.04	0	0
Hey1	2.06	4.18	0.00000527	0.0002328
Heyl	-2.97	-7.84	0.03376654	0.36639369
Hhip	8.56	377.95	0	0
Hif3a	2.61	6.12	0.02392166	0.28727329
Hlf	2.79	6.89	0.001749	0.03571895
Hmgcll1	-2.25	-4.77	0.0002448	0.00685
Hmgcs2	3.05	8.31	5.867E-08	3.913E-06
Homer2	1.71	3.28	0.00002799	0.001009
Hr	2.17	4.50	0	0
Hsh2d	-2.28	-4.87	0.0304634	0.34110341
Hspb1	-1.81	-3.51	0.0004049	0.01047722
Icosl	4.91	30.13	0.04178389	0.42728682
Id4	-2.00	-3.99	0.00003126	0.001118
Ifitm5	3.17	8.99	0.02790481	0.31921913
Igdcc3	2.72	6.59	0.01062832	0.15654826
Igf2	2.68	6.40	0	0
Igfbp3	4.16	17.82	0	0
Igfbp6	3.54	11.62	8.354E-10	7.19E-08
Il16	-1.63	-3.10	0.00009989	0.003093
Il17re	-3.11	-8.64	1.409E-08	1.034E-06
Il1rn	-3.60	-12.10	0	0
Isg20	1.61	3.05	1.206E-09	1.017E-07
Islr2	2.21	4.63	0.0206714	0.2577319
Itga10	1.72	3.30	0.0101719	0.15159079
Itga2	2.06	4.16	0.00995	0.14926952
Itga8	-1.90	-3.73	5.049E-13	6.821E-11
Itgb7	2.09	4.25	0.0006929	0.01660479
Kcnab1	1.55	2.92	3.48E-11	3.678E-09
Kcnf1	1.64	3.11	0.04375559	0.44086163
Kcnj16	2.90	7.44	0.04307742	0.43676967
Kcnj8	7.66	202.18	7.772E-16	1.38E-13
Kcns1	3.78	13.75	0.005647	0.09528698
Kif26a	4.11	17.23	0	0
Kirrel3	-1.72	-3.30	0.0003884	0.01014493
Klf4	1.72	3.28	0	0
Krt13	-1.53	-2.89	0.0001609	0.004711
Krt15	-1.51	-2.86	0.000105	0.003235
Lama2	1.53	2.88	5.019E-09	3.916E-07
Lama5	2.98	7.92	1.455E-06	0.00007342

Lctl	-2.52	-5.73	0.0006079	0.01477642
Lepr	2.39	5.24	8.268E-11	8.237E-09
Lgi2	4.38	20.80	0.000738	0.01749397
Lgr4	1.93	3.81	0	0
Lhfpl2	-1.77	-3.42	0	0
Lifr	-1.64	-3.12	0	0
Lims2	2.56	5.88	0	0
Lin7a	-4.57	-23.67	0.0004672	0.01186876
Liph	2.05	4.13	0.04292877	0.43589773
Lmod1	-1.63	-3.09	2.478E-11	2.687E-09
Lpar3	-2.39	-5.23	0.001617	0.03361638
Lrrc72	4.91	30.13	0.04335339	0.43868469
Lrrn3	-1.67	-3.18	2.64E-12	3.201E-10
Lrrtm2	1.98	3.95	1.332E-15	2.317E-13
Ly6g2	1.62	3.07	0.00003952	0.001373
Lypd1	-4.06	-16.68	0	0
Lypd2	4.59	24.11	0	0
Magi1	2.37	5.19	0	0
Mamstr	3.11	8.64	1.832E-14	2.919E-12
Map7d2	-2.55	-5.84	0.0005767	0.0141851
Mapt	1.84	3.57	0.04170524	0.42693681
Matn3	-2.27	-4.84	3.173E-06	0.0001473
Mdfi	-2.13	-4.37	0.00448	0.07871576
Mdga1	-1.76	-3.38	0.0004007	0.01038966
Megf10	-2.45	-5.48	0	0
Megf11	2.11	4.32	0.01998671	0.25129674
Mfap4	-1.52	-2.86	6.307E-08	4.174E-06
Mfsd13b	-2.04	-4.11	0.02123442	0.26302323
Mfsd4a	-5.59	-48.10	0.03090231	0.34435539
Mgam	2.48	5.57	1.524E-07	9.316E-06
Mgst2	-1.50	-2.84	0.03176348	0.35095365
Mlip	-2.99	-7.96	1.204E-07	7.544E-06
Mlph	1.54	2.91	0.003625	0.06573831
Mmrn2	-2.26	-4.80	0.01685101	0.22258283
Mrc1	-2.34	-5.06	0.01439767	0.19808903
Mrgprh	5.65	50.28	0.02172153	0.26683985
Mtss1	1.75	3.37	5.786E-09	4.431E-07
Mustn1	1.73	3.31	0	0
Mylk2	-1.63	-3.10	0.02597655	0.30398811
Mylk3	-3.03	-8.20	6.855E-12	8.016E-10
Myom1	-2.14	-4.40	0.00416	0.07392292
Myzap	1.95	3.87	1.945E-11	2.177E-09
N4bp3	2.33	5.04	8.545E-07	0.00004498
Nat8f5	-1.56	-2.94	0.004819	0.08357625
Ndnf	3.13	8.77	0	0
Ndrg2	3.25	9.51	3.789E-07	0.00002135
Neb	-1.50	-2.84	0.02201447	0.26891861
Nell2	2.36	5.14	0.00233	0.04531933
Ngef	1.93	3.81	0.02726012	0.31474956
Nhs	2.83	7.09	2.368E-12	2.899E-10
Nkd1	-2.14	-4.42	0	0
Nkd2	5.48	44.67	0.02340827	0.28183767
Nmb	-2.01	-4.03	0.0002228	0.006293
Nnmt	-1.52	-2.86	0.00001052	0.0004346
Nox1	-2.01	-4.04	0.009569	0.14478057
Npcd	5.66	50.54	0.03433892	0.37115731
Npr1	1.81	3.49	0.00001866	0.0007138
Npr3	-2.44	-5.42	0	0
Nr1h3	-1.83	-3.55	0.02604308	0.30447625
Nsg2	3.67	12.77	0	0
Ntn4	1.71	3.27	0	0
Ntn5	2.28	4.87	0.00003467	0.001221
Nyx	-1.61	-3.04	0.04299263	0.43631228
Olfml2a	2.16	4.47	0.00192	0.03849352
Otor	-1.67	-3.17	0.00001284	0.0005168
P2rx1	3.17	8.99	0.01870551	0.24003206
P2rx5	-2.97	-7.83	0.03648317	0.38692001
Pabpc4l	-2.54	-5.82	0.04482605	0.44698333
Palld	-1.66	-3.16	0	0
Panx3	2.55	5.85	7.511E-12	8.758E-10
Pate2	-1.88	-3.67	0.01417282	0.19609416

Pcdhga7	1.73	3.32	0.04055651	0.41883976
Pcdhgc4	-2.08	-4.23	0.02548299	0.30032087
Pde3a	2.05	4.16	0	0
Pde9a	-2.69	-6.44	5.051E-10	4.534E-08
Pdzd2	1.84	3.57	0	0
Pdzk1ip1	1.80	3.48	0.0007846	0.01840065
Penk	2.33	5.02	0	0
Pgf	1.57	2.96	0.0004348	0.01114059
Pheta2	-2.39	-5.26	0.03867701	0.40322035
Phex	-1.74	-3.35	0	0
Pi16	2.53	5.79	0	0
Pigz	3.03	8.18	0.0003408	0.009056
Piwil2	-2.97	-7.83	0.02776792	0.3186544
Plac8	1.79	3.46	0.001911	0.0384136
Platr3	-2.69	-6.43	0.01923214	0.24506937
Plcxd1	-2.34	-5.06	0.01882639	0.24143474
Plxdc1	3.13	8.75	1.665E-15	2.861E-13
Plxnc1	1.57	2.97	1.102E-06	0.00005727
Ppp2r2b	2.63	6.20	0.02385617	0.28665176
Prlr	-5.62	-49.30	0.03166571	0.35005874
Proser2	1.76	3.38	0.002801	0.05278839
Prr7	-2.13	-4.36	0.003786	0.06824248
Prx	2.09	4.25	0	0
Psd4	-1.82	-3.54	5.093E-09	3.959E-07
Ptch1	4.15	17.74	0	0
Ptch2	5.43	43.09	1.761E-12	2.188E-10
Ptchd1	-1.58	-2.98	2.127E-11	2.361E-09
Ptchd4	-2.23	-4.70	9.084E-07	0.00004764
Ptger4	5.82	56.52	0	0
Ptp4a1_1	1.85	3.61	0.01133983	0.16516353
Ptprv	1.54	2.91	0.0006012	0.01466686
Ptprz1	-1.90	-3.72	1.521E-14	2.451E-12
Ptx3	-1.75	-3.36	0	0
Rab17	2.11	4.31	0.02473372	0.29398056
Rap1gap	-1.74	-3.33	0.02205437	0.26918587
Rapgef3	1.70	3.25	8.438E-15	1.415E-12
Rasl11b	3.85	14.41	0	0
Rassf9	-2.31	-4.95	0	0
Rflna	2.90	7.46	0.04206829	0.42921456
Rfpl4b	-2.11	-4.31	0.01624261	0.2163418
Rgcc	-2.03	-4.09	3.713E-13	5.115E-11
Rgs17	-1.63	-3.09	0.0001061	0.003262
Rgs4	-1.59	-3.01	0	0
Rgs7	-2.03	-4.08	0.01617951	0.21577682
Rgsl1	5.17	35.97	0.03280454	0.35941209
Rhou	-2.04	-4.12	0	0
Rhpn2	1.69	3.23	1.811E-11	2.038E-09
Ripor2	2.26	4.81	0	0
Rnf128	-2.12	-4.35	0	0
Rtn4r	2.18	4.53	0.002443	0.04730625
Rtn4rl1	3.03	8.16	0	0
Rubcnl	2.34	5.07	0.00007899	0.002513
Sap25	6.16	71.63	0.02044837	0.2556383
Sap30	-1.89	-3.70	0	0
Scin	1.71	3.27	7.281E-06	0.0003132
Scrg1	-3.38	-10.38	9.728E-13	1.265E-10
Scube3	-2.14	-4.40	1.166E-12	1.488E-10
Selp	-1.90	-3.73	6.277E-10	5.493E-08
Sema3e	1.53	2.89	0.001061	0.02368079
Sema3g	1.75	3.36	0.007043	0.11373127
Sfrp1	-1.57	-2.98	0	0
Sfrp2	-3.53	-11.53	0	0
Sgms2	1.93	3.80	0	0
Slc17a8	2.25	4.75	0.04643743	0.45999943
Slc22a23	1.64	3.11	2.274E-11	2.492E-09
Slc25a34	-1.58	-3.00	0.00002296	0.0008556
Slc26a7	-2.11	-4.32	1.09E-13	1.62E-11
Slc27a3	1.81	3.52	0	0
Slc43a1	1.51	2.86	0.006737	0.10994573
Slc52a3	2.40	5.28	0.006846	0.11131678
Slc5a7	-1.80	-3.49	0.02144576	0.26446392

Slc6a4	3.60	12.17	0.007104	0.11441115
Slc6a6	1.89	3.71	0	0
Slc8a1	-1.96	-3.89	0	0
Slco2b1	2.99	7.96	0.003518	0.06415533
Slurp1	5.17	35.97	0.00005521	0.001841
Smoc1	2.09	4.27	0.00002307	0.0008582
Snapc1l	-3.89	-14.84	0.01577085	0.21174738
Sncaip	-2.75	-6.75	0	0
Sostdc1	7.87	233.58	0	0
Sox8	1.97	3.92	0.004643	0.08113005
Sp110	1.73	3.31	0.02481073	0.29464419
Sp7	1.99	3.98	0.0443163	0.44381772
Sparcl1	-1.86	-3.63	2.655E-08	0.00000185
Sprr1a	1.56	2.95	0.000506	0.01270149
Sprr2j-ps	2.38	5.20	0.02111263	0.26205897
Sprr2k	2.12	4.34	0.01573447	0.21132683
Sprr3	4.32	20.03	9.146E-13	1.197E-10
Sptbn5	1.84	3.57	0.03284488	0.35964297
St8sia2	3.57	11.85	0	0
Stc1	-1.91	-3.76	4.441E-16	8.095E-14
Steap4	3.56	11.80	0	0
Stk32b	3.86	14.50	6.631E-12	7.775E-10
Stx1b	2.07	4.19	0.03678473	0.38903095
Stxbp6	2.25	4.76	1.132E-14	1.854E-12
Styk1	1.57	2.97	0.00002304	0.0008579
Svopl	-2.69	-6.45	0.04549032	0.45211966
Syt8	2.25	4.74	0.04003046	0.41474104
Sytl2	-1.56	-2.95	0	0
Taco1os	-1.51	-2.84	0.03520684	0.3772174
Tagln	-1.52	-2.87	2.89E-11	3.085E-09
Tbx2	2.11	4.31	8.034E-07	0.00004245
Tceal3	-2.18	-4.53	0.0104481	0.15438409
Tdrd9	1.77	3.41	1.867E-08	1.341E-06
Tec	3.46	10.98	0	0
Tent5c	3.29	9.76	3.119E-13	4.325E-11
Tfcp2l1	2.10	4.29	0.03884574	0.40482866
Tgfbi	-2.13	-4.39	0	0
Tgtp1	1.98	3.94	0.00162	0.03366733
Tgtp2	1.78	3.43	3.537E-13	4.889E-11
Thbs2	-1.69	-3.22	0	0
Thsd4	5.07	33.58	0.0001184	0.003581
Tlr2	-1.62	-3.07	0	0
Tmem119	1.57	2.97	0	0
Tmem221	5.60	48.44	0.00002714	0.0009834
Tmem74	-1.70	-3.24	7.128E-07	0.000038
Tnfaip6	-1.66	-3.15	0	0
Tnip3	6.84	114.71	0.00417	0.07400337
Tnni1	-1.53	-2.89	7.213E-06	0.0003107
Tns1	1.80	3.48	0	0
Tpd52	2.22	4.65	0	0
Trabd2b	3.47	11.10	0	0
Tro	-1.52	-2.87	0.0000661	0.002154
Trpv1	2.11	4.32	0.01601644	0.21414929
Tsc22d3	2.42	5.37	0	0
Tspan11	2.58	5.98	0	0
Tspan18	1.77	3.42	1.378E-07	8.534E-06
Tspan7	1.67	3.19	0	0
Tst	1.56	2.95	9.282E-10	7.923E-08
Twist2	1.67	3.19	0	0
Txlnb	3.15	8.88	0.002619	0.04994108
Uckl1os	3.15	8.88	0.031114	0.3458833
Ucp2	3.11	8.62	1.376E-13	2.001E-11
Unc93a	4.91	30.13	0.04561153	0.4531085
Upk3b	2.67	6.36	0	0
Vill	1.64	3.12	0	0
Vit	2.54	5.81	0	0
Wdr38	2.21	4.63	0.02426879	0.28994048
Wfdc1	5.96	62.22	0.01316019	0.18490271
Wfdc18	-2.94	-7.67	0.00001176	0.0004783
Wfdc3	2.33	5.03	0	0
Wnt10b	1.73	3.32	0.04761339	0.46847034

Wnt11	-2.04	-4.11	0.00003773	0.001321
Wnt2	-1.62	-3.07	0.00001356	0.0005417
Xkrx	-1.71	-3.26	0.04583683	0.45502187
Zbp1	2.19	4.55	9.012E-10	7.709E-08
Zbtb16	2.51	5.70	0.0002516	0.007007
Zc2hc1c	1.87	3.66	0	0
Zfp935	-6.76	-108.69	0.0210201	0.26123193
Zfp969	-6.10	-68.37	0.03800679	0.3975238

Supplementary Table 4: Genes that were differentially expressed upon activation of Hh signaling after 7 days. RNA-Seq data. C3H10T1/2 cells were treated with 1.5 µM purmorphamine and DMSO and were compared to samples that were treated with DMSO. Log_2 fold changes of at least ± 2 with a p-value ≤ 0.05 were considered as significantly up- or down regulated.

Gene	Log_2 fold change	Fold change	p-value	FDR p-value
38231	-2.19	-4.55	0.002723	0.04621325
1500009L16Rik	-2.09	-4.27	0	0
1700028I16Rik	-2.10	-4.29	0.01345535	0.16259349
1700028M03Rik	-4.33	-20.11	0.001293	0.02475623
1700084E18Rik	-2.16	-4.45	0.04427319	0.40281072
2310047D07Rik	-2.90	-7.45	0.00962	0.12580994
2610528A11Rik	-3.67	-12.70	0.00001312	0.0004491
4732419C18Rik	-4.78	-27.41	0.04724008	0.42164
4921525O09Rik	2.46	5.49	0.0337439	0.33049548
4930474H06Rik	-2.07	-4.21	0.04113442	0.3819062
4930486L24Rik	5.78	55.01	0.0464665	0.41712924
4930488L21Rik	-2.47	-5.56	0.008554	0.11473502
4930558J18Rik	-2.15	-4.44	0.0003295	0.007647
4933417E11Rik	-2.52	-5.72	0.02826672	0.28884646
4933425D22Rik	2.87	7.33	0.03073746	0.30702889
5031415H12Rik	-4.91	-30.04	0.04533695	0.40972076
A430010J10Rik	3.37	10.37	0.02171281	0.23549517
A830012C17Rik	2.39	5.26	0.02263647	0.24369935
A830052D11Rik	-4.78	-27.42	0.04635105	0.41654074
Abcc9	3.28	9.72	0	0
Ackr4	-2.91	-7.51	0	0
Acox2	-2.19	-4.57	2.049E-08	1.203E-06
Acp5	2.87	7.33	0.03791903	0.35965785
Acp6	2.11	4.30	0.000371	0.008504
Acsbg2	-3.41	-10.63	0.01955553	0.21756573
Actrt3	3.24	9.45	0.01479116	0.17485906
Adam23	-2.20	-4.60	0	0
Adamts15	2.17	4.49	0	0
Adcy10	-5.25	-37.97	0.02655853	0.27564218
Adipoq	-2.62	-6.16	0.001467	0.02756385
Adtrp	-2.29	-4.88	0.04827311	0.42837253
Ahsg	2.69	6.46	0.002406	0.04179322
AI838599	2.26	4.80	0.001754	0.03208355
Aim2	2.31	4.96	0.003772	0.05991156
Akr1c18	3.32	9.97	0	0
Akr1c19	2.50	5.65	0.003815	0.0604754
Akr1cl	-2.52	-5.74	0.02018831	0.22282409
Alpl	6.57	94.84	0	0
Angpt4	2.70	6.51	0.00000743	0.0002692
Ankrd33b	2.05	4.13	4.441E-16	6.943E-14
Aox3	2.51	5.70	1.23E-08	7.541E-07
Apoc1	-2.94	-7.70	0.0005176	0.01121799
Apol9b	2.18	4.53	0	0
Arhgap27	3.13	8.76	0.0005005	0.01090502
Arhgap27os2	3.13	8.74	0.02311428	0.24755678
Arhgap9	5.29	39.21	0.02801385	0.28680196
Asb15	2.22	4.67	0.04176465	0.38581742
Asphd2	-4.17	-18.01	0.001452	0.02735389
Astn1	2.01	4.04	0.00624	0.08919948
Atp8a1	2.33	5.04	0.04068912	0.37870367

B830017H08Rik	-3.48	-11.13	0.01375902	0.16518348
Bace2	-2.33	-5.03	0	0
Bambi	-2.60	-6.08	0	0
Bbox1	5.70	51.94	0.01724034	0.19724939
Bcl11b	4.98	31.61	0.03768674	0.35794969
Bend5	-2.76	-6.79	0.005278	0.07832641
Bglap	2.45	5.48	0.0385196	0.36402181
Bmp3	2.73	6.63	0.03812604	0.36112896
Btn1a1	2.42	5.35	8.323E-06	0.0002985
C1qtnf12	-2.82	-7.07	0.001135	0.02223827
C4bp	-3.84	-14.33	0.00002316	0.000743
Calr4	-2.03	-4.07	0.006819	0.09612495
Car9	-3.18	-9.09	4.382E-09	2.917E-07
Card10	3.37	10.34	0.00002769	0.0008735
Card14	2.45	5.47	0.02871277	0.29176168
Cbfa2t3	4.29	19.58	0.001339	0.0254827
Ccdc3	5.02	32.36	0	0
Ccdc33	3.13	8.74	0.01572087	0.18412914
Ccl17	-2.09	-4.26	0.007132	0.09980582
Ccl5	-3.24	-9.45	0.0008935	0.01807963
Ccl8	2.36	5.12	2.889E-07	0.00001401
Cd53	2.09	4.25	1.454E-07	7.374E-06
Cdh5	6.36	82.25	0.007488	0.103563
Cdhr1	-3.39	-10.47	2.767E-07	0.00001348
Ces1f	3.23	9.39	0.0001276	0.003389
Cfap161	-2.80	-6.95	0.02546392	0.26713755
Cgref1	-2.42	-5.35	6.265E-07	0.00002855
Chst8	7.45	174.28	0.001507	0.02820246
Clca2	-3.13	-8.76	2.876E-08	1.644E-06
Clca4a	-3.07	-8.41	0.03314032	0.32573025
Cldn1	3.38	10.41	0	0
Cldn2	3.09	8.54	0	0
Clic6	6.18	72.61	0.01093905	0.13861369
Clvs1	-2.31	-4.95	0.02097972	0.22967648
Cngb1	3.01	8.04	0.02801855	0.28680196
Cnmd	-5.34	-40.41	0.00005739	0.001689
Cntnap5b	-2.34	-5.05	5.78E-08	3.113E-06
Coch	4.90	29.93	0.0002224	0.005512
Col14a1	2.72	6.59	1.539E-11	1.457E-09
Col15a1	-3.06	-8.33	1.499E-14	1.98E-12
Col23a1	3.68	12.78	0	0
Col27a1	-2.60	-6.04	1.437E-06	0.00006165
Col4a3	3.86	14.57	2.685E-06	0.0001093
Col4a4	3.06	8.32	1.11E-16	1.81E-14
Col9a1	-3.48	-11.19	0.0003276	0.007618
Col9a2	-2.02	-4.05	0.040579	0.37835583
Colec10	-2.86	-7.26	0	0
Cp	2.73	6.62	0	0
Cpvl	-2.14	-4.40	0.00001902	0.000624
Cpz	4.30	19.72	8.569E-10	6.221E-08
Crxos	5.38	41.76	0.02596992	0.27081248
Csdc2	-2.10	-4.29	3.703E-07	0.00001759
Ctsh	2.21	4.61	0	0
Cyfip2	2.42	5.34	4.591E-09	3.047E-07
Cyp27b1	-2.79	-6.92	0.04132697	0.38284769
Cyp2b10	3.54	11.65	0.00009179	0.002556
Cyp4a12b	6.64	99.64	0.006364	0.09060322
Cytl1	2.58	6.00	1.057E-11	1.023E-09
Dchs2	-2.22	-4.66	0	0
Dcn	2.22	4.67	0	0
Dennd2d	3.08	8.48	0.0005416	0.01169039
Dgki	-2.53	-5.77	4.369E-06	0.0001682
Dio3os	-4.91	-30.05	0.04108826	0.38165273
Dkk2	-2.13	-4.36	1.11E-16	1.81E-14
Dnaic2	-3.20	-9.19	0.0002711	0.006478
Dnajc6	5.09	34.10	0.0372342	0.35501761
Doc2b	5.55	46.85	0.01957592	0.21767655
Dusp27	-4.44	-21.67	0.0006163	0.01314542
Dusp4	-2.06	-4.17	2.757E-06	0.0001116

E130310I04Rik	-2.94	-7.65	0.0385971	0.36418593
Ear2	-2.09	-4.26	0.01744842	0.19883959
Efcab1	-2.79	-6.92	0.04172074	0.38563965
Egfl6	-2.43	-5.38	0.001588	0.02947777
Eln	-2.73	-6.63	6.17E-12	6.221E-10
Entpd2	3.58	11.96	0	0
Etv4	-2.09	-4.26	0.004302	0.06641502
Eya1	4.86	29.02	0.04238523	0.39005437
Eya2	7.17	143.62	0.002424	0.04196199
Faim2	2.16	4.47	6.512E-06	0.0002403
Fam131c	-2.55	-5.86	0.005011	0.07526313
Fam177a2	-2.32	-4.99	0.005419	0.08004487
Fam227a	2.85	7.23	0.04570192	0.41221594
Fat2	5.41	42.66	0.02508365	0.26381123
Fcgbp	5.96	62.15	0.01208321	0.14940694
Fcrlb	-4.81	-28.00	0.00001021	0.0003603
Fer1l6	-3.24	-9.44	0.0006322	0.01345746
Fgf1	4.52	22.97	0.0008078	0.01664431
Fibcd1	-4.06	-16.68	3.296E-07	0.00001589
Fmnl1	3.00	8.03	0.02973287	0.29943045
Fmo1	2.49	5.60	0	0
Foxo6	2.46	5.49	0	0
Frmd5	2.42	5.34	0	0
Fstl4	-2.51	-5.68	0.0008638	0.01759766
Fut7	5.45	43.59	0.02654835	0.27563552
Fyb2	-3.30	-9.88	0.01115244	0.14056047
G0s2	-2.12	-4.34	2.004E-13	2.37E-11
Gabra3	4.64	24.93	0	0
Gabre	2.20	4.61	4.875E-10	3.68E-08
Gadl1	-2.17	-4.49	0.02150056	0.23390617
Gas7	2.39	5.23	1.665E-15	2.456E-13
Gdf15	-2.31	-4.97	0.02570687	0.26880804
Gdf6	-2.03	-4.08	1.98E-10	1.602E-08
Gfpt2	2.99	7.96	0	0
Gipc2	3.49	11.22	6.973E-06	0.0002549
Gli1	8.14	282.67	0	0
Gm11629	-3.41	-10.61	0.01336897	0.16199151
Gm11973	-2.21	-4.63	0.02998548	0.3013927
Gm12108	-2.31	-4.95	0.01181252	0.14694919
Gm12199	2.93	7.61	0.001774	0.03237278
Gm12319	4.73	26.48	0.04965343	0.43782911
Gm12764	2.24	4.73	0.02088723	0.22890409
Gm13293	-3.78	-13.71	1.008E-07	5.266E-06
Gm13889	-3.92	-15.12	0.003544	0.05696285
Gm14440	8.40	337.67	0.002812	0.04753864
Gm14444	-2.94	-7.66	0.03087997	0.30830488
Gm14705	-2.39	-5.23	0.00798	0.10874956
Gm15222	-2.81	-7.00	9.572E-06	0.0003403
Gm15246	-2.40	-5.27	0.0004153	0.009361
Gm15635	4.73	26.47	0.04664549	0.41828631
Gm17501	-2.43	-5.40	7.115E-06	0.0002594
Gm20109	2.22	4.66	0.04401074	0.40147293
Gm21698	3.40	10.56	0.007141	0.09989573
Gm2619	2.23	4.68	0.00005549	0.00164
Gm2629	5.09	34.14	0.03563305	0.34367614
Gm26744	-2.76	-6.76	0.004432	0.06808329
Gm26771	-2.65	-6.26	1.595E-06	0.00006788
Gm26902	-3.67	-12.75	0.006021	0.0867142
Gm2694	-2.72	-6.60	0.01492299	0.17601872
Gm26965	5.63	49.50	0.03986597	0.37332331
Gm28035	-5.85	-57.71	0.04250308	0.39096653
Gm28052	-5.51	-45.53	0.0433776	0.39699875
Gm28539	4.46	22.06	0.02968214	0.29899169
Gm28710_1	-2.59	-6.04	5.252E-09	3.447E-07
Gm29417	-2.12	-4.35	0.03228115	0.31928554
Gm29674	-2.46	-5.50	0.0000866	0.002438
Gm30339	-2.79	-6.92	0.04914058	0.43414617
Gm34756	-2.48	-5.56	0.00002058	0.0006701
Gm36107	-2.19	-4.56	0.0002732	0.00651

Gm3854	-2.48	-5.56	0.01062712	0.13620139
Gm38947	-4.02	-16.25	0.006151	0.08823786
Gm40117	2.22	4.66	0.04764573	0.42406729
Gm42788	-2.28	-4.85	0.0399258	0.37363419
Gm43653	-2.51	-5.72	0.03894281	0.36686747
Gm45218	2.15	4.44	0.0189327	0.21182198
Gm45717	5.61	48.96	0.02541373	0.26674513
Gm47336	-4.78	-27.42	0.0464321	0.41700691
Gm47547	-4.91	-30.10	0.0472417	0.42164
Gm48336	-2.94	-7.66	0.02596334	0.27081248
Gm48791	-4.66	-25.33	0.0004261	0.009572
Gm48898	2.34	5.07	0.03967515	0.37175304
Gm49319	-2.41	-5.31	0.0288012	0.29251792
Gm49325	6.69	103.53	0.01525255	0.17939906
Gm49335	-3.19	-9.14	0.01985977	0.22018764
Gm49392	-2.63	-6.20	0.006016	0.08668764
Gm49510	-6.07	-67.37	0.0311913	0.31081842
Gm50241	-2.91	-7.50	0.00923	0.12177865
Gm50253	3.69	12.90	0.0039	0.061432
Gm50332	-2.08	-4.23	0.02154842	0.23418263
Gm50457	-5.16	-35.70	0.00009321	0.002594
Gm5144	-2.79	-6.92	0.0009036	0.01825603
Gm5532	2.03	4.10	0.02110753	0.23061346
Gm5860	-2.15	-4.45	0.009702	0.12667664
Gm9903	-2.02	-4.05	0.04819474	0.42776799
Gng13	3.70	12.98	0.005597	0.08183589
Gpr39	-2.82	-7.08	0	0
Grem1	-2.30	-4.94	0	0
Grem2	-2.31	-4.98	0.001481	0.0277787
Grp	2.02	4.05	0.0008473	0.01732913
Grtp1	2.86	7.28	0.00153	0.02853839
Gvin1	-6.28	-77.90	0.02547397	0.26717585
Gykl1	-4.78	-27.41	0.04898173	0.43355475
H19	2.35	5.11	1.212E-13	1.471E-11
H2-Aa	2.73	6.63	0.04847607	0.42989941
Hapln1	-3.50	-11.30	0.000308	0.007218
Hbb-bs	3.71	13.09	0.00003673	0.00113
Hbb-y	2.76	6.75	0.003177	0.05215426
Hectd2os	-4.94	-30.74	0.04472195	0.40614393
Hhip	11.61	3121.74	6.93E-07	0.00003138
Hlf	3.20	9.20	1.664E-08	9.978E-07
Hmcn2	-2.61	-6.11	0.006748	0.09524089
Hmgcs2	2.82	7.05	1.708E-06	0.00007222
Hoxb4	-2.12	-4.35	0.03442257	0.33564615
Hpse	2.09	4.27	0	0
Ifi205	3.82	14.08	0.0002623	0.006303
Igf2	3.46	11.00	0	0
Igfbp3	5.11	34.52	0	0
Igfbp6	3.22	9.32	3.554E-07	0.00001692
Igsf23	2.11	4.32	0.007684	0.10575751
Il17re	-3.38	-10.38	1.385E-12	1.513E-10
Il18bp	2.03	4.08	2.733E-07	0.00001333
Il1rn	-4.39	-21.00	0	0
Il27ra	-4.78	-27.41	0.04757089	0.42381694
Itga9	-2.36	-5.12	0	0
Itgb7	2.62	6.14	0.0001999	0.005007
Itih3	5.96	62.12	0.0116994	0.14599943
Kcna4	-3.06	-8.32	0.004829	0.07296131
Kcnj8	8.59	384.38	0	0
Kcnk2	-2.28	-4.87	0.0006928	0.01453269
Kcnma1	-3.33	-10.06	0.002583	0.04418698
Kif26a	4.45	21.83	1.332E-15	2E-13
Krt15	-2.81	-6.99	3.986E-08	2.212E-06
Krt79	-2.63	-6.17	0.01711524	0.19638306
Lctl	-2.55	-5.84	0.00001066	0.0003745
Lepr	3.64	12.46	0	0
Lgi2	4.69	25.83	3.32E-14	4.303E-12
Lhfpl2	-2.27	-4.81	0	0
Limch1	-2.37	-5.15	7.354E-11	6.346E-09

Lims2	2.22	4.65	0	0
Lin7a	-3.34	-10.13	0.00001657	0.0005513
Lmod1	-2.70	-6.48	0	0
Lrrc72	5.70	51.93	0.01678287	0.19390186
Lrrtm2	2.26	4.78	4.874E-12	4.975E-10
Lypd1	-4.26	-19.20	0	0
Lypd2	7.04	131.43	0	0
Mamstr	2.93	7.64	6.177E-10	4.588E-08
Map7d2	-2.05	-4.15	0.0001721	0.004395
Matn3	-2.62	-6.14	1.185E-08	7.295E-07
Mcam	-4.11	-17.26	0.00147	0.02760355
Mdfi	-2.10	-4.29	0.01054864	0.13532023
Megf10	-2.15	-4.45	0	0
Megf11	2.45	5.45	0.02895787	0.29375174
Meig1	2.16	4.46	0.0004294	0.009626
Methig1	5.32	40.08	0.0316584	0.31472177
Mettl7a3	2.25	4.75	0.0006157	0.01313975
Mgam	2.54	5.82	1.995E-08	1.173E-06
Mlip	-2.42	-5.37	9.33E-08	4.905E-06
Mmp13	4.09	17.08	0.00204	0.03639249
Mrgprh	3.55	11.69	0.0122349	0.15083328
Mylk3	-2.34	-5.06	8.157E-09	5.191E-07
Myo15	-4.90	-29.81	0.04596299	0.41420326
Myrf	-2.37	-5.17	0.014718	0.17429031
Nat1	-2.31	-4.95	0.02164615	0.2348779
Nav2	-2.55	-5.85	3.284E-11	2.987E-09
Ndnf	2.99	7.93	0	0
Ndor1_1	-8.74	-428.75	0.0004929	0.01077691
Ndrg2	4.48	22.33	1.751E-07	8.742E-06
Ndst3	-4.38	-20.75	0.001219	0.02359927
Nell2	2.25	4.77	0.01065079	0.13626368
Nhs	3.19	9.12	2.735E-09	1.871E-07
Nipal2	2.90	7.47	0.04445075	0.40416198
Nkain4	-2.24	-4.71	0.0004139	0.009335
Nkd1	-2.71	-6.55	0	0
Nkd2	2.62	6.13	0.004715	0.07151243
Nkx3-1	-5.58	-47.78	0.02288365	0.24561135
Npr3	-3.78	-13.72	0	0
Nptx1	-2.63	-6.17	0.01827644	0.20608147
Nr1h4	-2.79	-6.92	0.03387499	0.33115773
Ntn5	2.89	7.43	0.0002827	0.006704
Olfm3	2.34	5.07	0.04435282	0.40335939
Olfml2a	2.75	6.74	0.003335	0.05436573
Otor	-3.62	-12.30	2.887E-15	4.085E-13
Padi2	4.45	21.89	0.001245	0.02402313
Pagr1a	-2.99	-7.93	0.01806081	0.20427284
Palld	-2.40	-5.27	0	0
Pctp	2.24	4.73	7.779E-09	4.963E-07
Pde3a	2.01	4.02	0	0
Pde9a	-2.28	-4.85	4.572E-07	0.00002135
Pdzrn4	-3.07	-8.40	0.02043289	0.22481023
Pglyrp1	2.32	4.98	0.005949	0.08592615
Pi16	2.76	6.78	0	0
Pik3r6	2.60	6.07	0.0000132	0.0004512
Piwil4	-2.15	-4.45	0.006959	0.09787141
Plac8	2.91	7.51	4.617E-08	2.532E-06
Platr22	-2.39	-5.26	0.01727449	0.19745043
Plcb2	-2.79	-6.92	0.03357697	0.32924671
Pls1	-2.05	-4.15	4.987E-06	0.0001887
Plxdc1	3.82	14.14	0	0
Ppp1r14c	-4.91	-30.05	0.0390363	0.36758225
Ppp2r2b	2.76	6.76	0.0009386	0.01888232
Prkcz	-2.02	-4.06	0.01577855	0.18459754
Prlr	-3.09	-8.53	0.001809	0.03285215
Prune2	-2.09	-4.27	0	0
Ptch1	3.58	11.95	0	0
Ptch2	4.42	21.45	9.66E-09	6.073E-07
Ptchd4	-5.36	-41.08	5.395E-08	2.936E-06
Ptger4	6.29	78.29	0	0

Ptprq	-2.14	-4.40	1.11E-15	1.679E-13
Ptx3	-2.03	-4.08	0	0
Pycard	5.09	34.05	0.03562491	0.34367614
Qrich2	-2.41	-5.31	0.02655129	0.27563552
Rab11fip1	3.44	10.86	0.008158	0.11063208
Rab11fip4	3.23	9.37	0.02056676	0.22604483
Ramp1	7.00	128.34	0.003122	0.05144657
Rasgrp3	-2.04	-4.11	0.00001597	0.0005336
Rasl11b	3.68	12.79	0	0
Rassf6	-5.52	-45.97	0.02005696	0.22178486
Rassf9	-2.07	-4.19	0	0
Rec114	5.29	39.22	0.02578926	0.26946714
Ren1	3.16	8.92	0	0
Rflna	3.23	9.37	0.02077289	0.22789031
Rgs7	-2.38	-5.22	0.004174	0.06487173
Rhou	-2.15	-4.44	0	0
Ripor2	2.00	4.01	1.053E-11	1.022E-09
Ripply1	2.20	4.58	0.001079	0.02129623
Rn7s1	-4.12	-17.35	0.0001204	0.003236
Rnase2b	3.01	8.07	0.02949345	0.29737802
Rnase6	2.31	4.97	0.004383	0.06749069
Rorb	-2.12	-4.35	0.02963516	0.29859054
Rtn4r	2.41	5.31	0.005907	0.08546802
Rtn4rl1	3.07	8.39	0	0
Rubcnl	2.05	4.15	0.002352	0.04104198
Samd5	-2.08	-4.22	0.002894	0.04861688
Scrg1	-4.03	-16.35	9.481E-14	1.167E-11
Scube3	-2.25	-4.76	8.064E-10	5.896E-08
Serpinb5	-2.54	-5.82	1.085E-07	5.638E-06
Serpinb6b	-2.79	-6.92	0.03795886	0.35995385
Serpine1	-3.06	-8.32	0	0
Sfrp1	-2.13	-4.37	0	0
Sfrp2	-3.24	-9.42	0	0
Skap1	-2.79	-6.92	0.04463327	0.40555649
Slc22a23	2.38	5.19	1.288E-14	1.712E-12
Slc26a7	-2.61	-6.11	0	0
Slc5a1	-2.52	-5.74	0.01758648	0.20008519
Slc5a7	-3.41	-10.63	0.01023541	0.13207313
Slc6a2	-5.68	-51.18	0.01724272	0.19724939
Slco1c1	5.90	59.78	0.01374362	0.1650935
Slco2b1	6.90	119.62	3.651E-08	2.043E-06
Slurp1	7.29	156.41	0.001971	0.03535151
Sncaip	-3.32	-9.98	0	0
Sohlh1	3.64	12.45	0.0004039	0.009133
Sorbs2	2.76	6.79	1.081E-10	9.099E-09
Sostdc1	9.35	654.27	0	0
Sphkap	-3.07	-8.40	0.01805845	0.20427284
Spink10	-2.62	-6.16	0.003221	0.05274622
Spocd1	5.19	36.57	0.03463797	0.33727382
Sprr3	2.64	6.22	0.00004552	0.001375
Sptbn4	-3.19	-9.13	0.01971445	0.21875069
St8sia2	4.83	28.47	0	0
Stc1	-2.13	-4.39	0	0
Steap4	4.35	20.43	0	0
Stk32b	4.21	18.56	0	0
Svopl	-3.91	-15.05	0.00216	0.03823714
Syt12	-2.44	-5.44	1.868E-08	1.108E-06
Tec	3.75	13.48	0	0
Tent5c	5.61	48.92	0	0
Tfcp2l1	3.50	11.35	0.01098332	0.1389323
Thsd4	2.97	7.86	0.00004758	0.001431
Tmc3	2.87	7.33	5.326E-06	0.0002001
Tmem100	3.39	10.46	0.01785568	0.20254068
Tmem171	4.86	29.01	0.04225035	0.38928218
Tmem221	6.66	101.45	0.005322	0.07885716
Tmem88b	2.41	5.31	0.01116817	0.14067376
Tnfrsf19	-6.11	-68.97	0.01036858	0.13346144
Tnfsf18	3.46	11.00	0.00001538	0.000516
Tnip3	4.63	24.72	3.247E-06	0.0001294

Tnni1	-2.33	-5.04	2.644E-11	2.453E-09
Tomm6os	-2.00	-4.01	0.007872	0.107535
Tpd52	2.39	5.26	0	0
Trabd2b	2.84	7.14	0	0
Trdn	2.74	6.68	0.00001409	0.000479
Trim30d	-2.28	-4.87	0.00004765	0.001432
Trim63	-3.05	-8.26	0.0003227	0.007513
Tspan11	3.17	8.98	0	0
Ucma	-3.20	-9.17	0.003044	0.05040927
Ucp2	2.32	5.00	7.788E-09	4.963E-07
Unc93a2	3.30	9.82	0.004312	0.06653771
Vipr1	3.14	8.82	0.03641835	0.34907263
Vit	2.15	4.45	0	0
Wfdc1	4.31	19.81	0.00002107	0.0006817
Wfdc18	-2.36	-5.15	0.00004432	0.001343
Wfdc3	2.80	6.96	0	0
Wnt10b	-2.63	-6.17	0.01431174	0.17063061
Wnt11	-3.48	-11.18	0	0
Zbp1	2.28	4.85	1.116E-12	1.226E-10
Zfp935	4.67	25.38	0.009252	0.12198876
Zfp969	-5.92	-60.48	0.03360596	0.32945367

10.2.2 Genes differentially regulated by Picoberin

Supplementary Table 5: Genes that were differentially expressed upon Picoberin treatment for 24 h. RNA-Seq data. C3H10T1/2 cells were treated with 1.5 µM purmorphamine and 1 nM Picoberin and were compared to samples treated with 1.5 µM purmorphamine and DMSO. Log_2 fold changes of at least ± 1 with a p-value ≤ 0.05 were considered as significantly up- or down regulated.

Gene	Log_2 fold change	Fold change	P-value	FDR p-value
1010001B22Rik	-2.04	-4.11	0.026936544	0.99995467
1700056N10Rik	-1.84	-3.58	0.044886923	0.99995467
1700120C14Rik	-1.98	-3.94	0.044449031	0.99995467
4732414G09Rik	-2.75	-6.72	0.002368	0.584994053
4933406C10Rik	2.17	4.50	0.049630788	0.99995467
6330562C20Rik	1.06	2.08	0.014165403	0.99995467
A430105J06Rik	-1.35	-2.55	0.044705118	0.99995467
Abca4	1.06	2.08	0.010109637	0.99995467
Abca8a	-1.04	-2.06	0.012037413	0.99995467
Acp6	1.06	2.08	0.018525969	0.99995467
Adh7	1.00	2.00	0	0
Ahrr	3.75	13.47	5.621E-13	1.955E-09
Aldh3a1	2.68	6.43	0	0
Asgr1	1.35	2.56	0.0006056	0.279418935
AV356131	-1.54	-2.90	0.001328	0.420428955
B230398E01Rik	5.09	34.09	0.048126474	0.99995467
BC067074	1.92	3.79	0.007234	0.99995467
Bcam	-2.82	-7.05	0.047196692	0.99995467
Bdh1	1.20	2.29	0.037472092	0.99995467
Bdkrb2	1.43	2.69	0.013755306	0.99995467
Bean1	-1.58	-3.00	0.015541955	0.99995467
C130036L24Rik	-1.44	-2.71	0.005109	0.883014872
C230035I16Rik	-1.47	-2.77	0.029147459	0.99995467
C530005A16Rik	1.03	2.05	0.003385	0.706564981
Cadm4	-2.82	-7.07	0.003079	0.687002856
Camk1g	1.72	3.31	0.003139	0.687002856
Car8	-1.60	-3.02	0.004222	0.812074965
Carmil2	-2.48	-5.59	0.032823311	0.99995467
Ccdc24	1.20	2.30	0.010337147	0.99995467
Ccno	1.29	2.45	0.00001222	0.010200627
Cdh6	3.09	8.51	0.025495739	0.99995467
Cerox1	-1.68	-3.20	0.044642542	0.99995467
Ces1d	-2.82	-7.05	0.039316866	0.99995467

Chd7	1.44	2.71	0.009476	0.99995467
Clec10a	1.81	3.52	0.018712549	0.99995467
Col4a4	-2.75	-6.73	0.002002	0.528246267
Cyfip2	1.54	2.91	0.0006934	0.302786446
Cyp1a1	6.72	105.36	0.007901	0.99995467
Cyp1b1	1.59	3.00	0	0
Dlx4	-2.50	-5.64	0.014193606	0.99995467
Dpep1	1.42	2.67	0	0
Efnb3	-1.61	-3.06	0.016833944	0.99995467
Eln	-1.16	-2.24	0.00487	0.861450171
Fam222a	1.40	2.63	0.006898	0.99995467
Frmd4b	2.57	5.93	0.037846616	0.99995467
G0s2	1.08	2.11	0.0001901	0.111792831
Garem2	-1.05	-2.07	0.00428	0.815716484
Gbp10	1.48	2.79	0.006107	0.984971345
Gbp6	-5.74	-53.38	0.016449175	0.99995467
Gfra2	1.24	2.37	0.049139706	0.99995467
Gm10425	1.15	2.22	0.025991815	0.99995467
Gm11934	-2.98	-7.89	0.045549295	0.99995467
Gm12932	2.72	6.61	0.043700115	0.99995467
Gm14440	6.31	79.39	0.033058015	0.99995467
Gm14443	-2.04	-4.12	0.004449	0.836475989
Gm15337	1.17	2.26	0.001194	0.396418784
Gm15728	-1.12	-2.18	0.026445275	0.99995467
Gm19385	-1.94	-3.85	0.01759706	0.99995467
Gm19705	-1.21	-2.31	0.042585656	0.99995467
Gm2026	-1.03	-2.04	0.026290589	0.99995467
Gm20324	1.58	3.00	0.041655969	0.99995467
Gm20337	-1.07	-2.10	0.024622948	0.99995467
Gm20427	-5.81	-56.13	0.039615849	0.99995467
Gm20711	-1.84	-3.59	0.048137746	0.99995467
Gm21680	2.28	4.86	0.030808402	0.99995467
Gm21992	-1.20	-2.30	0.047600884	0.99995467
Gm28052	6.00	64.09	0.036821147	0.99995467
Gm30873	1.12	2.17	0.021345497	0.99995467
Gm33055	2.72	6.61	0.048415985	0.99995467
Gm34376	2.66	6.31	0.022860254	0.99995467
Gm3468	2.39	5.23	0.042650015	0.99995467
Gm34756	-1.78	-3.43	0.004747	0.857889492
Gm35853	3.52	11.48	2.518E-09	0.000005005
Gm3636	-1.73	-3.31	0.010873989	0.99995467
Gm37800	-1.31	-2.48	0.015086755	0.99995467
Gm38910	-2.10	-4.29	0.035654167	0.99995467
Gm43517	-2.33	-5.04	0.004682	0.857889492
Gm44503	-5.70	-52.09	0.040486807	0.99995467
Gm45606	1.85	3.60	0.027533901	0.99995467
Gm45799	1.24	2.36	0.00004291	0.03093086
Gm45890	-1.84	-3.57	0.030875938	0.99995467
Gm46447	-2.00	-4.01	0.020670898	0.99995467
Gm47939	-2.00	-3.99	0.037120014	0.99995467
Gm49776	6.07	67.41	0.032814656	0.99995467
Gm49804	-1.94	-3.83	0.01275184	0.99995467
Gm50203	1.85	3.60	0.033998353	0.99995467
Gm50364	-5.28	-38.85	0.046237704	0.99995467
Gpc1	1.08	2.11	0	0
Gprc5a	1.20	2.30	0	0
H1f3	1.21	2.31	0.047679789	0.99995467
H4c3	-3.12	-8.69	0.026580476	0.99995467
Hey2	-1.33	-2.52	0.006111	0.984971345
Hipk4	1.77	3.40	0.041768961	0.99995467
Hist1h2ao	-6.21	-74.18	0.020494758	0.99995467
Hmx2	-5.33	-40.09	0.027516	0.99995467
Homer2	1.17	2.25	0.037284975	0.99995467
Hoxa9	-1.18	-2.26	0.026971577	0.99995467
Igsf1	-2.10	-4.29	0.02741292	0.99995467
Il1rapl1	1.68	3.21	0.047638793	0.99995467
Il31ra	2.45	5.47	0.0001702	0.101508897
Il34	-1.84	-3.58	0.033522408	0.99995467
Il7	2.85	7.22	0.047682403	0.99995467
Inhbb	1.18	2.27	3.8E-09	0.000007211
Irx3os	3.09	8.52	0.021784873	0.99995467

Itgb7	1.27	2.41	0.003193	0.687002856
Jag2	-1.70	-3.24	0.026861307	0.99995467
Kcne4	-1.11	-2.16	0.004182	0.812036405
Kcnu1	2.98	7.90	0.035137112	0.99995467
Krt13	-1.61	-3.05	0.000002565	0.002677
Krt7	2.74	6.70	0.004605	0.850575878
Krt80	1.82	3.53	4.131E-11	1.232E-07
Krt87	2.57	5.94	0.001915	0.515763159
Lgr6	2.30	4.94	0.0003878	0.199840291
Lif	1.19	2.28	0.006919	0.99995467
Lncenc1	-1.84	-3.57	0.013546008	0.99995467
Lpxn	1.42	2.68	0.039586489	0.99995467
Lrrn3	1.47	2.76	6.768E-10	0.000001569
M1ap	2.44	5.43	0.003167	0.687002856
Megf6	1.42	2.68	0.034305546	0.99995467
Meig1	1.77	3.40	0.038721282	0.99995467
Mettl7a2	-2.49	-5.62	0.034782445	0.99995467
Mfap2	1.27	2.41	0.003275	0.690425699
Mpp4	-1.98	-3.94	0.045533468	0.99995467
Mylk2	-1.62	-3.08	0.021431419	0.99995467
n-R5-8s1	-1.57	-2.96	0.015794528	0.99995467
Nfe2	-1.84	-3.58	0.026194477	0.99995467
Nkd2	3.75	13.45	0.000003416	0.003395
Nmnat2	1.04	2.05	0	0
Nox1	1.77	3.41	0.015502876	0.99995467
Npcd	5.48	44.73	0.049767928	0.99995467
Nppc	-3.13	-8.75	0.018633436	0.99995467
Nupr1l	1.26	2.40	0.043664554	0.99995467
Otor	-1.22	-2.33	0.002348	0.584994053
Otulinl	1.21	2.32	1.512E-09	0.000003188
Pla2r1	1.53	2.89	0.013769037	0.99995467
Plekhh1	-1.31	-2.47	0.018764899	0.99995467
Plp1	1.95	3.87	0.020985733	0.99995467
Ppp1r14c	1.76	3.39	0.001419	0.438749204
Prg4	1.22	2.33	0.034978606	0.99995467
Prkch	-1.25	-2.37	0.022258103	0.99995467
Prl2c2	1.10	2.14	0.007015	0.99995467
Prl2c3	1.09	2.12	0.031268647	0.99995467
Prrt4	1.16	2.24	0.035506295	0.99995467
Psmb8	1.01	2.02	0.015378374	0.99995467
Pstpip2	1.02	2.03	0.008934	0.99995467
Ptch2	-3.13	-8.76	0.019314179	0.99995467
Ptchd4	1.15	2.22	0.008381	0.99995467
Rdh9	-1.56	-2.94	0.002659	0.623537516
Rnf144b	1.32	2.50	0.024278838	0.99995467
Rpl10	-1.05	-2.08	0.00005472	0.037442762
Rpl9-ps6	1.21	2.31	0.001599	0.463582546
Scn8a	1.17	2.25	0.036809963	0.99995467
Sec1	2.00	3.99	0.025610669	0.99995467
Serpina3n	2.07	4.18	0.034066979	0.99995467
Slc12a8	1.28	2.42	0.028960528	0.99995467
Slc14a1	3.79	13.87	0.000005336	0.00495
Slc26a7	-1.23	-2.34	0.003042	0.687002856
Sostdc1	-1.16	-2.23	0.003883	0.779223073
Sox8	-1.63	-3.10	0.033102831	0.99995467
Sprr3	-2.20	-4.60	0.046470325	0.99995467
Spx	1.77	3.40	0.033069256	0.99995467
Syn3	-1.11	-2.15	0.023088951	0.99995467
Syngr3	1.66	3.17	0.015950518	0.99995467
Tiparp	1.14	2.21	0	0
Tmc8	2.48	5.58	0.032834714	0.99995467
Tmem95	1.14	2.21	0.041720906	0.99995467
Tsacc	1.02	2.02	0.033697189	0.99995467
Tspan18	-1.79	-3.46	0.000006537	0.005805
Ttc16	-1.84	-3.57	0.014491709	0.99995467
Unc13a	1.13	2.19	0.039530133	0.99995467
Vpreb1	-1.04	-2.06	0.031941243	0.99995467
Wfdc12	-1.02	-2.03	0.038760697	0.99995467
Xdh	1.40	2.64	0	0
Zfp969	-5.98	-63.28	0.030620816	0.99995467
Zyx	1.08	2.12	0	0

Supplementary Table 6: Genes that were differentially expressed upon Picoberin treatment for 48 h. RNA-Seq data. C3H10T1/2 cells were treated with 1.5 µM purmorphamine and 1 nM Picoberin and were compared to samples treated with 1.5 µM purmorphamine and DMSO. Log_2 fold changes of at least ± 1 with a p-value ≤ 0.05 were considered as significantly up- or down regulated.

Gene	Log_2 fold change	Fold change	p-value	FDR p-value
1200007C13Rik	3.00	7.99	0.02804924	0.99988719
1700023F02Rik	3.47	11.08	0.008336	0.99988719
2810405F17Rik	2.85	7.22	0.03232234	0.99988719
2810455O05Rik	-1.81	-3.50	0.02669965	0.99988719
3010003L21Rik	-1.44	-2.71	0.04128186	0.99988719
3110083C13Rik	-1.30	-2.46	0.03486487	0.99988719
4930478M13Rik	5.44	43.43	0.01798926	0.99988719
4930547M16Rik	1.46	2.76	0.02115724	0.99988719
5430403N17Rik	-1.13	-2.19	0.003938	0.99988719
5730405O15Rik	3.00	7.99	0.02397267	0.99988719
9130604C24Rik	-1.63	-3.09	0.02969752	0.99988719
9230116L04Rik	3.00	7.99	0.02884517	0.99988719
Abcg4	2.85	7.23	0.03294253	0.99988719
Ahrr	3.86	14.54	3.105E-09	0.0000108
Aldh3a1	1.34	2.53	0	0
Alpl	-1.19	-2.28	0.0000255	0.03012756
Areg	1.58	2.99	0.03105862	0.99988719
Arhgdig	-1.96	-3.90	0.02963113	0.99988719
Arhgef15	1.98	3.94	0.04571412	0.99988719
Artn	1.17	2.26	7.688E-07	0.001515
Asgr1	2.62	6.16	0.00001307	0.01759418
Awat2	-1.79	-3.45	0.03827693	0.99988719
BC147527	2.59	6.03	0.01673762	0.99988719
Bdh1	2.47	5.53	0.006818	0.99988719
Bdkrb2	2.47	5.54	0.007876	0.99988719
C2	2.09	4.26	0.03186826	0.99988719
Ccl17	-1.95	-3.87	0.02059603	0.99988719
Ccn5	1.05	2.07	1.332E-15	1.854E-11
Ccno	1.62	3.08	3.527E-08	0.0001052
Cdh5	-1.33	-2.52	0.009148	0.99988719
Col14a1	1.42	2.68	0.003304	0.99988719
Col2a1	1.17	2.25	9.533E-13	7.959E-09
Col4a4	-1.35	-2.54	0.007987	0.99988719
Cpvl	1.57	2.98	0.02119087	0.99988719
Cyfip2	1.58	2.99	0.0005057	0.29316707
Cyp1a1	5.04	32.82	0.02948407	0.99988719
Cyp1b1	1.47	2.77	0	0
D830035M03Rik	-1.66	-3.15	0.0448073	0.99988719
Duoxa1	-1.26	-2.40	0.04177951	0.99988719
Fam221b	-1.18	-2.27	0.04400201	0.99988719
Fhod3	1.39	2.61	0.0007485	0.38642607
Fibcd1	-2.99	-7.93	0.00655	0.99988719
Fry	-1.60	-3.03	0.01174974	0.99988719
Gadl1	-2.02	-4.05	0.01453527	0.99988719
Gdf6	1.93	3.80	0.006147	0.99988719
Gm10425	1.18	2.27	0.02509123	0.99988719
Gm11940	-1.87	-3.65	0.02280078	0.99988719
Gm12022	-3.07	-8.38	0.03326473	0.99988719
Gm12166	-1.53	-2.89	0.02459337	0.99988719
Gm12319	1.63	3.09	0.04930418	0.99988719
Gm14440	-7.30	-157.43	0.009987	0.99988719
Gm15832	-3.03	-8.15	0.03626276	0.99988719
Gm16677	-1.76	-3.38	0.04839241	0.99988719
Gm17494	-1.32	-2.50	0.02875903	0.99988719
Gm2026	1.23	2.34	0.009438	0.99988719
Gm20628	-2.94	-7.66	0.0401114	0.99988719
Gm20662	5.07	33.64	0.03654351	0.99988719
Gm20721	-1.03	-2.04	0.0180176	0.99988719
Gm26826	2.62	6.17	0.007563	0.99988719
Gm26920	3.37	10.32	0.01842862	0.99988719
Gm27030	1.49	2.81	0.02211601	0.99988719
Gm28818	-1.48	-2.79	0.01650059	0.99988719
Gm30794	1.71	3.28	0.008045	0.99988719

Gm33508	3.13	8.76	0.01538937	0.99988719
Gm34655	2.10	4.28	0.02362819	0.99988719
Gm35551	2.23	4.68	0.03922092	0.99988719
Gm35853	2.07	4.21	0.0001377	0.10267894
Gm38477	-1.42	-2.67	0.003798	0.99988719
Gm41396	3.25	9.53	0.01651141	0.99988719
Gm42788	1.38	2.61	0.03129313	0.99988719
Gm43549	-5.77	-54.52	0.02586424	0.99988719
Gm45669	-3.57	-11.86	0.01391996	0.99988719
Gm45716	1.54	2.90	0.01181257	0.99988719
Gm45767	-2.27	-4.81	0.04739541	0.99988719
Gm47428	-3.57	-11.87	0.003007	0.99355383
Gm48228	-5.04	-32.79	0.04149257	0.99988719
Gm48275	-6.47	-88.83	0.0222675	0.99988719
Gm48488	-1.04	-2.06	0.02527505	0.99988719
Gm49257	1.98	3.94	0.04666903	0.99988719
Gm49317	1.34	2.54	0.04172133	0.99988719
Gm49325	-7.91	-239.82	0.004342	0.99988719
Gm49361	-5.43	-43.25	0.03482074	0.99988719
Gm49494	-2.33	-5.03	0.02342949	0.99988719
Gm49496	5.57	47.53	0.03183917	0.99988719
Gm49544	-1.16	-2.23	0.006881	0.99988719
Gm50069	-1.58	-2.99	0.007517	0.99988719
Gm50169	-3.58	-12.00	0.01372153	0.99988719
Gm50241	2.62	6.13	0.02128116	0.99988719
Gm50462	1.02	2.03	0.006125	0.99988719
Gm5148	-1.45	-2.74	0.02012382	0.99988719
Gpr156	-1.61	-3.05	0.01478946	0.99988719
Grem1	1.04	2.05	9.257E-12	6.44E-08
Gstp2	1.45	2.74	0.02108656	0.99988719
Gvin1	6.42	85.56	0.01990825	0.99988719
H3c10	-2.47	-5.54	0.02721524	0.99988719
H3c2	-5.57	-47.44	0.02574761	0.99988719
H3c3	2.59	6.00	0.01943626	0.99988719
Hist1h2br	-8.14	-281.89	0.001806	0.6793566
Icosl	-5.32	-40.08	0.0257343	0.99988719
Il18bp	1.03	2.04	0.006133	0.99988719
Il1rapl1	-2.03	-4.09	0.01503207	0.99988719
Il31ra	3.13	8.74	0.002496	0.86121783
Inhbb	1.24	2.36	8.573E-08	0.0002386
Ism1	-1.05	-2.07	0.004266	0.99988719
Kbtbd6	-1.15	-2.23	0.02746585	0.99988719
Kcnf1	1.96	3.89	0.01336564	0.99988719
Kif26a	-1.15	-2.22	0.0002155	0.14762938
Klk10	-2.80	-6.96	0.0393026	0.99988719
Krt13	-1.32	-2.50	0.0004587	0.27353969
Krt80	1.21	2.32	0.0001211	0.0976484
Krt87	2.59	6.01	0.02124619	0.99988719
Lcp1	-1.16	-2.23	0.02791077	0.99988719
Lrrn3	1.53	2.90	3.355E-11	2.001E-07
Lsmem2	2.79	6.93	0.0107599	0.99988719
Lypd2	-3.43	-10.74	0.00001073	0.01492621
Mafb	3.00	7.99	0.02388357	0.99988719
Maneal	-1.69	-3.23	0.04386242	0.99988719
Meox1	1.98	3.94	0.0364435	0.99988719
Mettl7a3	-2.25	-4.74	0.01960768	0.99988719
Mst1	2.36	5.13	0.03232734	0.99988719
Muc2	2.85	7.22	0.03324271	0.99988719
Nkd2	1.45	2.73	0.03843164	0.99988719
Nox1	2.64	6.22	0.001386	0.59010619
Olfr77	-2.50	-5.64	0.01039771	0.99988719
Pcolce2	-1.29	-2.45	0.0005712	0.32188318
Pigz	-2.27	-4.81	0.02783403	0.99988719
Pla2g4c	-1.29	-2.44	0.003065	0.99941224
Prss23os	-2.41	-5.33	0.007967	0.99988719
Prss57	1.43	2.69	0.03435396	0.99988719
Psmb8	1.11	2.16	1.147E-06	0.002082
Pstpip2	1.33	2.51	0.008708	0.99988719
Ptch2	-1.26	-2.40	0.004933	0.99988719
Ptchd4	1.12	2.17	0.009172	0.99988719
Pth1r	-1.02	-2.03	0.003941	0.99988719

Pygm	-1.95	-3.87	0.02614686	0.99988719
Qrich2	-1.49	-2.80	0.04949131	0.99988719
Rasd1	3.12	8.70	0.03122419	0.99988719
Rps18-ps4	-2.08	-4.23	0.00438	0.99988719
Scin	-3.18	-9.06	0.001701	0.65752424
Sema4a	1.80	3.49	0.038154	0.99988719
Serpina1e	-1.88	-3.67	0.03673694	0.99988719
Sfn	-1.20	-2.30	0.0171967	0.99988719
Slc11a1	-1.62	-3.08	0.04522881	0.99988719
Slc14a1	3.06	8.37	0.001152	0.52840497
Slc1a2	-1.80	-3.48	0.003481	0.99988719
Slc22a4	-1.66	-3.15	0.04415578	0.99988719
Slc2a3	2.22	4.68	0.03139229	0.99988719
Slc2a6	1.11	2.15	0.000124	0.0976484
Slurp1	-3.54	-11.65	0.006801	0.99988719
Sostdc1	-1.05	-2.07	1.44E-08	0.00004624
Sox6	3.57	11.86	0.008979	0.99988719
Sprr3	-1.05	-2.07	0.03563979	0.99988719
Sptbn5	-2.75	-6.75	0.009085	0.99988719
Tbc1d8	-1.32	-2.50	0.04955127	0.99988719
Trim36	1.96	3.89	0.02157776	0.99988719
Tspan18	-1.08	-2.11	0.001622	0.63881613
Tubb4a	4.84	28.70	0.04651312	0.99988719
Tymp	1.19	2.27	0.007294	0.99988719
Unc13c	-1.14	-2.20	0.04328444	0.99988719
Upk3b	-1.25	-2.37	0.001276	0.56046463
Wfdc12	-1.11	-2.16	0.01357244	0.99988719
Xlr	-1.72	-3.30	0.008808	0.99988719

Supplementary Table 7: Genes that were differentially expressed upon Picoberin treatment for 96 h. RNA-Seq data. C3H10T1/2 cells were treated with 1.5 µM purmorphamine and 1 nM Picoberin and were compared to samples treated with 1.5 µM purmorphamine and DMSO. Log_2 fold changes of at least ± 1 with a p-value ≤ 0.05 were considered as significantly up- or down regulated.

Gen	Log_2 fold change	Fold change	p-value	FDR p-value
2310069B03Rik	2.26	4.81	0.02390672	0.99994106
2310074N15Rik	1.14	2.20	0.02554264	0.99994106
2610204G07Rik	2.48	5.57	0.002333	0.70058853
4833417C18Rik	-1.32	-2.50	0.02113336	0.99994106
4921507P07Rik	-1.09	-2.13	0.03684777	0.99994106
4930534H03Rik	-3.32	-9.96	0.02275081	0.99994106
4930563E18Rik	-2.80	-6.97	0.005112	0.99994106
6430550D23Rik	1.46	2.75	0.03804302	0.99994106
7420700N18Rik	1.72	3.29	0.02408685	0.99994106
Abca13	-3.32	-9.99	0.009139	0.99994106
Ahrr	7.28	155.18	1.238E-06	0.00272
AI838599	-2.73	-6.64	0.03001406	0.99994106
Akap5	-1.28	-2.43	0.004574	0.98927185
Apob	3.63	12.42	0.03479214	0.99994106
Arhgap36	-1.57	-2.97	0.00006413	0.05819898
Artn	1.27	2.41	9.454E-13	5.637E-09
Atp2a1	-2.80	-6.97	0.006635	0.99994106
Ccno	1.23	2.35	0.00004678	0.04649486
Cd69	2.48	5.57	0.04870536	0.99994106
Cdx1	2.48	5.57	0.01973654	0.99994106
Chst5	3.34	10.14	0.01170324	0.99994106
Clic5	-1.04	-2.06	0.03674484	0.99994106
Cmbl	1.40	2.64	0.04353311	0.99994106
Col2a1	2.04	4.11	0	0
Ctla2a	-1.14	-2.21	0.002517	0.70988659
Cyp1b1	1.50	2.84	0.00001972	0.02494687
Dnajb13	-1.49	-2.81	0.01662187	0.99994106
Egf	-1.27	-2.41	0.01488211	0.99994106
Etaa1os	-1.53	-2.88	0.03175615	0.99994106
Exoc3l2	-1.99	-3.98	0.0333847	0.99994106

Fabp2	-2.80	-6.97	0.0001138	0.09256231
Far2	-1.62	-3.06	0.02234311	0.99994106
Fetub	-1.02	-2.02	0.006503	0.99994106
Gad1os	2.06	4.16	0.02380108	0.99994106
Gal3st3	2.99	7.94	0.03567141	0.99994106
Gast	-1.99	-3.98	0.04610538	0.99994106
Gbp8	1.63	3.10	0.001099	0.44985501
Gm10244	-1.31	-2.47	0.002015	0.6276162
Gm11007	-1.98	-3.95	0.00009612	0.08188716
Gm11615	-1.99	-3.98	0.02031787	0.99994106
Gm12166	1.33	2.51	0.03984479	0.99994106
Gm12474	1.72	3.29	0.008148	0.99994106
Gm16287	1.72	3.29	0.01166013	0.99994106
Gm16741	-1.99	-3.98	0.04856501	0.99994106
Gm16853	-1.99	-3.98	0.02808513	0.99994106
Gm19589	1.72	3.29	0.03417733	0.99994106
Gm20005	1.72	3.29	0.02213458	0.99994106
Gm2007	-2.80	-6.97	0.04466299	0.99994106
Gm2093	1.72	3.29	0.03350251	0.99994106
Gm27010	-1.69	-3.22	0.002248	0.6849862
Gm29609	1.59	3.01	0.02858557	0.99994106
Gm29797	-2.80	-6.97	0.002474	0.70988659
Gm30146	2.97	7.86	0.00761	0.99994106
Gm32171	-1.99	-3.98	0.0210339	0.99994106
Gm32834	1.36	2.57	0.0002725	0.18386811
Gm34376	-3.31	-9.94	0.02771644	0.99994106
Gm35853	2.04	4.12	0.00167	0.54887354
Gm36107	-2.29	-4.90	0.04422033	0.99994106
Gm36279	1.28	2.42	0.02139378	0.99994106
Gm36634	2.48	5.57	0.01695149	0.99994106
Gm37988	-1.17	-2.24	0.01762009	0.99994106
Gm39307	-2.80	-6.97	0.02899505	0.99994106
Gm42109	1.04	2.05	0.02273079	0.99994106
Gm42417	5.96	62.16	0.008484	0.99994106
Gm44731	1.72	3.29	0.001743	0.56415292
Gm44973	-1.98	-3.96	0.02598877	0.99994106
Gm45463	1.24	2.37	0.01170112	0.99994106
Gm47257	1.72	3.29	0.00926	0.99994106
Gm49397	-1.99	-3.98	0.03489137	0.99994106
Gm4952	-1.09	-2.13	0.04562078	0.99994106
Gm49864	-1.23	-2.34	0.0484184	0.99994106
Gm50081	2.48	5.57	0.01076774	0.99994106
Gm50336	1.72	3.29	0.0407711	0.99994106
Gm8332	1.65	3.13	0.01735851	0.99994106
Grem1	1.10	2.15	0	0
Guca1a	1.72	3.29	0.004326	0.981492
H4c2	2.22	4.66	0.01169649	0.99994106
Hes7	2.08	4.24	0.01214134	0.99994106
Inhbb	1.29	2.44	1.028E-06	0.00272
Iqub	-1.99	-3.98	0.0294161	0.99994106
Itga2	-2.11	-4.31	0.001391	0.50192365
Kcnj16	-3.10	-8.57	0.02635663	0.99994106
Kif17	-1.09	-2.13	0.04232654	0.99994106
Lbhd2	1.72	3.29	0.03093854	0.99994106
Lhx5	-1.99	-3.98	0.004167	0.96627823
Lmx1b	2.97	7.86	0.04221732	0.99994106
Lrrc23	1.72	3.29	0.02972838	0.99994106
Lrrn3	2.36	5.14	1.633E-08	0.00006196
Maats1	2.48	5.57	0.004253	0.97853123
Mamdc2	4.27	19.27	0.01407334	0.99994106
Mettl7b	-1.03	-2.04	0.004019	0.95630203
Ninj2	-1.99	-3.98	0.04827011	0.99994106
Nox1	1.61	3.05	0.0003649	0.23263622
Nrgn	1.72	3.29	0.04108367	0.99994106
Oacyl	2.97	7.86	0.008028	0.99994106
Olfr11	-1.99	-3.98	0.02784717	0.99994106
Olfr18	2.97	7.86	0.02165854	0.99994106
Olfr77	-1.63	-3.10	0.01518284	0.99994106
Oscar	3.64	12.43	0.02027602	0.99994106

Otulinl	1.15	2.23	0.0001268	0.09798755
Pik3cg	3.34	10.14	0.02806236	0.99994106
Ppara	-1.99	-3.98	0.004892	0.99994106
Prr7	1.97	3.90	0.03127493	0.99994106
Ptcra	2.97	7.86	0.04966691	0.99994106
Rhov	-1.03	-2.04	0.005004	0.99994106
Slc13a2	-2.80	-6.97	0.001147	0.45619897
Slc4a5	-3.32	-9.96	0.02479361	0.99994106
Slc5a2	-1.99	-3.98	0.001148	0.45619897
Slc6a1	2.48	5.57	0.004404	0.98768531
Smco2	1.72	3.29	0.01923259	0.99994106
Syne4	-1.03	-2.04	0.01649939	0.99994106
Tnn	3.34	10.14	0.01673101	0.99994106
Tph1	1.90	3.72	0.01565272	0.99994106
Trim66	4.09	16.99	0.02333589	0.99994106
Ucp3	-1.99	-3.98	0.009263	0.99994106
Ugt1a5	-2.28	-4.84	0.02661276	0.99994106

Supplementary Table 8: Genes that were differentially expressed upon Picoberin treatment for 7 days. RNA-Seq data. C3H10T1/2 cells were treated with 1.5 µM purmorphamine and 1 nM Picoberin and were compared to samples treated with 1.5 µM purmorphamine and DMSO. Log_2 fold changes of at least ± 1 with a p-value ≤ 0.05 were considered as significantly up- or down regulated.

Gene	Log_2 fold change	Fold change	p-value	FDR p-value
41883	2.45	5.45	0.01543897	0.99996605
1600012P17Rik	-1.52	-2.87	0.03681801	0.99996605
1700008J07Rik	1.97	3.93	0.03694791	0.99996605
1810026B05Rik	1.24	2.37	0.01259614	0.99996605
2610027K06Rik	1.38	2.60	0.00919	0.99996605
2610507B11Rik	-3.23	-9.36	0.03851005	0.99996605
4930534H03Rik	1.28	2.42	0.0009194	0.37997082
6720483E21Rik	1.17	2.26	0.03948823	0.99996605
8030462N17Rik	1.39	2.62	0.003558	0.88406534
9130019O22Rik	-1.61	-3.06	0.009202	0.99996605
9530026P05Rik	-2.68	-6.39	0.00004909	0.04269103
A430105J06Rik	1.18	2.27	0.04317658	0.99996605
Abcc9	-1.02	-2.02	0.04150253	0.99996605
Acoxl	1.18	2.26	0.002612	0.75019006
Adamts9	1.30	2.46	0.03355125	0.99996605
AI413582	1.31	2.48	0.0007469	0.32475386
AI467606	-1.19	-2.28	0.04377772	0.99996605
Aktip	1.87	3.66	0.02496403	0.99996605
Aldh3a1	6.12	69.38	0.009318	0.99996605
Antxr2	3.62	12.28	0.000377	0.20396706
Aox2	-1.05	-2.08	0.01058059	0.99996605
Artn	1.38	2.61	1.11E-16	1.159E-12
Bfsp1	1.24	2.37	0.03607633	0.99996605
Bhlhb9	-1.29	-2.44	0.04397245	0.99996605
Bloc1s4	-2.61	-6.10	0.004687	0.99996605
Bloc1s6os	1.12	2.18	0.0001855	0.11554264
C430049B03Rik	2.35	5.10	0.01763149	0.99996605
Calhm2	1.30	2.47	0.02847005	0.99996605
Cbfa2t2	-5.33	-40.11	0.04318961	0.99996605
Ccar1	-1.40	-2.63	0.04666087	0.99996605
Ccdc146	-1.12	-2.17	0.008846	0.99996605
Ccdc85c	-1.29	-2.44	0.03325441	0.99996605
Ccnq	-2.12	-4.35	0.02454532	0.99996605
Cdc5l	2.34	5.07	0.02776616	0.99996605
Chd4	2.00	3.99	0.01663912	0.99996605
Chst8	-1.06	-2.08	0.04132611	0.99996605
Cmtm4	2.95	7.73	0.008099	0.99996605
Cnr1	1.03	2.05	4.405E-07	0.001021
Col2a1	1.19	2.28	0	0
Cpxm1	5.37	41.29	0.04956302	0.99996605
Cr2	-1.15	-2.22	0.007813	0.99996605
Crebbp	1.85	3.59	0.04847334	0.99996605

Crim1	1.03	2.04	0.04678953	0.99996605
Crispld1	1.16	2.24	0.001934	0.64596268
Cryl1	1.86	3.64	0.006736	0.99996605
Ctbp1	3.99	15.91	0.003362	0.8504269
D030007L05Rik	1.09	2.13	0.007874	0.99996605
Dclk2	2.70	6.52	0.004058	0.94115076
Ddx25	3.02	8.09	0.02668024	0.99996605
Dennd4a	-1.14	-2.21	0.008593	0.99996605
Dmtn	1.58	2.98	0.04010954	0.99996605
Dnajc6	2.07	4.20	0.002982	0.78349275
Dync1li1	1.02	2.03	0.001277	0.47596779
Echdc3	1.56	2.96	0.001176	0.44222733
Eif2s3x	1.88	3.67	0.04703925	0.99996605
Eif4ebp3	1.55	2.94	0.02386817	0.99996605
Enpp3	7.68	204.95	0.002245	0.69942128
Epor	-3.37	-10.31	0.01402653	0.99996605
Evi2a	2.24	4.72	0.04208466	0.99996605
Exo1	-8.43	-345.42	0.00495	0.99996605
Exoc3	1.02	2.02	0.00103	0.40907176
Fa2h	-1.68	-3.20	0.02122683	0.99996605
Fam207a	1.72	3.29	8.905E-09	0.00003717
Fam234a	3.00	8.01	0.04204184	0.99996605
Fam43a	2.86	7.24	0.03729165	0.99996605
Fam72a	-2.03	-4.10	0.02464094	0.99996605
Fbln1	-2.20	-4.60	0.02696526	0.99996605
Fbxw9	1.98	3.94	0.04501041	0.99996605
Fem1a	1.31	2.47	0.02563143	0.99996605
Fgf7	1.46	2.75	0.0001929	0.11835878
Foxp3	-1.22	-2.34	1.522E-07	0.0004234
Frmd5	-1.21	-2.31	0.02558401	0.99996605
Fzd5	-1.12	-2.17	0.0123668	0.99996605
Gask1a	-1.20	-2.30	0.0002469	0.14117963
Gfm2	-1.06	-2.09	0.009989	0.99996605
Gipr	-2.41	-5.30	0.04168973	0.99996605
Gm10010	1.20	2.30	0.0002107	0.12387943
Gm10549	1.33	2.51	0.0004091	0.21114719
Gm11007	-1.02	-2.02	0.0006975	0.3132125
Gm12474	1.43	2.69	0.01993992	0.99996605
Gm12976	-1.96	-3.90	0.02204855	0.99996605
Gm14149	1.03	2.04	0.003066	0.79362812
Gm15541	-1.62	-3.08	0.004534	0.99996605
Gm17455	-1.46	-2.76	0.008732	0.99996605
Gm20005	-1.58	-2.99	0.01419549	0.99996605
Gm22314	3.17	8.98	0.02175677	0.99996605
Gm25259	1.78	3.43	0.03033721	0.99996605
Gm29427	5.83	56.79	0.02862532	0.99996605
Gm34759	-2.52	-5.72	0.025646	0.99996605
Gm41495	1.62	3.07	0.008173	0.99996605
Gm42802	1.00	2.00	0.0007158	0.31788941
Gm45012	-2.03	-4.08	0.001775	0.60748264
Gm45437	-6.73	-106.21	0.02042732	0.99996605
Gm4544	1.36	2.58	0.01855296	0.99996605
Gm48529	-2.03	-4.10	0.03712458	0.99996605
Gm49804	-1.65	-3.13	0.003726	0.9068246
Gm50399	-3.18	-9.05	0.02130239	0.99996605
Gm50455	1.51	2.84	0.03503923	0.99996605
Gm5431	-1.50	-2.83	0.02953063	0.99996605
Gm7628	-3.35	-10.19	0.003591	0.88693156
Gna12	-1.42	-2.68	0.02834485	0.99996605
Gpat3	-3.28	-9.68	0.0177283	0.99996605
Gpr31b	-1.74	-3.34	0.04784031	0.99996605
Grem1	2.38	5.20	0	0
H3f3b	-1.85	-3.60	0.04636639	0.99996605
H6pd	-1.10	-2.14	0.02264793	0.99996605
Hdgf	2.07	4.19	0.04791258	0.99996605
Hemgn	1.96	3.89	0.001414	0.51374371
Hmmr	-3.02	-8.08	0.0009623	0.39379867
Hnrnpul1	1.18	2.26	0.01159293	0.99996605
Il1rl1	1.37	2.59	0.01018927	0.99996605
Ippk	-1.01	-2.02	0.0369725	0.99996605
Itpr2	2.85	7.22	0.04312006	0.99996605

Kcnu1	2.25	4.76	0.005508	0.99996605
Kif3b	2.01	4.02	0.004572	0.99996605
Krt13	1.37	2.58	0.008853	0.99996605
Ldhd	-1.60	-3.03	0.01324166	0.99996605
Lgi2	-1.19	-2.28	0.0152926	0.99996605
Lhx2	1.20	2.30	0.00879	0.99996605
Lrfn4	-1.28	-2.43	3.665E-06	0.0051
Lrriq3	1.99	3.96	0.004859	0.99996605
Med31	1.78	3.43	0.03702408	0.99996605
Mphosph8	1.81	3.51	0.002634	0.75019006
Mrgpre	1.53	2.89	0.03393998	0.99996605
Msrb3	1.31	2.47	0.0243238	0.99996605
Nanos1	1.36	2.57	0.02073055	0.99996605
Nat8f4	3.16	8.96	0.02048729	0.99996605
Ndufaf3	-1.18	-2.27	0.02627231	0.99996605
Nectin2	2.07	4.20	0.02291312	0.99996605
Nhs	-1.24	-2.37	0.02927385	0.99996605
Nmnat1	-1.71	-3.26	0.03207718	0.99996605
Nt5e	-1.65	-3.15	0.04970132	0.99996605
Ntpcr	5.00	31.98	0.04186628	0.99996605
Olfr10	-1.01	-2.02	0.003075	0.79362812
Olfr11	-1.67	-3.18	0.03641609	0.99996605
Opn1mw	2.01	4.03	0.03800337	0.99996605
Pak1	-1.04	-2.05	0.007915	0.99996605
Parp6	-1.82	-3.52	0.001633	0.5681078
Pcdha5	2.04	4.10	0.01226308	0.99996605
Pcdhga8	2.10	4.30	0.004128	0.94526206
Pcdhgc4	2.59	6.00	3.348E-06	0.004819
Pecam1	-1.40	-2.63	0.03577952	0.99996605
Pef1	-1.35	-2.56	0.0005021	0.24128386
Phf24	2.67	6.36	0.04636949	0.99996605
Pigz	-1.37	-2.58	0.01039723	0.99996605
Pmm2	-2.84	-7.17	0.04258795	0.99996605
Polr2c	-2.03	-4.10	0.03511928	0.99996605
Ppp1r12c	2.35	5.10	0.00897	0.99996605
Prr5l	-1.23	-2.35	0.03819877	0.99996605
Prrg2	1.38	2.60	0.008311	0.99996605
Psmg2	-1.04	-2.05	0.04629616	0.99996605
Ptpra	1.25	2.38	0.003891	0.92804451
Ptx3	5.14	35.29	0.03429392	0.99996605
Rdh16f1	5.71	52.50	0.04320004	0.99996605
Rgs3	1.25	2.39	0.003086	0.79362812
Rims4	2.01	4.03	0.03287863	0.99996605
Rny3	1.22	2.33	0.002232	0.69942128
Samd4	-3.17	-8.98	0.02227572	0.99996605
Sec22b	1.24	2.37	0.02158873	0.99996605
Selenbp1	1.11	2.17	2.072E-06	0.003326
Sephs2	2.38	5.21	0.02181927	0.99996605
Sh2d4b	2.23	4.70	0.04389959	0.99996605
Slc16a7	-1.33	-2.51	0.02756254	0.99996605
Slc22a4	6.14	70.37	0.02758044	0.99996605
Slc2a6	2.26	4.81	0	0
Slc30a3	-1.52	-2.87	0.02309077	0.99996605
Slc38a6	1.42	2.67	4.138E-09	0.00001919
Slc7a4	1.78	3.44	0.000045	0.04083242
Smagp	3.02	8.09	0.02764399	0.99996605
Smim9	1.80	3.48	0.02536428	0.99996605
Snx25	-1.94	-3.85	0.04572325	0.99996605
Sorl1	-1.56	-2.94	0.01579783	0.99996605
Sort1	2.38	5.21	0.03616549	0.99996605
Sp100	-1.63	-3.10	0.01277976	0.99996605
Spink10	2.13	4.38	0.03616471	0.99996605
Srp54a	1.98	3.93	0.0254858	0.99996605
St3gal3	-1.06	-2.08	0.0304449	0.99996605
Stk11	-1.31	-2.47	0.01746444	0.99996605
Tbc1d8	1.86	3.62	0.01953001	0.99996605
Thoc3	1.23	2.35	0.001461	0.52122526
Tle1	-1.10	-2.14	0.04116289	0.99996605
Tmem64	-2.12	-4.35	0.02041284	0.99996605
Tnfrsf1b	1.07	2.10	0.01530977	0.99996605
Tpm3-rs7	1.54	2.92	0.005364	0.99996605

Tspan2	1.15	2.22	0.00342	0.85492015
Ttc3	1.40	2.63	0.03651142	0.99996605
Ttc32	-1.03	-2.04	0.01096464	0.99996605
Ube2m	-2.82	-7.08	0.04115273	0.99996605
Ufc1	-1.23	-2.34	0.009809	0.99996605
Upk3b	1.49	2.80	3.998E-06	0.005384
Usp13	1.02	2.03	0.03147603	0.99996605
Vill	1.36	2.57	2.393E-12	1.427E-08
Vwf	2.46	5.49	0.02285375	0.99996605
Wdhd1	-1.68	-3.20	0.01633623	0.99996605
Zbed3	-8.34	-324.21	0.005991	0.99996605
Zbtb41	-3.45	-10.94	0.01143177	0.99996605
Zdhhc7	-2.22	-4.65	0.04861716	0.99996605
Zfp523	-1.29	-2.45	0.02733631	0.99996605

10.3 Global proteome profiling results

Supplementary Table 9: Proteins that were altered upon Picoberin treatment for 24 h. Proteome profiling data. C3H10T1/2 cells were treated with 1.5 µM purmorphamine and 1 nM Picoberin and were compared to samples treated with 1.5 µM purmorphamine and DMSO. Log_2 fold changes of at least ± 0.2 with a p-value ≤ 0.05 were considered as significantly up- or down regulated.

Protein name	Gene name	log_2 fold change	p-value
Alcohol dehydrogenase class 4 mu/sigma chain	Adh7	0.27	0.015
Aldehyde dehydrogenase. dimeric NADP-preferring	Aldh3a1	0.53	0.006
Coiled-coil domain-containing protein 127	Ccdc127	-0.23	0.041
Collagen alpha-1(II) chain;Collagen alpha-1(II) chain;Chondrocalcin	Col2a1	0.22	0.014
Cytochrome P450 1B1	Cyp1b1	0.87	0.019
Gremlin-1	Grem1	0.34	0.013
Histone H4	Hist1h4a	-0.22	0.001
Serine/threonine-protein kinase TAO3	Taok3	0.25	0.035
TATA box-binding protein-like protein 1	Tbpl1	-0.28	0.046
Xanthine dehydrogenase/oxidase;Xanthine dehydrogenase;Xanthine oxidase	Xdh	0.41	0.04

Supplementary Table 10: Proteins that were altered upon Picoberin treatment for 48 h. Proteome profiling data. C3H10T1/2 cells were treated with 1.5 µM purmorphamine and 1 nM Picoberin and were compared to samples treated with 1.5 µM purmorphamine and DMSO. Log_2 fold changes of at least ± 0.2 with a p-value ≤ 0.05 were considered as significantly up- or down regulated.

Protein name	Gene name	log_2 fold change	p-value
39S ribosomal protein L23. mitochondrial	*Mrpl23*	-0.2	0.000
Acyl-CoA desaturase 1	*Scd1;Scd3;Scd4*	-0.21	0.009
AKAP_110 domain-containing protein	*Akap11*	0.42	0.033
Alcohol dehydrogenase class 4 mu/sigma chain	*Adh7*	0.35	0.001
Aldehyde dehydrogenase. dimeric NADP-preferring	*Aldh3a1*	0.57	0.002
Caspase-12; Caspase	*Casp12*	0.28	0.028
Cytochrome P450 1B1	*Cyp1b1*	0.85	0
Endosialin	*Cd248*	-0.2	0.019
Interferon gamma inducible protein 47	*Ifi47*	0.2	0.004
Interferon-induced guanylate-binding protein 1	*Gbp1; Gbp2b*	0.23	0.017
Malignant T-cell-amplified sequence 2	*Mcts2*	0.55	0.027
Mannosyl-oligosaccharide 1.2-alpha-mannosidase IA	*Man1a1*	-0.24	0.030
N-acetylglucosamine-1-phosphotransferase subunits alpha/beta;N-acetylglucosamine-1-phosphotransferase	*Gnptab*	-0.21	0.002

subunit alpha;N-acetylglucosamine-1-phosphotransferase subunit beta			
NAD(P)H dehydrogenase [quinone] 1	*Nqo1*	0.2	0.004
Retinoblastoma-binding protein 5	*Rbbp5*	-0.25	0.002
RING finger and SPRY domain-containing protein 1	*Rspry1*	-0.2	0.047
Sorting nexin-15	*Snx15*	0.42	0.015
Stathmin-2	*Stmn2*	-0.25	0.008
Tenascin	*Tnc*	-0.22	0.042
Tetratricopeptide repeat domain 39D	*Ttc39d*	-0.22	0.03
Transforming growth factor beta-2;Latency-associated peptide	*Tgfb2*	-0.23	0.049
U3 small nucleolar RNA-interacting protein 2	*Rrp9*	0.32	0.036
Xanthine dehydrogenase/oxidase;Xanthine dehydrogenase;Xanthine oxidase	*Xdh*	0.37	0.015

Supplementary Table 11: Proteins that were altered upon Picoberin treatment for 96 h. Proteome profiling data. C3H10T1/2 cells were treated with 1.5 µM purmorphamine and 1 nM Picoberin and were compared to samples treated with 1.5 µM purmorphamine and DMSO. Log_2 fold changes of at least ± 0.2 with a p-value ≤ 0.05 were considered as significantly up- or down regulated.

Protein name	Gene name	log_2 fold change	p-value
60S ribosomal protein L27	*Rpl27*	0.2	0.001
AKAP_110 domain-containing protein	*Akap11*	0.34	0.031
Alcohol dehydrogenase class 4 mu/sigma chain	*Adh7*	0.26	0.015
Aldehyde dehydrogenase. dimeric NADP-preferring	*Aldh3a1*	0.39	0.004
Carnitine O-palmitoyltransferase 1. brain isoform	*Cpt1c*	0.23	0.047
Cytochrome P450 1B1	*Cyp1b1*	0.59	0.003
DNA polymerase lambda	*Poll*	0.28	0.015
Ephrin type-A receptor 2	*Epha2*	0.31	0.013
Histone H1.2	*Hist1h1c*	0.21	0.036
Histone H1.3	*Hist1h1d*	0.2	0.032
Inactive serine protease PAMR1	*Pamr1*	-0.21	0.049
Insulin-like growth factor-binding protein 3	*Igfbp3*	-0.27	0.018
Insulin-like growth factor-binding protein 5	*Igfbp5*	-0.2	0.039
NAD(P)H dehydrogenase [quinone] 1	*Nqo1*	0.23	0.021
Protein phosphatase 1 regulatory subunit 37	*Ppp1r37*	0.21	0.018
Structural maintenance of chromosomes flexible hinge domain-containing protein 1	*Smchd1*	0.34	0.011
Tetratricopeptide repeat domain 39D	*Ttc39d*	-0.35	0.013

Supplementary Table 11: Proteins that were altered upon Picoberin treatment for 7 days. Proteome profiling data. C3H10T1/2 cells were treated with 1.5 µM purmorphamine and 1 nM Picoberin and were compared to samples treated with 1.5 µM purmorphamine and DMSO. Log_2 fold changes of at least ± 0.2 with a p-value ≤ 0.05 were considered as significantly up- or down regulated.

Protein name	Gene name	log_2 fold change	p-value
5-nucleotidase domain-containing protein 1	*Nt5dc1*	0.23	0.008
Alcohol dehydrogenase class 4 mu/sigma chain	*Adh7*	0.31	0.046
Cytochrome P450 1B1	*Cyp1b1*	0.61	0.023
E3 ubiquitin-protein ligase DTX3L	*Dtx3l*	0.23	0.017
HECT domain-containing protein	*Gm15800*	0.21	0.04
Insulin-like growth factor-binding protein 3	*Igfbp3*	-0.31	0.043
Insulin-like growth factor-binding protein 5	*Igfbp5*	-0.25	0.017
Interferon gamma inducible protein 47	*Ifi47*	0.21	0.018
NAD(P)H dehydrogenase [quinone] 1	*Nqo1*	0.28	0.014

Protein name	Gene name	log_2 fold change	p-value
Rho-related GTP-binding protein RhoQ	*Rhoq*	-0.25	0.016
T-cell-specific guanine nucleotide triphosphate-binding protein 1	*Tgtp1*	0.2	0.019
Tetratricopeptide repeat protein 27	*Ttc27*	-0.22	0.049
Transmembrane protein 256	*Tmem256*	0.24	0.039
Uncharacterized protein C11orf98 homolog	*Ints5*	-0.25	0.015

CURRICULUM VITAE

PERSONAL INFORMATION:

Surname:	Flegel
Name:	Jana Erika
Date of birth:	21.11.1992
Date of birth:	Ostercappeln
Citizenship:	German

EDUCATION:

11/1017 – 05/2022: **PhD student at the Max Planck Institute of Molecular Physiology**

Research topic:
Identification and Characterization of inhibitors of Hh-induced osteoblast differentiation

Advisor: Prof. Dr. Dr. h.c. H. Waldmann

11/1016 – 09/2017: **Master of Sciences in Chemical Biology, TU Dortmund**

Master thesis:
Validation of a bi-tetrahydropyridine derivative as an inhibitor of the Hedgehog signaling pathway

Advisor: Prof. Dr. Dr. h.c. H. Waldmann

10/1012 – 08/2015: **Bachelor of Sciences in Chemical Biology, TU Dortmund**

Bachelor thesis:
Cloning and expression of Akt-1 mutants for investigation of the binding mode of allosteric inhibitors

Advisor: Prof. Dr. D. Rauh

Eidesstattliche Versicherung (Affidavit)

Flegel, Jana Erika

Name, Vorname
(Surname, first name)

159198

Matrikel-Nr.
(Enrolment number)

Belehrung:	Official notification:
Wer vorsätzlich gegen eine die Täuschung über Prüfungsleistungen betreffende Regelung einer Hochschul- prüfungsordnung verstößt, handelt ordnungswidrig. Die Ordnungswidrigkeit kann mit einer Geldbuße von bis zu 50.000,00 € geahndet werden. Zuständige Verwaltungs- behörde für die Verfolgung und Ahndung von Ordnungs- widrigkeiten ist der Kanzler/die Kanzlerin der Techni- schen Universität Dortmund. Im Falle eines mehrfachen oder sonstigen schwerwiegenden Täuschungsversu- ches kann der Prüfling zudem exmatrikuliert werden, § 63 Abs. 5 Hochschulgesetz NRW.	Any person who intentionally breaches any regulation of university examination regulations relating to deception in examination performance is acting improperly. This offence can be punished with a fine of up to EUR 50,000.00. The competent administrative authority for the pursuit and prosecution of offences of this type is the chancellor of the TU Dortmund University. In the case of multiple or other serious attempts at deception, the candidate can also be unenrolled, Section 63, paragraph 5 of the Universities Act of North Rhine-Westphalia.
Die Abgabe einer falschen Versicherung an Eides statt ist strafbar.	The submission of a false affidavit is punishable.
Wer vorsätzlich eine falsche Versicherung an Eides statt abgibt, kann mit einer Freiheitsstrafe bis zu drei Jahren oder mit Geldstrafe bestraft werden, § 156 StGB. Die fahrlässige Abgabe einer falschen Versicherung an Eides statt kann mit einer Freiheitsstrafe bis zu einem Jahr oder Geldstrafe bestraft werden, § 161 StGB.	Any person who intentionally submits a false affidavit can be punished with a prison sentence of up to three years or a fine, Section 156 of the Criminal Code. The negligent submission of a false affidavit can be punished with a prison sentence of up to one year or a fine, Section 161 of the Criminal Code.
Die oben-stehende Belehrung habe ich zur Kenntnis genommen:	I have taken note of the above official notification.

Ort, Datum
(Place, date)

Unterschrift
(Signature)

Titel der Dissertation:
(Title of the thesis):

Ich versichere hiermit an Eides statt, dass ich die vorliegende Dissertation mit dem Titel selbstständig und ohne unzulässige fremde Hilfe angefertigt habe. Ich habe keine anderen als die angegebenen Quellen und Hilfs- mittel benutzt sowie wörtliche und sinngemäße Zitate kenntlich gemacht.	I hereby swear that I have completed the present dissertation independently and without inadmissible external support. I have not used any sources or tools other than those indicated and have identified literal and analogous quotations.
Die Arbeit hat in gegenwärtiger oder in einer anderen Fassung weder der TU Dortmund noch einer anderen Hochschule im Zusammenhang mit einer staatlichen oder akademischen Prüfung vorgelegen.	The thesis in its current version or another version has not been presented to the TU Dortmund University or another university in connection with a state or academic examination.*

*Please be aware that solely the German version of the affidavit ("Eidesstattliche Versicherung") for the PhD thesis is the official and legally binding version.

Ort, Datum (Place, date)

Unterschrift (Signature)